DEPARTAMENT D'ASTRONOMIA I ASTROFISICA

ASTEROSEISMOLOGY AND MASS LOSS IN BE STARS.
STUDY WITH CoRoT.

PASCUAL DAVID DIAGO NEBOT

UNIVERSITAT DE VALÈNCIA
Servei de Publicacions
2010

Aquesta Tesi Doctoral va ser presentada a València el dia 28 d'octubre de 2010 davant un tribunal format per:

- Dr. Rafael Garrido Haba
- Dr. Ennio Poretti
- Dr. Luis Manuel Sarro Baro
- Dr. Enrique Solano Márquez
- Dra. Julia Suso López

Va ser dirigida per:
Dr. Juan Fabregat Llueca
Dr. Juan Gutiérrez Soto

Programa de Doctorado en Física Teórica, Nuclear y Astrofísica, 514-185-C

VNIVERSITAT
Ⓓ✪VALÈNCIA

Asteroseismology and mass loss in Be stars. Study with CoRoT

Pascual David Diago Nebot
Pascual.Diago@uv.es

Observatori Astronòmic
VNIVERSITAT ⒹVALÈNCIA

Departament d'Astronomia i Astrofísica
VNIVERSITAT ⒹVALÈNCIA

Esta tesis doctoral fue impresa el 1 de septiembre de 2010.

Ilustraciones de la portada:
Arriba: Cúmulo abierto de las Pleiades (Messier 45). Fotografía formada por composición de distintas placas fotográficas tomadas en el Observatorio de Monte Palomar en 1986 y 1989. Composición y copyright: Davide De Martin.
Abajo: Silueta del Montí (Onda), fotografía tomada por Pascual D. Diago y Sahila Aparici. Procesada con PixInsight (http://pixinsight.com/) por Vicent Peris.

Diseño de la portada: LiO.Web.Design, contacto lio.web.design@gmail.com.

b

Dr. Juan Fabregat Llueca (Universitat de València) y
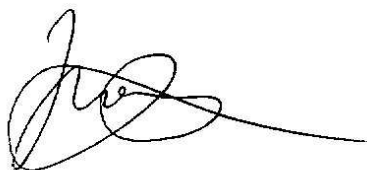**Dr. Juan Gutiérrez-Soto** (Instituto de Astrofísica de Andalucía – CSIC)

CERTIFICAN:

Que la presente memoria, "**Asteroseismology and mass loss in Be stars. Study with CoRoT**", ha sido realizada bajo su dirección, por Pascual David Diago Nebot, y que constituye su tesis doctoral para optar al grado de Doctor en Físicas.

Y para que quede constancia y tenga los efectos que corresponda, firman el presente certificado en Valencia, a 1 de septiembre de 2010.

Firmado: Juan Fabregat Llueca   Firmado: Juan Gutiérrez-Soto

d

a Sahila...

Contents

II   Study of pulsating Be stars with CoRoT   143

8   The CoRoT space mission   145

9   The study of Be stars with CoRoT   171

10 Be stars in the exoplanet fields of CoRoT   185

11 The Be star HD 50 209   197

Introduction

The interiors of the stars are among the most difficult parts of the Universe to observe. Essentially, asteroseismology tries to make use of the oscillations to prove the stellar interiors, which are not directly observable. The basic principles of asteroseismology are, to a certain extent, similar to those developed and employed by Earth seismologists. Asteroseismology relies on advanced mathematical descriptions of oscillations in a three-dimensional body and numerical modeling. It is therefore a prominent example of interdisciplinary science.

The general aim of this work is the study of Be stars with the CoRoT space mission. Classical Be stars are B-type stars that exhibit line emission over the photospheric spectrum. The excess is attributed to a circumstellar gaseous component that is commonly accepted to be in the form of an equatorial disk. The mechanisms responsible for the production and dynamics of the circumstellar gas are still not constrained. Observations of non-radial pulsation beating phenomena connected to outbursts point toward a relevance of pulsation, but this mechanism cannot be generalized. In this regard, the observation of classical Be stars with the high-precision CoRoT satellite is providing important keys to understand the physics of these objects and the nature of the Be phenomenon.

In order to study the light variations of the selected stars we use photometric and spectroscopic observations. These observations allow us to extract frequencies, amplitudes and phases of these variations. As we will show, these light variations can be connected with pulsations on the stellar surface. For carrying out the frequency analysis we have developed a new code based on standard Fourier analysis. The point is that this code, called PASPER, allows the frequency analysis of large sets of light curves in an automatic mode.

This Ph.D. thesis is arranged as follows: in Chapter 1, Chapter 2 and Chapter 3 we describe the scientific framework of this project. Chapter 1 gives a brief description on Asteroseismology, the technique to dive into the interior of the stars. Chapter 2 presents the current status of Be stars and emphasizes the relevance of pulsations in these emission-line B-type stars. Finally, Chapter 3

describes the basics of the Fourier analysis and the rudiments of the time series analysis. In this Chapter, we introduce the PASPER code for the frequency analysis of photometric light curves.

At the early begin of this Ph.D. thesis, the CoRoT satellite was still on ground getting ready for the launch. At this time, we were performing and improving our PASPER code and we needed some variable stars to check the performance of our methods. In this context, we perform a search for short-period B and Be star variables in the low metallicity environment of the Magellanic Clouds. This study constitutes the Part I of this Ph.D. thesis. This Part has a double goal: i) to test the frequency analysis codes; and ii) to detect observationally β Cephei and SPB-like B-type pulsators in low metallicity environments, actually not predicted by the pulsational theory and models. This Part is organized in four Chapters: Chapter 4 depicts the scientific context for the search of B-type pulsators in the Magellanic Clouds. An overview of the MACHO survey and the description of the B and Be studied samples are given in Chapter 5. Finally, Chapter 6 and Chapter 7 describe the results and discussion for the SMC and LMC studies, respectively.

Part II is devoted to the study of Be stars with the CoRoT space mission. This Part is also organized in four Chapters: Chapter 8 depicts a complete review on the CoRoT mission, describing the spacecraft, the different observing programmes and the mission design. Chapter 9 presents the CoRoT Be Team, a collaboration for the study of Be stars using the CoRoT data. We describe some general remarks about the instrumental effects present in the CoRoT light curves and information on the frequency analysis of the CoRoT data. In Chapter 10 we describe the results on the analysis of three Be stars from the CoRoT exoplanet field. Finally, in Chapter 11 we present the results on the frequency analysis of the late Be star HD 50 209, observed in the seismology field of the CoRoT satellite. The analysis of this Be star has revealed up to sixty frequencies, grouped in six different and separated sets, attributed to g-mode pulsations.

Finally, in Chapter 12 we resume the main conclusions of the whole project, including prospects and future work to be done. An addendum with all the published results derived from this project has been added in Chapter 13.

Part III encloses the Appendixes. Appendix A provides a brief summary of this work in Spanish. A complete description on basic equations of non-radial oscillation is given in Appendix B. Appendix C contains the user guide of the PASPER code. The user guide of the KURTZ_BOS code is given in Appendix D. Finally, Appendix E contains additional plots that complete the results of the Small Magellanic Cloud given in Chapter 6.

You tell me that you've heard every sound there is
And your bird can swing
But you can't hear me, you can't hear me.

John Lennon

1

Asteroseismology

Every star, including our Sun, is a self-gravitating gaseous sphere that radiates an enormous amount of energy to the outer space. Energy radiated from the surface of a star is generated in the deep interior by thermo-nuclear reactions. A star, born out of an interstellar cloud, spends most of its life in the hydrogen-burning main-sequence stage. As a star consumes its nuclear fuel, it evolves by changing its internal structure. A star is by no means a quiet object, but is in a sense a kind of heat engine exhibiting various activities. Some stars blow out stellar winds from their surfaces with speeds ranging up to a few thousand kilometres per second, while some others change its volume or temperature just as a human body breathes rhythmically.

The theory of stellar pulsation was originally developed in order to explain the oscillations of classical variable stars such as the Cepheids and RR Lyrae stars. However, in recent years, pulsation phenomena have also been discovered in many stars that were regarded as non-pulsating stars before, such as our Sun itself, white dwarfs, early-type O and B stars with slow and rapid rotation, etc. By using these oscillations, we can probe, in the case of the Sun, its internal structure, just as one probes the interior of the Earth by using data of seismic waves. This new field of research is thus called "helioseismology". The same method may in principle apply to stellar pulsations, called "asteroseismology" in this case. Asteroseismology is at the present moment still in its infancy, but it has the potential to become a major field of stellar physics.

The physical basis for understanding stellar pulsations has been described with great clarity by many authors. Classic texts in this matter are Cox (1980), Unno et al. (1989) or Christensen-Dalsgaard and Berthomieu (1991). Recently, Aerts et al. (2010) have published the first book dedicated to asteroseismology. Moreover, different reviews in asteroseismology (Brown and Gilliland 1994; Kurtz 2006) and in helioseismology (Christensen-Dalsgaard 2002) can be found in the literature. In this work, we only try to give a brief report on asteroseismology, so we refer to the above mentioned works for a complete review.

1.1   The Music of the Spheres

In Pythagoras (c. 556–475 BC) time[1], people believe that there was a natural harmony for everything, that music, mathematics and what we now call physics were intimately related. In particular, they believed that the motions of the Sun, Moon, planets and stars generated musical sounds: the *Music of the Spheres* (see Koestler 1959). A century after Pythagoras, Plato (c. 427–347 BC) said that "a siren sits on each planet, who carols a most sweet song, agreeing to the motion of her own particular planet, but harmonising with all the others" (see Brewer 1894). Two millennia after Plato, Johannes Kepler (1571–1630) did admit that "no sounds are given forth", but still held that "the movements of the planets are

---

[1]Introduction partly reproduced from Kurtz (2006).

modulated according to harmonic proportions". The Music of the Spheres never left artistic thought or disappeared from the language, but as a "scientific" idea it faded from view with Kepler's Laws of motion of the planets.

In the opening paragraph of his now-classic book, *The Internal Constitution of the Stars* (Eddington 1926), Sir Arthur Stanley Eddington lamented:

> At first sight it would seem that the deep interior of the sun and stars is less accessible to scientific investigation than any other region of the universe. Our telescopes may probe farther and farther into the depths of space; but how can we ever obtain certain knowledge of that which is hidden behind substantial barriers? What appliance can pierce through the outer layers of a star and test the conditions within?

However, Eddington would have actually been amazed and delighted to know that now we are able to *see* inside the stars. Stars are not quiet places. They are noisy, they have sound waves inside them. Those sounds cannot get out of a star, of course. But for many kinds of stars, the sound waves make the star periodically swell and contract, get hotter and cooler. With our telescopes we can see the periodic changes in the brightness of the star, the periodic motion of its surface moving up-and-down, back-and-forth. Thus, we can detect the natural oscillations of the star and *hear* the sounds inside them, ringing like giant bells. This is the birth of asteroseismology. Therefore, the answer to the Eddington's question would be "Asteroseismology, the real Music of the Spheres".

1.2   Stellar pulsation

When the gas in the stellar interior oscillates periodically due to a perturbation from its equilibrium state, the stellar temperature and radius will fluctuate accordingly, which becomes visible by means of periodic changes in brightness and radial velocity. Hence, the observed signatures of stellar pulsations find their ori-

gin in small displacements of the stellar layers. In Section 1.3 we will describe the mechanism that feeds the regular periodic oscillations present in stars.

To describe the theory of stellar pulsations, one considers a spherically symmetric star in equilibrium upon which small perturbations are superimposed. We consider stars as 3-dimensional spheres, so their natural oscillation modes have nodes in three orthogonal directions. These nodes are concentric radial shells (r), lines of latitude (θ) and lines of longitude (φ). For a spherically symmetric star the solutions to the equations of motion have displacements in the (r, θ, φ) directions. The solutions of the equations of motion on the condition that oscillations must have components in each of these directions can be found from the equations of hydrodynamics, given in Appendix B. By considering these equations to first order perturbation, we obtain the following solutions depending on the time (t) and the spherical harmonics[2]:

$$\xi_r(r, \theta, \varphi, t) = a(r) Y_\ell^m(\theta, \varphi) \, e^{(i \, 2\pi\nu t)} \tag{1.1}$$

$$\xi_\theta(r, \theta, \varphi, t) = b(r) \frac{\partial Y_\ell^m(\theta, \varphi)}{\partial \theta} \, e^{(i \, 2\pi\nu t)} \tag{1.2}$$

$$\xi_\varphi(r, \theta, \varphi, t) = \frac{b(r)}{\sin \theta} \frac{\partial Y_\ell^m(\theta, \varphi)}{\partial \varphi} \, e^{(i \, 2\pi\nu t)} \tag{1.3}$$

where ξ_r, ξ_θ and ξ_φ are the displacements, $a(r)$ and $b(r)$ are amplitudes, ν is the oscillation frequency[3] and $Y_\ell^m(\theta, \varphi)$ are the spherical harmonics given by

$$Y_\ell^m(\theta, \varphi) = \sqrt{\frac{2\,\ell+1}{4\pi} \frac{(\ell-m)!}{(\ell+m)!}} \; P_\ell^m(\cos\theta) \, e^{(i\,m\varphi)} \tag{1.4}$$

that represents the dependence of the mode on the angular variables θ and φ for a star with a spherically symmetric equilibrium configuration. And $P_\ell^m(\cos\theta)$ are Legendre polynomials given by

$$P_\ell^m(\cos\theta) = \frac{(-1)^m}{2^\ell \, \ell!} \, (1 - \cos^2\theta)^{\frac{m}{2}} \, \frac{d^{l+m}}{d\,\cos^{\ell+m}\,\theta} \, (\cos^2\theta - 1)^\ell \tag{1.5}$$

where we remember that θ is measured from the pulsational pole, the axis of

---

[2]Here the displacements are written in complex form which is a mathematical convenience. The physically meaningful quantities are obtained by taking the real parts. See Appendix B

[3]More precisely, the *cyclic* frequency, later we also introduce the *angular* frequency $\omega = 2\,\pi\,\nu$.

symmetry. Note that the spherical harmonics are usually defined such that the integral of $|Y_\ell^m|^2$ over the unit sphere equals 1, as secured by the normalisation constant

$$c_{\ell m} \equiv \sqrt{\frac{2\ell+1}{4\pi} \frac{(\ell-m)!}{(\ell+m)!}} \qquad (1.6)$$

Using the spherical harmonics the oscillation modes can be defined by three quantum numbers:

- n is the number of radial nodes and is called the *overtone* of the mode[4].

- ℓ is the *spherical degree* of the mode and specifies the number of surface nodes that are present.

- m is the *azimuthal order* of the mode, where $|m|$ specifies how many of the surface nodes (ℓ) are lines of longitude (lines that pass through the rotation axis of the star). It follows therefore that the number of surface nodes that are lines of latitude is equal to $\ell - |m|$. The wave-numbers ℓ and m are both integers, with $m = -\ell, ..., \ell$, so there are $2\ell+1$ m-modes for each degree ℓ.

In stellar oscillation theory one distinguishes two different types of pulsation modes: radial and non-radial oscillation modes that we will describe in the following Section. A more detailed description on basic equations of stellar pulsation can be found in the Appendix B. For a complete review we refer to Unno et al. (1989) and Aerts et al. (2010).

1.2.1 Radial pulsation

The radial oscillation is an oscillation whereby the star rhythmically expands and contracts while keeping its spherical symmetry. The system of differential equations that describes the radial displacement defines a Sturm-Liouville eigenvalue problem with an infinite number of discrete eigenvalues and eigenfrequencies. In

---

[4]Sometimes denoted as k, particularly amongst those working on pulsating white dwarf stars.

this case, only radial movements occur and the oscillation can be described in a one-dimensional parameter space, with $\ell = 0$, and hence also $m = 0$. Radial oscillations are characterised by the radial wave number n, which indicates the number of nodes of the eigenfunctions between the centre and the surface of the star. The mode with the smallest eigenvalue is the *fundamental radial mode* ($n = 0$). This mode has no node between the stellar centre and the atmosphere and hence all mass elements in the interior of the star will periodically move in the same direction. The mode with one node ($n = 1$) is called the *first radial overtone.* In this case the mass elements on either side of the node will move in opposite directions. The modes with n nodes are called the n-th radial overtones.

The radial mode is the usual pulsation mode of Cepheid variables and RR Lyrae stars, amongst others. There are Cepheid variables, RR Lyrae stars and δ Scuti stars that pulsate in the fundamental and first overtone radial modes. Radial pulsations are also present in massive stars, like β Cephei or Be stars (see Walker et al. 2005b, for a study of the pulsations of the Oe star ζ Oph).

1.2.2   Non-radial pulsation

When both radial and transverse motions occur in the stellar interior, the spherical symmetry of the star will not be preserved and we speak of non-radial oscillations. In this case three pulsational parameters are needed to characterise the oscillation: the radial wavenumber n, the degree ℓ and the azimuthal number m. The latter two describe the angular dependence of the oscillation and are determined by the spherical harmonic $Y_\ell^m(\theta, \varphi)$. A non-radially oscillating star is subdivided in different regions of which some move periodically inwards while others move simultaneously outwards. Nodal lines and surfaces indicate the borders between the different regions of opposite motion.

Fig. 1.1 illustrates the radial component of different types of non-radial oscillation modes with different inclination angles (i). Based on the values of ℓ and m we can distinguish three types:
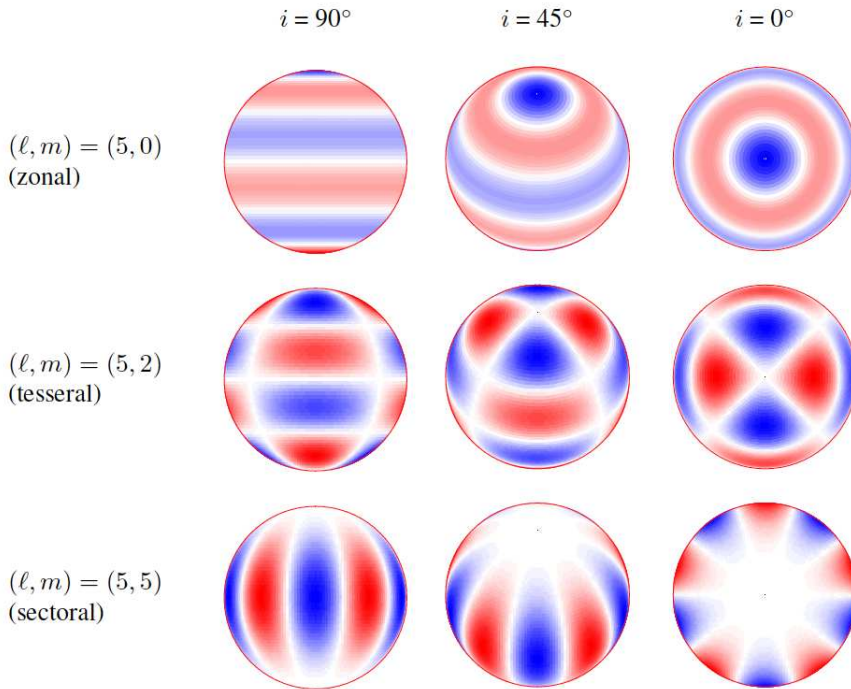
Figure 1.1: *Snapshot of the radial component of different non-radial oscillation modes for different inclination angles (i). The first column depicts the star seen equator-on, the second column under an inclination angle of 45° and the third column shows the star pole-on. From top to bottom we give an example of a zonal, tesseral and sectoral mode ($\ell = 5$). Blue velocity regions of the star are moving towards us, while red regions are moving away from us. The black dots denote the poles. The white nodal lines are mass elements with zero radial component of the pulsational velocity. Figure courtesy of K. Uytterhoeven.*

- *Zonal or axisymmetric modes* are modes that satisfy $m = 0$.

- *Sectoral modes* are the ones for which $\ell = |m|$ is valid.

- *Tesseral modes* are those with $0 \neq |m| \neq \ell$.

Note that we have treated radial oscillations as a special case of non-radial oscillations whereby $\ell = 0$, i.e., radial modes do not induce nodal lines on the surface. All modes that satisfy $1 \leq \ell$ are non-radial pulsation modes. A mode

with $\ell = 1$ or $\ell = 2$ is sometimes called a dipole mode, respectively quadrupole mode.

1.2.3 Historical background

The early history of studies on stellar pulsation was concisely described in the introduction of the famous textbook *The Pulsation Theory of Variable Stars* (Rosseland 1949). It is interesting to see that the theory of non-radial pulsation developed by Kelvin (1863) preceded the theory of radial pulsation developed by Ritter (1879). However, the Cepheids have been the chief concern of pulsation theory, which was founded by Eddington as summarised in his book *The Internal Constitution of the Stars* (Eddington 1926). In spite of the remarkable progress in the development of the theory of radial pulsation, the theoretical study of non-radial pulsation remained largely within academic circles until recently. But the work of Pekeris and Cowling should be mentioned. Pekeris (1938) obtained the exact analytic solution for adiabatic non-radial oscillations in the homogeneous compressible model. Cowling (1941) extended the study for the polytrope model. For a description of these and other studies, readers can refer to the comprehensive article by Ledoux and Walraven (1958).

Ledoux developed the study of non-radial pulsations in 1951 (see Ledoux 1951). He suggested that non-radial oscillations could explain the double periodicity and the large temporal variations in the broadening of spectral lines observed in β Canis Majoris (a prototype of β Cephei type variable stars). Osaki (1971) examined Ledoux's theory by calculating line profiles for a star undergoing non-radial oscillations and compared the result with observations available at that time. He also suggested (Osaki 1974) a possible mechanism for the origin and maintenance of β Cephei pulsation based on non-radial oscillation.

The discovery of the five-minute Solar oscillations by Leighton et al. (1962) was also epoch-making. A number of interesting theories had been proposed to explain this phenomenon (see Stein and Leibacher 1974). Some fifteen years later, Deubner (1975) succeeded in resolving observed oscillations into discrete modes

in the so-called diagnostic diagram. A comparison between his observation and theoretical eigenfrequencies of non-radial modes calculated by Ando and Osaki (1975) has established that the solar five-minute oscillations are global non-radial p-modes of the Sun with high spherical harmonic degree ℓ ($\ell = 200 - 1\,000$). Furthermore, low-degree ℓ ($\ell = 0 - 5$) and intermediate-degree ℓ ($\ell = 1 - 200$) have also been detected.

Since the late 1960s and early 1970s, pulsations and oscillation-related phenomena have been observed in many stars that were regarded as non-pulsating stars before. They include white dwarfs, hot subdwarfs, Ap stars, γ Dor stars, and early type O and B stars. It is now believed that non-radial oscillations are responsible for variability observed in these stars in most cases. Along with these observational developments, much progress has been made in the theoretical side of non-radial oscillations theory. Since the middle of the 1970s, full equations of linear adiabatic and non-adiabatic non-radial oscillations have been solved numerically for realistic stellar models with the help of computers. The introduction of the so-called propagation diagram, the phase diagram and the concept of "wave trapping" (Scuflaire 1974; Unno 1975; Osaki 1975; Shibahashi and Osaki 1976) have greatly improved the understanding on non-radial oscillation in stars.

A number of theoretical problems remain to be studied. Among them are non-linear problems, including the mixing of matter due to finite oscillations, oscillations in the presence of a strong magnetic field or rotation, and energy and momentum transport by waves. Both theory and observation are still in progress, so further developments can be expected in the near future.

1.2.4   The effect of rotation

From Eqs. 1.1 and 1.4 we can derive that for modes with $m \neq 0$ the exponentials in the two equations combine to give a time dependence that goes as $e^{-i(2\pi\nu t - m\varphi)}$. This phase factor in the time dependence means that the $m \neq 0$ modes are travelling waves. Conventionally, we assign positive values of m to modes that propagate in the same direction as the stellar rotation (*pro-grade modes*), and

negative values of m to modes that travel in the opposite direction of the stellar rotation (*retrograde modes*). In most cases the pulsation axis is assumed to coincide with the rotation axis.

It is straightforward to see, from a purely geometrical argument, that rotation affects the observed frequencies. Let us assume the angular velocity Ω to be uniform and consider an oscillation frequency $\nu_{n\ell 0}$ in the co-rotating frame of the star, this frequency is independent of m ($m = 0$) and it is unaffected by the rotation. Then, the observed frequency ($\nu_{n\ell m}$) satisfies the relation:

$$\nu_{n\ell m} = |\nu_{n\ell 0} - m\,\Omega| \tag{1.7}$$

Thus, an observer in the inertial frame finds ($2\ell + 1$) different frequencies that split uniformly depending on the m number. This is called *rotational splitting*.

This description is obviously incomplete. Even in the case of uniform rotation, the effects of the Coriolis force must be taken into account in the rotating frame, causing a contribution to the frequency splitting. This was discussed by Ledoux (1951) in a study of the β Cephei star β Canis Majoris (β CMa). In the *observer's frame of reference* the Ledoux rotational splitting relation for an uniformly rotating star is

$$\nu_{n\ell m} = \nu_{n\ell 0} + m\,(1 - C_{n\ell})\,\Omega \tag{1.8}$$

where $C_{n\ell}$ is the *Ledoux constant*, a mode-dependent and model-dependent quantity with values below 1. Furthermore, in general the angular velocity $\Omega(r, \theta)$ is a function of the depth in the star and the position in the surface. Nevertheless, the effect of the Coriolis force is often small, and Eq. 1.7 is approximately correct if Ω is replaced by a suitable average of the position-dependent angular velocity.

1.2.5 Pressure and gravity modes

There are two main sets of solutions to the equation of motion for a pulsating star, and these lead to two types of pulsation modes: the *pressure* and the *gravity*

modes. For the pressure modes, or p-modes, the pressure is the primary restoring force for a star perturbed from equilibrium. These p-modes are acoustic waves and have gas motions that are primarily vertical. For the gravity modes, or g-modes, buoyancy is the restoring force and gas motions are primarily horizontal. Both p- and g-modes of high order can be described in terms of propagation rays (see also Gough and Toomre 1991; Gough 1993, for a complete review). The propagation ray descriptions provide illuminating graphical representations of mode properties. This representation also forms the basis for powerful asymptotic descriptions of the modes. In Fig. 1.2 we show the propagation rays for sound and gravity waves in cross-section of a Sun-like star.
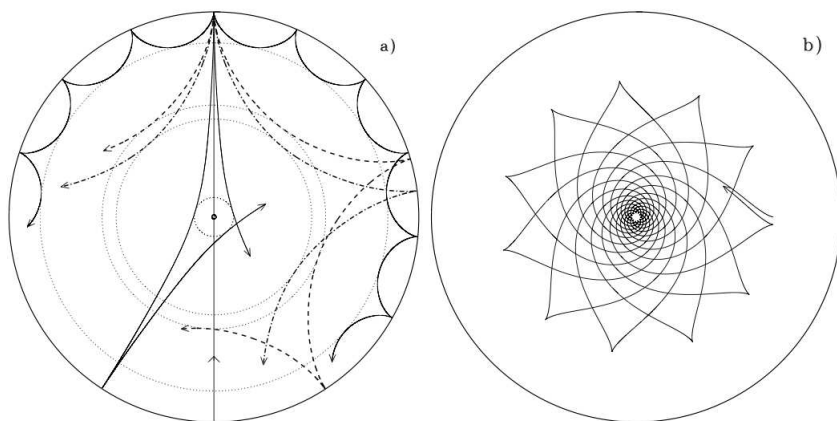
Figure 1.2: *Sound and gravity propagation rays in cross-section of a Sun-like star. The acoustic ray paths, panel a), are bend by the increase in sound speed with depth until they reach the inner turning point (indicated by the dotted circles) where they undergo total internal refraction. At the surface the acoustic waves are reflected by the rapid decrease in density. Shown are rays corresponding to modes of frequency $3\,000\,\mu$Hz and degrees (in order of increasing penetration depth) $\ell = 75, 25, 20$ and 2. The line passing through the centre schematically illustrates the behaviour of a radial mode. The g-mode ray path, shown in panel b), corresponds to a mode of frequency $190\,\mu$Hz and degree 5 and is trapped in the interior. This figure illustrates that g-modes are sensitive to the conditions in the very core of the star. Figure taken from Cunha et al. (2007).*

The peculiarity of the non-radial oscillations compared with the radial oscillations is that the system of differential equations together with the boundary conditions is in general not a Sturm-Liouville eigenvalue problem (as described in Appendix B). Only in two special cases of approximations the system becomes

so and leads to an infinite number of eigenfrequencies and eigenvalues: for very high frequencies ($\nu^2 \to \infty$) and for very low frequencies ($\nu^2 \to 0$). This property corresponds physically to the existence of the two kinds of restoring forces described above, pressure and gravity. Therefore, there are two sequences of the eigenvalues:

Pressure modes (p-modes): For a given ℓ, occurs $\nu_n^2 \to \infty$ as $n \to \infty$.

Gravity modes (g-modes): For a given ℓ, occurs $\nu_n^2 \to 0$ as $n \to \infty$.

For a given order n, the frequency is higher for the modes with larger ℓ. Some eigenvalues (square of oscillation frequencies) of a polytropic model are shown in Fig. 1.3 as an example.
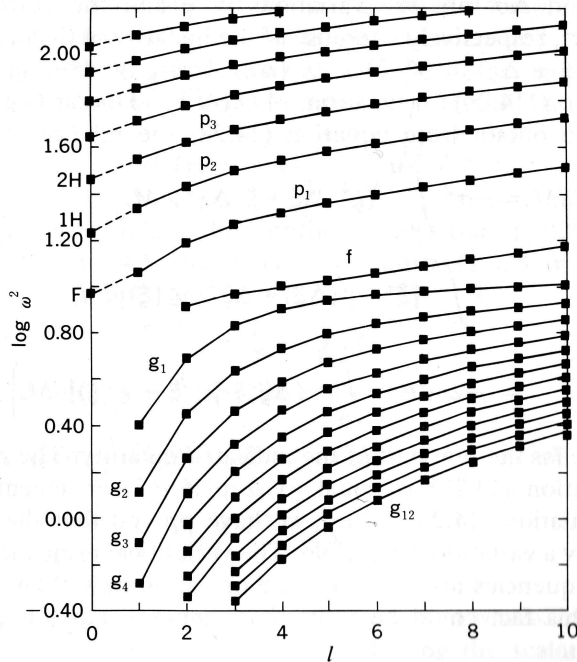
Figure 1.3: *The square of the dimensionless eigenfrequency, $\omega^2 = \nu^2 R^3/GM$, versus the index ℓ of spherical harmonics $Y_\ell^m(\theta, \varphi)$ for the adiabatic pulsations of the polytrope with $N = 3$. The radial pulsations corresponds to $\ell = 0$. Figure taken from Unno et al. (1989).*
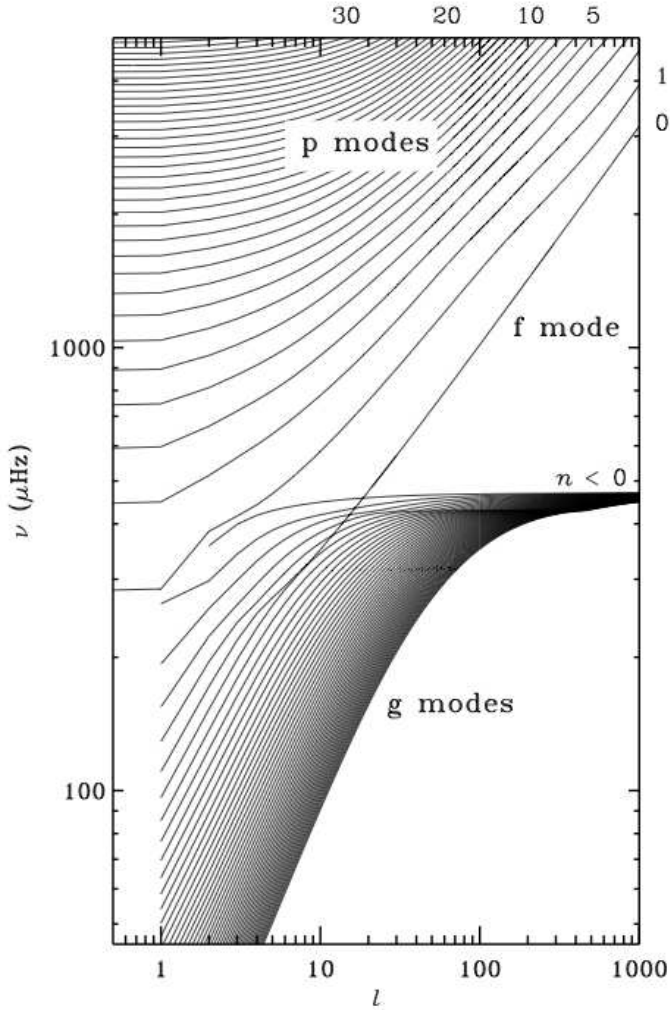
Figure 1.4: *The frequency of the modes versus their degree ℓ for a Solar model. The figure clearly illustrates the general property of p-modes that the frequency increases with overtone n and degree ℓ. For g-modes frequency decreases with higher overtone, but increases with n if we use the convention that n is negative for g-modes. Frequency still increases with degree ℓ for g-modes, just as it does for p-modes. Some values of the overtone n are given for the p-modes lines in the upper right of the figure. Note that while continuous lines are shown for clarity, the individual modes are discrete points, corresponding to integer ℓ, which are not shown here. Figure courtesy of Jørgen Christensen-Dalsgaard.*

There are three important properties of p- and g-modes to be mentioned here:

1. As the number of radial nodes increases, the frequencies of the p-modes increase but the frequencies of the g-modes decrease, as shown in Fig. 1.3 for a polytropic model and in Fig. 1.4 for a Solar model.

2. The p-modes are most sensitive to conditions in the outer part of the star, whereas g-modes are most sensitive to conditions in the deep interior of the star[5] as shown in Fig. 1.2.

3. For p-modes and $n \gg \ell$, Tassoul (1980) found an asymptotic relation for the pulsation frequencies, becoming approximately equally spaced. This is usually observed in the p-modes of the Sun and Sun-like stars. On the other hand, for g-modes and $n \gg \ell$, Tassoul (1980) found an asymptotic relation for the periods and not for the frequencies. In this case, the periods are approximately equally spaced. For a recent review, see Miglio (2006).

The oscillation frequencies associated to p-modes, occupy the high frequency domain and the motions are dominated by the radial displacement component. According to the radial order n, the p-modes are denoted as p_1 (fundamental mode), p_2 (first overtone), p_3 (second overtone), etc. In analogy with the radial modes, the eigenfrequency $\nu(p_i)$ increases with increasing n:

$$0 < \nu(p_1) < \nu(p_2) < \nu(p_3) < ...$$

Radial pulsation modes can be seen as special cases of p-modes, with $\ell = 0$.

Gravity modes, on the other hand, have low frequencies and the oscillations of the mass elements are dominated by transverse motions. As g-modes always have an horizontal component, g-modes never can be purely radial, and hence $1 \leq \ell$. Similar to p-modes, a g-mode with radial order n is noted g_n. The g-modes are divided into two classes: the dynamically unstable ($\nu^2 < 0$) g^--modes and the oscillatory ($\nu^2 > 0$) g^+-modes. As we will consider only the oscillatory g^+-modes, hereafter we refer to them as g-modes. The absolute value of the eigenfrequency

---

[5]Except in white dwarfs where the g-modes are sensitive mainly to conditions in the stellar envelope.

$|\nu(g_i)|$ decreases with increasing radial order n in case of g-modes (g^+-modes), with limiting value 0. The relation between subsequent eigenfrequencies is thus given by:

$$0 < \frac{1}{|\nu(g_1)|} < \frac{1}{|\nu(g_2)|} < \frac{1}{|\nu(g_3)|} < ...$$

We distinguish a third type of mode, the f-mode, which only exists for $\ell > 1$. The eigenfrequencies of f-modes are intermediate between those associated to the p-modes and the g-modes. Note that $\nu = 0$ for the f-mode for $\ell = 1$. This mode corresponds to the trivial solution which describes a parallel displacement of the whole star. The f-mode always have $n = 0$ and it is situated between the p-mode and g-mode zones, therefore the following relation is satisfied:

$$0 < ... < \nu(g_i) < ... < \nu(g_1) < \nu(f) < \nu(p_1) < ... < \nu(p_i) < ...$$

In the interior of the star, the pressure and gravity modes propagate in the radial direction, but have an oscillatory behaviour depending on the properties of the waves. The propagation diagram, given essentially by Scuflaire (1974), contains the so-called *trapping regions* or *mode cavities*. Outside these regions the amplitude of the modes decrease. The g-modes have large amplitudes near the centre of the star, while p-modes reach high amplitudes in the outer stellar layers. From an asteroseismology point of view the g-modes are more interesting as they penetrate deepest in the star. In Fig. 1.5 we show the p- and g-mode cavities (labelled as P and G, respectively) for a stellar model of $1.8M_\odot$. We finally mention that, during the course of the evolution of a star, its modes may become of mixed nature, i.e., an oscillatory behaviour in an inner g-mode cavity but in an outer p-mode cavity. In such a case the P and G mode cavities are situated closer to each other. For more details on physic nature and propagation of the oscillation modes we refer the interested reader to Appendix B and the text books Unno et al. (1989) and Aerts et al. (2010).

In a rapidly rotating star, other types of modes, called the r-modes, are predicted to be unstable. The restoring force for these modes is exclusively attribute to the Coriolis force (see for e.g. Savonije 2005; Townsend 2005; Lee 2006). The r-modes, or *toroidal modes*, are characterised by purely transverse motions.
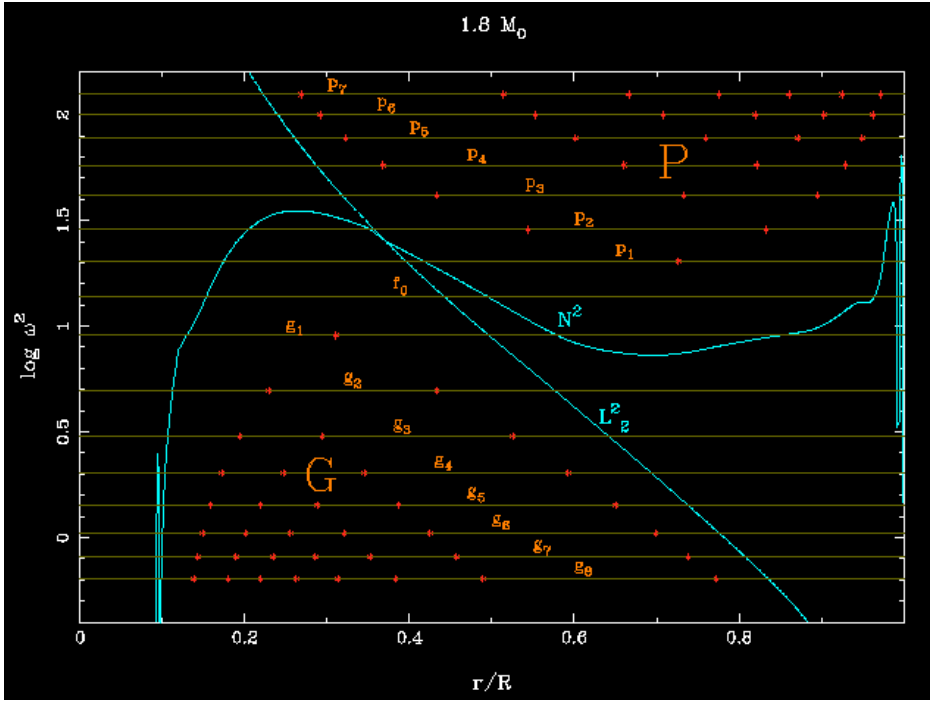
Figure 1.5: *Propagation diagram of a stellar model of $1.8\,M_\odot$. The equilibrium model originates from Antonio Claret, and the frequencies were calculated by Rafael Garrido. The vertical axis gives the oscillation frequencies of the model in natural units of the star, meaning that their square is divided by GM/R^3, and the horizontal axis gives the radius, with $R = 1$ being at the stellar surface. Each point is an oscillation node, which is a point in the stellar radius where the oscillation amplitude is zero. The diagram also indicates the Brunt-Väisälä frequency (N) which is the natural frequency of vertical oscillations of a fluid element that is allowed to oscillate freely in the interior of a star. The Lamb frequency (L), which is the frequency of a horizontal wave, is also shown in the diagram, for the spherical harmonics with $\ell = 2$, scaled to the sound speed in that region. The denominations "P" and "G" refer then also to depths in the stellar interior where the waves that are able to pass through have the character of pressure or gravity waves. The eigenfrequencies and node positions of the modes are indicated as dashed lines and bullets. Figure courtesy of Andrés Moya.*

1.2.6   Observational evidences of non-radial pulsations

It has been well established that variable stars such as Cepheids, RR Lyrae and Mira variables are pulsating stars and their pulsations are explained in terms of simple radial, spherically symmetric pulsations. That is, their variations in light and radial velocity are caused by alternate expansion and contraction of a star as a whole. On the other hand, for non-radial oscillations in which the stellar form periodically deviates from the spherical shape, observational evidence for their existence was rather meager. In fact, before 1970, the pulsation of β Cephei stars was the only case in which non-radial oscillation was suspected as a possible cause of stellar variability. Actually, non-radial oscillation has been found in different pulsating stars.

In Unno et al. (1989) we can find an interesting explanation of direct and indirect observational evidences for non-radial pulsations. For brevity, in this work, we only refer to amplitude variations during the oscillations. But there are a lot of observational signatures of non-radial pulsations as photometric variations, phase shifts during eclipses, line profile variations, amplitude and phase variations in different colours, etc.

Amplitude modulation: the beating phenomenon

In some variable stars, amplitudes of pulsations in the light curve and/or in the radial velocity curve are know to be modulated with periods much longer than the principal period, as illustrated in Fig. 1.6. This is the so-called *beating phenomenon*. The simplest explanation may be the simultaneous excitation of two oscillations with nearly equal periods. In the case of radial pulsations it is difficult for two oscillations with the nearly equal periods to occur. But in the case of non-radial oscillations, the existence of nearly equal periods can be easily explained in terms of the rotational splitting of eigenfrequencies of non-radial modes with the same quantum numbers n and ℓ but differing in m, i.e., the lifting of the degeneracy of non-radial modes in the presence of rotation. In stars with high rotational rates the beating phenomenon can also be due to the presence of close

modes with different degree ℓ, for example, $\ell = 1$ and $\ell = 3$ or $\ell = 2$ and $\ell = 4$.

In order to better understand the beating phenomenon observed in a star, we explain below its mathematical description. The sum of two waves is given by the following equation:

$$A_1 \sin(F_1\ t + \varphi_1) + A_2 \sin(F_2\ t + \varphi_2) =$$

$$= (A_1 + A_2) \sin \tfrac{1}{2}((F_1 + F_2)\ t + \varphi_1 + \varphi_2) \cdot \cos \tfrac{1}{2}((F_1 - F_2)\ t + \varphi_1 - \varphi_2) +$$

$$+ (A_1 - A_2)\ \cos \tfrac{1}{2}((F_1 + F_2)\ t + \varphi_1 + \varphi_2) \cdot \sin \tfrac{1}{2}((F_1 - F_2 t + \varphi_1 - \varphi_2))$$

$$(1.9)$$

where F_1 and F_2 represent the frequencies, A_1 and A_2 the associated amplitudes and φ_1 and φ_2 the corresponding phases. Now let us suppose that two frequencies are nearly the same, so that $\tfrac{1}{2}(F_1 + F_2)$ is the average frequency, and is about the same as either one. However, $F_1 - F_2$ is much smaller than F_1 or F_2. That means that we can represent the solution with a high-frequency sine wave similar to the one we started with, but its "size" (i.e. amplitude) is slowly changing with a frequency which appears to be $\tfrac{1}{2}(F_1 - F_2)$. Although Eq. 1.9 means that the amplitude goes as $\tfrac{1}{2}(F_1 - F_2)$, what it is really telling us is that the high-frequency oscillations are contained between two opposed cosine curves (shown in Fig. 1.6). The modulation of the amplitude is at frequency $F_1 - F_2$. Therefore, we conclude that if we add two waves of frequencies F_1 and F_2, we will get a net resulting wave of average frequency $\tfrac{1}{2}(F_1 + F_2)$ which oscillates in strength with frequency $F_1 - F_2$.

Amplitude modulation also occurs in the case of non-radial oscillations if the symmetry axis of a non-radial mode is oblique to the rotation axis of a star. This possibility was first suggested by Kurtz (1982) to explain amplitude modulation observed in rapidly rotating Ap stars.
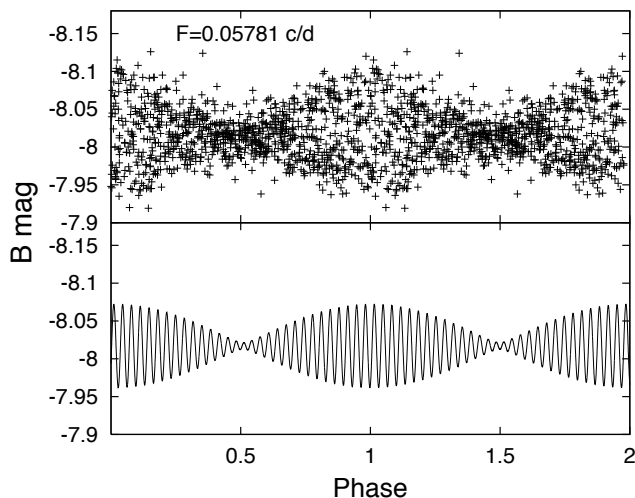
Figure 1.6: Top: *The Be star* SMC5_016544 *light curve folded with the beating frequency* $F = 0.05781 \, \mathrm{c\,d^{-1}}$ *produced by the frequencies* $F_1 = 1.70774 \, \mathrm{c\,d^{-1}}$ *and* $F_2 = 1.64993 \, \mathrm{c\,d^{-1}}$. Bottom: *Sum of the two sinusoidal functions. Figure courtesy of Juan Gutiérrez-Soto.*

1.3 Driving mechanism for stellar pulsations

As a star pulsates, it swells and contracts, heats and cools. For most of the interior of the star, energy is lost in each pulsation cycle, i.e., most of the volume of the star *damps* the pulsation. However, one needs to have a mechanism that *excites* the modes in the stars. This self-excitation is possible because a region in the star, usually a radial layer, gains heat during the compression part of the pulsation cycle. All other layers that lose heat on compression damp the pulsation. If this region succeeds in driving oscillation, the star functions as a heat engine, converting thermal energy into mechanical energy, thus we refer to this type of driving as a *heat-engine mechanism*.

Historically, Eddington in 1917 proposed the basic ideas behind this excitation mechanism that is able to produce unstable oscillations with large amplitudes. This theory, now known as the κ *mechanism*, was elaborated on, theoretically developed and refined by Zhevakin (1952, 1953, 1963), Cox and Whitney (1958), Baker and Kippenhahn (1962) and Cox (1980). We omit a detailed description of the working of the κ mechanism and refer to the paper of Pamyatnykh (1999) for an excellent overview. The driving force behind the κ or opacity mechanism is the behaviour of the opacity and the opacity gradient ∇_κ in the different stellar layers. The opacity κ is the absorption coefficient for radiation and depends on the abundance of different chemical elements and their distribution over their excitation and ionisation states (which is dependent on the density and the temperature).

To elaborate, the κ mechanism works when H and He (atomic species for instance) in the convective layer essentially block the radiative outflow due to their orbiting electrons absorbing photons. This causes a build up of heat energy, raising the temperature and pressure concordantly. This leads to a swelling as the radiative pressure begins to overcome the gravitational force acting inwards, upsetting the equilibrium. During this heating and expansion, the H and He can become ionised, which has the effect of reducing opacity. This allows more radiation to pass through the ionised material, which reduces the pressure of radiation (the *radiative damping*), causing the star to contract back towards its original equilibrium. A reduction in radiation pressure also cools the material, and so H and He recombine back into their atomic form at the same time, so the star is ready for the process to begin again.

For the κ mechanism to work there must be full of opacity, so major drivers of pulsation are, not at all surprisingly, H and He. Moreover, despite their abundances being so low, iron-group elements are still believed to play an important role in the opacity mechanism. The reason is that these elements have many electrons which can be excited into the many energy levels that iron has, and hence many of the outward travelling photons are absorbed in this way. It acts as a catalyst in the photon absorption process. This mechanism has been observed to function in Slow Pulsating B (SPB) stars and β Cephei as we see below, even if their abundance is so much lower than the H and He ones.

But, what selects the modes of pulsation in stars? And, what is the selection mechanism of the pulsation modes? These are complex questions for which the answer is not always known. The fundamental mode is strongly excited for many stars, as it is for musical instruments, but not for all. The position of the driving zone as well as the shape of the mode eigenfunctions determine which modes are excited, just as where a musical instrument is excited will determine which harmonics are played, and with what amplitude. Another requirement for modes to be excited by the κ mechanism concerns their periods of oscillation and is closely related to the time scales. We introduce the *dynamical time scale* as

$$\tau_{\mathrm{dyn}} \simeq \sqrt{\frac{R^3}{GM}} \simeq \sqrt{\frac{1}{G\bar{\rho}}} \tag{1.10}$$

where $\bar{\rho}$ stands for the average stellar density, G is the gravitational constant, R and M are the stellar radius and mass, respectively. It expresses the time the star needs to recover its equilibrium whenever the balance between the pressure and gravitational forces is disturbed by some dynamical process. The *thermal time scale*, also called the *Kelvin-Helmholtz time scale*, is defined as

$$\tau_{\mathrm{th}} \simeq \frac{GM^2}{RL} \tag{1.11}$$

where L is the star luminosity. This express the time a star can shine with gravitational potential energy as its only energy source, i.e., without a nuclear source. The great difference between the dynamical and thermal time scales shows that globally the heat loss during a pulsation period id very small, in other words, globally the oscillation is very nearly adiabatic. However, to investigate the excitation of the oscillations we need to work with local time scales in the driving zones that may have vastly different values than those listed above. Of particular relevance is the local thermal time scale of the driving zone, defined as

$$\tau_{\mathrm{th}} \equiv \int_r^R \frac{c_p\, T\, dm}{L} \tag{1.12}$$

where c_p is the heat capacity of the gas at constant pressure[6] (see Pamyatnykh 1999, for details).

---

[6]Note that we use m to denote the mass inside a given point in the star, in addition to the azimuthal order of a mode. With attention to context, this should not cause confusion.

With these definitions, another condition to be fulfilled in order to have driving by the κ mechanism is that the period of the oscillation must be similar to the thermal time scale in the driving zone. If the oscillation period is much longer than τ_{th}, then the driving layer will remain in thermal equilibrium and not be able to excite the mode. Typical values for τ_{th} in the driving zones of β Cephei, SPB and δ Scuti stars amount to 0.3 d, 3 d and 0.1 d, respectively.

1.4   Stellar pulsation across the H-R diagram

Oscillations can only be excited when a suitable combination of stellar luminosity, temperature, and chemical composition occurs, as we have seen in the previous Section. We can plot a standard *Hertzsprung-Russell diagram* (hereafter H-R diagram) identifying the different regions with pulsating stars. Fig. 1.7 shows this pulsation H-R diagram. An evident conclusion from this figure is that stellar oscillations occur in almost all phases of stellar evolution. However, there exists a particular region in the H-R diagram in which the density of pulsating stars is more outspoken than elsewhere. This region is situated between the two vertical dashed lines and is called the *classical instability strip*. The Cepheids, RR Lyrae stars, δ Scuti stars, rapidly oscillating Ap stars, γ Doradus stars and DAV white dwarfs are all situated in this strip. On the other hand, cool red giants, such as the Mira stars and irregular variables are situated along the red cool side of the classical instability strip. Concise overviews of stellar variability are available in Gautschy and Saio (1995, 1996) and Eyer and Mowlavi (2008).

The κ mechanism explains the stellar pulsations observed in these different types of stars. As the first developers of this theory already demonstrated, the opacity mechanism is acting on the He II ionisation zone responsible for the pulsations of Cepheids. This opacity bump causes as well the pulsations in δ Scuti stars, RR Lyrae stars and DBV white dwarfs. The H I-bump, on the other hand, leads to the pulsations in Mira variables and DAV white dwarfs. The H I-bump or He II-bump, however, does not explain the observed variability in the massive B-stars such as SPB stars and β Cephei stars, as the thermal time scales of these regions are too short in comparison to the pulsational periods (e.g. Christy 1966).
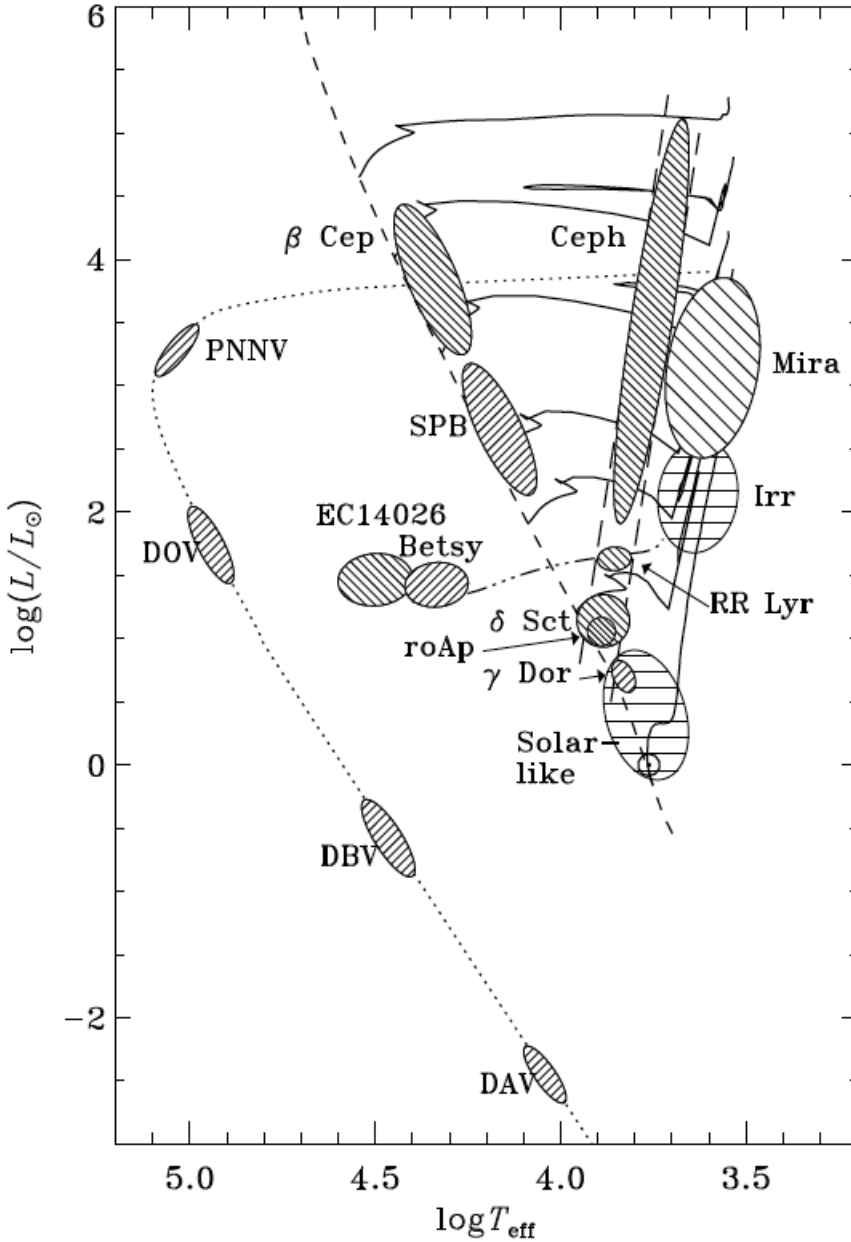
Figure 1.7: *A pulsation H-R diagram showing many classes of pulsating stars for which asteroseismology is possible. Figure courtesy of Jørgen Christensen-Dalsgaard.*

A suitable thermal time scale is found at the position of the metal[7] *Z-bump* (term for the opacity enhancement due to the iron-group elements) located at temperatures around $200\,000$ K. It took several decades to find convincing theoretical evidence for the Z-bump as driving layer in the B-type stars, due to the fact that the opacity maxim, calculated from the opacity tables of the heavy elements, were not high enough to produce a pulsationally unstable region. A breakthrough came in the early nineties with the new results provided by Rogers and Iglesias (1992) and Iglesias and Rogers (1996) in the Opacity Project At Livermore (OPAL[8]) and Seaton (1996) in the Opacity Project (OP[9]). Based on the new opacity values, Dziembowski and Pamyatnykh (1993) and Gautschy and Saio (1993) succeeded in explaining the p-mode and g-mode pulsations of the B-type stars in terms of the κ mechanism acting in the partial ionisation zones of the heavy elements of the iron group.

1.4.1 Description of β Cephei and SPB stars

A significant fraction of main-sequence B-type stars are known to be variable. The whole main-sequence in the B spectral domain is populated by two well characterised classes of pulsators: the β Cephei stars and the Slowly Pulsating B stars. β Cephei stars do pulsate in low-order p-modes and g-modes with periods similar to the fundamental radial mode while SPB stars are high-radial order g-mode pulsators with periods longer than the fundamental radial one. Both types of stars pulsate due to the κ mechanism activated by the metal opacity bump (Cox et al. 1992). The κ mechanism in β Cephei and SPB stars has an important dependence on the abundance of iron-group elements, and hence the respective instability strips will depend on the metallicity of the stellar environment. In Fig. 1.8 we show the efficiency of the κ mechanism in representative models of β Cephei and SPB variables. These stars are located in the middle of corresponding instability domains in the H-R diagram. The masses of the models are 12 and $4\,M_{\odot}$, and effective temperatures are $23\,800$ K and $12\,450$ K, respectively.

---

[7]In astrophysics, the abundance of elements heavier than He (collectively known as "metals") is referred as the *metallicity* and labelled Z.

[8]http://opalopacity.llnl.gov/opal.html.

[9]http://cdsweb.u-strasbg.fr/topbase/op.html.
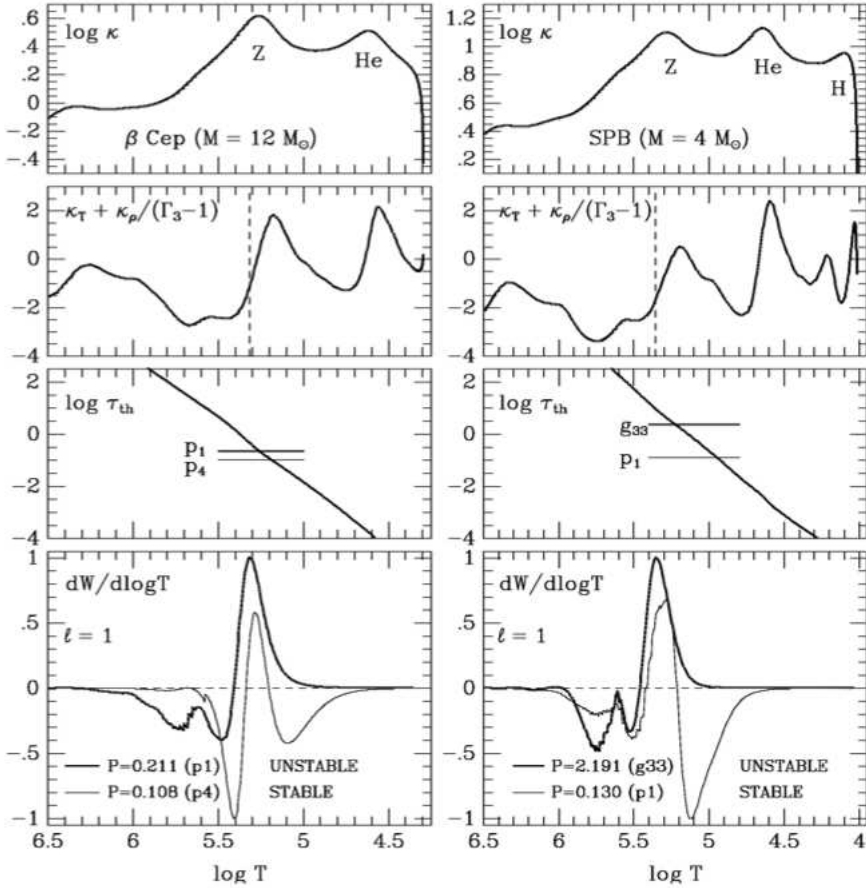
Figure 1.8: *Opacity bump regions* (top panels). *Opacity* (κ), *opacity derivative* ($\kappa_T + \kappa_\rho/(\Gamma_3-1)$), *thermal time-scale* (τ_{th}) *in days, and differential work integral* ($dW/d\log T$, *arbitrary units, positive driving zones), for selected pulsation modes* ($\ell = 1$), *plotted versus temperature for two representative models of* β *Cephei* (left column) *and SPB* (right column) *variables. All models have initial chemical composition* $X = 0.70$ *and* $Z = 0.02$. *Dashed vertical lines mark the position of the maximum driving for the unstable modes shown in the lower panels. Horizontal lines in the* τ_{th} *diagrams correspond to the periods of selected modes. Figure taken from* Pamyatnykh (1999).
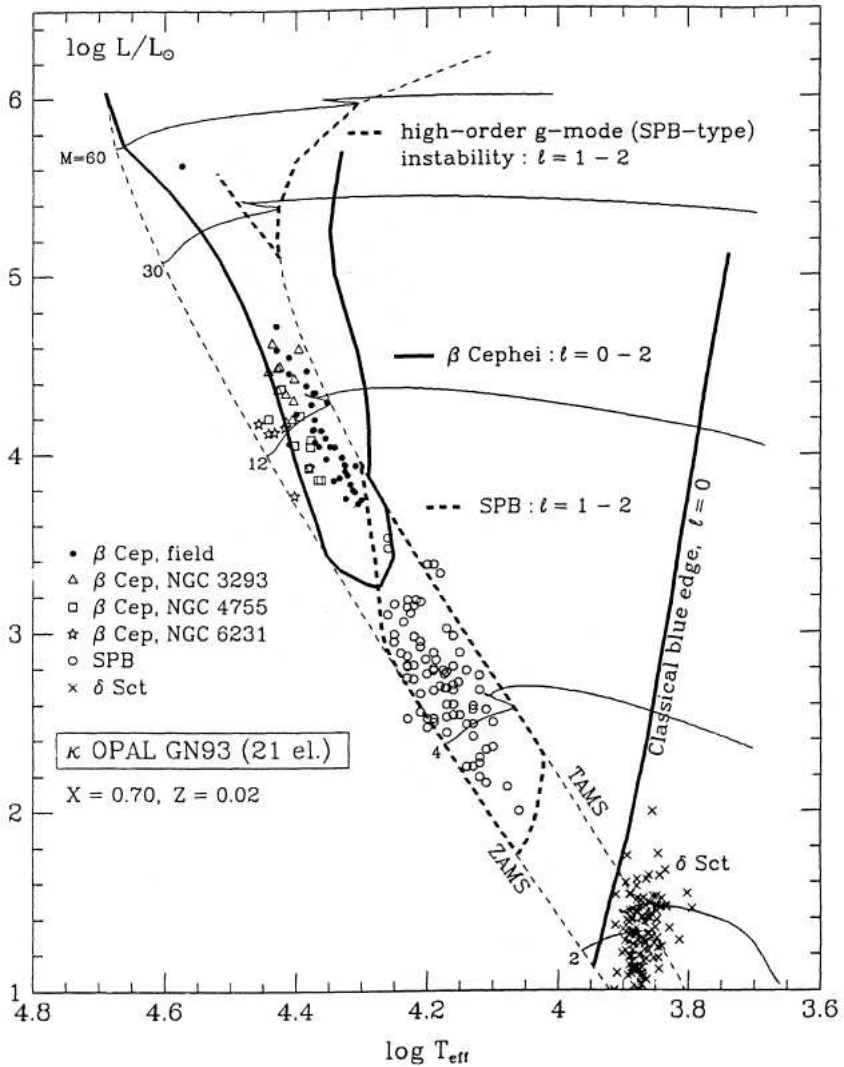
Figure 1.9: *Instability domains for modes with $\ell \leq 2$ of B-type stars along the upper main sequence, computed using the* OPAL *opacities (Iglesias and Rogers 1996). In the calculation of the stellar models, rotation and convective overshooting are not taken into account and initial abundances of $X = 0.70$ and $Z = 0.02$ are adopted. A few evolutionary tracks for the indicated values of $M/M_\odot$ are shown. As described in the picture labels, solid line depicts the β Cephei instability strip and dashed line depicts the SPB instability strip. Figure taken from Pamyatnykh (1999).*

Fig. 1.9 shows the position of the β Cephei and SPB stars in the upper main sequence that exhibit unstable modes with $\ell \leq 2$, calculated by Pamyatnykh (1999) using the revised tables of OPAL opacities from 1996 (Iglesias and Rogers 1996). Such a theoretically derived region is called the theoretical instability strip for β Cephei and SPB stars. The location of the strip is sensitive to several different parameters, such as metallicity, rotation and the value of the convective overshooting distance. The theoretical instability strips do not completely correspond to the observed ones. A comparison between observations and theory is therefore important to constrain the stellar parameters.

In the following we will present a brief description of these two pulsating B stars. An excellent overview over β Cephei and Slowly Pulsating B stars for which Geneva photometry is available is given by de Cat (2002) in the form of an online catalogue[10].

β Cephei stars

The variability of the prototype of this class of variable stars, β Cephei, was discovered by Frost (1902). The β Cephei variables are early-B stars with spectral types B0.5 to B2, luminosity class II-III to V. The β Cephei stars exhibit coherent short-period light and radial velocity variations. They are main-sequence or slightly evolved stars in the core H burning stage. Today, about 100 bona fide β Cephei stars are known, but numerous new candidate members have been found from large surveys in the Magellanic Clouds as well as in our own Galaxy (Pigulski 2005; Kołaczkowski et al. 2004, 2005, 2006; Narwid et al. 2006; Sarro et al. 2009). Assuming that all these faint variable stars are indeed β Cephei this more than doubles the number of class members to over 200.

Pulsation periods of β Cephei variables range from about 3 to 8 hours and are associated with low-order p-modes and/or g-modes. As mentioned at the beginning of this Section, their driving mechanism was not understood for a long time. In contrast to several other variable classes of stars (e.g. δ Scuti stars, RR Lyrae stars), the region of ionisation of He I can not destabilise β Cephei stars. It

---

[10]See http://www.ster.kuleuven.ac.be/~peter/Bstars/.

was not until 1993, when new atomic data became available, that it became clear that the classical κ mechanism acting on iron-peak elements deep in the envelope of the star causes the pulsations in these stars (see Dziembowski and Pamyatnykh 1993; Gautschy and Saio 1993).

Smith (1980) argued that the main pulsation modes of β Cephei stars are radial. The observed main modes are indeed usually radial, but non-radial pulsations have also been detected. β Crucis is a well-known β Cephei star for which only non-radial modes are observed (so far) (Aerts et al. 1998). A large fraction of the β Cephei stars are multiperiodic, which causes beating phenomenon with periods of weeks to months. An overview of the properties of the β Cephei class was provided by Stankov and Handler (2005).

SPB stars

The Slowly Pulsating B (SPB) stars were first introduced by Waelkens (1991) as a distinct group of variables B2 to B9 stars, with masses ranging from 2 to 7 $M_\odot$ showing multiperiodic light variations. Typical periods are 0.5 to 3 days, thus too long and unstable to be associated with β Cephei variability. The HIPPARCOS mission greatly increased the number of known SPB stars: only 12 SPBs were known before HIPPARCOS while 72 new SPB candidates were discovered with this satellite (Waelkens et al. 1998). This is not surprising, since oscillation periods of the order of 1 day are hard to detect from the ground (see Chapter 3 for details in this matter). Currently there are about 40 bona fide SPB stars known in the Galaxy, and more than 100 suspected.

The SPBs are situated in the main sequence, just below the β Cephei stars in the H-R diagram, as shown in Fig. 1.9. Like for the β Cephei stars, the κ mechanism has to be invoked to explain the instabilities (Dziembowski et al. 1993). The light and line-profile variations are interpreted in terms of non-radial pulsations of high-order g-modes (Dziembowski and Pamyatnykh 1993). Most of the SPBs are multiperiodic, which causes beating phenomenon with periods of months to years. A detailed study of SPBs therefore needs observations with a sufficiently long time-base.

The SPBs are considered to be slow rotators[11], with $V \sin i \leq 100 \, \mathrm{km \, s^{-1}}$, but the extensive list of candidate SPBs contains rapidly rotating stars. A spectroscopic follow-up campaign is needed to exclude binarity and/or rotational modulation as causes of the observed variations.

1.5   Asteroseismology from the Space

Asteroseismology is being revolutionised in the present days. The amount of data coming from our ground-based telescopes is being strengthened using the new advantages of the space missions. With little telescopes orbiting the Earth we can improve the asteroseismic data. This is possible because we can obtain continuous observations of the target stars. The absence of gaps in the light-curves allow us to obtain accurate calculations of the oscillation frequencies and hence, a better modelling for the stellar pulsations. With the new observational opportunities provided by the space missions in asteroseismology, which will complement the coverage of the H-R Diagram with ground based observations, we may expect to be able to address some of the unsolved problems in the modelling of stellar structure and evolution.

The first asteroseismic mission was the MOST[12] (Microvariability and Oscillations of STars, see Walker et al. 2003) photometric satellite, launched on June 2003. This mission has undertaken more than 64 primary campaigns and obtained observations of more than 850 secondary stars of which near 180 are variable. More than half of these variable stars pulsate, with the majority being B-type stars. MOST has detected a large number of SPB stars with variations that are characteristic of g-modes (Walker 2008).

The CoRoT[13] (Convection, Rotation and planetary Transits, described in detail in Chapter 8) space mission was launched on December 2006. As docu-

---

[11] If the equatorial rotation is given by V and the inclination of the polar axis relative to the line of sight from the Earth is given by i. Then, the radial velocity as viewed from Earth is given by $V \sin i$.

[12] http://www.astro.ubc.ca/MOST/.

[13] http://corot.oamp.fr/ and http://smsc.cnes.fr/COROT/.

mented in a recently published special Volume 506 of *Astronomy & Astrophysics*, the initial results from the CoRoT mission are very promising in asteroseismic matters. In Section 8.7 we describe a review on the recent results of the CoRoT mission.

The KEPLER[14] mission is the most recent one. It was launched on 7th of March 2009 with the primary science objective of finding Earth-like planets. KEPLER will also provide precise photometry for a large number of stars. At the time this Ph.D. thesis is been written, the very early data from the KEPLER mission are being analysed, through an intense and coordinated effort in the KEPLER Asteroseismic Science Consortium[15] (KASC), with a view towards publication in during 2010. Given the continuing operations of MOST and CoRoT and the very extensive data to be obtained with KEPLER it is clear that coming years will see a huge effort in the analysis of asteroseismic data, with a corresponding increase in our information on and, one may hope, understanding of stellar properties.

On a somewhat longer timescale there is hope that the PLATO[16] mission (PLAnetary Transits and Oscillations, see Catala and the PLATO consortium 2008) will provide detailed asteroseismic data on tens of thousands of stars.

Despite the impressive success of space-based asteroseismic investigations, there is still a need for ground-based observations. As found early in observations of the Sun (Harvey 1988) the intrinsic stellar noise is much higher, relative to the oscillations, in photometric observations than in observations of Doppler velocity. Velocity observations can be carried out from the ground, the main limiting factor being the access to the required instrumentation, at several sites to ensure continuous data and over a sufficient length of time. This motivates the establishment of dedicated facilities. An example is the SONG[17] (Stellar Observations Network Group) project (Grundahl et al. 2009), aiming to establish a network of eight observatories, with a suitable world-wide distribution, equipped with 1-m telescopes and high-resolution spectrographs to carry out asteroseismic Doppler-velocity observations. The SONG network is expected to be operational

---

[14]http://kepler.arc.nasa.gov/.
[15]http://astro.phys.au.dk/KASC/.
[16]http://www.oact.inaf.it/plato/PPLC/Home.html.
[17]http://astro.phys.au.dk/SONG/.

in 2011. Another promising proposal is to set up the SIAMOIS (Sismomètre
Interférentiel A Mesurer les Oscillations des Intérieurs Stellaires - Seismic Inter-
ferometer to Measure Oscillations in the Interior of Stars, see Mosser et al. 2008)
facility for Doppler velocity observations on Dome C in Antarctica.

Now, in 2010, we are entering in a new era of asteroseismology. Major diffi-
culties in the descriptions of stellar interiors that arose in the second half of the
20th Century may now be in part addressed and solved by asteroseismology with
unprecedented precision, in part due to the facilities of the space-based missions.
As it has been so well put by Eyer and Mowlavi (2008), *now is the time to be an
asteroseismologist.*

Baby, you can drive my car,
Yes, I'm gonna be a star,
Baby, you can drive my car,
And maybe I'll love you.

Paul McCartney

2

Be stars

On 23$^{\text{rd}}$ of August 1866, Padre Angelo Secchi, director of the observatory of the Collegio Romano, wrote a letter to the editor of the *Astronomische Nachrichten*, reporting "une particularité curieuse de l'etoile γ Cassiopée". Instead of Balmer line absorption as in Sirius or Vega, it would have "une ligne lumineuse très-belle et bien plus brillante que tout le reste du spectre" (Secchi 1866). This was the first emission-line star detected and the first report of a Be star.

More than 120 years later, Collins (1987) gave the definition for a Be star as "a non-supergiant B star whose spectrum has or had at some time, one or more Balmer lines[1] in emission", which is still in use today as working definition (see

---

[1]The Balmer series or Balmer lines is the designation of one of a set of six different named series describing the spectral line emissions of H.

Jaschek et al. 1981, for the first definition of this sort). In Fig. 2.1 we show an artist conception of a Be star. With the understanding of the processes of emission line formation in the early 20th century it became clear that these lines must come from the circumstellar environment, not from the star itself. Nowadays, all the observational characteristics are explained with a gaseous disk that is formed of material ejected from the star. Be stars are generally accepted to rotate rapidly, what has been impressively confirmed by interferometric measurements of the rotational distortion of Achernar (α Eridani, Domiciano de Souza et al. 2003). However, rotation alone is probably not sufficient to form the disk, but an additional ejection mechanism is required, such as a magnetic field or non-radial stellar pulsation. The transient nature of the Be phenomenon is most likely connected to the nature of that secondary process, but the details are currently still being discussed. A review on the research of Be stars from the early work of Merrill and Struve can be found in Slettebak (1988). For a recent review on classical Be stars see Porter and Rivinius (2003).

The wide interest in this *Be phenomenon* is illustrated by the number of meetings since the last IAU Colloquium 175 dedicated to *The Be Phenomenon in Early-type Stars* (Smith et al. 2000). Up to now, there have been numerous other meetings with significant contributions from Be star researchers. In this Chapter we bring a review on Be star properties and their relation with non-radial pulsations.

2.1 Be stars and their properties

More precisely, a Be star is defined as a main sequence star or slightly evolved non-supergiant, late-O, B or early-A type which show or have shown at least once emission lines of H in its spectrum, mainly Hα, due to the presence of a decretion circumstellar disk. The designation is combined by the spectral type, commonly B, and the lowercase *e* denoting emission in the spectral classification system. They often rotate fast and exhibit light and line-profile variations at different timescales. Be stars also often display either enhancements (*outbursts*) or fadings of their brightness, depending on whether they are seen rather pole-

on or equator-on. The study of Be stars during these phases, simultaneously in spectroscopy and photometry, is very important as it could provide new clues to the Be phenomenon. In particular, one could study the link between mass-loss episodes and the pulsational properties of the star. Outbursts are frequent in Galactic and Magellanic Be stars, especially in the earlier ones (Hubert et al. 2000; Mennickent et al. 2002). However, simultaneous observations of an outburst in spectroscopy and photometry are fairly rare.
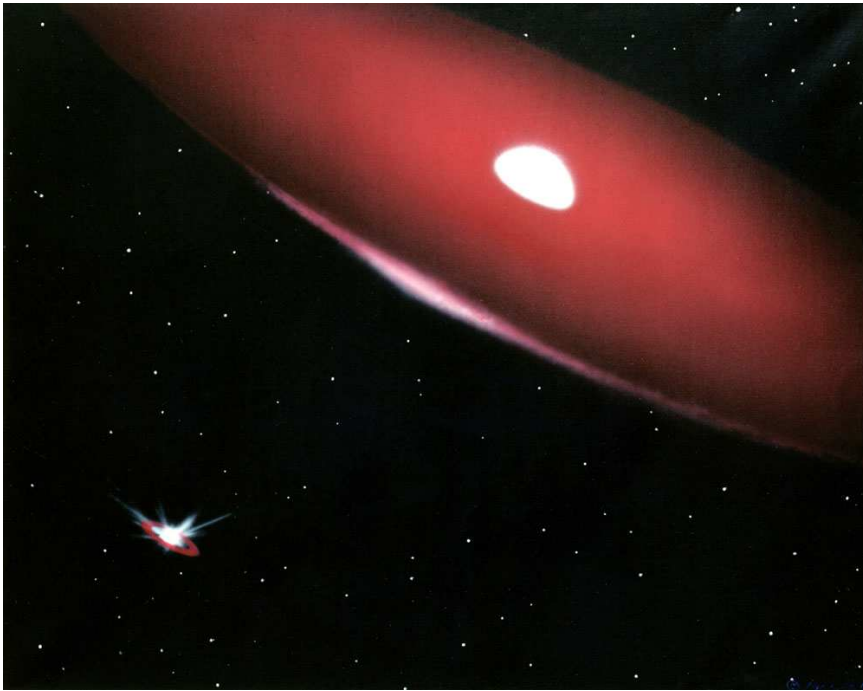
Figure 2.1: *The Be star ϕ Per, illustrated below by Bill Pounds, is a classical Be star with an evolved, stripped down, He star companion. Figure courtesy of Bill Pounds.*

2.1.1 Evolutionary status

Their observational definition places Be stars on, or just off, the main sequence. Are Be stars "born" or do they evolve from B to Be stars? The evolutionary status of classical Be stars is a frequently raised and yet unsolved question. The main issue is to determine whether the Be phenomenon appears at a given stage in the evolutionary track of every B star, or if it originates in the conditions of formation of some stars, which include fast rotation among other facts. Several modern studies of the Be star population of young open clusters point towards the presence of an evolutionary enhancement of the Be phenomenon in the second half of the B stars main sequence lifetime (see Fabregat and Torrejón 2000; Keller et al. 2000, 2001; Fabregat 2003, for example).

2.1.2 Be stars and metallicity

About 20% of all B stars are Be stars in our Galaxy, however this fraction depends on the metallicity (Martayan et al. 2006a, 2007b). Therefore, in other environments with lower metallicity, the fraction of Be stars over B stars can be much higher (Maeder et al. 1999). About 50% of the B stars in the SMC cluster NGC 330 were found to be Be stars by Feast (1972). This high fraction, compared to 10 to 20% in the Milky Way (MW), was confirmed by subsequent studies done by Grebel and Richtler (1992), Grebel et al. (1996), Mazzali et al. (1996), Keller et al. (1999) and more recently, by (Martayan et al. 2006a, 2007b). A pronounced difference between the Be star content in the Magellanic Cloud clusters and in the MW was found by Grebel et al. (1993) and also obtained by Maeder et al. (1999). Fig. 2.2 shows the relation between the fraction Be/(B+Be) and the local average metallicity. The trend is quite clear for the various magnitude intervals considered. For the sample of the locations of the SMC, LMC, Galactic interior and Galactic exterior, there seems to be a clear decrease of the fraction of the relative number of Be stars with the local average initial metallicity. Preliminary results by Royer et al. (2004) could confirm this metallicity effect, although they use limited stellar samples.
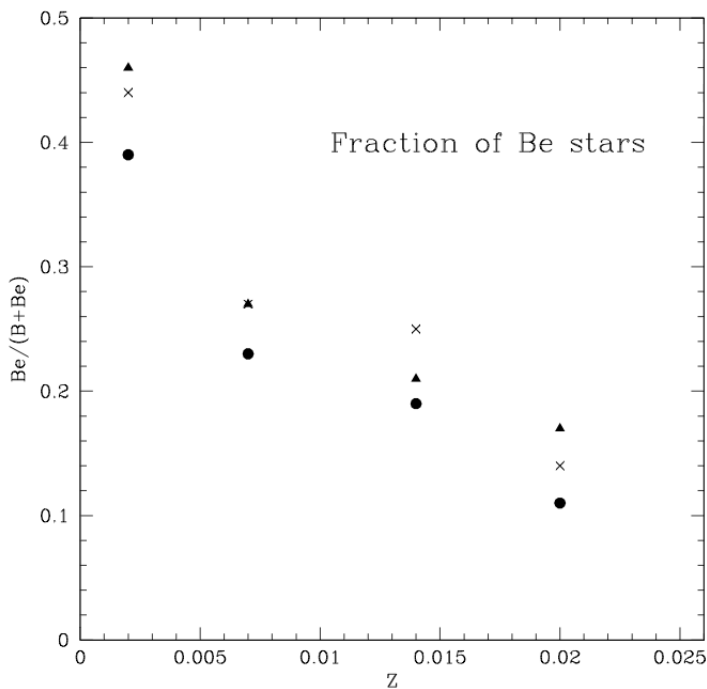
Figure 2.2: *Relation between the number ratio* Be/(B+Be) *and the local metallicity for four groups of clusters studied by Maeder et al. (1999) (SMC, LMC, Galactic interior and Galactic exterior). To test the validity of the results, the number counts were made in different magnitude intervals, the dots refer to counts made in the magnitude interval* $V = -5, -1.4$ mag, *the crosses to the interval* $V = -5, -2$ mag *and the triangles to the interval* $V = -4, -2$ mag. *Figure taken from Maeder et al. (1999).*

2.1.3 Rapid rotation

The Be phenomenon is closely related to fast rotation. An important feature of Be stars is that they are known to be fast rotators (typically $V \sin i \sim 250 \, \text{km s}^{-1}$). Slettebak (1982) published a large set of line widths along with spectral types for Be stars. It is commonly assumed that the observed photospheric line broadening measured in velocity units is the real $V \sin i$ of the star. However, the study of Collins and Truax (1995) illustrates the effects of high rotation on observational derivation of $V \sin i$: they find that stars with rotation values above $\sim 80\%$ of

critical speeds are likely to produce underestimates of the true rotation speed of the star (also see Stoeckley 1968). This is partly due to the gravitational darkening caused by rotation. With the equatorial belts less prominent because of this darkening, the largest component in the photospheric line broadening arises from an intermediate latitude, thereby producing a line width narrower than that from a uniformly bright stellar disk. Hence, for high rotation, this yields an underestimate of the $V \sin i$ values of the star. Is thus necessary to apply corrections to the observed velocity rates in high rotating stars, in particular in Be stars. Frémat et al. (2005) developed a calculation code to account for the effects carried by fast rotation on observed spectra of early-type B stars, obtaining that Be stars are rotating at an average value of angular velocity to breakup velocity (Ω/Ω_c) of 88% in our Galaxy. Moreover, the rapid rotation of Be stars changes their position in the H-R diagram, making difficult to see how they fit into the stellar evolutionary sequence, as we will see in detail in Chapter 5 (Figs. 5.4 and 5.5). Depending on the inclination, the combination of oblateness and gravity darkening can displace a B star from the *zero-age main sequence* (ZAMS) into the sub-giant and giant regions, causing it to appear more evolved than it really is.

2.1.4   Circumstellar envelope

It is generally accepted that the envelope of Be stars is flattened by their high rotational velocities. Interferometry observations provided direct evidence for the presence of such a disk (e.g. Quirrenbach et al. 1997; Vakili et al. 1998; Stee 2000, see Fig. 2.3). However, as mentioned above, the rotation rates of Be stars are always lower than the critical velocities at which the centrifugal force balances gravitation at the equator. Thus, the centrifugal force by itself is inadequate to explain the formation of a disk around these stars. Moreover, most disks around Be stars seem to be Keplerian rather than co-rotating (Meilland et al. 2006). It is generally agreed that the circumstellar disk is formed by episodic mass ejections. However, different mechanisms are proposed (see Section 2.2).
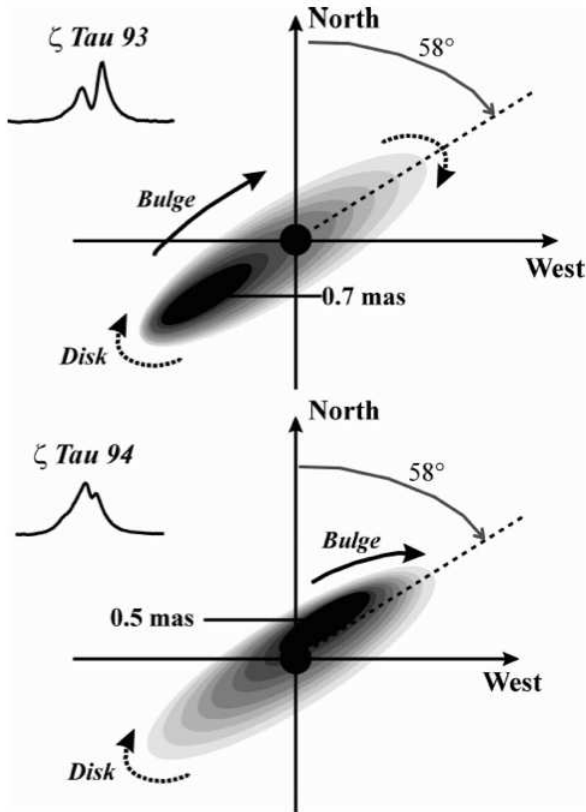
Figure 2.3: *Interferometric detection of the disk of the Be star ζ Tau in 1993 and 1994, providing direct evidence that the envelope is flattened. Figure taken from Vakili et al. (1998).*

As mentioned at the beginning of this Section, the emission lines of Hα in the spectrum of Be stars come from the circumstellar disk. Line emission from other atomic ions might be present as well, in particular in red He I lines or Fe II lines, but is typically much weaker. Other observational characteristics include optical linear polarisation and often infrared radiation that is much stronger than in ordinary B-type stars, called infrared excess. The infrared excess and the polarisation result from the scattering of stellar light in the disk, while the line emission is formed by re-processing stellar ultraviolet light in the gaseous disc. As the Be nature is transient, Be stars might exhibit a normal B-type spectrum

at times, and hitherto normal B stars may become Be stars. In Fig. 2.4 we show the Hα spectra of the Be star 60 Cyg star taken at different moments compared to a synthetic spectrum for a star of similar spectral type.
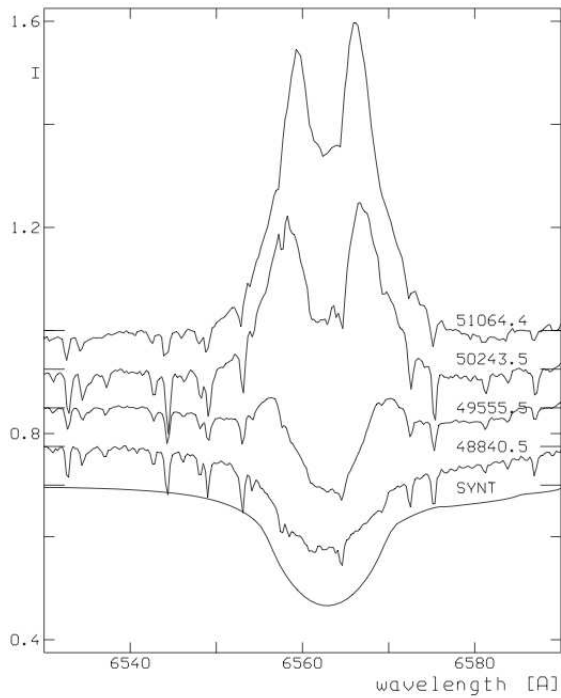
Figure 2.4: *Examples of the Hα profile of the Be star* 60 Cyg *in the non-emission, intermediate and emission phase. The bottom spectrum is a synthetic profile of this star. The upper spectra were obtained at different times over 6-year interval, between* HJD 2 448 840.5 *and* 2 451 064.4*. Figure taken from* Koubský et al. (2000)*.*

2.1.5 Photometric variability

Be stars show two different types of photometric variability, with different origin and time scale:

Short-term variability: It ranges from 0.1 to $2 - 3.5$ days. It is produced by rotation, pulsations, magnetic fields and wind. In the following, we make longer discussion about the origin of this variability. To establish a criterion, we consider as short-period variations those with frequencies higher than $0.3 \, \mathrm{c \, d^{-1}}$. In early Be stars short periodic light and *line profile variability*[2] are nearly omnipresent and superimposed to the longer one. In Fig. 2.5 we depict the line profile variability of the Mg II for the Be star ω CMa. Hubert and Floquet (1998), based on HIPPARCOS[3] observations, found that this short-term is present in 86% of early Be stars, in 40% of intermediate sub-spectral range types (B4e-B5e) and in only 18% of late Be stars. This fact could be due to the variability detection level of current instrumentation, since the amplitude of pulsations in late sub-types is expected to be lower from theory.

Long-term variability: It is produced by changes in the structure, size and density of the circumstellar envelope. Variations are irregular and sometimes quasi-periodic, with time scales of weeks or months to decades. Some stars present outburst episodes or high and low states in its light curves with a total duration of weeks or months.

This timescales usually appears together and often superimposed in Be stars. In many cases Be stars show multiple periods due to multiple pulsation modes present in the star. Further detailed studies of well-observed objects led to a complete and consistent multi-mode modelling of the observed variations (Rivinius et al. 2001; Maintz et al. 2003; Neiner et al. 2005a).

---

[2]As depicted in Fig. 2.4, a *line profile* is an isolated spectral line in the spectrum of a star. Whenever the shape of such a line profile varies in time, one speaks of *line profile variations*. The line profile variations are either caused by intrinsic surface velocity changes, or a non-uniform temperature, gravity or chemical element distribution across stellar surface or a combination thereof.

[3]HIPPARCOS Project: http://www.rssd.esa.int/index.php?project=HIPPARCOS.
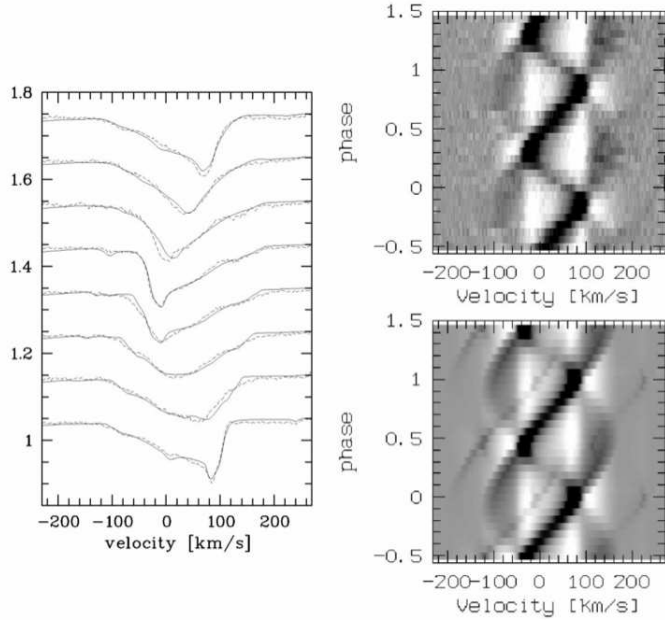
Figure 2.5: *Observed short-term periodic line profile variability of Mg* II *4 481 in ω* CMa, *modelled as non-radial pulsations in the absolute profiles* (left panel) *and residual gray-scale representation* (right panel, with the top panel as the data and the lower panel as the model). *Figure taken from* Maintz et al. (2003).

2.2 The Be phenomenon

Since the discovery of Be stars over 140 years ago (Secchi 1866), the ejections of stellar material into a circumstellar disk, called the Be phenomenon, have remained puzzle. Since rotation is not enough to eject this matter, another mechanism is needed to provide additional angular momentum. Several explanations have been proposed:

- Be stars could be binaries and the ejections triggered by tidal effects. A study from Fabregat and Torrejón (2000) conclude that, despite the consistency, the model of the close binary evolution does not provide a satisfactory explanation to the Be star phenomenon. Moreover, it has to be considered

that this model is ad hoc, because it only justifies the formation of a rapidly rotating B star, but does not explain how the Be phenomenon arises from it. It is important to mention that a study from Van Bever and Vanbeveren (1997) reveals that only a minority of Be stars (less than 20% and possibly as low as 5%) can be due to close binary evolution.

- A magnetic field could force matter to follow magnetic field lines. In the case of a simple dipole for example, matter would leave the star from the magnetic poles and follow the field lines towards the magnetic equator. The particles coming from both hemispheres would then collide at the magnetic equator where they could stay confined if the magnetic field is strong enough. A possible detection of a magnetic field has been announced for the Be star ω Ori (Neiner et al. 2003), although subsequent attempts to confirm this detection with new generation instrumentation have failed. Therefore, even through this mechanism could explain the presence of a co-rotating disk for some Be stars, this currently does not seem to be the most common way of forming Be stars.

- The beating of pulsation modes in Be stars could provide some angular momentum and, in combination with the fast rotation, allow to reach the critical limit at which ejections can occur. Many Be stars are indeed known to pulsate (e.g. Walker et al. 2005a,b; Gutiérrez-Soto et al. 2007b). Its important to mention the work of Rivinius et al. (1998a,b, 2001) who showed, thanks to a spectroscopic study, that the beating of pulsation modes in the Be star μ Cen seems to coincide with the ejections of matter from that star. This result, however, could not be obtained for other Be stars from the ground. The idea to explain the Be phenomenon is that a constructive interference wave due to several close pulsation modes can produce a pulsation with sufficient amplitude to ejects mass to the exterior of the star and create the flattened equatorial disk around the Be star where the Hα emission comes from, in addition, the disk seems to be mainly replenished during transient mass loss episodes. Another important result comes from the analysis of the space-based mission CoRoT (Auvergne et al. 2009, see Chapter 8 for more details). Thanks to the high-precision photometric data, Huat et al. (2009a) shows that the data of HD 49 330 provides a correlation similar to the one proposed by Rivinius et al. (1998b).

Nowadays, non-radial pulsations combined to the near break-up rotational velocity have been proposed as mechanisms that could give rise to the additional amount of momentum needed to cause mass ejection. Up to now, this statement has been confirmed only for the Be star μ Cen, for which Rivinius et al. (2001) found that the beating produced by the non-radial pulsation modes, with low identical degree ℓ and identical azimuthal order m, determine the times of mass loss events. The question is: Is this fact valid for all Be stars?

2.3 Pulsating Be stars

As mentioned above in the text, Be stars are variable stars with different time scales and broad range of amplitudes. Periods ranging from 0.3 to 2 days have been measured in most of the studied early Be stars but in only 30% of later ones (Hubert and Floquet 1998). The first claim of non-radial oscillations in Be stars dates back to 1982, when Baade (1982a,b) discovered complex line profile variations for the star ω CMa. Baade (1982a) attributed the short periodic line profile variability to non-radial pulsations. However, Balona (1990, 1995) argued on statistical grounds that the periods were better explained by stellar rotation and attributed the line profile variability to stellar spots, and later, to co-rotating clouds. Finally, the proponents of both pulsation and starspot hypotheses above agreed that the detection of photospheric multiperiodicity would decide the issue in favour of non-radial pulsations (Baade and Balona 1994).

In this Ph.D. thesis we assume that the periodic variations detected in the studied B and Be stars are due to pulsations. As mentioned above, it is not easy to discriminate between pulsation and rotational modulation, specially for stars showing only one period in their variations. The keys that support our statement are:

- The stars detected variables are located in the instability strips for β Cephei or SPB stars or close to them. In the case of Be stars, early-type Be stars are located in the H-R diagram at the lower border of the instability domain of the β Cephei stars, while mid- and late-type Be stars are mixed with SPB

stars. It is thus not surprise that the κ mechanism ignites p- and/or g-mode pulsations in Be stars like in these two types of pulsators: short-period p-modes are expected in early Be stars and long-period g-modes in mid- to late-type Be stars. As a matter of fact, theoretical calculations made by Balona and Dziembowski (1999) revealed the existence of unstable p and g non-radial pulsation high-degree modes in the B temperature range that are compatible with some observed periods. For example, Balona and Kambe (1999) and Jankov et al. (2000) for ζ Oph, Janot-Pacheco et al. (1999) for η Cen, Hubert et al. (1997) for 48 Per or Floquet et al. (1996) for 48 Lib.

- Variability due to rotational modulation needs the existence of inhomogeneities in the the photosphere, and the only physical mechanism proposed to produce this effect is the presence of magnetic fields. However, the external layers of Be stars are completely radiative and, as explained above, the existence of magnetic fields in Be stars should be rather rare and weak. A recent study carried by Silvester et al. (2009) with the ESPaDOnS and NARVAL high-resolution spectropolarimeters shows no evidence of magnetic field in the two Be stars HD 148 184 (χ Oph) and HD 181 615 (υ Sgr). In fact, no magnetic field has been consistently detected so far in any Be star, despite very accurate recent searches with state of the art techniques and instrumentation performed in several tens of Be stars (Wade 2010).

In spite of taken into account that only observations cannot allow us to distinguish between pulsation or rotational modulation, it is clear that pulsation seems to be the more convincing argument to explain periodic short-term variations in the light curves of B-type stars. Moreover, the existence of pulsations in these stars is commonly supported by theoretical models. Recently, short-term variations observed in different Be stars are being modelled as non-radial pulsations, as we will show in the following.

The MOST satellite as well as detect multiple periods in Be stars has revealed a rich spectrum of frequencies associated with radial and non-radial pulsations in several Be stars. For example, ζ Oph (O9.5Ve, Walker et al. 2005b, associated with p-modes), HD 163 868 (B5Ve, Walker et al. 2005a, associated with g- and r-modes) and the late Be star β CMi (B8Ve, Saio et al. 2007, associated with

g-modes). In Fig. 2.6 we report the frequency model spectrum for the Be star HD 163 868.

More recently, Rivinius et al. (2003) report an extensive summary of the detection of short period line profile variations due to oscillations in hot Be stars. They monitored 27 early-type Be stars spectroscopically during six years and found 25 of them to be line profile variables at some level. For several of their targets the variability was interpreted in terms of non-radial oscillations with $\ell = m = +2$. Almost all stars in the sample also show traces of outburst-like variability rather than a steady star-to-disk mass transfer. The authors interpret the disk formation in terms of multi-mode beating in combination with fast rotation.

The results coming from the space-based mission CoRoT, launched on December 2006, are confirming p-mode and g-mode non-radial pulsations in Be stars from the MW. As an example we cite the cases of the late Be star HD 50 209 (B8IVe, Diago et al. 2009a), HD 49 330 (B0.5IVe, Huat et al. 2009a; Floquet et al. 2009), HD 175 869 (B8IIIe, Gutiérrez-Soto et al. 2009b) and HD 181 231 (B5IVe, Neiner et al. 2009a). In addition, for the Be star HD 49 330, Floquet et al. (2009), show that the detected frequencies are attributed to high degree p-modes with $\ell = 4$ and 6, respectively, using relations for moderate rotators, in lack of models appropriate for fast rotating stars. Ejection of matter has been observed in the emission quantities at the epoch of minimum flux observed in the CoRoT light curve for this star, just before the steep increase of brightness which characterises the outburst itself as commonly observed in Be stars. The ejection coincides with the constructive beating of the two main frequencies observed during the outburst phase of the CoRoT light curve as shown in Huat et al. (2009a).

These discoveries suggest that the oscillations detected in Be star show multitude of different behaviour, which is in full accordance with those of β Cephei stars and SPB stars. This fact supports the argument stated above for consider the detected B and Be star short-period variables as non-radial pulsators showing p- and/or g-modes. In the near future we will be able to test whether the beating of pulsation modes provides the additional angular momentum needed to eject material from the star and create a circumstellar disk. If the pulsations are indeed the trigger of ejections, the long-lasting mystery of the Be phenomenon

will finally be solved. A brief review on the pulsations of Be stars can be found in Neiner and Hubert (2009).
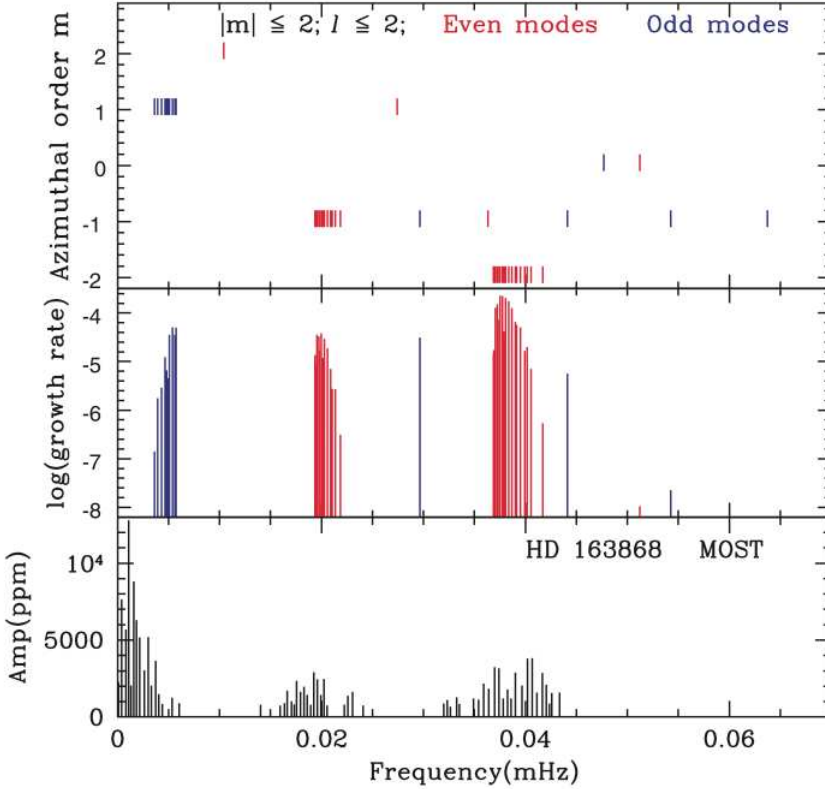
Figure 2.6: Top and middle panels: *Frequencies and growth rates of excited pulsations in a 6 $M_\odot$ main-sequence model with a rotational frequency of 0.016 MHz. Only low latitudinal degree ($\ell \leq 2$) and low azimuthal order ($|m| \leq 2$) modes are shown. Red and blue lines show even and odd modes, respectively. For even (odd) modes, pulsational perturbations are symmetric (antisymmetric) to the equator. Positive (negative) azimuthal orders, m, refer to retrograde (pro-grade) modes in the co-rotating frame of the star. Odd modes at ~ 0.005 MHz are high-order r-modes, while most of the others are high-order g-modes.* Bottom panel: HD 163 868 *amplitude spectrum from* MOST. *Figure taken from Walker et al. (2005a).*

I can show you,
That when it starts to rain,
Everything's the same,
I can show you, I can show you.

John Lennon & Paul McCartney

3

Analysis tools

The detection of a periodic signal in unevenly time series is not always easy. The criterion is by nature rather complicated and in order to obtain the correct period different methods have been developed. These techniques are not always suited for all type of time series. In addition, the methods usually give several solutions, which can be produced by the noise of the light curve or even by the method. The window spectrum, the aliases, the possibility of multiperiodicity and many other factors make this search very laborious.

Besides the complication discussed above, a serious difficulty arises when the irregular light variations which are sometimes present in Be stars have a time scale comparable to the underlying periodic variations. In these cases it is not possible to obtain the correct period with any certainty. In addition, long-term

activity is nearly always present, which increases the noise in the light curves.

The components of the Lagrangian displacement vector given in Eqs. 1.1, 1.2 and 1.3 in Chapter 1 contain a time-dependent factor: $e^{i\nu t}$. It is therefore clear that stellar oscillations give rise to periodic variations of the physical quantities which translate in periodic variations of observables, such as the brightness, the colours, the radial velocity and the spectral line profiles. In the current Chapter we study a method to derive the time-dependence of such observables of pulsating stars.

As we have said, there are different techniques to do a frequency analysis: the two most frequently used methods are the *Fourier periodogram* (based on Fourier analysis) and the *Phase Dispersion Minimisation* (PDM) described in Stellingwerf (1978). Several other methods still exist in the literature (some of them based on Bayesian statistics, like those described in Bretthorst 2003; White et al. 2010, and references therein), but almost all of them are derived from the two basic methods outlined here.

We have opted for use techniques based on Fourier analysis because they are better for sinusoidal variations, while PDM gives a better result when a single period in a multiple-wave light curve is present. Next, we will describe the method followed by our group in order to derive the periodicity of unevenly time series.

3.1   Fourier analysis

In period analysis based on Fourier techniques one tries to define a function for testing frequencies in such a way that it reaches an extremal for the test frequency that is close to the true frequency present in the data. The plot of this function is called the *periodogram*. The Fourier analysis uses the frequency domain, that has advantages for periodic processes, while time domain are well suited for the random case, as we will see below. We first recall some useful properties of Fourier analysis and subsequently introduce different periodograms.

The *Fourier transform* of a function $f(t)$ that fullfills the necessary conditions of continuity and finiteness is given by

$$F(\nu) := \mathscr{F}(f(t)) = \int_{-\infty}^{\infty} f(t)e^{-2\pi i\ \nu t}dt \tag{3.1}$$

The Fourier transform of the constant function $f(t) = 1$ is the *Dirac's delta function*, defined as

$$\delta(\nu) := \int_{-\infty}^{\infty} e^{-2\pi i\ \nu t}dt = \begin{cases} \infty & \text{, if } \nu = 0, \\ 0 & \text{, if } \nu \neq 0. \end{cases} \tag{3.2}$$

which has the following properties:

$$\int_{-\infty}^{\infty} \delta(\nu)\, d\nu = 1 \quad \text{and} \quad \int_{-\infty}^{\infty} \delta(\nu - \nu_0)\, g(\nu)\, d\nu = g(\nu_0) \tag{3.3}$$

Period determination from Fourier analysis is based on the fact that the Fourier transform $F(\nu)$ of a function $f(t)$, which is a pure sine wave of frequency ν_0, is only different from zero for $\nu = \pm\nu_0$. The demonstration goes as follows, let be $f(t)$ a periodic function (a sine wave) with frequency ν_0, i.e.:

$$f(t) = A\, e^{2\pi i\ \nu_0 t} \tag{3.4}$$

then, the Fourier transform is

$$F(\nu) = A\, \delta(\nu - \nu_0) \tag{3.5}$$

Thus, the resulting function of the transformation is only different from 0 in $\nu = \pm\nu_0$. Then, if we have a multiperiodic function which can be written in terms of a sum of n harmonic functions with frequencies $\nu_1, ..., \nu_n$ and amplitudes $A_1, ..., A_n$, i.e.:

$$f(t) = \sum_{k=1}^{n} A_k e^{2\pi i\ \nu_k t} \tag{3.6}$$

and his Fourier transform is given by

$$F(\nu) = \sum_{k=1}^{n} A_k \; \delta(\nu - \nu_k) \tag{3.7}$$

Hence, $F(\nu)$ is a sum of n δ-functions which are different from zero for the frequencies $\pm\nu_1, ..., \pm\nu_n$.

However, this is not true when we deal with a discrete data sampling and with a finite data length. Most procedures for estimating $F(\nu)$ from a finite amounts of data give rise to a result which can be expressed as the convolution of the true $F(\nu)$ with a *spectral window*, as we will see below.

For real data, we must use the *discrete Fourier transform* (DFT), which can be defined for an arbitrarily sampled data set $(X_j = X(t_j),\ j = 1, 2, ..., N)$ as

$$DFT_N(\nu) := \sum_{j=1}^{N} X(t_j) \; e^{-2\pi i \; \nu t_j} \tag{3.8}$$

In the same way as we did before, if the data set is constant and equal to 1 for all t_j, the DFT will be

$$\delta_N(\nu) := \sum_{j=1}^{N} e^{-2\pi i \; \nu t_j} \tag{3.9}$$

It is clear that DFT_N differs from F, but we can associate them with each other through the *window function*, defined as

$$w_N(t) := \frac{1}{N} \sum_{j=1}^{N} \delta(t - t_j) \tag{3.10}$$

It's easy to probe, using the definition of the window function and the properties of the Dirac function, that the observed Fourier transform DFT_N can be transferred to an integral form:

$$\frac{DFT_N(\nu)}{N} = \int_{-\infty}^{\infty} X(t) \; w_N e^{-2\pi i \; \nu t} dt \tag{3.11}$$

The discrete Fourier transform of the window function is called the *spectral window* $W_N(\nu)$, defined as follows,

$$W_N(t) := \frac{1}{N} \sum_{j=1}^{N} e^{-2\pi i \, \nu t_j} = \frac{\delta_N(\nu)}{N} \qquad (3.12)$$

Now, if we apply the spectral window to a continuous data set it gives us a sampled data.

If we define the *convolution of two functions F and G in the frequency domain* as

$$F(\nu) * G(\nu) := \int_{-\infty}^{\infty} F(\nu - \sigma) \, G(\sigma) \, d\sigma \qquad (3.13)$$

then the DFT_N/N will be the convolution of the true Fourier transform with the spectral window:

$$DFT_N(\nu)/N = F(\nu) * W_N(\nu) \qquad (3.14)$$

Therefore, the DFT of a pure sine wave will be different from the Fourier transform of the same function. The difference can be described in the frequency domain as an interference between frequencies. It is usually possible to recognise two types of interferences:

- Interference from nearby frequencies, which is usually described by a spectral window and is primarily a product of the finite length of the data.

- Interference from distant frequencies, which is usually called *aliasing*, and is a product of the data spacing.

For continuously recorded data, aliasing does not exist, while for equally spaced data, it exists in its most extreme form. For general arbitrary data spacing, which is usually our case, it is not possible to make such a separation of the two effects.

From Eq. 3.14 we can see that if $F(\nu)$ is a delta function at frequency ν_0, the quantity $DFT_N(\nu)/N$ will reproduce the shape of the spectral window, centred on ν_0, i.e. $W_N(\nu - \nu_0)$. Since $W_N(\nu)$ may well be significantly different from

zero at frequencies different from $\nu = 0$, there may be interference between the different frequencies present in the data. The point is that the behaviour of the data distribution is all contained in the spectral window, which can be calculated from the data spacing and does not depend on the data themselves. Typically, a plot of the amplitude of $W(\nu)$ versus frequency shows a reasonably well defined central peak at $\nu = 0$, with a width of T^{-1} in frequency and some subsidiary peaks corresponding to peculiarities in the data spacing, being T the time span of the data points. The phenomenon is called *aliasing* and the false frequencies, *alias frequencies*.
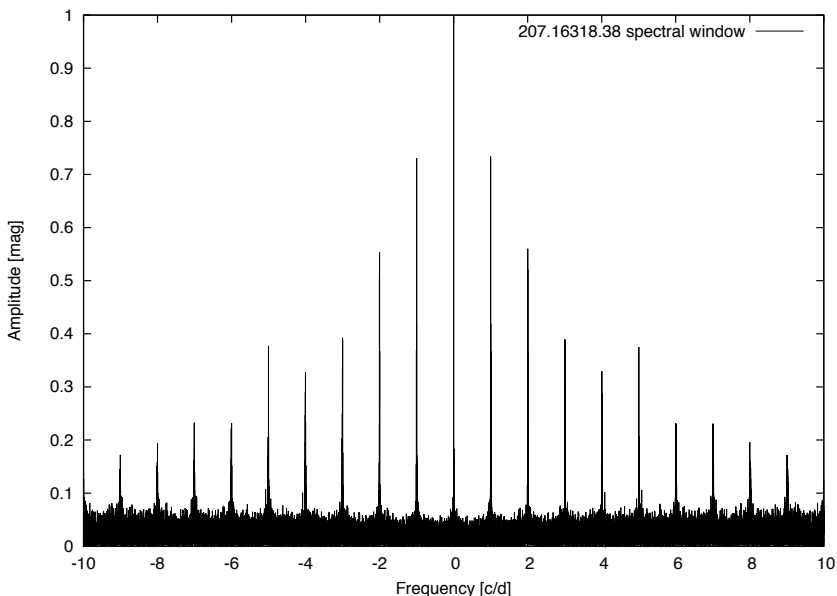
Figure 3.1: *Example of spectral window of a star from the* MACHO *project. We can see a typical 1-day alias pattern present. The length of the observations ($\sim 1\,960$ days) produce a very thin width in the window peaks.*

In Fig. 3.1 it can be seen a typical spectral window for a star selected from the MACHO project (Alcock et al. 1999, see Chapter 5 for more details), with significant peaks in $1, 2, 3, 4, \ldots \mathrm{c\,d^{-1}}$ (and negative values also). This is because any set of observations necessarily has a one day periodicity in its data spacing, since an object can only be observed during night time. Hence a peak is present in a spectral window at the frequency corresponding to the period of one day.
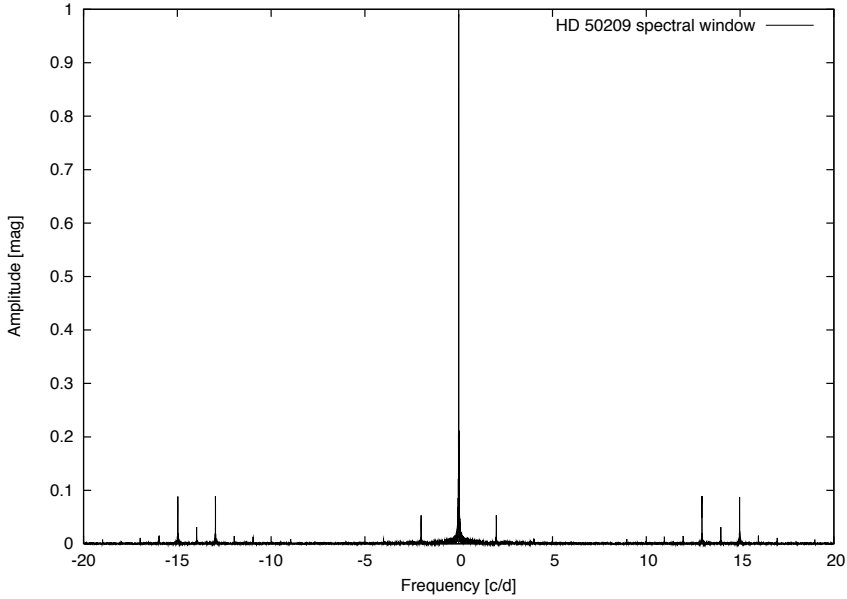
Figure 3.2: *Example of spectral window of the star* HD 50 209 *observed by the space mission* CoRoT. *In this case the 1-day alias pattern is not present as these observations were taken from the space. The peaks at the orbital frequency of the satellite* $(13.97 \, \mathrm{c\,d^{-1}})$, *the day-night frequency* $(2.007 \, \mathrm{c\,d^{-1}})$ *and its aliases are also present. In this case, the time span of the observations was* 136 *days.*

This will be the *1-day alias* ($\nu_A = 1 \, \mathrm{d^{-1}}$), which we can see in Fig. 3.1. Thus, for observing campaigns from only one site, there should be aliases in the transform at frequencies $\nu = \nu_A + \nu_0$ and $\nu = \nu_A - \nu_0$. In the other hand, for data collected from the space, the 1-day alias pattern is not present in the spectral window as we can see in Fig. 3.2.

Let's see some mathematical properties of the spectral window, assuming that the measurements are equidistant in time, i.e., $t_j = t_0 + \Delta t$. In that case, the spectral window is

$$W_N(\nu) = \frac{1}{N} \sum_{j=1}^{N} e^{2\pi i \ \nu \ t_0} \cdot e^{2\pi i \ \nu \ j \Delta t} = \frac{\sin \pi \nu N \Delta t}{N \sin \pi \nu \Delta t} \tag{3.15}$$

See Aerts (2005) or Aerts et al. (2010) for the details. Therefore, we can see that $W_N(\nu)$ has the following properties:

- It is symmetric: $W_N(\nu) = W_N(-\nu)$

- It is periodic with period $1/\Delta t : \forall n,\ W_N(\nu) = W_N(\nu + n/\Delta t)$

- For small values of ν,

$$W_N(\nu) \simeq \frac{\sin \pi\nu\, N\Delta t}{N\pi\nu\Delta t} = \frac{\sin \pi\nu\, T}{\pi\nu\, T} \tag{3.16}$$

  for $T = N\Delta t$, i.e., the *time span*. This function is usually called the *sinc function*[1].

In brief, $W_N(\nu)$ is approximately like an infinite row of sinc functions spaced $1/\Delta t$ apart. We see that for equally spaced data, $W_N(\nu)$ takes the value of unity at an infinite set of frequencies $\nu_n = n/\Delta t$. For unequally spaced data, the periodicity and symmetry properties will not be generally true. However, we may expect that $W_N(\nu)$ will take large values, perhaps near unity (as it can be seen in Fig. 3.1), at frequencies far from $\nu = 0$.

In general, the time sampling provides an upper limit for the high-frequency range. The highest useful frequency to search for is called the *Nyquist frequency*, which is $1/2\Delta t$. The intuitive meaning of this frequency is that if the observations were made every 1 h, one cannot search for instance for periods of about 1 min. It is also important to note that the concept of the Nyquist frequency disappears for unequally spaced data. Then, in theory, the periodogram for such cases could be extended to very high frequencies.

Now we have some knowledge about the different results we obtain when we deal with finite data. Let's see the periodograms.

---

[1] $\operatorname{sinc}(x) := \frac{\sin x}{x}$

3.1.1 Classical periodogram

For detecting periods, we use the periodogram instead of the DFT_N, since this is a complex function. The periodogram or, also called, *power spectrum*, is proportional to the real part of the discrete Fourier transform. The *classical periodogram* is defined as

$$P_N(\nu) := \frac{1}{N}|DFT_N(\nu)|^2 = \frac{1}{N}\left\{(\sum_{j=1}^{N} X_j \sin{(2\pi\nu\,t_j)})^2 + (\sum_{j=1}^{N} X_j \cos{(2\pi\nu\,t_j)})^2\right\} \tag{3.17}$$

If the signal we are searching for is a pure cosine wave ($X(t_j) = A\,cos(2\pi\nu_0\,t_j)$), the periodogram will take the value

$$P_N(\nu_0) = \frac{1}{N}\left\{\sum_{j=1}^{N} A\cos{(2\pi\nu_0\,t_j)}\sin{(2\pi\nu_0\,t_j)}\right\}^2 + \frac{1}{N}\left\{\sum_{j=1}^{N} A\cos^2{(2\pi\nu\,t_j)}\right\}^2 \tag{3.18}$$

Then, for a large value of N we have that

$$\sum_{j=1}^{N} A\cos{(2\pi\nu_0\,t_j)} \approx 0 \quad \text{and} \quad \sum_{j=1}^{N} \cos^2{(2\pi\nu\,t_j)} \approx N/2 \tag{3.19}$$

and so $P_N(\nu) \approx A^2 N/4$. At other values of ν, the terms in the sum are randomly positive and negative, and the resulting cancellation yields to a small sum. Hence the presence of a sinusoid is indicated by large values in P. And we can derive the *amplitude at frequency* ν as:

$$A(\nu) = 2\,\sqrt{\frac{P_N(\nu)}{N}} \tag{3.20}$$

3.1.2 Lomb-Scargle periodogram

Lomb (1976) and Scargle (1982) defined a improved definition of the periodogram. This definition is preferable for:

- Its value does not change when all time values t_j are replaced by $t_j + T$.

- The statistical distribution of the estimator is easy to use (Scargle 1982).

- Is equivalent to the *least-square fitting* of sine waves to the data.

The *Lomb-Scargle* periodogram is defined as follows

$$P_N(\nu) := \frac{1}{2} \left\{ \frac{[\sum_{j=1}^N X_j \cos(2\pi\nu(t_j - \tau))]^2}{\sum_{j=1}^N X_j \cos^2(2\pi\nu(t_j - \tau))} + \frac{[\sum_{j=1}^N X_j \sin(2\pi\nu(t_j - \tau))]^2}{\sum_{j=1}^N X_j \sin^2(2\pi\nu(t_j - \tau))} \right\} \tag{3.21}$$

where τ is the reference epoch, which is chosen in such way that

$$CS \equiv \sum_{j=1}^N X_j \cos(2\pi\nu(t_j - \tau)) \sin(2\pi\nu(t_j - \tau)) = 0 \tag{3.22}$$

or, equivalently

$$\tan(4\pi\nu\tau) = \frac{\sum_{j=1}^N \sin(4\pi\nu t_j)}{\sum_{j=1}^N \cos(4\pi\nu t_j)} \tag{3.23}$$

The following definitions are introduced to simplify the periodogram:

$$\begin{cases} CC \equiv \sum_{j=1}^N \cos^2[2\pi\nu(t_j - \tau)], & SS \equiv \sum_{j=1}^N \sin^2[2\pi\nu(t_j - \tau)] \\ \\ XC \equiv \sum_{j=1}^N X_j \cos[2\pi\nu(t_j - \tau)], & XS \equiv \sum_{j=1}^N X_j \sin[2\pi\nu(t_j - \tau)] \end{cases} \tag{3.24}$$

Hence, the Lomb-Scargle periodogram is rewritten as:

$$P_N(\nu) = \frac{1}{2} \left\{ \frac{(XC)^2}{CC} + \frac{(XS)^2}{SS} \right\} \tag{3.25}$$

And it takes the value $A^2 N/4$ for harmonic signal with frequency ν_1 and for sufficiently large N. As in the classical periodogram, the *amplitude at frequency* ν is:

$$A(\nu) = 2\sqrt{\frac{P_N(\nu)}{N}} \tag{3.26}$$

3.2 Significance criteria

During a frequency analysis, one needs to adopt a stop criterion to decide whether or not a candidate frequency is still *significant* or not. For obvious reasons, this aspect of frequency analysis has received a lot of attention. To derive the significance of a frequency one needs to know the distribution function of the employed frequency statistic.

The method used by our group in order to determine whether the frequencies are statistically significant or not is the *signal to noise amplitude ratio requirement* (SNR) described in Breger et al. (1993). This method basically consists in the calculation of the SNR of each peak in the periodogram. To calculate the SNR of each peak, the signal (S) is the amplitude of the peak for each frequency obtained. And the noise (N) is assumed to be the average amplitude, within a $5\,\mathrm{c\,d^{-1}}$ frequency interval, of the residual periodogram after the *prewhitening* of all the frequencies detected. The interval of frequencies where it is calculated depend on the frequencies one is studying. Breger et al. (1993) shown that for a multi-site campaign a $S/N \geq 4$ might be a good criterion to distinguish between peaks due to real frequencies and noise. Note that the criterion is conservative, by using amplitudes rather than power, i.e., amplitude squared.

3.3 Error determination

Since period finding techniques have many false frequencies, we need an estimation on how good is the frequency we obtain. This is made by astronomers with several approaches. The most common procedure, in the Fourier transform methods, is by using the half-width of the side lobe of the peak in the periodogram, which is $\sim 1/T$, with T the time span. This approach is known as the *Rayleigh criterion*. This error determination is not always accepted by all the authors. Schwarzenberg-Czerny (1991) argued that this criterion is insensitive to the *signal to noise ratio* and thus does not reflect quality of observations. Therefore, this is an upper limit of the error. However, Kallinger et al. (2008) propose a

less conservative criterion, based on Monte-Carlo simulations, by using $1/(2T)$ or $1/(4T)$.

Following Montgomery and O'Donogohue (1999), the expected error in a frequency ν for uncorrelated observations can be derived from the equation

$$E_\nu = \frac{\sqrt{6}}{\pi} \cdot \frac{E_n}{A \cdot \sqrt{N} \cdot T} \tag{3.27}$$

where A/E_n indicates the SNR (i.e., E_n stands for the average error on each of the data points), N is the number of observations and T the time elapsed between the first and the last data point. As noted by Schwarzenberg-Czerny (1991), correlations in the residuals of fitting have to be taken into account multiplying the error frequency by $\sqrt{D}$, where D is the correlation length. D can be estimated by performing an auto-correlation analysis of the residuals.

3.4   Searching for multiple periods

The basic method for searching multiperiodicity is *prewhitening* the frequency found in the periodograms. The procedure is as follows:

1. Find the most probable frequency with the methods discussed above.

2. Knowing the first frequency, make a least-squared fitting to determine the amplitude and phase of the oscillation.

3. Remove this frequency from the light curve in the time domain. This is usually called *prewhitening* the frequency.

4. Repeat the first instruction.

5. This process is made until the frequency founded has a S/N less than 4, as mentioned in Breger et al. (1993).

This is no the best technique, since periods may interfere between them. We need a non-linear method. In this way, we also use techniques which fit a number

of simultaneous sinusoidal variations in the time domain and does not rely on prewhitening. These techniques make a least-squared fitting to the frequencies and in the process, their aliases are automatically removed from the data. For this purpose we use two different methods, both of them based on *non-linear multi-parameter fitting codes* and described in the Subsection 3.5.3. We combine both non-linear methods with those linear ones (based on the prewhitening of found frequencies).

3.5 Frequency analysis codes

Different methods have been used and developed by our group to extract the maximum amount of information from the light curves.

3.5.1 Search for frequencies

In the first stage, we search for frequencies in the light curves using a code based on the standard Fourier transform. This code is PASPER (Diago et al. 2008a), developed by P. D. Diago in collaboration with R. Garrido and J. Gutiérrez-Soto. An important advantage of this code is the batch analysis mode, very useful for long sets of observations.

PASPER calculates the amplitude and the power spectrum for a wide range of frequencies, respectively, identifies the frequency corresponding to the maximum peak in the Fourier space and then fits a sinusoidal function by means of least-squares fitting to this frequency in the time domain. PASPER is based on the classical discrete Fourier transform (Deeming 1975), using the Lomb-Scargle periodogram. The amplitude computed by PASPER is given in magnitudes. When a frequency is found, it is prewhitened by subtracting the corresponding synthetic sinusoidal light curve and a new search begins for the most powerful frequency in the residuals. The stop criterion for the frequency search is the one described in Breger et al. (1993) and explained above in the text.

In Appendix C we provide the complete user guide of PASPER, with a deep description on the different subroutines and the installation notes.

3.5.2 Testing the pasper code

Different codes are used in the CoRoT Be Team for extracting information from the light curves provided by the CoRoT satellite. The codes used for the search of frequencies are PASPER (Diago et al. 2008a), CLEANest (Foster 1995), CLEAN-NG and TiSAFT (Huat et al. 2009b) and Period04 (Lenz and Breger 2005).

Recently, Gutiérrez-Soto et al. (2009b) perform a comparison of the frequencies detected in the CoRoT B8IIIe star HD 175 869 star. In this work a frequency analysis was performed using PASPER, CLEANest, CLEAN-NG and TiSAFT. The results obtained in this comparison are summarised in Fig. 3.3. We can see that the differences between the frequencies obtained for HD 175 869 are less than the frequency resolution in most cases, as is evident in the top panel of Fig. 3.3. Only three of the detected frequencies differ by little more than the frequency resolution and have small amplitudes. Therefore, all methods infer similar values for the frequencies with the largest amplitude.

Another comparison was performed to the residuals after the prewhitening of F_1 and its harmonics. Again, PASPER, CLEANest, CLEAN-NG and TiSAFT detected similar frequencies within the frequency resolution, except for two cases, as shown in the bottom panel of Fig. 3.3.

3.5.3 Improve the frequency determination

The second stage consists of improving with non-linear least-squares fitting methods (local minimum) the estimation of initial frequencies detected with the method described above. We employed the codes BOSSIRR and KURTZ_BOS, developed by M. Bossi and J. Gutiérrez-Soto, respectively.
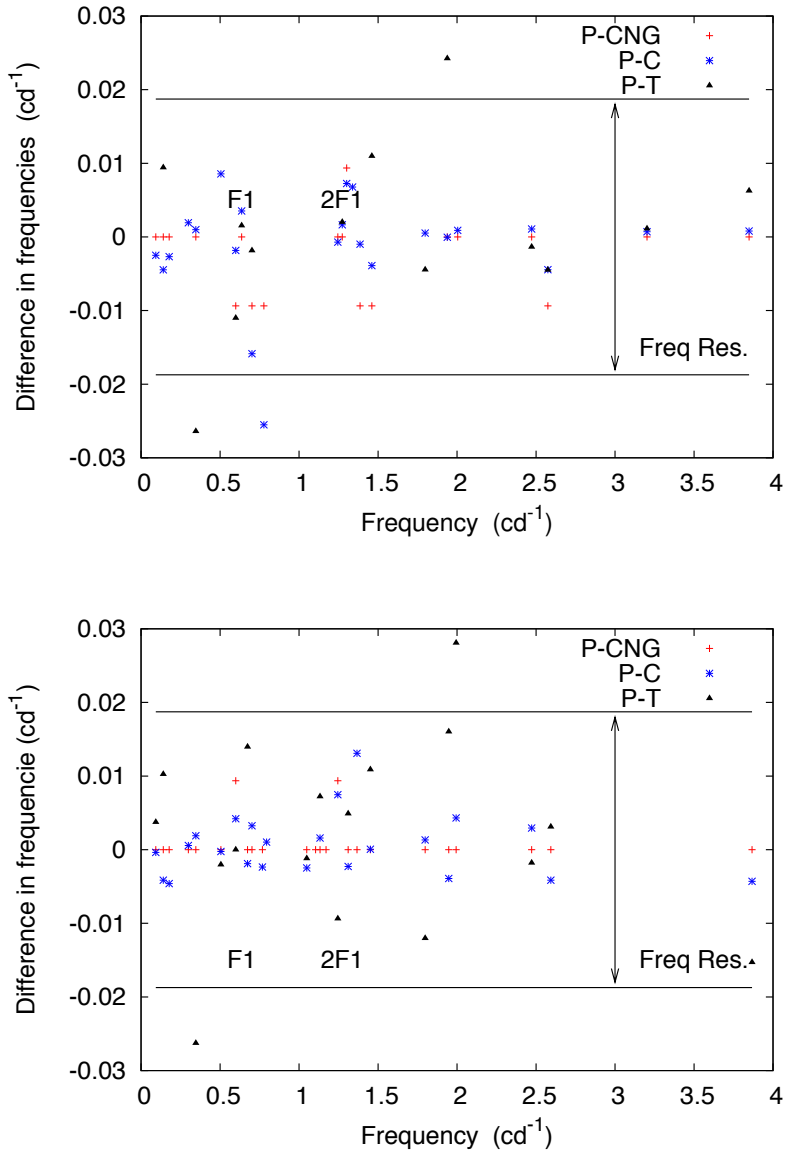
Figure 3.3: *Red crosses, blue asterisks, and black triangles represent the differences for* PASPER *and* CLEAN-NG, PASPER *and* CLEANEST, *and* PASPER *and* TISAFT, *respectively.* Top: *Differences in frequencies given by the different methods applied to the detrended and corrected* CoRoT *light curve.* Bottom: *Differences in frequencies given by the different methods applied to the residuals after prewhitening F_1 and its harmonics. Figure courtesy of Juan Gutiérrez-Soto.*

The BOSSIRR routine

Once we have obtained a preliminary set of significant frequencies for each star and filter, we perform a non-linear multi-parameter fitting based on the method described by Vaníček (1971), also explained in detail by Zerbi et al. (1997) and Martín et al. (2003) . This code simultaneously adjusts all the frequencies, allowing the fit to move over a wide range in frequency (global fitting) in order to obtain the minimum variance.

The KURTZ_BOS routine

The KURTZ_BOS code is a powerful tool to perform frequency analysis and improve the frequency determination. The search for frequencies is done by the program KURTZ_BOS in an automatic mode using the efficient algorithm described in Kurtz (1985). Once a frequency has been detected, it scans a small range around this frequency to determine the minimum variance. The improved frequency is prewhitened from the data and another frequency is found in the residuals with the Kurtz algorithm. The code, then adjusts simultaneously the two frequencies allowing them to move to obtain the best fit. This method is iterated until a maximum number of frequencies is reached.

In Appendix D we provide the complete user guide of KURTZ_BOS.

3.5.4   Determination of the amplitudes and phases

To determine the amplitudes and phases of each detected frequency, we used a linear least squares fitting subroutine `freqPyLSQ` of the code PASPER. Another method used for this purpose is AMPHI, written by B. Leroy, which is based on the SVD algorithm developed in the GSL library (Galassi et al. 2006). In this implementation, the matrix components are discarded if the ratio of singular values falls below a user-specified tolerance.

Part I

B-type pulsations in low metallicity environments

Newspaper taxis appear on the shore,
Waiting to take you away.
Climb in the back with your head in the Clouds,
And you're gone.

John Lennon

4

Study of B-type pulsations in the Magellanic Clouds

At the early begin of this Ph.D. thesis (October 2005), the CoRoT satellite was still on ground getting ready for the launch in December 2006. At this time, we were performing and improving our PASPER code and we needed some variable stars to check the performance of our methods. In this context, the search for short-period B and Be star variables in the low metallicity environment of the Magellanic Clouds (MCs) is an interesting starting point whose scientific context is explained in the following. This study will constitute the first part of this Ph.D. thesis.

This part of the Ph.D. thesis, based on the searching for B-type pulsators in the MCs, is arranged as follows: in this Chapter we present the aims and definitions. Chapter 5 depicts an overview of the MACHO survey and the B and Be samples of the study. Finally, in Chapters 6 and 7 we describe the results and discussion for the SMC and LMC studies, respectively. Moreover, a comparison between the SMC and LMC results with those obtained for the MW has been added to the latter Chapter.

4.1 Aims of the study

As mentioned in Chapter 1, stellar pulsation in main-sequence B-type stars is driven by the κ mechanism due to the Fe-group opacity bump. As we will describe in the following, the current models predict a vanishing of the instability strips in the B spectral domain as decreasing the metallicity (Z). For this reason, the Small Magellanic Cloud (SMC) and the Large Magellanic Cloud (LMC) are suitable objects to test these predictions.

This search for short-term variations in B-type stars from the low metallicity environments of the MCs has two main goals:

1. To search for short-term periodic variability in both B and Be star samples from the SMC and the LMC for which Martayan et al. (2006a) and Martayan et al. (2007b) calculated accurate fundamental physical parameters. This is an important key because the fundamental parameters allow us to place the detected variable stars in a theoretical H-R diagram.

2. To make a detailed comparison between the pulsating B and Be stars found in the MCs and in the Milky Way (MW). For thus, we will present a discussion on the effects of metallicity and the rotational velocities, both related with non-radial pulsations.

4.2 The Magellanic Clouds

Magellan and his crew had a lot of time to study the southern sky during their famous voyage around the world (1519-1522). As result, two fuzzy cloud-like objects in the southern sky are now known as the clouds of Magellan or the Magellanic Clouds (MCs). These star clouds are small irregular galaxies, satellites of our larger MW spiral galaxy.

The LMC and its neighbour and relative, the SMC, both shown in Fig. 4.1, are conspicuous objects in the southern hemisphere, looking like separated pieces of the MW with to the naked eye. Roughly $21°$ apart in the night sky, the true distance between them is about $75\,000$ light years. Until the discovery of the Sagittarius Dwarf Elliptical Galaxy in 1994, they were the closest known galaxies to our own, about $170\,000$ and $240\,000$ light years distant, for the LMC and SMC respectively. They are also two of the most distant objects that can be seen with the naked eye.

There is almost no doubt that both Clouds are gravitationally bound to the MW. Even so, both are currently moving away from us at $76\,\mathrm{km\,s^{-1}}$ and $22\,\mathrm{km\,s^{-1}}$ (LMC and SMC, respectively). However, their gravity has affected our Galaxy as well, distorting the outer parts of the galactic disk and making the Magellanic Clouds to resemble disrupted barred spiral galaxies. The SMC together with the LMC, the Andromeda Galaxy, our MW and over 30 galaxies conform the Local Group.

Aside from their different structure and lower mass, they differ from our Galaxy in two major ways:

- First, they are gas-rich. A relatively higher fraction of their mass is H and He compared to the MW. As we have mentioned above, observation and theoretical evidence suggests that the MCs have been greatly distorted by tidal interaction with the MW as they orbit around it. For this, streams of neutral H surrounds and connects both Clouds and trails away from them toward and beyond the south galactic pole of the MW. This huge sea and

river of hydrogen is known as the Magellanic Stream.

- They are also more metal-poor than the MW. The youngest stars in the LMC and in the SMC have a metallicity of 0.5 and 0.25 times solar metallicity, respectively. Both are detected because of their nebulae and young stellar populations, but as in our own Galaxy, their stars range from the very young to the very old, indicating a long stellar formation history. Actually both Clouds are experiencing massive stellar production, for example, the Tarantula Nebula (30 Doradus or NGC 2070) in the LMC.

Figure 4.1: *Diffuse starlight and dark nebulae along the southern Milky Way arc over the horizon and sprawl diagonally through this gorgeous night scape. The breath-taking mosaic spans a wide $100°$, with the rugged terrain of the Patagonia, Argentina region in the foreground. Along with the insider's view of our own galaxy, the image features our outside perspective on two irregular satellite galaxies - the Large and Small Magellanic Clouds. Recorded on January 28th of 2007, the scene also captures the broad tail and bright coma of Comet McNaught, the great comet of 2007. Figure courtesy of Miloslav Druckmuller.*

The LMC and the SMC were one of the favoured locations by the MACHO collaboration to search for gravitational lensing by dark stellar objects in the halo of our Galaxy. In Chapter 5 we describe in detail the MACHO Project. The results obtained in this project have sharpened and deepened the mystery of dark matter in galaxies.

4.3   Scientific rationale of the study

As we have mentioned in Chapter 1, both SPB and β Cephei stars are B-type star pulsators near the main sequence and their pulsations are driven by the κ mechanism operating in the Fe-group elements, not on H or He. Pamyatnykh (1999) showed that the theoretical instability domains shrink down with decreasing value of Z. This study reveals that the β Cephei and SPB instability strips practically vanish at $Z < 0.01$ and $Z < 0.006$, respectively. Miglio et al. (2007a,b) computed new calculations based on OPAL and updated OP opacities and different metal mixtures and found that for the lowest metallicity considered ($Z = 0.005$), only SPB-type modes are excited. They do not predict β Cephei pulsations at this metallicity. In Fig. 4.2 we depict the instability strips obtained by Miglio et al. (2007b) for β Cephei and SPB star models.

More recently, Salmon et al. (2009) compute new opacity tables for the "Small Magellanic Cloud B stars mixture" by making use of the OP and OPAL opacities. They conclude that $Z \geq 0.007$ is required to excite β Cephei modes and $Z > 0.004$ for SPB mode excitation. The new calculations are depicted in Fig. 4.3 for reference.

The metallicity of the MCs has been measured to be around $Z = 0.002$ for the SMC and $Z = 0.007$ for the LMC according to Maeder et al. (1999, and references therein). Therefore, taking together the above mentioned theoretical constraints and assuming the similarity between the SMC and LMC B star metal mixtures, it is expected to find a very low occurrence of β Cephei and SPB pulsators in the LMC and no β Cephei nor SPB stars in the SMC.
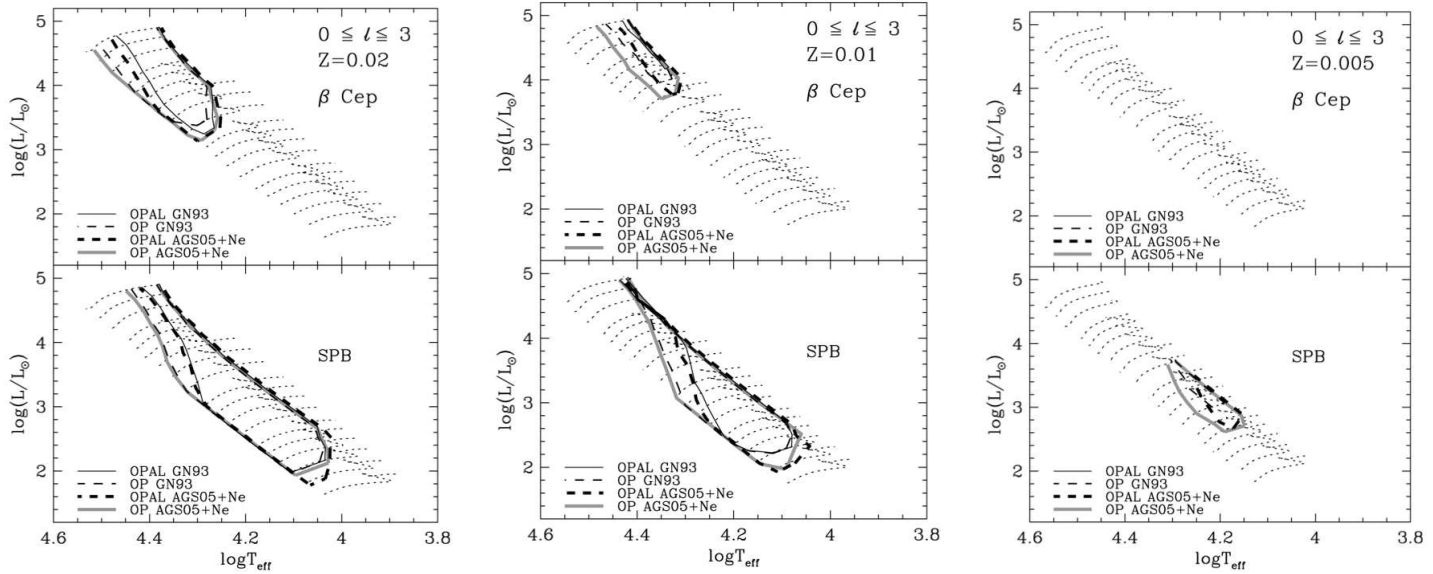
Figure 4.2: *Instability strips of β Cephei and SPB-type pulsations in the H-R diagram computed by* Miglio et al. (2007b) *for Z = 0.02 (left), Z = 0.01 (centre) and Z = 0.005 (right). Evolutionary tracks are represented by dotted lines. Figure taken from* Miglio et al. (2007b).
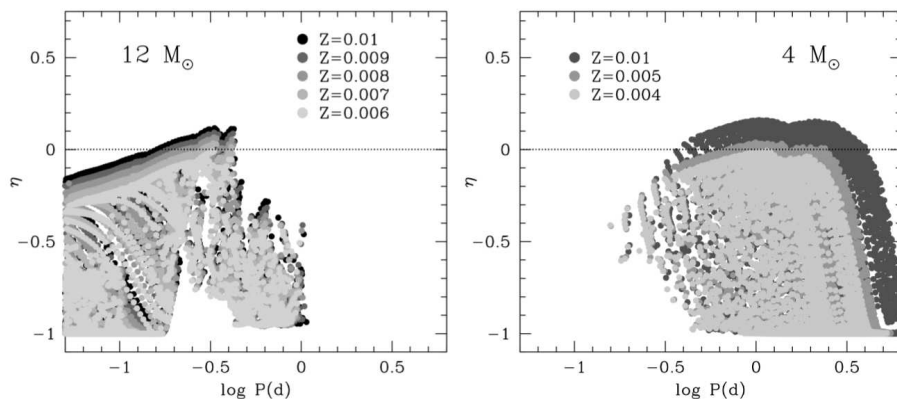
Figure 4.3: *Measurement of instability of β Cephei (left panel) $\ell = 0, 1$ and 2 modes, and SPB (right) high order $\ell = 1$ and 2 g-modes as a function of the mode period $\log P(d)$. Region with $\eta > 0$ means unstable mode, while $\eta < 0$ means stable mode. Models along the main-sequence evolution of 12 and $4\,M_\odot$ for different values of the metal mass fraction Z and the SMC B stars metal mixture are considered. Figure taken from Salmon et al. (2009).*

Searches for β Cephei variable stars in the MCs had already been undertaken. The first was carried out by Sterken and Jerzykiewicz (1988). By means of the photoelectric photometry these authors studied six late O/early B-type stars. For the same purpose, Kubiak (1990) searched the young LMC cluster NGC 1712. These searches resulted in the discovery of some variables, but none of a convincing β Cephei-type pulsation mainly because of the small statistical sample observed. Another search for β Cephei stars was performed by Balona (1992, 1993) and Balona and Jerzykiewicz (1993) in NGC 2004 and 2100 in the LMC and in NGC 330 in the SMC. A similar CCD search was also carried out by Kjeldsen and Baade (1994) in NGC 2122 in the LMC and NGC 371 in the SMC. No variable of β Cephei-type was found by any of these authors.

Another large class of stars populating the B-type main sequence are the Be stars, described in detail in Chapter 2. As pulsating Be stars occupy the same region of the H-R diagram as β Cephei and SPB stars, it is generally assumed that pulsations have the same origin, i.e., $p-$ and/or g-mode pulsations driven by the κ mechanism associated with the Fe bump. The current theoretical models

are not suitable to describe the pulsational characteristics of Be stars, due to the high rotational velocity of these objects. However, recent developments are contributing to progress on this issue (e.g. Reese et al. 2006).

However, during the last years the number of B-type candidate pulsators in the low metallicity environment of the MCs has steadily increased (see, for example, Pigulski and Kołaczkowski 2002; Kołaczkowski et al. 2004, 2006; Diago et al. 2008a; Karoff et al. 2008; Sarro et al. 2009) suggesting that pulsations are still driven by the κ mechanism even in low metallicity environments. Fig. 4.4 shows B-type pulsator candidates for the SMC obtained in recent studies. The apparent disagreement between observations and theory remains an enigma. In this context, the observational study of β Cephei and SPB star pulsations in objects of different metallicity is of great importance. It was already pointed out by Sterken and Jerzykiewicz (1988) that with their lower than Galactic metallicities and relatively small interstellar absorption, the LMC and SMC are among the best objects for such a study.
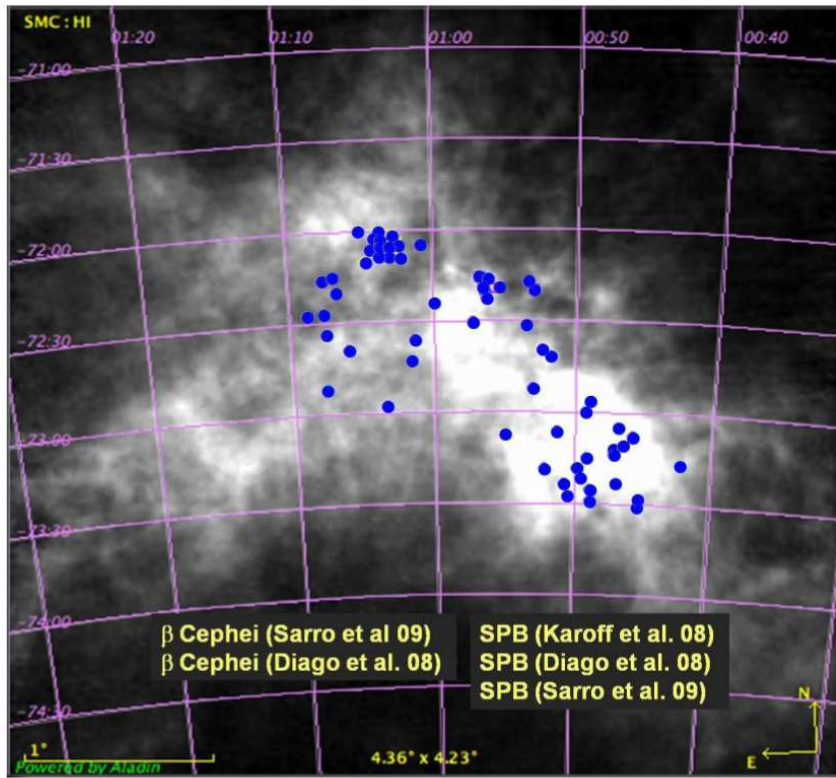
Figure 4.4: *Map of column density of the neutral hydrogen in the SMC. The brighter is the colour, the higher is the density. Coloured dots correspond to SPB and β Cephei candidates from different works. Figure taken from Salmon et al. (2009) and powered by* ALADIN *(http: // aladin. u-strasbg. fr/).*

I read the news today, oh boy,
Four thousand holes in Blackburn, Lancashire.
And though the holes were rather small,
They had to count them all;
Now they know how many holes it takes to fill the Albert Hall.

John Lennon

5

The MACHO Project and the data analysis

As we have shown in the previous Chapter, the MCs are two suitable objects to study the effects of the metallicity in the pulsating B-type stars. In this Chapter we describe the B and Be samples analysed in our study. The data was retrieved from the MACHO database, a survey that has monitored the light variations of millions of stars from the LMC, SMC and the Galactic bulge to detect gravitational lensing effects. Finally, we will describe the frequency analysis process.

For our study we have selected more than 150 B and Be stars identified in Martayan et al. (2006a, hereafter M06) for the LMC and more than 300 B and Be stars identified in Martayan et al. (2007b, hereafter M07) for the SMC. The determined fundamental astrophysical parameters for these stars allow us to place the periodic variables studied in the theoretical H-R diagram in order to better

understand their nature and to map the regions of pulsational instability at the LMC and SMC metallicity. A preliminary discussion of some of the pulsating Be stars found in this work has already been presented by Martayan et al. (2006b), Martayan et al. (2007a) and Martayan et al. (2008b).

The search for periodic variability has been done by analysing the photometric time series provided by the MACHO project (Alcock et al. 1999, described in the following Section). The reason to select this survey rather than others is that the time span of the MACHO observations is large enough to provide a very high frequency resolution in the spectral analysis and hence allow us to distinguish between very close frequencies. The average time span of observations in each light curve is about 2 690 days.

5.1 The MACHO project

MACHO (Massive Astrophysical Compact Halo Object) is a general name for any kind of astronomical body that might explain the apparent presence of dark matter in galaxy halos. A MACHO is a small chunk of normal baryonic matter, which emits little or no radiation and drifts through interstellar space. Since MACHOs would not emit any light of their own, they would be very hard to detect. MACHOs may sometimes be black holes or neutron stars as well as brown dwarfs or unassociated planets. White dwarfs and very faint red dwarfs have also been proposed as candidate MACHOs. A MACHO may be detected when it passes in front of or nearly in front of a star and the MACHOs gravity bends the light, causing the star to appear smaller and brighter in an example of gravitational lensing known as gravitational microlensing. Several groups have searched for MACHOs by searching for the microlensing amplification of light.

The MACHO Project[1] is a microlensing survey experiment (Alcock et al. 1999) that monitors the brightness variations of about 60 million stars in the MCs and the Galactic Bulge. This project is a collaboration between American, Australian, and British astronomers to search for MACHOs using a special-purpose

---

[1] http://wwwmacho.anu.edu.au/
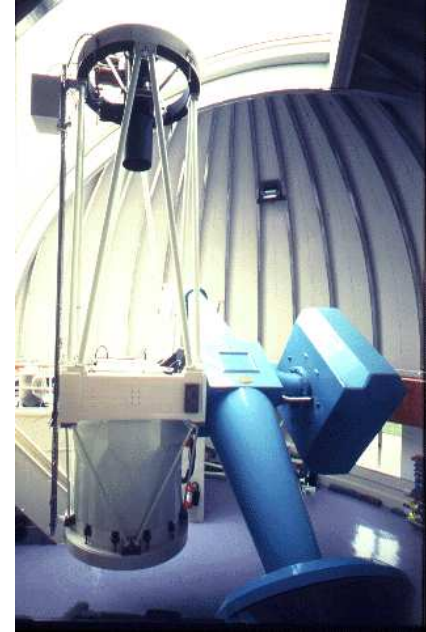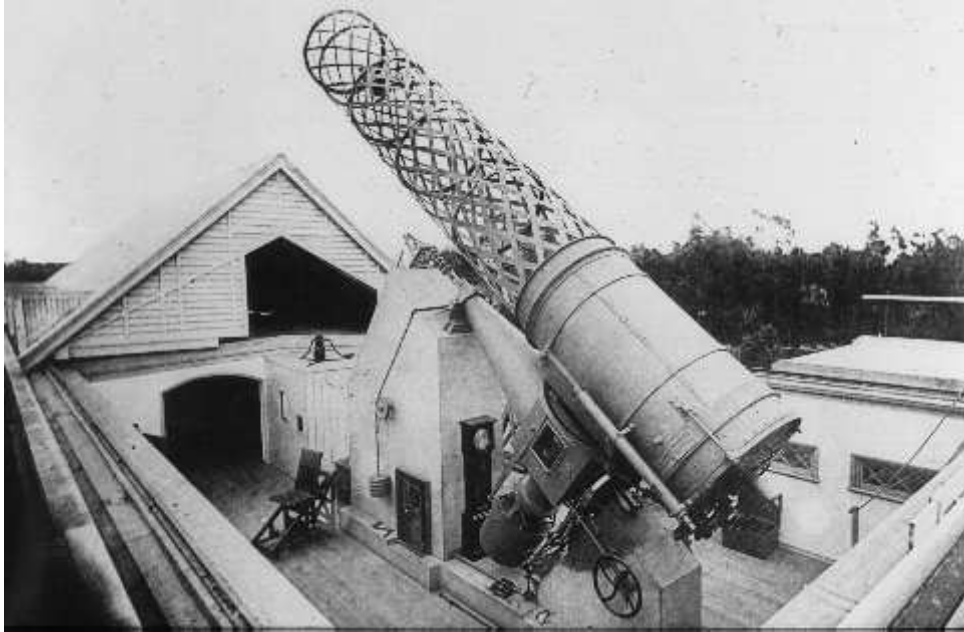
Figure 5.1: Left: *The Great Melbourne Telescope in* 1910. Right: *The telescope in the* MACHO *era. The original polar axis, declination-axis and mirror cell are evident. Figure taken from the* MACHO *website* http://wwwmacho.anu.edu.au/.

charged coupled device camera on the 1.27-meter telescope of the Mount Stromlo
and Siding Spring Observatories. Operated by the Australian National Observa-
tories they are located on Mount Stromlo (near Canberra) at an altitude of 770 m
in Australia. The MACHO Project is led by Charles Alcock at the Lawrence
Livermore National Laboratory, California.

The primary aim of this project is to test the hypothesis that a significant
fraction of the dark matter in the halo of the MW is made up of MACHOs. The
signature of these objects is the occasional amplification of the light from stars
by the gravitational lens effect. The amplification can be large, but events are
extremely rare: it is necessary to monitor photometrically several million stars
for a period of years in order to obtain a useful detection rate. They have taken
more than 27 000 images with this system since June 1992.

5.1.1   Telescope optics and configuration

The telescope used in the MACHO program is a renovation of the Great Mel-
bourne Telescope (Robinson and Grubb 1869) built in 1868 by Grubb in Dublin.
An illustration at its commissioning stage in Melbourne is shown in Fig. 5.1. At
the time and for several decades following it was the largest steerable telescope in
the world. In 1953, the telescope was transferred to Mount Stromlo Observatory,
and renovated by installing a Pyrex (DURAN) glass mirror of 1.27-meter aper-
ture and replacing the manual control of the slewing and setting motions with
motors. This telescope was selected for the MACHO survey because it had sub-
stantial aperture and could be dedicated to the continuous observational schedule
required. Today the telescope looks like in Fig. 5.1.

The telescope uses a 1.27-meter aperture paraboloidal primary mirror made by
Grubb-Parsons (UK). The wide-field prime-focus corrector incorporates a dichroic
element to allow simultaneous two-colour observations. The corrector provides flat
focal plane images over a field of 60 arcmin. The astronomical imaging system
incorporates a total of eight 2048×2048 pixel CCDs into two focal planes, to allow
simultaneous imaging in two wavelength regions, centred on 560 nm and 710 nm.

The two MACHO passbands are non-standard (see Fig. 5.2). The blue band covers $437 - 590$ nm with an effective wavelength of about 520 nm, and the red band covers $590 - 780$ nm with an effective wavelength of about 690 nm. Simultaneous observations of stellar fields in two passbands allows colour information to be obtained even in non-photometric weather conditions. These colour data are important for the MACHO program because there is a need to differentiate between gravitational lensing which is an achromatic amplification of the background star light and the intrinsic variability of stars which is usually associated with temperature changes leading to colour changes in the stellar light curve. Further details of the MACHO camera system are provided in Stubbs et al. (1993) and Marshall (1994).
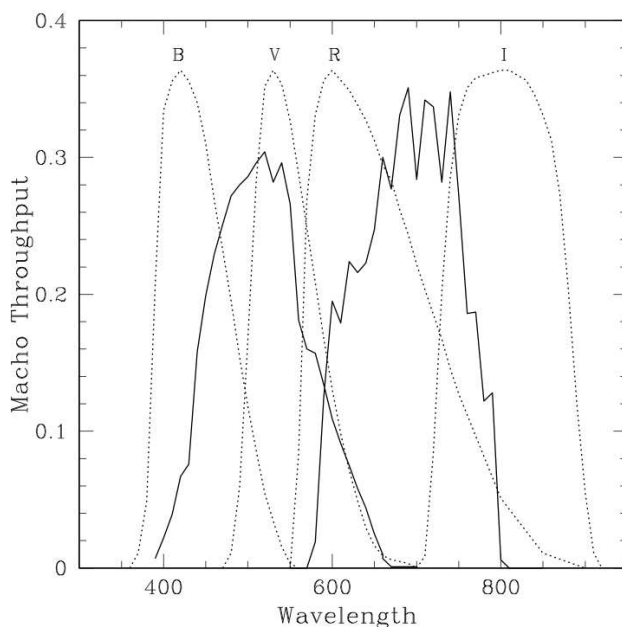
Figure 5.2: *Approximate instrumental throughput for the blue and red* MACHO *image data. A throughput of one would indicate no loss of light. Wavelength is in units of* nm. *These response functions include dichroic, filters and CCDs. However, the wife-field optics corrector has not been included. Uncertainty in these functions is* $\sim 20\%$. *Also shown are normalised standard passbands B, V, R and I from Bessell (1990). Figure taken from Alcock et al. (1999).*

The telescope is operated on all clear night-time hours using typical exposures of $300\,\mathrm{s}$. The limiting magnitude in average seeing is $V \sim 20.5\,\mathrm{mag}$ with photometric errors depending on the crowding of images in the dense stellar fields used in the MACHO surveys. For a complete overview of the telescope system we refer to Hart et al. (1996).

5.1.2 The MACHO data system

Since the MACHO cameras produce data at a prodigious rate, it is highly desirable to have a data pipeline that is both automatic and computationally efficient. Raw image data from the cameras passes down a fibre optic line to $128\,\mathrm{Mb}$ of buffer memory on a VME Bus extension to a Sun Sparc IPC. The images are then written to magnetic disk and copied to tape. While the images are resident on disk, 4-processor Solbourne reduces the data to photometric measurements using the custom built PSF fitting photometry routine, SoDOPHOT (originally based on DOPHOT5, see Alcock et al. 1999, for details). The photometric output includes a number of parameters and flags designed to help identify possible photometric problems. The quantities output include the PSF fit χ^2, measures of cosmic ray contamination and the fraction of the PSF that is lost to bad pixels, and a seeing-dependent crowding estimator.

The MACHO database contains (in 1999) about 80 billion photometric measurements, a significant fraction of all astronomical photometry. Alcock et al. (1999) describes the calibration of MACHO two-colour photometry and transformation to the standard Kron-Cousins V and R system. Calibrated MACHO photometry may be properly compared with all other observations on the Kron-Cousins standard system, enhancing the astrophysical value of these data. For about 9 million stars in the LMC bar, independent photometric measurements of about $20\,000$ stars with $V \lesssim 18\,\mathrm{mag}$ in field-overlap regions demonstrate an internal precision $\sigma V = 0.021$, $\sigma R = 0.019$, $\sigma(V - R) = 0.028\,\mathrm{mag}$. The accuracy of the zero-point in this calibration is estimated to be $\pm 0.035\,\mathrm{mag}$ for stars with colours in the range $-0.1 < (V - R) < 1.2\,\mathrm{mag}$. A comparison of calibrated MACHO photometry with published photometric sequences and new Hubble

Space Telescope (HST) observations shows agreement (see Alcock et al. 1999, for reference). The current calibration zero-point uncertainty for the remainder of the MACHO photometry database is estimated to be ± 0.10 mag in V or R and ± 0.04 mag in $(V - R)$.

The MACHO data is labelled using the *Field.Tile.Sequence* triplet. For example, the star labelled 207.16317.116 means that this star is from the field 207 (thus it is on the SMC), the corresponding tile is 16317 and the sequence is 116. Searches through the *Web-based Image and Data Access*[2] can be made on a range of parameters by specifying each of these parameters in the corresponding field on the search form. The parameters are predominantly concerned with identification of the stars for which photometry is to be retrieved. A precise star identification using the MACHO *Field.Tile.Sequence* triplet can be entered, in which case the photometry for that star only will be retrieved, or cone search parameters can be entered and the photometry for stars closest to the centre point of the specified region will be retrieved. The total number of stars for which photometry will be retrieved in the case of a cone search is limited. Since April 2009 these query services are deprecated and may be removed at any time. The new MACHO data services are fully compliant with current Virtual Observatory service standards, as specified by the International Virtual Observatory Alliance[3] (IVOA). For full information on service standards, refer to the IVOA standards documentation.

5.1.3 SMC and LMC MACHO fields

As mentioned above, the MACHO Project has monitored brightness variations of stars in the LMC, SMC and Galactic bulge. The total sky area monitored is approximately 40, 3, and 45 square degrees in the LMC, SMC, and Galactic bulge, respectively. Each star is represented in the MACHO database by a time-series of two-colour photometric measurements. In some cases, stars are counted in the database two or three times because the survey fields overlap on the sky. In Fig. 5.3 we depict the squared fields of the LMC and SMC, respectively.

---

[2]http://wwwmacho.anu.edu.au/Data/MachoData.html.
[3]http://www.ivoa.net/.
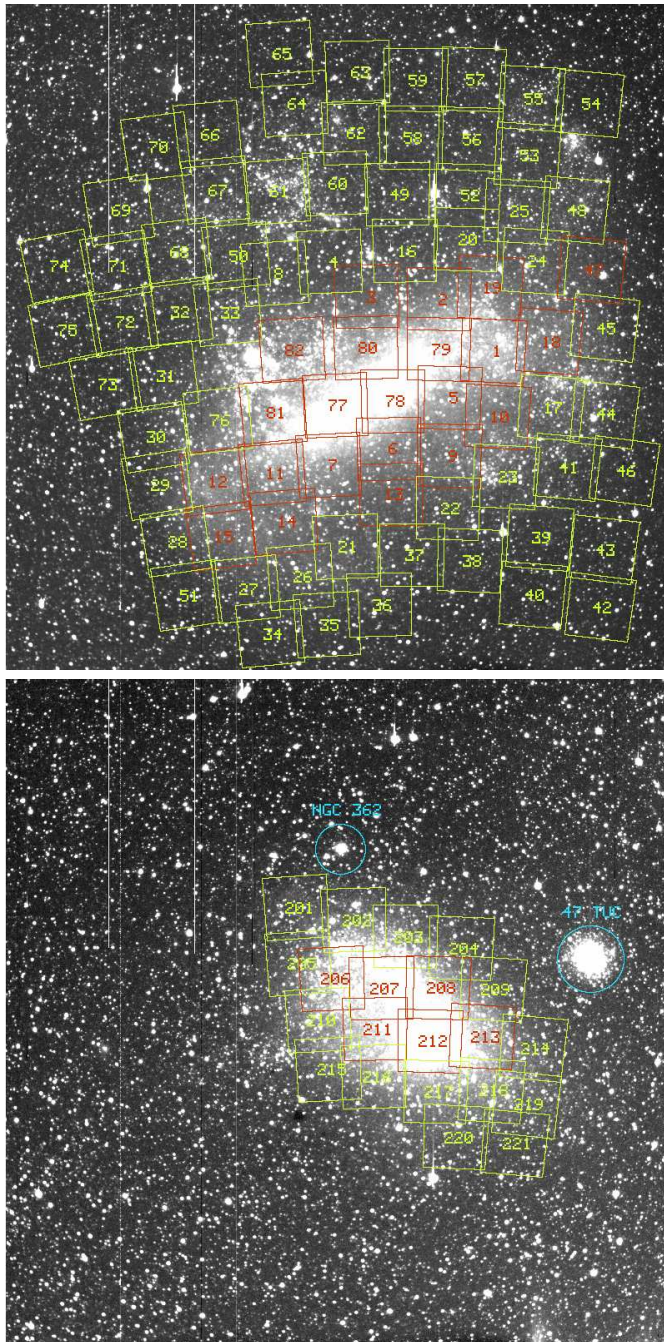
Figure 5.3: Top: *The LMC observed fields.* Bottom: *The SMC observed fields. Figure taken from the* MACHO *website* http://wwwmacho.anu.edu.au/.

5.2   Data analysis

M06 and M07 analysed spectroscopic data of a significant sample of B stars from the LMC and SMC, respectively, obtained with the ESO/VLT[4] FLAMES spectrograph[5] in MEDUSA mode. The stars studied in the SMC cluster NGC 330 by M07 are located in the MACHO field 207, and those studied in the LMC clusters NGC 2004 and EIS LMC 33 by M06 are located in the MACHO fields 60 and 61.

A total amount of 198 absorption-line B stars and 131 Be stars were studied in the SMC field NGC 330 by M07. The V magnitude of these selected targets ranges from 13.5 to 18.8 mag. Concerning the LMC, a total of 106 absorption-line B stars and 47 Be stars were studied by M06, with V magnitudes ranging from 13.7 to 17.8 mag. The targets of each sample were identified in the MACHO database using the coordinates given by M06 and M07 and downloaded using their MACHO *Field.Tile.Sequence* name. The data is given in ASCII column format. For the frequency analysis we extracted the columns containing the *time*, *R magnitude*, *B magnitude*, *R error* and *B error* information. In each light curve the datapoints with erroneous measurements were deleted. Our final SMC and LMC samples are summarised in Table 5.1 and explained in detail in the Subsections 5.2.2 and 5.2.3.

Table 5.1: *Final number of B and Be stars included in our SMC and LMC samples for the study of short-term variability.*

	B stars	Be stars
SMC	183	126
LMC	99	22

5.2.1   Fundamental parameters

To study the effects of metallicity and evolution on the appearance of the Be phenomenon in the B stars population, M06 and M07 observed several fields in

---

[4]The Very Large Telescope (VLT) at the European Southern Observatory (ESO): http://www.eso.org/public/teles-instr/vlt.html.

[5]Fibre Large Array Multi Element Spectrograph (see Pasquini et al. 2002, for details): http://www.eso.org/sci/facilities/paranal/instruments/flames/.

the LMC and SMC, respectively. Thanks to the FLAMES-GIRAFFE multi-fibres spectrograph on the ESO/VLT-UT2, the authors obtained spectra of 520 stars in the LMC-NGC 2004, LMC-EIS 33 and SMC-NGC330 regions using two settings at medium resolution: $R = 8\,600$ (for the red setting which contains Hα) and $R = 6\,400$ (for the blue setting which contains Hγ, Hδ, He I 4 026 Å, 4 388 Å and 4 471 Å). The latter setting was used to obtain fundamental parameters of the stars by fitting the observed spectrum with theoretical spectra.

M06 and M07 used the GIRFIT code (see Frémat et al. 2006, for details) to calculate the fundamental parameters of the selected stars: effective temperature (T_{eff}), surface gravity ($\log g$), projected rotational velocity ($V \sin i$) and radial velocity (RV) for each star of the samples. This procedure fits the observations with synthetic spectra interpolated in a grid of stellar fluxes computed with the SYNSPEC programme and from model atmospheres calculated with TLUSTY (Hubeny and Lanz 1995, see references therein) or/and with ATLAS9 (Kurucz 1993; Castelli et al. 1997). The grid of model atmospheres was computed with abundance adopted from Korn et al. (2002) for the LMC and from Jasniewicz and Thevenin (1994) for the SMC.

They took into account the effects of fast rotation (stellar flattening and gravitational darkening) for high rotating B stars and for all Be stars to correct their apparent fundamental parameters. The fast rotation makes the star more evolved and cooler than it is actually, as it is shown in Fig. 5.4 and Fig. 5.5 for the LMC and SMC, respectively. In order to correct for the gravity darkening and stellar flattening effects, M06 and M07 used the FASTROT code (Frémat et al. 2005) and derived the "parent non-rotating counterpart" (pnrc, see Frémat et al. 2005) stellar parameters ($T_{\mathrm{eff}}^{\mathrm{o}}$, $\log g_{\mathrm{o}}$ and $V \sin i^{\mathrm{true}}$) for a given Ω/Ω_c. The ratio of the mean angular velocity to the breakup velocity (Ω/Ω_c) for each sub-sample of Be stars in the MCs was calculated using the formula given in Chauville et al. (2001) and M06. M07 derived the mean value of Ω/Ω_c for B and Be stars in the LMC and SMC, the results are presented in Table 5.2.
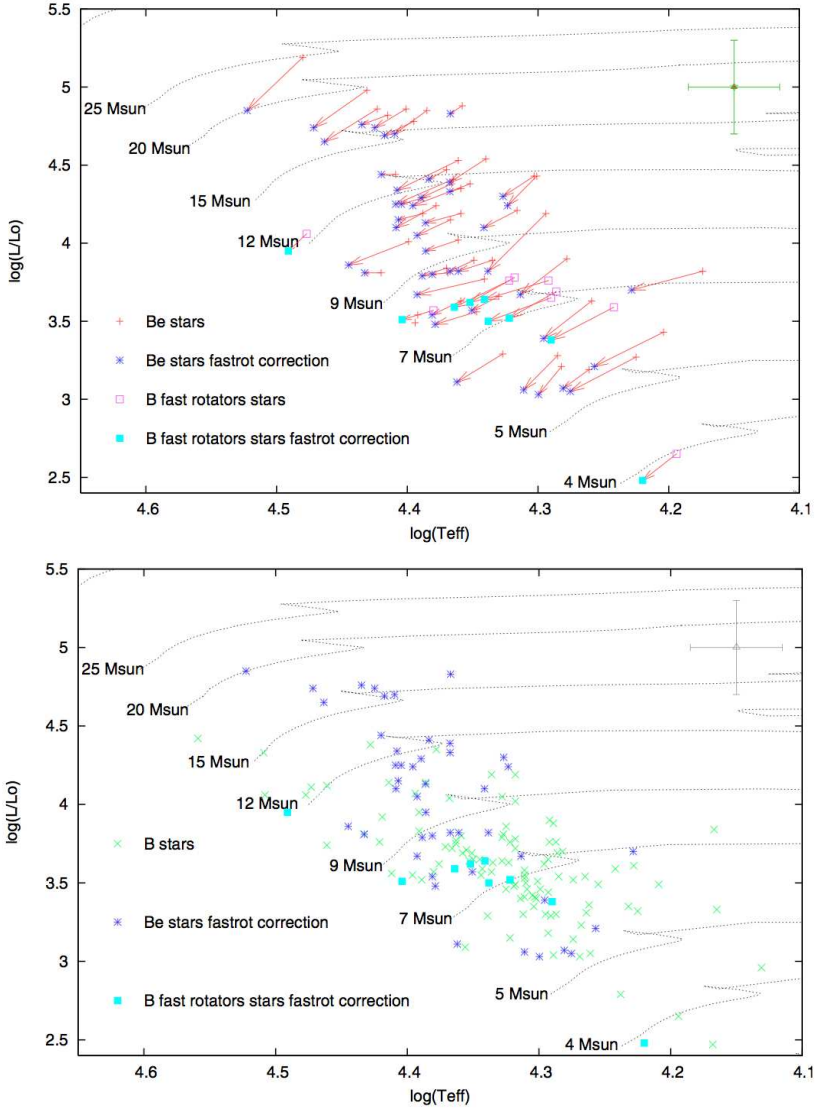
Figure 5.4: *H-R diagrams for the studied LMC B stars, including rapid rotators, and for Be stars in* M06. *Top: the effects of fast rotation are taken into account with* $\Omega/\Omega_c = 85\%$ *for Be stars and rapidly rotating B stars. Bottom: B stars and fast rotators (Be and B stars) corrected for their fast rotation.* Common: *the adopted metallicity for the LMC comes from* Korn et al. (2002) *and* Rolleston et al. (1996). *Green "×" represent B stars, red "+" represent Be stars with their apparent parameters, and blue "∗" Be stars corrected with* FASTROT *with* $\Omega/\Omega_c = 85\%$. *Pink empty squares represent rapidly rotating B stars with their apparent parameters, and filled blue squares, rapidly rotating B stars corrected with* FASTROT *with* $\Omega/\Omega_c = 85\%$. *Typical error bars are shown in the upper right corner of the figure. Figure taken from* M06.
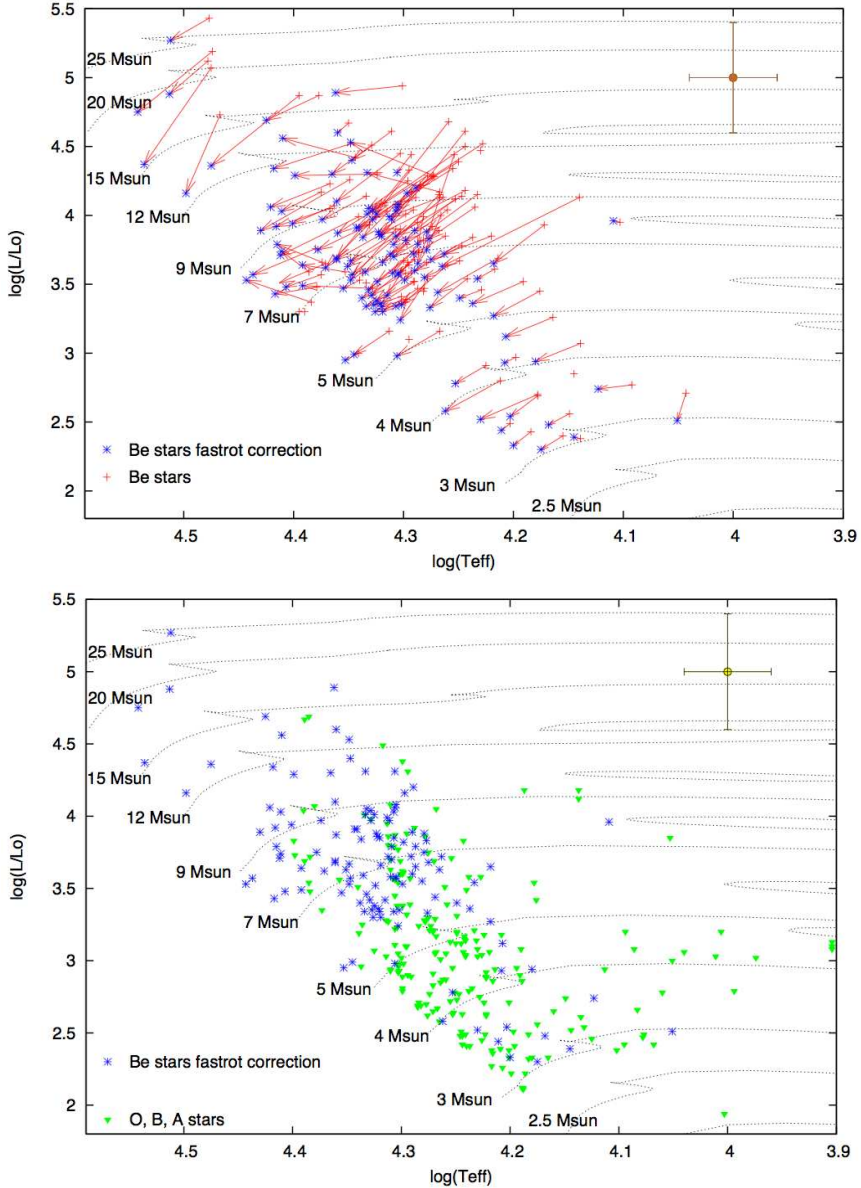
Figure 5.5: *H-R diagrams for the SMC B and Be stars studied in M07. Top: The effects of fast rotation are taken into account with $\Omega/\Omega_c = 95\%$ for Be stars. Bottom: B stars and fast rotators (Be stars) corrected for their fast rotation. Common: The adopted metallicity for the SMC is $Z = 0.001$. Red "+" represent Be stars with their apparent parameters, blue "$*$" Be stars corrected with FASTROT with $\Omega/\Omega_c = 95\%$, and green triangles B stars. Typical error bars are shown in the upper right corner of the figure. Evolutionary tracks come from Schaller et al. (1992). Figure taken from M07.*

Table 5.2: Ω/Ω_c *ratios for the MCs samples obtained by* M06 *and* M07.

	LMC	SMC
Metallicity	0.007	0.002
Ω/Ω_c (B stars)	37%	58%
Ω/Ω_c (Be stars)	85%	95%

Concerning the rotational velocities between the SMC, LMC and the MW, both studies, M06 and M07, revealed an increase in $V \sin i$ with decreasing metallicity in B and Be stars populations. This trend was already observed by Maeder et al. (1999) in open clusters. These is an important key that we will discuss in the forthcoming Chapters. For more details we refer to M06 and M07 and references therein.

We refer the interested reader to M06 and M07 to retrieve the complete list of parameters for the selected targets. In the forthcoming Chapters we only mention the targets for which variability has been found.

5.2.2 The SMC sample

Among the initial sample of B stars, composed by 198 targets, four are not included in the MACHO database and eight more do not have measured errors in their photometry. From the remaining 186 stars, we consider three to be Be stars, since they show outbursts in their light curves (207.16317.116 and 207.16203.94) or long-term quasi-periodic variations (207.16204.182). These characteristics are typical of Be stars. The transient nature of the Be phenomenon can explain the non-detection by M07 of the Hα emission in these three stars. Therefore, the final sample of absorption-line B stars for which we have performed the frequency analysis is composed of 183 stars.

The initial sample of Be stars given in M07 is composed of 131 objects. Two of them are not present in the MACHO database, and two more do not have measured errors. On the other hand, we have added the three stars considered to be Be stars as explained in the above paragraph. Therefore, our sample of Be stars with MACHO photometry consists of 130 objects. Among them, four present a

very complex long-term light curve, with bursting behaviour and irregular high-amplitude variations, which prevents the search for short-term variability. The final Be star sample for which we have performed frequency analysis is hence composed of 126 stars.

5.2.3   The LMC sample

Among the initial sample of 106 B stars, the MACHO photometry of five of them is affected by poor data sampling or erroneous measurements. Two more objects present light curves with complex irregular variations. Due to the transitory nature of the Be phenomenon these two objects may be in fact Be stars that did not show emission at the time of M06 observations. The time series for all these objects do not allow accurate frequency analysis, and they have not been considered for further study within this work. The final sample of B stars to be analysed is thus reduced to 99 objects.

The initial Be star sample consists of 47 objects. Among them, eight targets show poor photometric data and erroneous measurements and were removed from the sample. Moreover, we dismiss 17 objects showing outbursts and/or complex irregular variations that cannot be removed with a polynomial fitting. The shape of their light curves is too complex and together with the poor sampling prevents us from performing the Fourier analysis. Therefore, the final Be star sample for the frequency analysis is reduced to 22 objects.

In Fig. 5.6 we show the distribution of both final object samples as a function of their spectral type for the LMC and SMC. The spectral classification has been taken from M07 (for the SMC) and from M06 (for the LMC). Note that in our LMC samples the majority of the stars have spectral types B3 or earlier. This is due to the fact that the late B-type stars are much fainter and difficult to observe at the LMC distance.
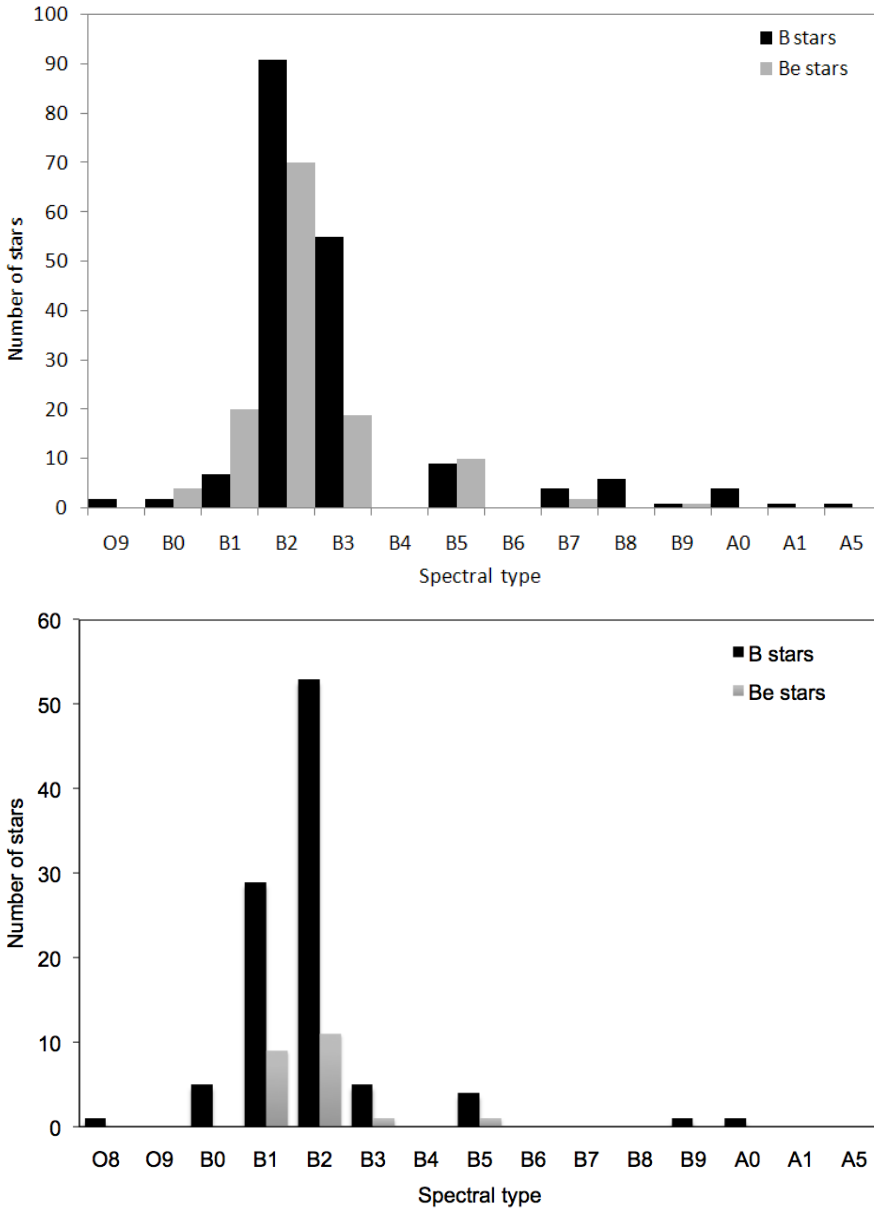
Figure 5.6: *Distribution of OAB and Be star samples for the SMC* (top) *and LMC* (bottom) *as a function of their spectral types.*

5.2.4 Frequency analysis

The search for periodic variability has been done by analysing the photometric time series retrieved from the MACHO Project. As mentioned above, the MACHO Project provides photometric instrumental magnitude for each star in two contiguous "blue" and "red" passbands, which we label as B and R in the following. The light curves have an average of 1 000 data points spanning 2 690 days. Two light curves of Be stars are depicted in Fig. 5.7 for the SMC and the LMC.

The frequency analysis was performed in both B and R datasets using standard Fourier techniques and linear least-squares fitting implemented in the code PASPER (Diago et al. 2008a). Then, the significant frequencies were improved with the non-linear least-squares methods BOSSIRR and KURTZ_BOS. Finally, amplitudes, phases and S/N for the improved frequencies were calculated. For a more details in the frequency analysis process we refer to Chapter 3. As an example, in Fig. 5.8 we depict the periodograms computed with PASPER for two Be stars from the SMC and LMC. A typical 1-day alias pattern is present in the spectral window of the MACHO data, since the observations were obtained at only one site.

The resolution in frequency for the majority of the stars of the SMC and LMC is $\sim 3.7 \times 10^{-4}$, following the Rayleigh criterion. The uncertainty on the detected frequencies is $1 - 5 \times 10^{-5}\,\mathrm{c\,d^{-1}}$ for the SMC sample and $\sqrt{3} \times 10^{-5}\,\mathrm{c\,d^{-1}}$ for the LMC sample. This value has been derived analytically using the formula given by Montgomery and O'Donogohue (1999), and taking into account the correlations in the residuals, as described by Schwarzenberg-Czerny (1991) (see Chapter 3 for more details).
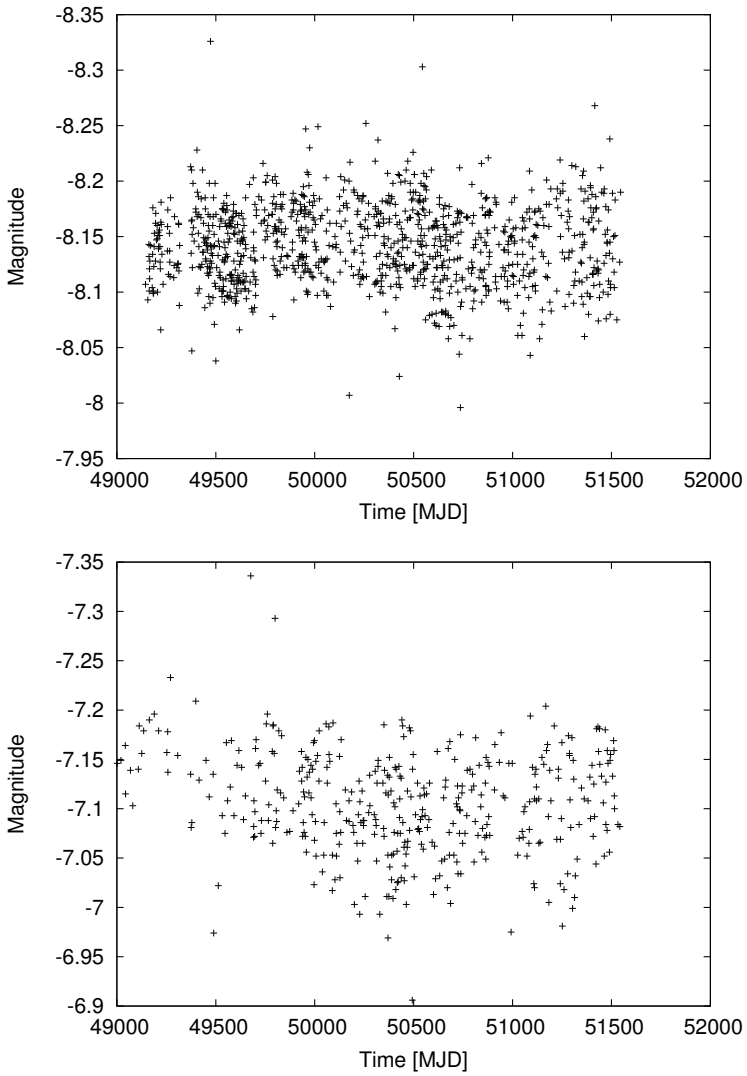
Figure 5.7: Left: *Light curve for the SMC Be star* 207.16262.58 *in the B filter.* Right: *Light curve for the LMC Be star* 61.8192.204 *in the B filter. The time scale is refereed to the modified Julian Day* (MJD) *that it is defined by the expression* MJD = JD - 2 400 000.5.
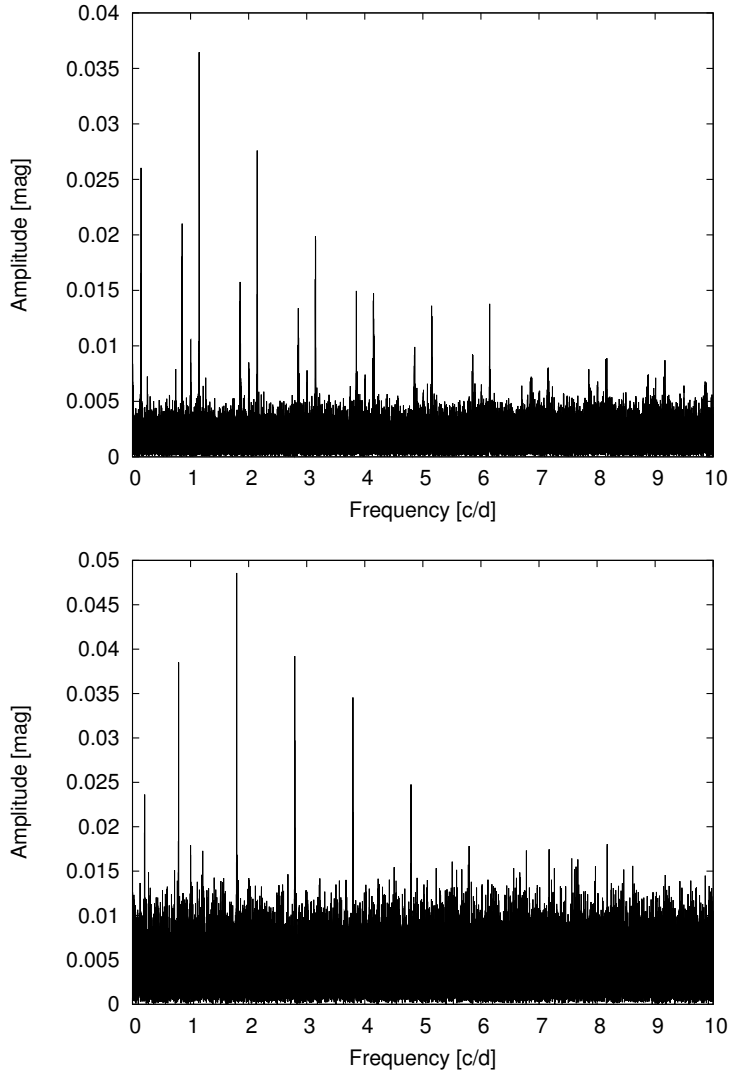
Figure 5.8: Left: *Periodogram for the SMC Be star* 207.16262.58 *in the B filter.* Right: *Periodogram for the LMC Be star* 61.8192.204 *in the B filter. The frequencies with more amplitude correspond to* $1.14 \, \mathrm{c \, d^{-1}}$ *for the SMC Be star and* $1.79 \, \mathrm{c \, d^{-1}}$ *for the LMC Be star. A common feature in our study is that the analysed stars from the SMC have better signal to noise ratios than those analysed in the LMC, as we can see in this picture.*

Sitting in an English garden, waiting for the Sun.
If the Sun don't come, you get a tan
From standing in the English rain.

John Lennon

6

Study in the Small Magellanic Cloud

As pointed in Chapter 4, the first aim of the study of B-type pulsations in the MCs is to search for short-term periodic variability in a significant sample of B and Be stars from the SMC and the LMC, for which the fundamental physical parameters were accurately calculated. This Chapter contains the results and the conclusions for the SMC B-type star samples. The samples and the data analysis have been described in the previous Chapter. The results on the SMC samples have been also published in Diago et al. (2008a, hereafter D08). Some of the Be stars studied here were previously analysed by Gutiérrez-Soto (2006, Ph.D. thesis and references therein).

6.1 Results

In this Section we present the results of the search of variability performed on the two samples of B and Be stars described above. A summary of these results is shown in Table 6.1.

Table 6.1: *Results of the variability search in the B and Be star samples for the SMC.*

	B stars	Be stars
Number of stars	183	130
Short-period variables	9	32
- single period	7	12
- multiple periods	2	20
Long-period variables	0	6
Eclipsing Binaries	3	1
Outburst/Irregular variability	0	5

6.1.1 Short-term variability

As mentioned in Chapter 2, we consider as short-period variations those with frequencies higher than $0.3\,\mathrm{c\,d^{-1}}$. In the sample of 183 absorption-line B stars we have found nine short-period variables. Two among them are multiperiodic. In the sample of Be stars, 126 have been analysed for short-term variability. A total of 32 Be stars have been found to be short-period variables, 20 among them being multiperiodic.

The detected frequencies with their amplitudes and phases for B and Be stars are presented in Tables 6.3 and Table 6.4, respectively. The targets detected variable are sorted by their EIS[1] identification name. The phase diagrams for each star folded with the detected frequencies are depicted in Fig. E.1 and Fig. E.2 to Fig. E.5 for B and Be stars respectively, available in the Appendix E.

---

[1] The ESO Imaging Survey (EIS) project is an ongoing effort to carry out public imaging surveys in support of VLT programmes. Background information on the original and future goals of the programme can be found in Renzini and da Costa (1997) and in a companion article by Renzini and da Costa (1999), both in The Messenger Journal.

Table 6.2: *Stars in the SMC sample showing the beating phenomenon. The beat frequencies are given in* $c\,d^{-1}$ *in cols. 4 and 5.*

| Star iD | | Sp. T. | Beat frequency | |
MACHO iD	EIS iD		B filter	R filter
207.16318.77	SMC5_004326	B	0.04841	-
207.16373.129	SMC5_016544	Be	0.05780	0.05790
207.16147.14	SMC5_021152	Be	0.01928	0.01926
207.16259.35	SMC5_045353	Be	0.02876	-

The amplitude variation due to the beating of two close frequencies is clearly seen in the light curves of four multiperiodic variables, when folded with the difference of the two frequencies. This effect is clearly seen in Fig. 6.1, for the star 207.16373.129, which is an example of a phase diagram folded with the beat frequency ($F_1 - F_2 = 0.057798\,c\,d^{-1}$ in this case). The plots of the complete set of stars showing this pattern and the list of the beat frequencies are presented in Fig. 6.2 and Table 6.2, respectively. The presence of the beating phenomenon confirms the existence of close frequencies in these stars.
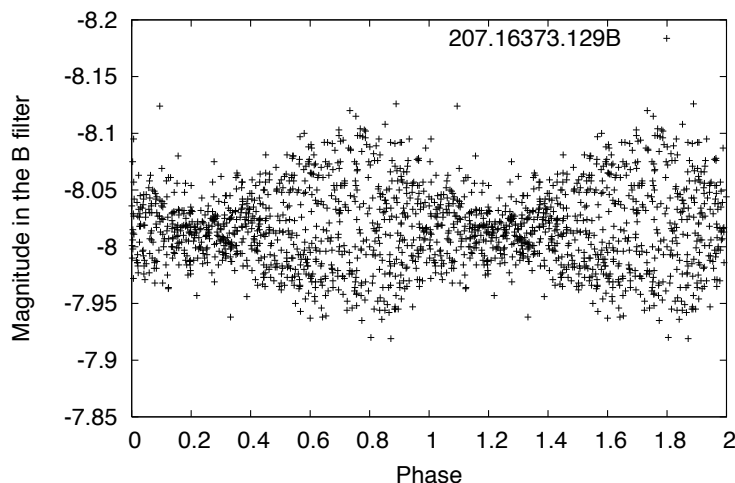
Figure 6.1: *Phase plot of the star* 207.16373.129 *in the B filter folded with the beat frequency* $(0.057798\,c\,d^{-1})$. *This indicates the presence of close frequencies with similar amplitudes.*

Table 6.3: *Pulsational characteristics of short-period variable absorption-line B stars in the SMC. We only present the frequencies detected with significant SNR. The symbol "-" indicates that the S/N for the detected frequencies in this filters are not enough to reach our criterion and they are not considered as significant frequencies. The targets are sorted by the* EIS *identification name.*

Star iD				B filter			R filter		
MACHO iD	EIS iD	Sp. T.	$V \sin i$ $[\mathrm{km\,s^{-1}}]$	Freq $[\mathrm{c\,d^{-1}}]$	Amp [mmag]	Phase [rad]	Freq $[\mathrm{c\,d^{-1}}]$	Amp [mmag]	Phase [rad]
207.16318.77	SMC5_004326	B1V	373 ± 30	3.63947	7.65	4.19	3.63950	9.23	4.09
				3.68789	6.52	4.76	-	-	-
207.16376.31	SMC5_004988	B2IV	134 ± 10	0.59378	6.14	3.42	0.59378	6.09	3.22
207.16374.240	SMC5_020451	B2V	243 ± 36	0.86186	21.69	5.90	-	-	-
207.16147.27	SMC5_038033	B2IV	76 ± 10	0.59241	15.14	0.61	0.59236	10.24	0.84
207.16376.49	SMC5_038311	B2IV	196 ± 30	0.59104	6.85	2.67	-	-	-
207.16375.56	SMC5_050662	B2IV	161 ± 24	1.19411	36.73	0.61	1.19410	39.20	0.67
				0.59707	12.79	1.06	0.59705	15.02	1.00
207.16318.27	SMC5_051147	B2IV	246 ± 25	1.31646	26.10	6.08	1.31647	26.90	6.04
207.16204.70	SMC5_052147	B2V	126 ± 13	1.04202	17.45	3.14	1.04196	14.91	3.68
207.16376.188	SMC5_087022	B2V	145 ± 22	0.55267	13.27	5.70	-	-	-

Table 6.4: *Pulsational characteristics of short-period variable Be stars in the SMC. We only present the frequencies detected with significant SNR. The symbol "-" indicates that the S/N for the detected frequencies in this filters are not enough to reach our criterion and they are not considered as significant frequencies. The targets are sorted by the* EIS *identification name. The* $V \sin i^{\mathrm{true}}$ *value is the observed* $V \sin i^{\mathrm{app}}$ *value corrected from fast rotation assuming* $\Omega/\Omega_c = 95\%$ *(see M07, for details).*

Star iD				B filter			R filter		
MACHO iD	EIS iD	Sp. T.	$V \sin i^{\mathrm{true}}$	Freq	Amp	Phase	Freq	Amp	Phase
			$[\mathrm{km\,s^{-1}}]$	$[\mathrm{c\,d^{-1}}]$	[mmag]	[rad]	$[\mathrm{c\,d^{-1}}]$	[mmag]	[rad]
207.16318.32	SMC5_000643	B3IVe	301 ± 28	3.69095	4.76	3.83	-	-	-
				1.65525	4.63	2.80	1.65555	8.86	0.68
207.16372.22	SMC5_002232	B2IIIe	261 ± 17	1.32656	25.31	6.17	1.32661	33.51	5.59
				1.32620	14.97	1.27	1.32616	18.03	1.88
207.16375.39	SMC5_004201	B5II-IIIe	550 ± 72	1.69005	45.88	2.16	1.69039	79.76	6.05
				1.69052	30.58	4.24	1.69050	55.69	2.25
				1.69086	24.53	4.76	1.68997	28.21	2.34
207.16315.67	SMC5_011991	B2IVe	207 ± 31	2.30208	4.38	1.01	-	-	-
207.16373.58	SMC5_013978	B3IIIe	311 ± 37	1.37946	15.50	0.48	1.37948	14.15	0.06
				0.59335	14.36	2.93	0.59336	15.42	2.78
207.16259.29	SMC5_014212	B2IIIe	229 ± 11	1.27691	23.48	4.91	1.27693	15.75	4.90
207.16259.30	SMC5_014271	B0IIIe	559 ± 35	4.16878	7.33	1.67	-	-	-
				4.08090	5.84	2.59	-	-	-
				4.24210	5.51	2.10	-	-	-
207.16373.63	SMC5_014727	B2IVe	333 ± 32	1.12290	16.65	4.04	-	-	-

Continues on next page...

... continued from Table 6.4.

MACHO iD	EIS iD	Sp. T.	$V \sin i^{\mathrm{true}}$ [km s^{-1}]	Freq [c d^{-1}]	Amp [mmag]	Phase [rad]	Freq [c d^{-1}]	Amp [mmag]	Phase [rad]
207.16259.41	SMC5_014878	B2IIIe	442 ± 20	3.50858	18.93	4.12	3.50877	8.79	2.36
				3.50846	11.90	2.59	-	-	-
207.16316.30	SMC5_016523	B2IIIe	454 ± 43	1.29297	40.29	0.93	1.29296	33.43	0.95
				1.29344	23.68	3.80	1.29341	20.92	3.90
207.16373.129	SMC5_016544	B2IVe	357 ± 34	1.70768	29.54	3.27	1.70776	32.97	2.46
				1.65011	22.46	1.32	1.64988	24.58	3.08
				1.64959	11.36	6.23	1.65029	12.90	0.41
207.16147.14	SMC5_021152	B2IIIe	218 ± 10	0.98514	19.25	2.55	0.98513	17.08	2.67
				1.00442	19.06	4.45	1.00439	17.01	4.67
207.16262.86	SMC5_025718	B2IIIe	280 ± 17	0.85851	16.26	3.86	0.85847	13.61	4.06
207.16376.43	SMC5_025829	B2III-IVe	286 ± 17	0.85031	7.56	2.25	0.85019	13.93	2.46
207.16205.141	SMC5_026689	B2Ve	425 ± 59	3.82424	10.24	5.79	-	-	-
207.16315.26	SMC5_037013	B2IIIe	148 ± 10	1.18149	15.70	2.17	1.18154	20.06	1.73
				1.21712	10.64	0.18	1.21707	9.48	0.14
				1.18116	8.39	0.01	1.18113	5.75	0.09
207.16373.30	SMC5_037137	B2IIIe	301 ± 10	-	-	-	0.38864	6.29	3.44
207.16316.99	SMC5_037158	B1IVe	448 ± 60	3.79973	16.21	1.90	-	-	-
				3.80111	12.79	2.51	-	-	-
				3.80020	12.34	2.92	-	-	-

Continues on next page...

MACHO iD	EIS iD	Sp. T.	$V \sin i^{\mathrm{true}}$ [km s^{-1}]	Freq [c d^{-1}]	Amp [mmag]	Phase [rad]	Freq [c d^{-1}]	Amp [mmag]	Phase [rad]
				3.80187	9.79	4.37	-	-	-
207.16259.57	SMC5_037162	B2IIIe	386 ± 55	0.88531	37.31	4.92	0.88532	39.17	4.79
				0.90613	19.21	5.61	0.90622	17.71	4.65
207.16315.41	SMC5_043413	B2IVe	294 ± 41	2.00731	6.74	2.21	2.00709	6.21	2.84
207.16373.132	SMC5_044898	B2III-IVe	418 ± 19	1.19626	15.28	0.14	1.19627	18.32	6.21
207.16259.35	SMC5_045353	B2IIIe	343 ± 10	0.59169	33.01	2.11	0.59168	42.01	2.26
				0.56293	8.65	2.46	-	-	-
				1.33684	7.26	4.94	-	-	-
207.16431.1732	SMC5_048047	B2IVe	238 ± 11	0.60530	5.86	5.52	0.60544	5.45	4.77
				1.15074	5.17	2.97	1.15909	4.86	4.01
207.16147.29	SMC5_049996	B2IIIe	490 ± 30	1.09797	18.75	2.68	1.09796	20.05	2.71
				1.00391	16.19	0.82	1.00394	18.70	0.59
207.16373.51	SMC5_064327	B3II-IIIe	312 ± 14	1.05025	9.19	0.54	-	-	-
207.16147.28	SMC5_074402	B2IIIe	437 ± 20	1.54904	5.30	0.88	-	-	-
				1.54956	4.96	3.75	-	-	-
207.16203.94	SMC5_079021	B2IV	-	3.48747	10.28	0.53	3.48753	8.47	2.19
				3.45715	4.19	2.89	-	-	-
207.16262.58	SMC5_080910	B2IVe	334 ± 15	1.14776	37.35	1.87	1.14771	38.84	1.93
				1.14806	11.65	4.34	-	-	-

... continued from Table 6.4.

MACHO iD	EIS iD	Sp. T.	$V \sin i^{\mathrm{true}}$ [km s^{-1}]	Freq [c d^{-1}]	Amp [mmag]	Phase [rad]	Freq [c d^{-1}]	Amp [mmag]	Phase [rad]
207.16375.41	SMC5_082042	B3IIIe	433 ± 22	2.48838	19.06	4.87	2.48833	12.10	5.37
				1.16624	16.80	2.66	1.16627	11.60	2.54
207.16373.24	SMC5_082819	B2IIIe	340 ± 10	-	-	-	0.38869	7.35	3.15
207.16203.47	SMC5_082941	B3IIIe	359 ± 16	0.62490	38.75	1.23	0.62499	26.85	0.66
				0.62470	17.16	2.73	0.62471	25.60	2.54
				0.15325	11.47	5.86	0.15325	8.00	5.86
207.16319.58	SMC5_086251	B2IVe	314 ± 19	4.12332	10.33	1.49	-	-	-
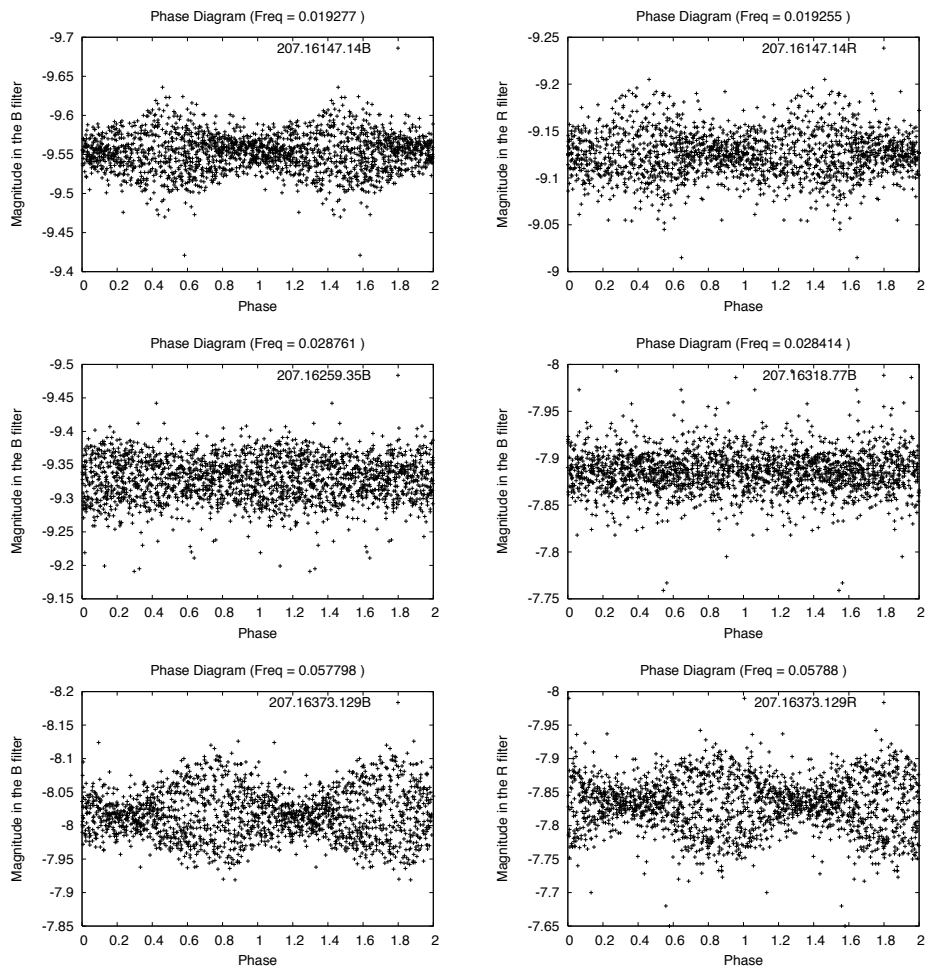
Figure 6.2: *Phase plots of the stars in the SMC showing the beating phenomenon.*

6.1.2   Long-term variability

In addition to the short-term variability, we have found periodic or quasi-periodic variations with frequencies lower than $0.333\,\mathrm{c\,d^{-1}}$ for six Be stars. The frequencies, amplitudes and phases are presented in Table 6.5. The folded light curves are depicted in Fig. 6.3.

Table 6.5: *Long-period variable Be stars in the SMC. We only present the frequencies detected with significant SNR. The symbol "-" indicates that the S/N for the detected frequencies in this filters are not enough to reach our criterion and they are not considered as significant frequencies. The targets are sorted by the* EIS *identification name.*

Star iD		B filter			R filter		
MACHO iD	EIS iD	Period [d]	Amp [mmag]	Phase [rad]	Period [d]	Amp [mmag]	Phase [rad]
207.16375.57	SMC5_004509	4.67	13.08	1.08	-	-	-
207.16316.21	SMC5_016461	27.16	88.80	5.84	27.15	85.46	5.57
207.16258.73	SMC5_041410	961.54	16.28	5.99	823.05	36.79	3.86
207.16319.11	SMC5_052688	8.13	5.06	6.02	-	-	-
207.16376.22	SMC5_078440	1162.79	117.32	1.16	1129.94	210.84	0.84
207.16204.182	SMC5_082379	9.73	10.96	2.54	9.73	16.12	2.81

One of these stars, 207.16316.21, has been discussed by Martayan et al. (2007a), who showed that it is an spectroscopic binary, and interpreted the light curve as produced by ellipsoidal variability.
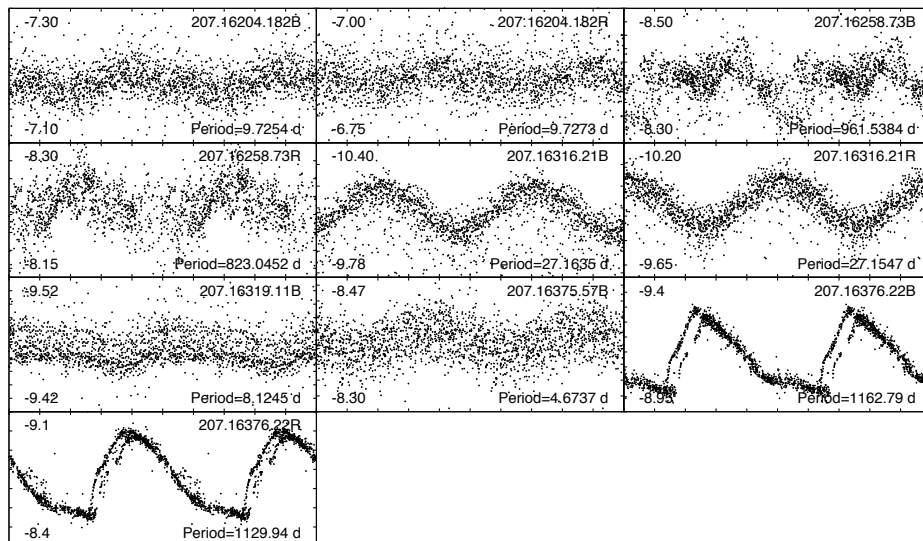
Figure 6.3: *Phase plots of the Be SMC stars showing long-term periodic variability. Phases span from 0 to 2. Magnitude range in the B or R filter is denoted inside each panel in the left side. In the right lower corner we show the period in* days.

6.1.3 Eclipsing binaries

The light curves of three absorption-line B and one Be stars are characteristic of eclipsing binaries. Periods for each binary star are listed in Table 6.6. Phase diagrams are depicted in Fig. 6.4 and Fig. 6.5 for B and Be stars respectively.

Table 6.6: *Eclipsing binaries in the SMC. Periods are given in days.*

MACHO iD	EIS iD	Sp. Type	Period
207.16203.296	SMC5_003809	B	0.8817
207.16318.41	SMC5_004534	B	4.0513
207.16316.160	SMC5_015429	Be	0.6523
207.16205.114	SMC5_053563	B	1.0148
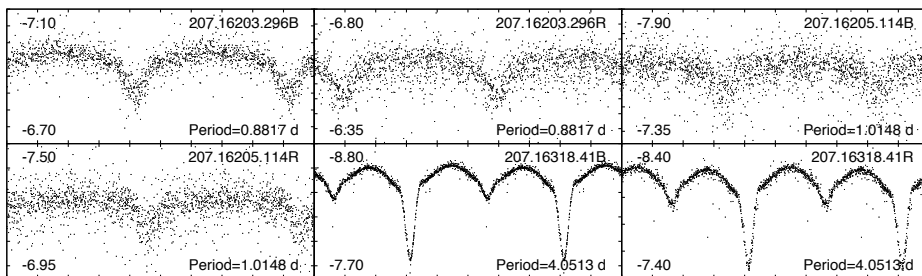
Figure 6.4: *Phase plots of eclipsing binaries in the sample of B stars. Axes and labels as in* Fig. 6.3.
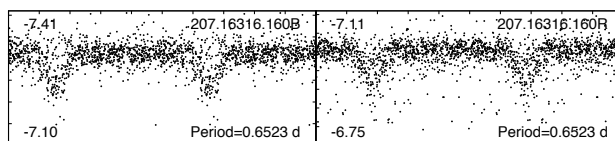
Figure 6.5: *The same as* Fig. 6.4 *for an eclipsing Be star. Axes and labels as in* Fig. 6.3.

6.1.4   Irregular variability

We have found a total of five Be stars showing outbursts or irregular variations, names depicted in Table 6.7. In four of them these variations prevented us from performing the frequency analysis to search for short-term variability, as stated before. In Fig. 6.6 we show the irregular light curves of these Be stars.

The star 207.16203.94 presents a photometric outburst at the end of the MA-CHO light curve. The data before the outburst does not show significant irregular variability, and therefore we have been able to perform frequency analysis using only the first part of the light curve. Short-period multiperiodic variability has been detected, see Table 6.4.

Table 6.7: *SMC Be stars showing irregular variability or outbursts.*

MACHO iD	EIS iD
207.16373.88	SMC5_073581
207.16317.116	SMC5_074305
207.16203.94	SMC5_079021
207.16372.13	SMC5_190576
207.16204.11	SMC5_744471
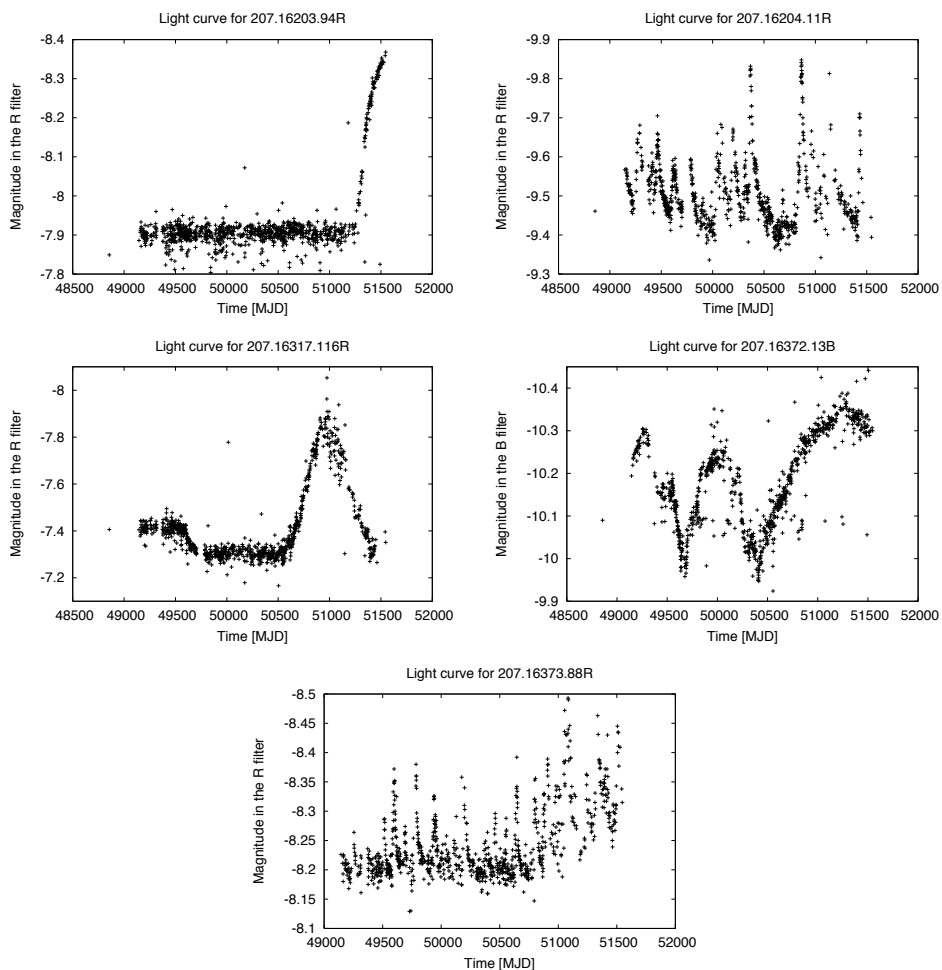
Figure 6.6: *Light curves of SMC Be stars showing outbursts and/or irregular variability. The time scale is refereed to the modified Julian Day (MJD) that it is defined by the expression* MJD = JD - 2 400 000.5.

6.2 Discussion

As mentioned in Chapter 2, the variability seen in Be stars can be produced by non-radial pulsations or/and rotational modulation. It is difficult to distinguish between them, specially for stars showing only one period in their variations. However, in order to have inhomogeneities in the photosphere we need the existence of a magnetic field, that has not been detected so far in any Be star. In addition, as the external layers of the Be stars are completely radiative, it implies that the magnetic field should be very rare. On the other hand, the theoretical models that support non-radial pulsations as the origin of these variations are more reliable. Therefore, in the following we assume that the detected short-term variability is produced by pulsations.

6.2.1 Pulsating B stars

We have found nine short-period variable absorption-line B stars. Their pulsational characteristics are presented in Table 6.3. In Fig. 6.7 we have represented their positions in the theoretical H-R diagram. The values of $\log T_{\mathrm{eff}}$ and $\log L/L_{\odot}$, as well as the spectral type and $V \sin i$, have been taken from M07. For comparison, we have also represented the theoretical boundaries of the β Cephei and SPB instability strips and the ZAMS line for solar metallicity. All pulsating B stars are restricted to a narrow range of temperatures, between $\log T_{\mathrm{eff}} = 4.24$ and $4.39 \, \mathrm{K}$.

In the bottom panel of Fig. 6.8 we display the period distribution of β Cephei and SPB stars in the Galaxy, from Stankov and Handler (2005) and de Cat (2002), respectively. In the top panel we have represented the period distribution of our sample of pulsating B stars in the SMC. All stars but one have periods longer than 0.5 days, characteristic of SPB stars. Star 207.16318.77 has two close periods in the range of the p-mode pulsators in the Galaxy. In addition, it is the hottest star in our sample ($\log T_{\mathrm{eff}} = 4.39 \, \mathrm{K}$). Thus, we propose that this star is a candidate to be a β Cephei variable in the SMC. In Fig. 6.9 we display the phase diagram folded with the two detected frequencies for this star together with the
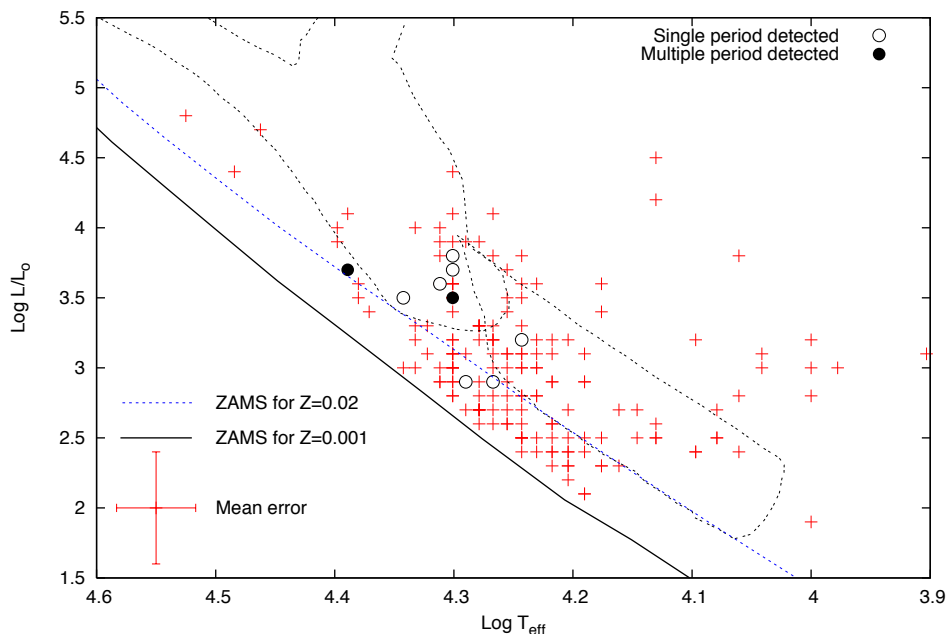
Figure 6.7: *Location of the B star sample in the theoretical H-R diagram. Single crosses represents stars in our sample, the void circles represents single period detection and filled ones multiple period detection. The β Cephei and the SPB boundaries (dashed lines) at solar metallicity have been taken from* Pamyatnykh (1999, *the upper region corresponds to β Cephei variables and the lower one to the SPB star variables, see* Fig. 1.9 *for details). The ZAMS at solar and SMC metallicity are from* Schaller et al. (1992).

periodogram derived from the frequency analysis. It should be noted, however, that the periods found are somewhat too long in order to correspond to p-modes of a little evolved star. This may well be a high-order g-mode pulsator, i.e. a SPB star. If this is the case, the SPB instability strip in the SMC is considerably shifted towards higher temperatures than predicted by the current models, as discussed in more detail below.

In addition, 207.16318.77 has a large rotational velocity $V \sin i = 370 \pm 30 \, \mathrm{km \, s^{-1}}$, while most β Cephei stars in the Galaxy are known to be slow rotators (Stankov and Handler 2005). However, these authors include in their list several fast-rotating bona fide β Cephei stars. They also suggest that the fact that most
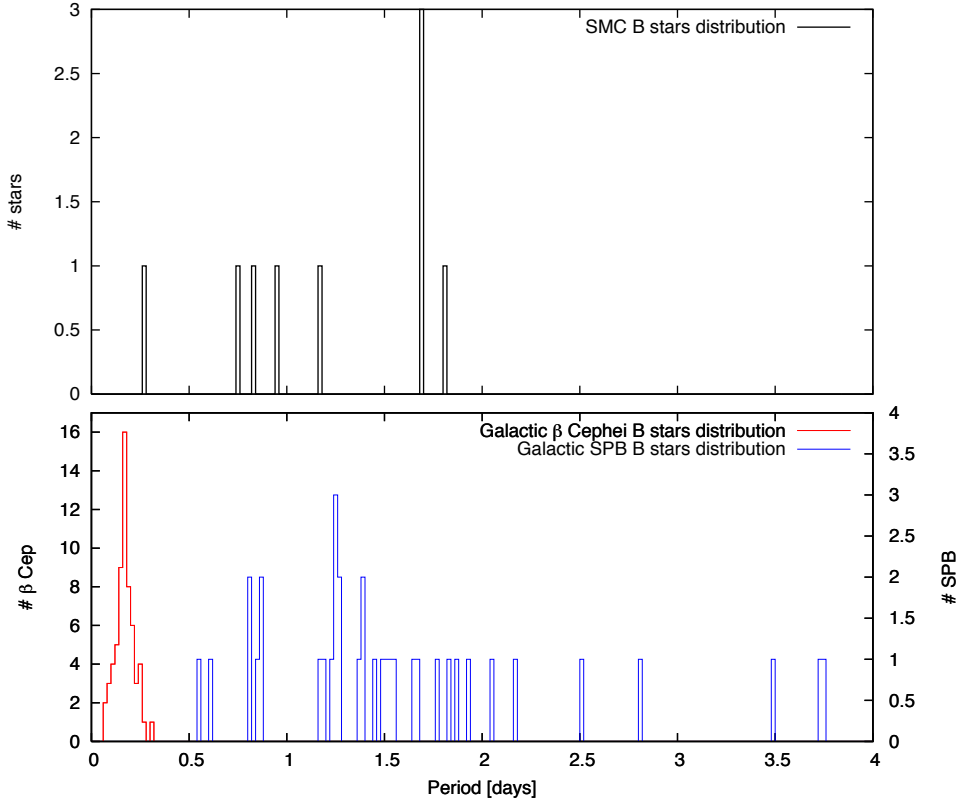
Figure 6.8: *Period distribution of the pulsating B stars found in our SMC sample* (top panel) *compared to the galactic β Cephei and SPB period distributions* (bottom panel). *All stars in our sample but one have periods longer than* 0.5 d, *characteristic of SPB stars.*

β Cephei stars are slow rotators can be a selection effect, as the highest-amplitude pulsators have the lowest rotational velocities.

If 207.16318.77 is indeed a β Cephei star, this would constitute an unexpected result, as the current stellar models does not predict *p*-mode pulsations at the SMC metallicity. However, as the assumed SMC metallicity is an average value, this particular case might correspond to a star with a higher metal content. A spectroscopic determination of its metallicity would be of great value to conclude on this issue.
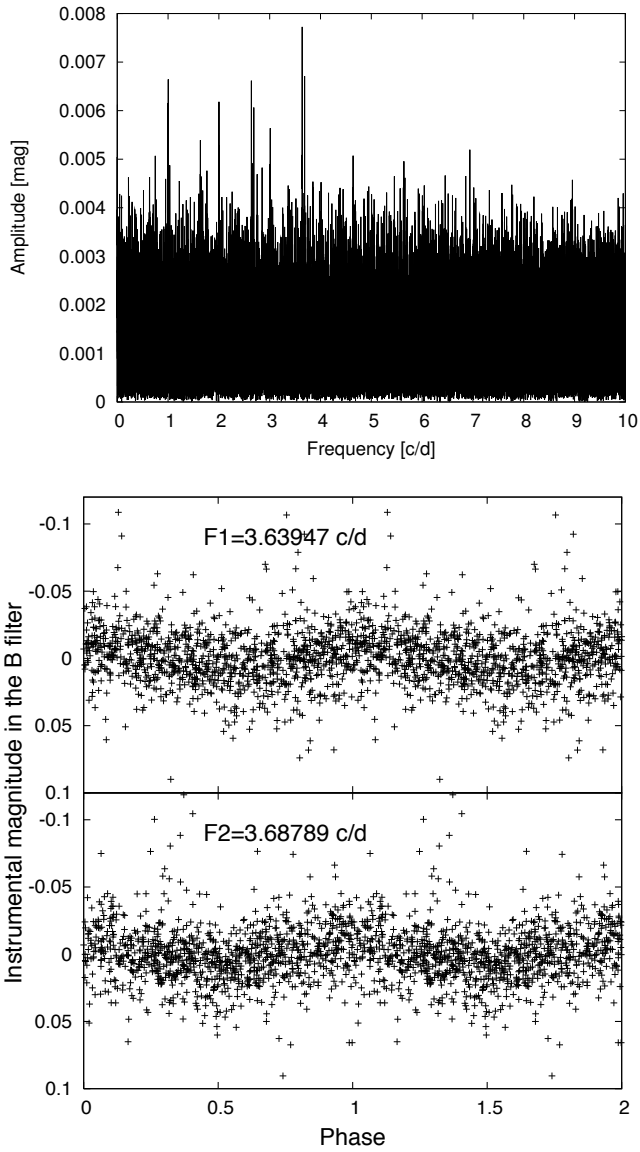
Figure 6.9: *Periodogram* (top) *and phase diagram* (bottom) *of the SMC β Cephei star* 207.16318.77 *folded with the two detected frequencies.*

The eight remaining pulsating stars in our sample are SPB variables. They are located in the main sequence of the H-R diagram, in the temperature range between $\log T_{\text{eff}} = 4.24$ and $4.35\,\text{K}$ (see Fig. 6.10). The region containing all the SPB stars is depicted with a dashed line. The high temperature limit is shifted towards hotter temperatures with respect to the instability strip at solar metallicity, represented in Fig. 6.7. It is also placed at temperatures higher than the ones predicted by the new computations by Miglio et al. (2007b) for $Z = 0.005$. The low-temperature limit is most likely of observational origin, due to the fact that there are few stars with lower temperatures in our sample, and their photometry is less accurate because of their faintness. In Fig. 6.11 we display an example of the phase diagrams corresponding to a multiperiodic SPB star together with the frequency spectrum. A puzzling circumstance regarding our sample of SPB stars is that none of them but one have been detected as multiperiodic. The only multiperiodic object has a secondary period which is exactly twice the pri-
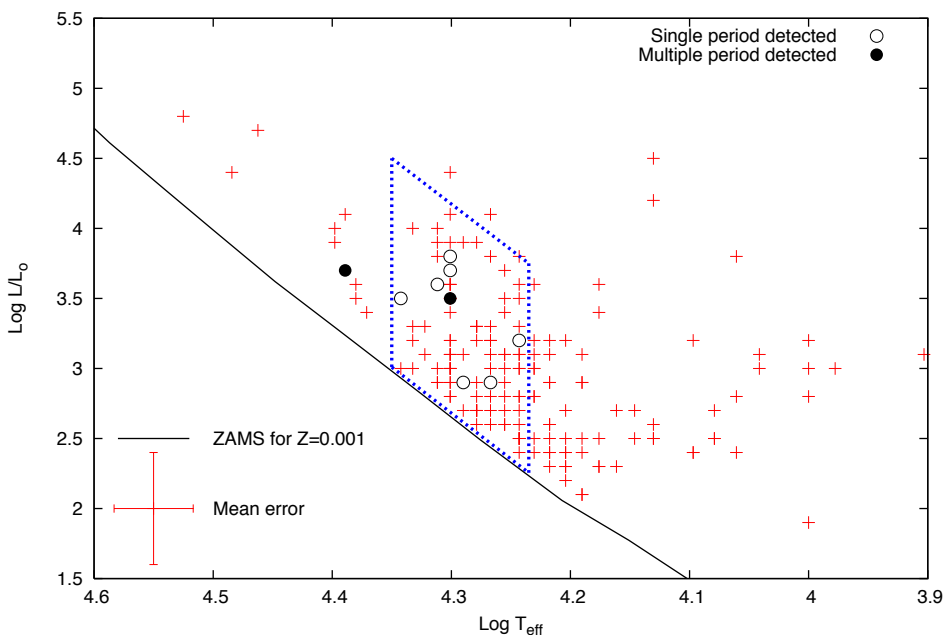
Figure 6.10: *Location of the SMC B star sample in the theoretical H-R diagram. The dashed line delimits the region which contains all SPB stars found in this work.*
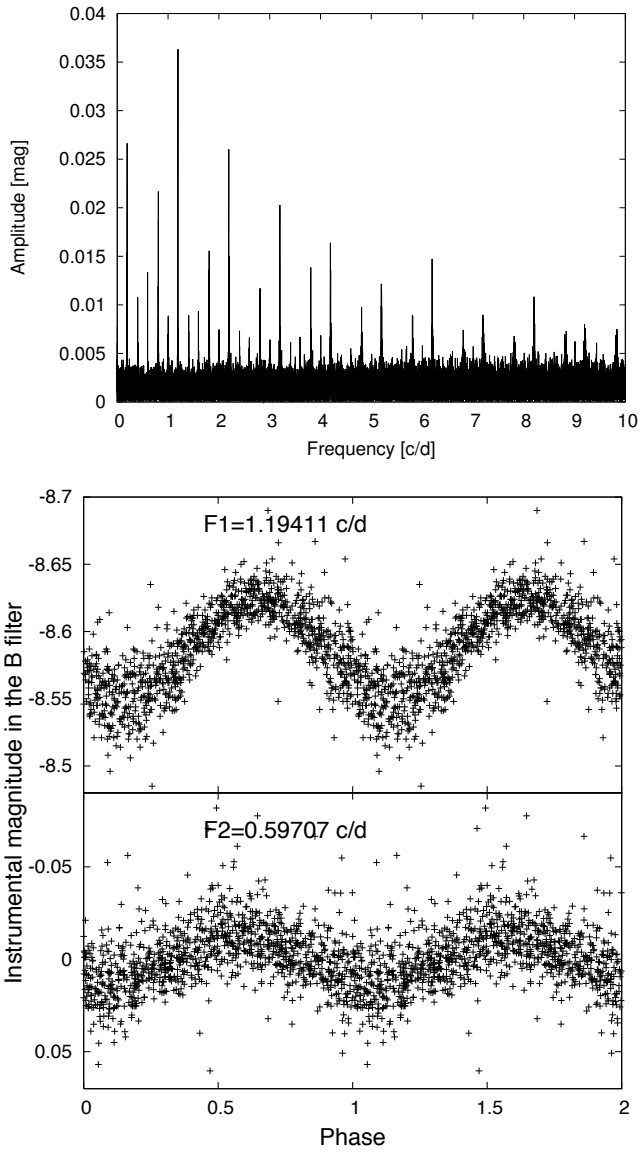
Figure 6.11: *Periodogram* (top) *and phase diagram* (bottom) *of the SPB star* 207.16375.56 *folded with the two detected frequencies.*

mary one, and hence even this object could be monoperiodic but with a non-sinusoidal light curve. This means that the variability in some of these stars might be not caused by pulsations, but by other phenomena like eclipsing or ellipsoidal binarity. It should be noted, however, that non of these stars have been detected as binary in the spectroscopic survey of Martayan et al. (2007a). In any case, we consider our figure of eight stars as an upper limit to the number of bonna-fide SPB stars in our sample.

SPB stars in the Galaxy are also characterised to have low-rotational velocities, although there are several cases of fast rotation (de Cat 2002). In our sample, SPB stars in the SMC have rotational velocities evenly distributed around the mean rotational velocity of absorption-line B stars ($V \sin i = 160 \, \mathrm{km \, s^{-1}}$, M07). Statistically, M06 and M07 found that B and Be stars with similar masses and ages rotate faster at low metallicity (in the SMC) than at high metallicity (in the MW). This result was the first confirmation, based on a significantly large star sample, of the theory from Maeder and Meynet (2001) about the behaviour of rotational velocities in respect of the metallicity for main sequence (SMC vs. MW) B and Be stars.

6.2.2 Pulsating Be stars

In Fig. 6.12 we have represented the pulsating Be stars in the theoretical H-R diagram. The values of the fundamental parameters of the Be stars are corrected for rapid rotation assuming $\Omega/\Omega_c = 95\%$ (M07). We have included in the figure the region where the SPB stars are located as described in the previous subsection. Most Be stars are placed inside or very close to this region, suggesting that most pulsating Be stars in the SMC are g-mode SPB-like pulsators. Three stars are significantly outside the strip towards higher temperatures (207.16259.30, 207.16259.41 and 207.16316.99). All of them are multiperiodic, with the detected periods lower than 0.3 days. Therefore, we propose that these stars may be β Cephei-like pulsators.
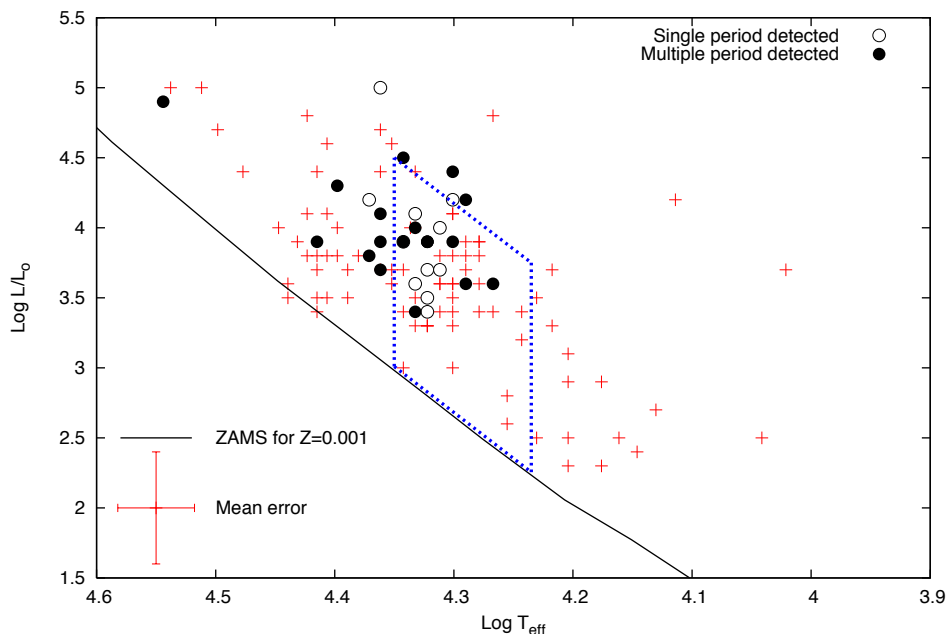
Figure 6.12: *Location of the Be stars in the theoretical H-R diagram. The dashed line represents the suggested SPB instability strip for the SMC.*

In the case of Be stars, the classification of short-term variables as β Cephei or SPB-type stars from the period distribution is more uncertain. As pointed in Eq. 1.7, the observed frequency is significantly affected by the high rotational velocity of the Be stars, according to the formula

$$\nu_{\rm obs} = |\nu_{\rm corot} - m\,\Omega|$$ (6.1)

where $\nu_{\rm obs}$ is the detected frequency, $\nu_{\rm corot}$ is the pulsational frequency in the co-rotating frame, Ω is the rotational frequency of the star and m is the azimuthal order of the pulsational mode. Therefore, if $\Omega \sim 1\,{\rm c\,d}^{-1}$ the value $\nu_{\rm obs}$ could be much different and we cannot make a good comparison.

As an example, we display in Fig. 6.13 the phase diagrams of the Be star 207.16259.35, folded with the detected frequencies. The periodogram for this star is given in the same plot.
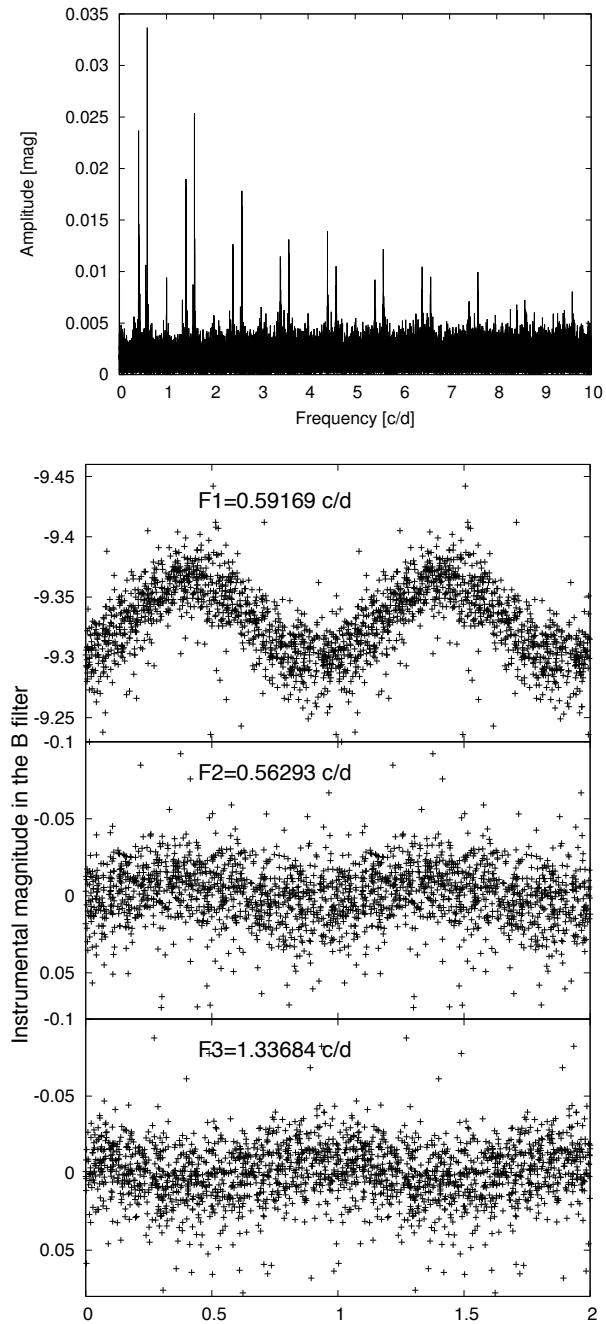
Figure 6.13: *Periodogram* (top) *and phase diagram* (bottom) *of the multiperiodic SMC Be star* 207.16259.35 *folded with the three detected frequencies.*

6.2.3   Degree of variability for the SMC star samples

The stellar samples searched for short-term variability in the SMC are composed of 183 absorption-line B stars and 126 Be stars. We have found nine pulsating stars among the former and 32 among the latter. This means that 4.9% of B stars and 25.3% of Be stars are short-term variables. If we restrict our comparison to the interval B2-B3, where most of the pulsating stars are found (see discussion below), the fraction of pulsating B and Be stars are 5.4% and 31.5% respectively.

Thus, the fraction of non-radial pulsators among the fast-rotating Be stars is much higher than the fraction among slow-rotating B stars. The same result was obtained for stars in the Galaxy by Gutiérrez-Soto et al. (2007a, hereafter G-S07). These results suggest that high-rotational velocity has the effect to trigger the development of non-radial pulsations in B stars, or to enhance the amplitude of existing modes to made them more easily detectable. As an alternative explanation, the prevalence of non-radial pulsations could be related to the yet unknown nature of the Be phenomenon.

To compare the percentage of variability between B stars in the SMC and in the Galaxy we will make use of the statistics of pulsating B stars presented by G-S07. We have only found one β Cephei candidate in the SMC, and hence no statistical comparison is possible. In the case of SPB stars, in an unbiased sample of 795 galactic bright B stars, G-S07 found 35 SPB stars, i.e. 4.4%. In the SMC we have found eight SPB stars among 183 stars, representing a fraction of 4.4%. Both percentages are identical, and both samples are statistically significant.

However, the above statistics is likely to be biased because in the galactic sample used by G-S07, most of the stars are of late B-type, while in our SMC sample most of the stars have spectral types B3 or earlier. This is due to the fact that the late B stars are much fainter and difficult to observe at the SMC distance. On the other hand, SPB stars are of spectral types B2 or later, both in the Galaxy and in the SMC. If we restrict our comparison to the B2-B3 spectral range, in the Galaxy we have 14 SPB stars among 160 B star, i.e. 8.8%. In the SMC we have eight SPB among 147 stars, representing 5.4%. Moreover, the much

larger dataset of the MACHO survey allows for a much more complete detection than the HIPPARCOS data, from which most of the known galactic SPB stars have been detected. Finally, the figure of eight SPB stars we have found in the SMC is to be considered as an upper limit as discussed previously in the text. This represents a lower fraction in the SMC than in the Galaxy as predicted by the current models.

All pulsating Be stars found in this work but one are of spectral types B3 or earlier. In fact, only 11 Be stars of the whole sample have later spectral types. The fraction of pulsating Be stars in the SMC is 27% in the B0-B3 interval. This percentage is to be compared with 74% found by G-S07 or 86% given by Hubert and Floquet (1998) for pulsating Be stars in the Galaxy. Therefore, in the case of Be stars, the prevalence of pulsations in the SMC is significantly lower than in the MW, as expected from the lower metallicity environment.

6.3   Conclusions

In this Chapter, we have searched for short-term variability in a sample of 183 absorption-line B stars and 126 Be stars in the SMC with accurately determined physical parameters. We have studied their position in the theoretical H-R diagram and mapped the regions of pulsational instability in the SMC.

We have found nine pulsating absorption-line B stars. Among them, eight have periods longer than 0.5 days, characteristic of SPB-type stars. The region occupied by the SPB stars in the SMC is shifted towards higher temperatures with respect to the galactic SPB instability strip and to the predictions of recent models for $Z = 0.005$. The remaining star presents two short periods within the range of the β Cephei variables. This fact and its high effective temperature lead us to propose that it is indeed a β Cephei star. This is an interesting result as current stellar models do not predict β Cephei pulsations at the SMC metallicity.

There are 32 pulsating stars among the Be star sample. Most of them are placed in the region occupied by the SPB stars in the H-R diagram of the SMC

and present periods longer than 0.5 days. They are most probably g-mode SPB-like pulsators. Three pulsating Be stars are significantly hotter and present much shorter periods, within the range of the β Cephei stars. We propose that they are β Cephei-like pulsators.

The prevalence of pulsations among Be stars is significantly higher than among absorption-line B stars, much like as in the Galaxy. We have found that 25.3% of Be stars present short-term variability, while only 4.9% of B star do pulsate. This result indicates that the high-rotational velocity either contribute to trigger the development of non-radial pulsations or to enhance the amplitude of the existing modes. Alternatively, the prevalence of non-radial pulsations could be related to the yet unknown nature of the Be phenomenon.

Both the fraction of SPB among B stars and pulsating Be stars among the whole sample of Be stars in the SMC are lower than in the Galaxy, indicating that the prevalence of pulsations is directly affected by the metallicity of the environment, as predicted by the current stellar models.

Well on the way, his head in a Cloud,
The man of a thousand voices talking perfectly loud.
But nobody ever ears him,
Or the sound he appears to make.

Paul McCartney

7

Study in the Large Magellanic Cloud

This Chapter contains the results and conclusions of the search for short-term variability in a large sample of LMC B-type stars for which we have accurate physical parameters. This study in the LMC completes the search for short-term periodic variability in the Magellanic Clouds, started in the previous Chapter for the SMC. We conclude with a comparison between the number of B-type pulsators obtained in the LMC, SMC and MW. A brief comment on Be stars presenting outbursts in the LMC and SMC samples has been added.

7.1 Results

In this Section we present the results of the search for variability in the LMC performed on the two samples of B and Be stars described in Chapter 5. A summary of these results is shown in Table 7.1. In this table we also present the patterns found in the stars excluded to the frequency analysis, for the sake of completeness.

7.1.1 Short-term variability

As assumed for the SMC, we consider as short-period variations those with frequencies higher than $0.3\,\mathrm{c\,d^{-1}}$. In the sample of 99 absorption-line B stars we have found seven short-period variables. One among them is multiperiodic. In the Be stars sample five Be stars have been found to be short-period variables with three among them being multiperiodic.

The detected frequencies with their amplitudes and phases for B and Be stars are presented in Tables 7.2 and 7.3 respectively. The phase diagrams for each star folded with the detected frequencies are depicted in Fig. 7.1 for B and Be stars.

Table 7.1: *Results of the variability search in the B and Be star LMC samples.*

	B stars	Be stars
Analysed stars	99	22
Short-period variables	7	5
- single period	6	2
- multiple periods	1	3
Ecl. Binaries	1	-
No-analysed stars	7	25
Long-period variables	-	4
Irr. variations / Outbursts	2	13
Bad data	5	8

Table 7.2: *Pulsational characteristics of short-period variable absorption-line B stars in the LMC. We only present the frequencies detected with significant SNR. The symbol "-" indicates that the S/N for the detected frequencies in this filters are not enough to reach our criterion and they are not considered as significant frequencies.*

Star iD				Proposed	B filter			R filter		
MACHO iD	EIS iD	Sp. T.	$V\sin i$ $[\,\mathrm{km\,s^{-1}}]$	variable type	Freq $[\,\mathrm{c\,d^{-1}}]$	Amp [mmag]	Phase [0,1]	Freq $[\,\mathrm{c\,d^{-1}}]$	Amp [mmag]	Phase [0,1]
60.7827.209	MHF57079	B1V	320 ± 50	β Cephei	3.00537	164.400	0.893	-	-	-
60.7949.60	MHF84042	B2V	194 ± 10	SPB	0.79875	10.321	0.447	0.79874	9.005	0.456
60.7950.34	MHF86995	B2.5IV	11 ± 20	β Cephei	3.46803	5.740	0.547	3.46801	9.553	0.626
61.8069.26	MHF57975	B2IV	345 ± 35	β Cephei	3.78259	8.077	0.388	-	-	-
61.8072.16	MHF124760	B1V	172 ± 10	β Cephei	-	-	-	4.87569	5.460	0.512
					-	-	-	3.51163	4.804	0.178
61.8190.26	MHF63084	B9.5III	26 ± 20	β Cephei	-	-	-	2.96853	5.879	0.748
61.8194.28	MHF144637	B2III-IV	202 ± 20	SPB	0.31078	30.454	0.188	0.31080	28.564	0.142

Table 7.3: *Pulsational characteristics of short-period variable Be stars in the LMC. We only present the frequencies detected with significant SNR. The symbol "-" indicates that the S/N for the detected frequencies in this filters are not enough to reach our criterion and they are not considered as significant frequencies. The $V \sin i^{\mathrm{true}}$ value is the observed $V \sin i^{\mathrm{app}}$ value corrected from fast rotation assuming $\Omega/\Omega_c = 85\%$ (see M06, for details).*

Star iD				Prop.	B filter			R filter		
MACHO iD	EIS iD	Sp. T.	$V \sin i^{\mathrm{true}}$ [km s^{-1}]	variable type	Freq [c d^{-1}]	Amp [mmag]	Phase [0,1]	Freq [c d^{-1}]	Amp [mmag]	Phase [0,1]
60.7830.14	MHFBe118784	B1III	404 ± 19	SPB	1.91014	20.736	0.455	1.91023	19.810	0.356
					-	-	-	0.69131	14.519	0.156
60.7952.33	MHFBe137325	B5III	263 ± 13	SPB	1.41387	6.939	0.614	-	-	-
60.8070.1905	MHFBe85028	B1.5IV	277 ± 13	SPB	2.56226	13.861	0.060	-	-	-
					1.44516	8.264	0.424	-	-	-
61.8192.204	KWBBe1055	B2IV	433 ± 67	SPB	1.79373	45.747	0.445	1.79370	50.016	0.503
					3.79310	18.978	0.146	-	-	-
61.8192.253	KWBBe1175	B2V	354 ± 100	SPB	1.67718	17.681	0.761	-	-	-
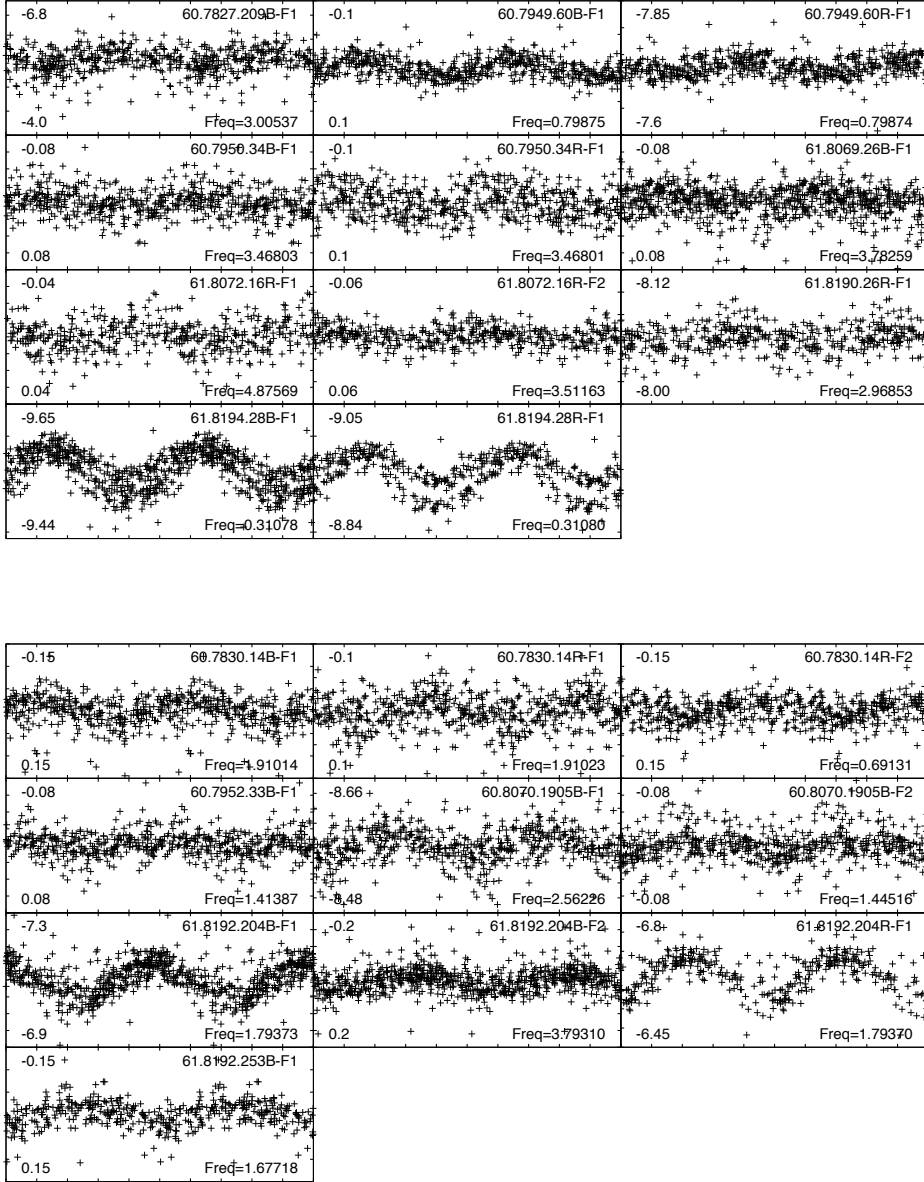
Figure 7.1: *Phase plots of absorption-line B (top) and Be (bottom) stars showing short-term variability folded with the frequency given in each panel. Phases span from 0 to 2. Magnitude range in the B or R filter is denoted inside each panel in the left side. In the right lower corner we show the frequency in $\mathrm{c\,d^{-1}}$. When the star is multiperiodic, the frequency used in the plot is given by the label F1 or F2 inside each panel.*

7.1.2   Eclipsing binaries

Among the B stars we have found one target displaying an eclipsing binary light curve with a period of 1 396 days and spectral type B2IV. The phase diagram is depicted in Fig. 7.2.
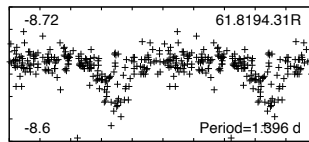
Figure 7.2: *Phase plots of the eclipsing binary star* 61.8194.31, *plotted with the corresponding period (in* days). *Axes as in* Fig. 7.1.
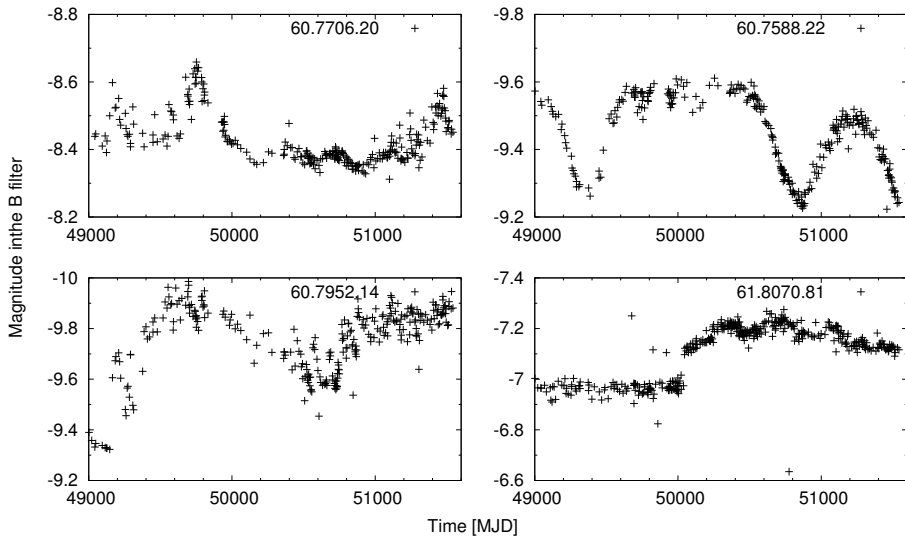
Figure 7.3: *Sample light curves of some Be stars showing outbursts or irregular variations. The time scale is refereed to the modified Julian Day* (MJD) *that it is defined by the expression* MJD = JD - 2 400 000.5.

7.1.3 Irregular variability and outbursts

Finally, we have included in Table 7.4 the list of irregular variable stars detected in both B and Be samples. These variations prevented us from performing a frequency analysis to search for short-term variability, as stated before. All Be stars in this list present photometric outbursts in their light curves spanning a large interval of time. In Fig. 7.3 we have depicted some light curves showing these outbursts or irregular variations.

Table 7.4: *Stars in the sample presenting outburst, irregular variations or long-period variations in the LMC.*

MACHO iD	EIS iD	Sp. T.	Comments
60.7949.52	MHF68257	B1.5V	irregular variations, B star
60.8073.63	MHF131570	B2V	irregular variations, B star
60.7828.21	MHFBe72704	B1.5III-IV	long-period, Be star
60.7831.25	MHFBe140012	B1.5III	long-period, Be star
60.7949.21	MHFBe77796	B1III-IV	long-period, Be star
61.8193.66	MHFBe119521	B1III	long-period, Be star
60.7588.22	MHFBe118313	B1III	outbursts / irr. var., Be star
60.7706.20	MHFBe55920	B1V	outbursts / irr. var., Be star
60.7830.16	MHFBe107877	B2III	outbursts / irr. var., Be star
60.7830.58	MHFBe108272	B2IV	outbursts / irr. var., Be star
60.7949.44	MHFBe66252	B1V	outbursts / irr. var., Be star
60.7952.14	MHFBe132205	B1III	outbursts / irr. var., Be star
60.7953.14	MHFBe155603	B1III	outbursts / irr. var., Be star
61.8070.81	KWBBe0874	B2V	outbursts / irr. var., Be star
61.8191.86	KWBBe0624	B2III	outbursts / irr. var., Be star
61.8192.58	KWBBe0152	B2III	outbursts / irr. var., Be star
61.8192.60	KWBBe0171	B2III	outbursts / irr. var., Be star
61.8192.76	MHFBe101350	B1IV	outbursts / irr. var., Be star
61.8192.88	KWBBe0344	B2IV	outbursts / irr. var., Be star

7.2 Discussion

7.2.1 Pulsating B stars in the LMC

We have found seven short-period variable absorption-line B stars. Their pulsational characteristics are presented in Table 7.2. In Fig. 7.4 we have represented their positions in the H-R diagram. The values of $\log T_{\text{eff}}$ and $\log L/L_{\odot}$, as well as the spectral type and $V \sin i$, have been taken from M06. For comparison, we have also represented the theoretical boundaries of the β Cephei and SPB instability strips, taken from Miglio et al. (2007a, see Fig. 4.2) for the metallicities $Z = 0.010$ and $Z = 0.005$. The ZAMS for the LMC metallicity (taken from Schaerer et al. 1993, at $Z = 0.008$) is also represented. In the case of the B stars, all of them are very close or inside the instability boundaries, except for one, that is extremely out of any instability strip.

In Fig. 7.5 we display the period distribution of β Cephei and SPB stars in the Galaxy, from Stankov and Handler (2005) and de Cat (2002), respectively. The top panel represents the period distribution of our sample of pulsating B stars in the LMC. All stars but two have periods shorter than 0.5 days, characteristic of β Cephei. In the top panel of Fig. 7.1 we display the phase diagrams for all pulsating B stars folded with the corresponding detected periods.

From the period distribution we consider five B stars as β Cephei variables. Among them, the hottest one (61.8072.16) presents two pulsating frequencies. Multiperiodicity is a common feature of the β Cephei stars. In Fig. 7.6 we display the phase diagrams for the multiperiodic star 61.8072.16 folded with the two detected periods. An additional feature is the high rotational velocities (with $V \sin i > 160 \, \text{km s}^{-1}$) of three of the detected pulsating B stars considered as β Cephei variables. These feature also occurs in the β Cephei variables detected in the SMC, where the detected β Cephei candidates have rotational velocities higher than in the MW. Stankov and Handler (2005) have reported several fast-rotating bona fide β Cephei stars in the Galaxy.
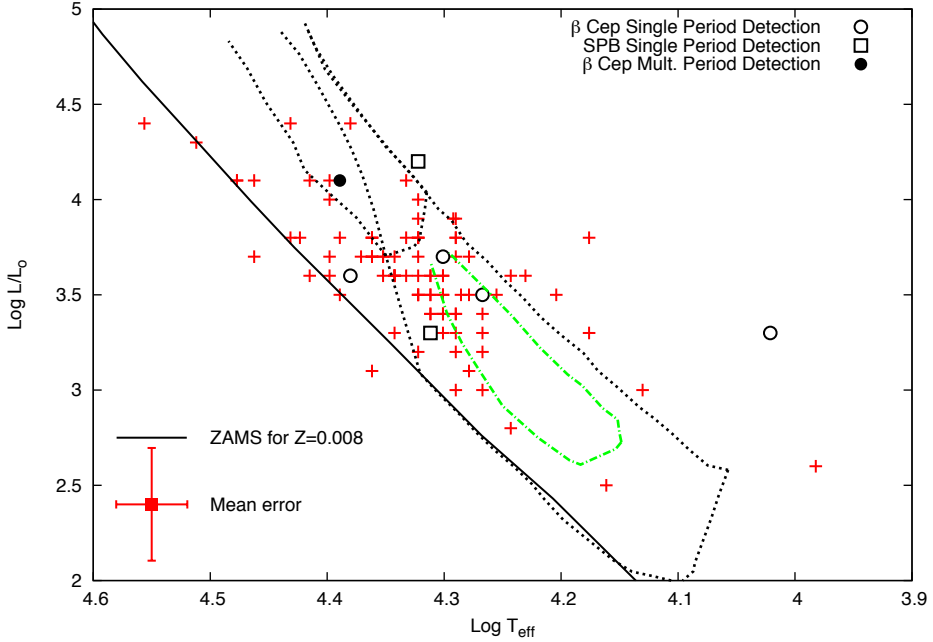
Figure 7.4: *Location of the LMC B star sample in the H-R diagram. Crosses represent stars not detected as short-period variables, empty circles β Cephei stars with single period detection, filled circles β Cephei stars with multiple period detection and empty squares SPB stars with single period detection. For Z = 0.010 we have depicted the β Cephei and SPB boundaries (dotted line). For Z = 0.005 only SPB boundary has been plotted (green dash-pointed line). Boundaries for both metallicities have been taken from Miglio et al. (2007a, see Fig. 4.2). The ZAMS at Z = 0.008 is from Schaerer et al. (1993).*

Concerning the stars considered as SPB variables stars (named as 61.7949.60 and 61.8190.28), they present periods typical of this class, and their position in the H-R diagram is inside or very close to the SPB instability strip for $Z = 0.010$ as seen in Fig. 7.4. As observed for the SMC in the previous Chapter, the SPB stars found in the LMC are placed towards higher temperatures with respect to the Galactic SPB instability strip.

It should be noted that the star with the longest period (61.8194.28) might be an ellipsoidal binary because of the shape of its phase diagram (see Fig. 7.1).
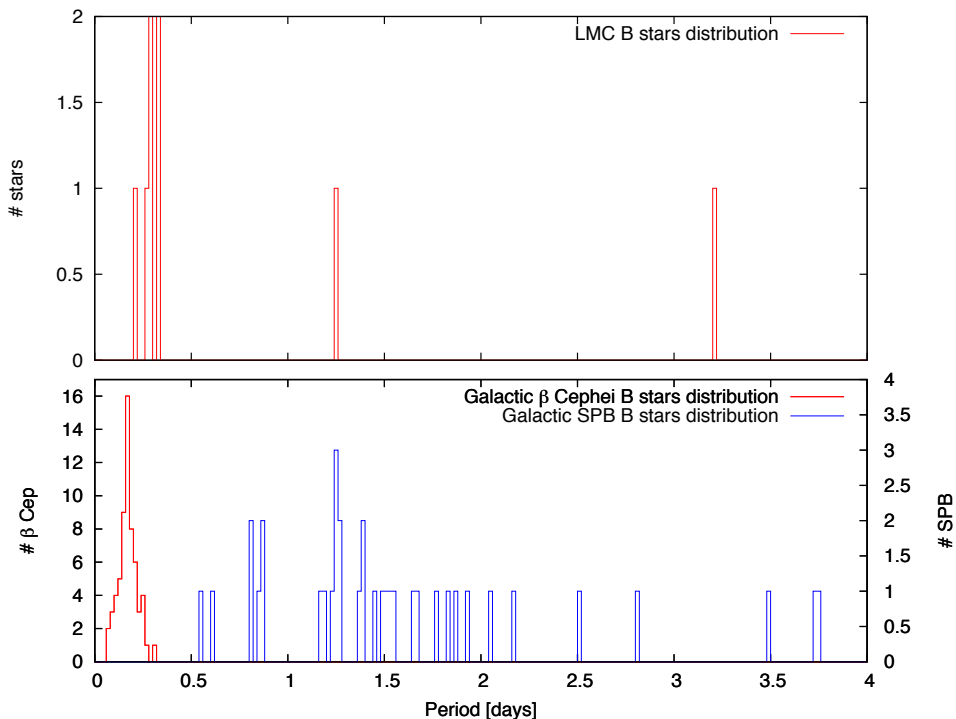
Figure 7.5: *Period distribution of the pulsating B stars found in the LMC sample (top panel) compared to the Galactic β Cephei and SPB period distributions (bottom panel). All stars but two have periods characteristic of β Cephei stars.*

If this is the case, the binary period will be twice the detected one, i.e., ~ 6.4 days. We have to mention however that it was not detected as binary in the spectroscopic data by M06.

Moreover, as the Be nature is transient, the two pulsating B stars that rotate faster (named as 60.7827.209 and 61.8069.26) could be in fact Be stars detected as normal B stars at the moment of the spectroscopic survey made by M06.

As mentioned in the SMC study, SPB stars in the MW are also characterised to having low-rotational velocities, although there are several cases of fast rotators (de Cat 2002). In our sample, the two detected SPB stars have rotational velocities slightly higher than the mean rotational velocity of absorption-line B

stars ($V \sin i \sim 119\,\mathrm{km\,s^{-1}}$) as calculated in M06. This fact could be due to the low metallicity environment of the LMC, as explained in the previous Chapter for the SMC.
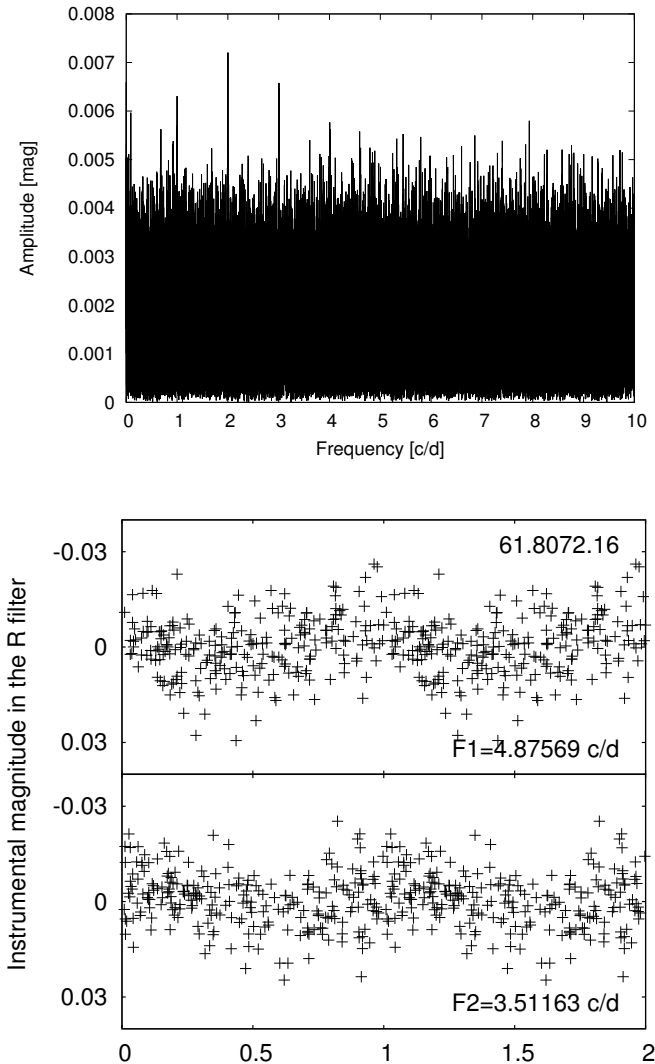
Figure 7.6: *Periodogram* (top) *and phase diagram* (bottom) *of the B star* 61.8072.16 *folded with the two detected frequencies. Note that two cycles are shown for clarity.*

7.2.2 Pulsating Be stars in the LMC

Our frequency analysis detects five short-period variable stars among the Be sample. Their fundamental parameters are presented in Table 7.3 (taken from M06). These values were corrected for rapid rotation assuming $\Omega/\Omega_c = 85\%$ (M06). In Fig. 7.7 we depict these short-term pulsating Be stars in the H-R diagram with the values of $\log T_{\text{eff}}$ and $\log L/L_\odot$ taken from M06.
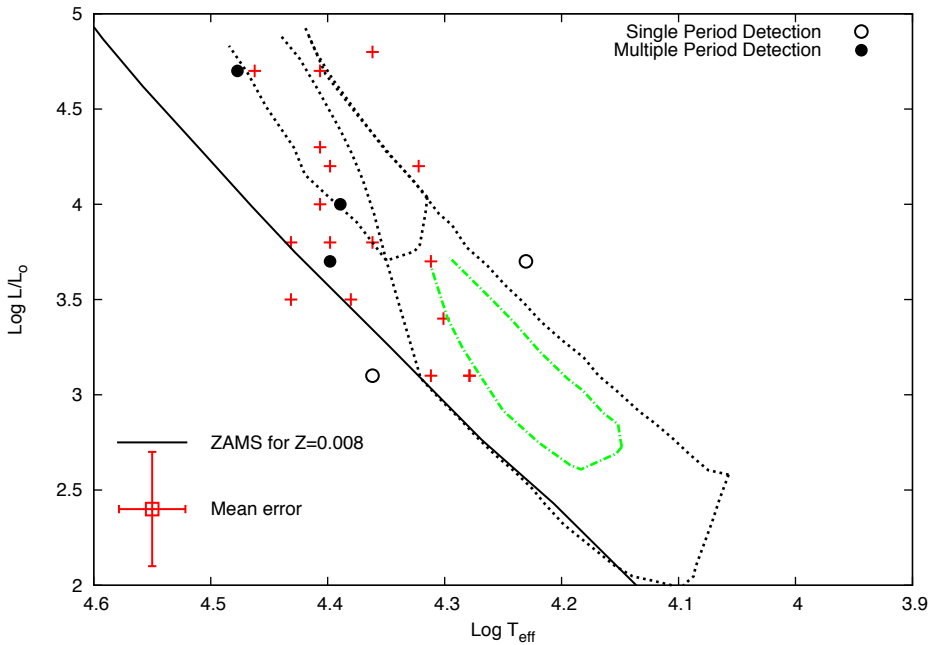
Figure 7.7: *Location of the LMC Be star sample in the theoretical H-R diagram. Single crosses represent stars in our sample, the empty circles represent single period detection and filled ones multiple period detection. The β Cephei and SPB boundaries at metallicities of $Z = 0.010$ (dashed line) and $Z = 0.005$ (green dash-pointed line) have been taken from Miglio et al. (2007a, see Fig. 4.2). The ZAMS at $Z = 0.008$ is from Schaerer et al. (1993).*

As explained for the pulsating Be stars detected in the SMC in Chapter 6, the classification of pulsating Be stars as β Cephei or SPB stars from the period distribution is more uncertain, due to the fast rotation of these stars. The observed

frequency is significantly affected by the high rotational velocity, according to Eq. 1.7. In any case, the periods obtained for the five short-term Be star variables place them into the *g*-mode SPB-like pulsators type. Moreover three of them (matching with those with higher temperatures) show multiperiodicity. In Fig. 7.8 we display a detail of the phase diagram for the Be star 61.8192.204, folded with the two detected frequencies, together with the periodogram.
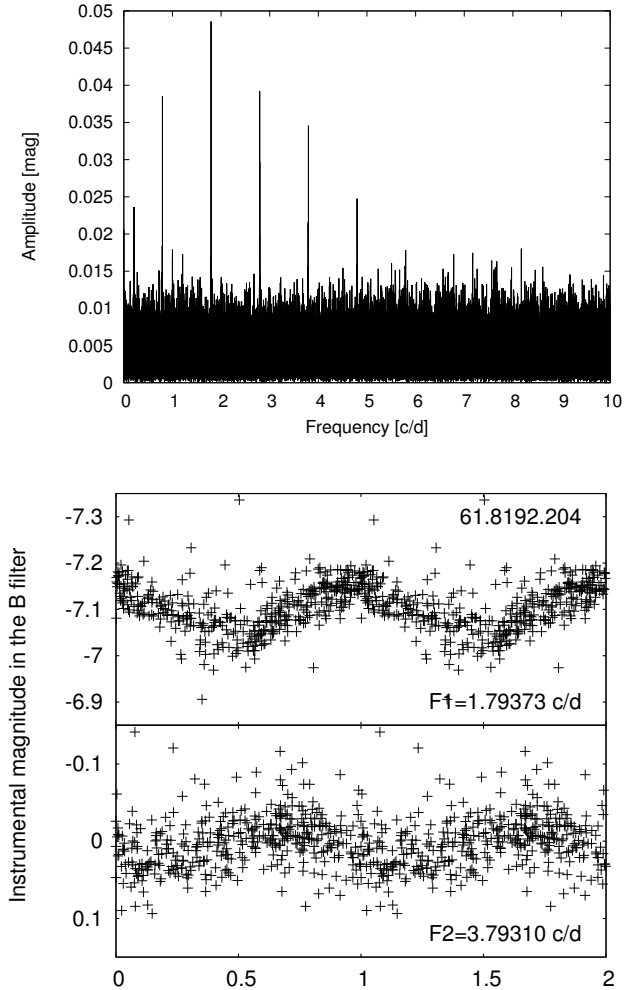
Figure 7.8: *Periodogram* (top) *and phase diagram* (bottom) *of the LMC Be star* 61.8192.20 *folded with the two detected frequencies. Two cycles are shown.*

7.2.3   Degree of variability for the LMC star samples

The samples analysed for short-term variability in the LMC are composed by 99 B stars and 22 Be stars. We have identified seven variables among the B star sample and five among the Be star sample. This means that 7% of B stars and 23% of Be stars are identified as short-term variables. These values indicate that in the LMC, the fraction of non-radial pulsators among the fast-rotating Be stars is much higher that the fraction among the slow-rotating B stars.

The same result was obtained for stars from the SMC by D08 (Chapter 6) and for stars from the MW by G-S07. As in the SMC, this fact supports the thesis that high rotational velocity has the effect of triggering the development of non-radial pulsators in B-type stars, or to enhance the amplitude of existing modes to make them more easily detectable. An alternative explanation comes from the fact that the prevalence of non-radial pulsations could be related to the yet unknown nature of the Be phenomenon.

7.2.4   Comparison of the pulsating B-type stars in the SMC, LMC and MW

A recent investigation on the photometric variability of Be stars from the SMC cluster NGC 330 made by Schmidtke et al. (2008) has revealed that pulsations are present in $\sim 30\%$ of their selected Be stars. This percentage is similar to the 25% obtained by D08 (Chapter 6) for the pulsating Be stars found in the SMC. To compare the degree of variability between B-type stars from the SMC, LMC and MW we make use of the statistics of pulsating B-type stars presented in G-S07 for the MW and in the previous Chapter for the SMC. Note that the B-type samples in the SMC and LMC are homogeneous and have an accurate determination of their fundamental parameters provided by M06 and M07, respectively.

The fraction of pulsating B and Be stars at the SMC, at the LMC and at the MW are reported in Table 7.5. The percentages of pulsating B and Be stars in the MW, given by G-S07, have been restricted to the early-type domain, since

Table 7.5: *Degree of pulsating B-type stars compared with the Ω/Ω_c values for the MW and MCs.*

	MW	LMC	SMC
Metallicity	0.02	0.007	0.002
Ω/Ω_c (B stars)	40%	37%	58%
Pulsating B stars	16%	7%	5%
Ω/Ω_c (Be stars)	88%	85%	95%
Pulsating Be stars	74%	23%	25%

all stars in the MC samples are B3 or earlier. We also provide the metallicity and the average rotational velocities with respect to the break-up velocity (Ω/Ω_c) for the SMC, LMC and MW. The latter value comes from M07 for the MCs (see Chapter 4 for more details) and from Frémat et al. (2005) for the MW.

As the SMC and LMC samples are homogeneous, the error in the fraction of pulsating stars is given by the Poisson distribution, i.e. $\sqrt{n}/n$, where n is the number of detected pulsating stars in each sample. Therefore, we find a percentage of $16\% \pm 3\%$ %, $7\% \pm 3\%$ and $5\% \pm 2\%$ of pulsating B stars in the MW, LMC and SMC, respectively and $74\% \pm 15\%$, $23\% \pm 10\%$ and $25\% \pm 4\%$ of pulsating Be stars in the MW, LMC and SMC, respectively.

As mentioned in Chapter 4 and according to the recent theoretical studies (Miglio et al. 2007a,b; Salmon et al. 2009) a decreasing trend in the metallicity of the stellar environment should decrease or practically vanish the occurrence of pulsations in B-type stars. On the other hand, for both B and Be stars, M07 shows, based on an observational study, that the lower the metallicity the higher the rotational velocities (Ω), confirming the theoretical results presented in Meynet and Maeder (2000) and Maeder and Meynet (2001). These theoretical results are explained by the fact that at low metallicity, the radiatively driven stellar winds are less efficient than at high metallicity. Thus, the mass-loss and the corresponding angular momentum loss are lower at low metallicities and then the stars rotate faster, increasing the linear rotational velocity of the star. On the other hand, the lower metallicity also produces a decrease of the stellar radius (Maeder and Meynet 2001) and makes the critical rotational velocity (Ω_c) to in-

crease. Then, the ratio between the rotational velocity and the break-up velocity (Ω/Ω_c) is due to the combination of both effects.

As shown in Table 7.5 the rotational rates of B stars in the LMC and the SMC are $\Omega/\Omega_c = 37\%$ and $\Omega/\Omega_c = 58\%$, respectively. These values are close to the one for the Galactic B stars, which is about $\Omega/\Omega_c \sim 40\%$. The effects of fast rotation in the stellar structure become significant at the rotational velocity with respect to the critical velocity $\Omega/\Omega_c \sim 70\%$ (Zorec et al. 2005; Frémat et al. 2005). Therefore, we conclude that the sample of B stars in the LMC and SMC are less affected by the fast rotation and consequently, as seen in Table 7.5 and predicted by the models, we only expect the effect of the lower metallicity reflected in a decrease of the pulsating stars fraction.

In the case of Be stars, the decreasing trend is also observed in Table 7.5, from higher to lower metallicity. Actually, we find much less pulsating Be stars in the MCs than in the MW. However, the fraction of pulsating Be stars in the SMC, despite its lower metallicity, is comparable with the one of the LMC. IN this case we propose that the higher rotational velocity of Be stars in the SMC balances the lower metallicity, and then the fraction of pulsators become similar in both LMC and SMC. As commented above, the fast rotation seems to play an important role in the pulsations, enhancing the non-radial pulsations or amplifying the existing modes. The significantly higher abundance of pulsators among Be stars with respect to B stars points towards the same conclusion.

7.2.5   Be stars presenting outbursts in the SMC and LMC

Outbursts have been more frequently observed in early Be stars. These phenomena seem to occur randomly, varying in strength and lifetime in each star. Our analysis shows that the percentage of Be stars presenting outbursts and/or irregular variations is significantly different in the SMC and the LMC. We found that 44% and 4% of Be stars, in the LMC and SMC, respectively, present outbursts or irregular variations in their light curves. In addition, the outbursts seen in the Be stars of the SMC are, in average, more energetic, i.e., have larger amplitudes.

This suggests that the mechanism(s) that produce(s) these outbursts or ejections of matter depend(s) on the metallicity of the environment. Similar results were obtained by Sabogal et al. (2005) with different samples of Be stars in the SMC and LMC. For Be stars in the Galaxy, Hubert and Floquet (1998) searched for the presence of outbursts and fading events in the HIPPARCOS data. They found that outbursts have been frequently and preferentially detected in early Be stars with rather low to moderate $V \sin i$. For the SMC, Mennickent et al. (2002) carried out an empirical classification based on the light curve appearance in a sample of $\sim 1\,000$ Be star candidates using the OGLE[1] II data (Soszynski et al. 2002). A deeper investigation of this effect is beyond the scope of the present work.

7.3   Conclusions

We have searched for short-term variability in a sample of 106 absorption-line B stars and 47 Be stars in the LMC with accurately determined physical parameters. We have studied their position in the H-R diagram and mapped the regions of pulsational instability in the LMC.

We have found seven pulsating absorption-line B stars. Among them, two stars are proposed to be SPB-like pulsators from their period distribution. As form the SMC, the position occupied by the SPB stars in the LMC in the H-R diagram seems to be shifted towards higher temperatures with respect to the Galactic SPB instability strip. The remaining five B stars present periods within the range of β Cephei variables. This fact and their high effective temperatures lead us to propose that they are indeed β Cephei stars.

In the Be star sample, we have detected five pulsating stars, three of them showing multiperiodicity. According to the observed periods, we interpret them as g-mode SPB-like pulsators.

---

[1]Optical Gravitational Lensing Experiment: http://ogle.astrouw.edu.pl/.

The prevalence of pulsations among the Be stars is significantly higher than among absorption-line B stars. We have found that 23% of Be stars present short-term variability, while only the 7% of B stars do pulsate. The same result was previously found in the SMC and the MW, supporting that the high rotational velocity either contributes to trigger the development of non-radial pulsations or to enhance the amplitude of the existing modes. Alternatively, the prevalence of non-radial pulsations in Be stars could be related to the still unknown nature of the Be phenomenon.

Finally, we have undertaken a comparison of the prevalence of pulsating B-type stars in the SMC, LMC and MW. We note a decrease of the rates of pulsating B-type stars with decreasing metallicity as expected from the theory. However, it is clear from this work (and other above mentioned studies) that pulsations are still driven in B-type stars at low metallicity environments, in contradiction with the predictions from recent calculations on stellar pulsation theory. This detection of pulsators at low-Z environments still remains an enigma.

In addition, we detect an increase of the rates of pulsating Be stars between the LMC and the SMC while the metallicity decreases. This may be explained by the fact that SMC Be stars rotate faster than their counterparts in the LMC. There is a similar trend in Ω/Ω_c for B stars, but their ratios are always lower than the minimal ratio from which the fast rotation effects on the stars are not negligible ($\Omega/\Omega_c \geq 70\%$). This fact could explain why there is an effect of the fast rotation between the LMC and SMC for Be stars and not for B stars.

Part II

Study of pulsating Be stars with CoRoT

Images of broken light which dance before me like a million eyes,
They call me on and on across the Universe.

John Lennon

8

The CoRoT space mission

Here begins the second part of this Ph.D. thesis: the study of pulsating Be stars with the CoRoT space mission. In this Chapter we present a detailed description of the CoRoT spacecraft and the mission scenario. Chapter 9 presents the CoRoT Be Team, a collaboration for the study of Be stars using the CoRoT data. We describe some general remarks about the instrumental effects present in the CoRoT light curves and information on the frequency analysis of the CoRoT data. In Chapter 10 we describe the results on the analysis of three Be stars from the exoplanet field. Finally, in Chapter 11 we present the results on the frequency analysis of the Be star HD 50 209.

8.1 CoRoT, from stars to habitable planets

CoRoT[1] (Convection, Rotation and planetary Transits) is one of the most important space missions today. The CoRoT Space Telescope is an experiment of astronomy dedicated to stellar seismology and search for extrasolar planets. The mission is led by the French Space Agency CNES[2] with a significant international participation: ESA[3], Austria, Belgium, Brazil, Germany and Spain. In brief, the spacecraft is equipped with a 27-cm diameter afocal telescope and a 4-CCD camera sensitive to tiny variations of the light intensity from stars. The CoRoT satellite was launched on 27th of December 2006 after successful development and integration phase.

For the first time, a spacecraft devoted to detect rocky exoplanets, like our own, and delve into the very centre of the stars has been launched. For many decades, European space organisations have been exploring the possibility of applying the technique of high precision photometry on very long durations in space to these two topics. The CoRoT mission is the first one of this kind. The new information on the stellar interiors provided by the seismology technique, as applied on almost all types of stars will revolutionise our picture of stellar formation and evolution. As stars are the major engines driving the changes of the composition of the Universe through the transformation of chemical elements and the building of metals from hydrogen, this will also have a strong impact on our understanding of the evolution of the Universe as a whole.

The initial concept of CoRoT was proposed already in 1993 by C. Catala, M. Auvergne and A. Baglin (see Catala et al. 1995) in answer to a call of ideas of CNES for "small missions", and was preselected in 1994 for a phase A competitive study and posterior launch. At that time it was designed as a second generation mission of asteroseismology only, following Evris (Baglin et al. 1993) and preceding large surveys like ESA's Eddington mission (actually cancelled) or Kepler mission launched on March 2009 by NASA (National Aeronautics and Space Administration) and actually on flight. In 1996, just after the discovery of

---

[1]Websites: http://corot.oamp.fr/ and http://smsc.cnes.fr/COROT/.
[2]Centre National d'Études Spatiales: http://www.cnes.fr/.
[3]European Space Agency: http://www.esa.int/.

Figure 8.1: *The CoRoT logo, designed by Patrice Amoyel, where the name of CoRoT is illuminated by a funny laughing Sun with eight petals. Figure taken from CoRoT website at CNES.*

the first giant exoplanet (Mayor and Queloz 1995) it was proposed a much richer scientific mission, in particular, including a planet finding objective.

The discovery of the first planets orbiting stars other than our Sun –exoplanets or extrasolar planets– in the last few decades has demonstrated that the hypothesis made since antiquity that our Solar System is not unique is true in fact. However, as always, Nature has demonstrated its capability to surprise us. Up to now, more than 450 exoplanets have been found[4] and all have shown properties different than what we find locally in our own planetary (Solar) system. Among the many differences, the fact is that everything found so far is significantly larger than the Terrestrial Planets in our own neighbourhood and this is a consequence of the bias introduced by ground based observations. Nevertheless, CoRoT was needed to make the first leap into the realm of the terrestrial planets. The CoRoT satellite, with its capability of detecting much smaller planets than so far observed, as well as determining the frequency of such objects as a function of size and distance from their primaries can tell us enormously much about how planetary systems form and under what boundary conditions the formation takes place. We will also be able to extrapolate the CoRoT results in a way that prepares the road for missions to come.

---

[4]See the Extrasolar Planets Encyclopaedia: http://exoplanet.eu/.

But, why going to space? It has been extensively demonstrated that photometry from the ground cannot reach the precision required to achieve the previous explained goals. From the ground, it is also almost impossible to have a good time coverage over several months with less than 10% interruptions. For both of them the spectroscopic alternative is not sensitive to the same objects, or would require huge networks of very large telescopes. So, there is a need to go to space for both stellar seismology and detection of small planets. The technique of very high precision stellar photometry with very long duration of observations, can be implemented in space with a reasonable size mission. But, unfortunately, this new field for space studies, which makes use of the stability properties of the spatial environment as well as the opportunity to make continuous measurements over a long time, had and still has difficulties to be selected by the National Space Agencies. The Canadian micro-satellite MOST[5] (Microvariability and Oscillations of STars) has now shown that even with a very small instrument and budget, one can detect tiny stellar oscillations that will never be seen from the ground.

8.2   The scientific objectives

The CoRoT mission has two concrete scientific programs working simultaneously on adjacent regions of the sky and both requiring long uninterrupted observations with very high photometric accuracy. The two goals for the CoRoT satellite are:

Stellar seismology: By studying the acoustical waves rippling across the surfaces of stars, with waves as high as a few meters, one can penetrate into the so far "invisible" stellar interiors and learn about the physics of stars. This is the engine driving the most important energy source in our universe, which creates the environment necessary for life on the surface of planets.

Search for exoplanets: Searching for rocky planets outside our Solar System, CoRoT is an important stepping stone in the European effort to find habitable, Earth-like planets around other stars.

---

[5]http://www.astro.ubc.ca/MOST/.

For thus, the two main programmes of the CoRoT mission have been named as *Seismology Programme* and *Exoplanet Programme*. The CoRoT satellite is measuring with a very high accuracy the brightness variations of selected stars, during very long periods of continuous observations (with ~ 150 days) and shorter periods of continuous observations (with ~ 21 days) for both main programmes. Moreover, to allow some additional science, different from doing seismology in the seismology field and planet finding in the exoplanet field, half of the short runs will be dedicated to the *Additional Programmes*.

8.2.1   The seismology programme of CoRoT

The seismology programme have two different objectives and subprogrammes: the *Core Programme* and the *Exploratory Programme*. The Core Programme is centred on a detailed study of a few stars, specially chosen to test the hydrodynamics of the internal layers and the physical state of stellar cores. The Exploratory Programme is devoted to detect oscillations in a large variety of stars and to classify the asteroseismologic properties in the H-R diagram. Here comes a brief description of both programmes.

The Core Programme

Its objective is to observe very precisely a small set of objects during 150 days. The general problem addressed by the CoRoT seismology Core Programme is the nature of transport processes in stellar interiors during the main sequence evolution stage and around it. This covers several aspects of transport, from convective heat transport to angular momentum transport, including overshooting, transport of chemical species, etc. Through these phenomena, CoRoT will decipher the main sources of uncertainty in the modelling of intermediate and moderate mass stars during a stage of evolution which represents about 90% of their life-time and has crucial consequences on their further evolution.

In the case of solar-like pulsators, it is well known that the characteristic features of the internal structure induce signatures in the oscillation frequencies at the level of $0.1\,\mu$Hz (1 cycle in about 100 days, see e.g. Gough 1990; Provost 2000). CoRoT needs this accuracy in frequency to have access to the profile of the modes and the rotational divisions, and for a precise measurement of the modal frequencies. For A and F stars close to main sequence, the CoRoT data will provide measurements of the size of the convective cores, the size of the outer convective zones and their helium content. In the case of moderate-mass stars as δ Scuti stars, a 150 days run provides accurate enough frequencies to tackle precise inversion of the rotational profile as demonstrated by Goupil et al. (1996).

During the long runs of this programme the CoRoT satellite has been observing one or two bright stars (primary targets) and several fainter ones in the surrounding field of view (secondary targets). The range of magnitudes for the stars observed in the seismology programme is $5.7 \leq V \leq 9.5$ mag.

The Exploratory Programme

The principal objective of the Exploratory Programme is to determine the domain of stellar parameters for which stellar oscillations can be detected. In consequence, one needs to observe a sample of objects with a large variety of stellar parameters, as mass, age, chemical composition, rotational state, etc, for which only a modest signal to noise ratio is needed. CoRoT has been studying all the different types of pulsating stars in the H-R diagram (see Fig. 1.7 in Chapter 1) and finding new ones.

A frequency resolution of 0.5 Hz is sufficient, corresponding to observations that last $20 - 30$ days. Stars with magnitudes less than about 9 mag are bright enough for these studies.

8.2.2 The Exoplanet Programme of CoRoT

Since the discovery of the first extrasolar planet (51 Peg b by Mayor and Queloz 1995), the understanding of the formation of planetary systems has improved drastically. After the study of the giant exoplanet class, the challenge is now to detect and characterise the Terrestrial exoplanet class (also known as telluric, rocky or inner exoplanet class, composed by silicate rocks). CoRoT is taking up the challenge with a planet finding programme whose main goal is to detect the first Terrestrial extrasolar planet with the transit method.

The transit method and the radial velocities method are the only ones which allow precise determination of the orbital period and the size of the planet. The problem is to detect the small luminosity decrease of a star when occulted by one of its planets, either a giant with a Jupiter mass or a small Terrestrial one (see Fig. 8.2). At the moment that this Ph.D. thesis is written, the smallest confirmed diameter of an exoplanet around a main-sequence star is that of CoRoT-7b, which is about 70% larger than Earth (Léger et al. 2009; Queloz et al. 2009).
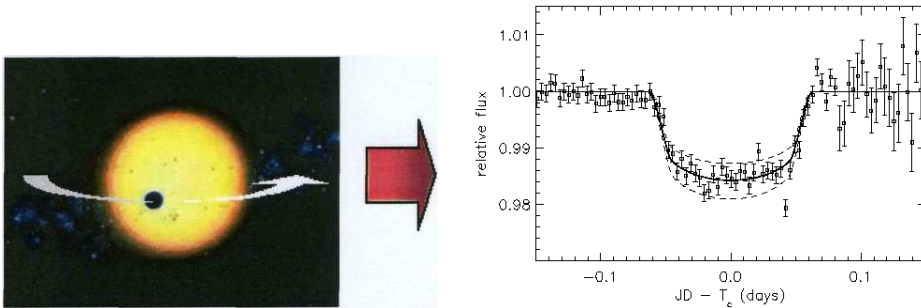
Figure 8.2: *The transit method for detecting planets. A decrease in the light of the star is observed when the planet is on the line of sight between us and the star. Figure courtesy of H. Deeg.*

A transit event is characterised by: i) A relative amplitude of 10^{-2} for a Jupiter-like planet and only 8×10^{-5} for an Earth-like one. And ii) A periodicity which ranges from a few days to several months. This implies a great necessity of high precision photometry and continuous observations during a long period.

Furthermore, this event may be observed only when the line of sight lies within the orbital plane of the planet. The associated geometrical probability is very low (0.5% for the Earth-like planets and 16% for 51 Peg b, see Bordé et al. 2001), so that a large number of stars must be monitored to have a chance to find a planet. For this reason, an amount of 12 000 stars per run, with a $11.5 \leq V \leq 16$ mag are being monitored continuously during 5 months on the two exoplanet CCDs of the CoRoT satellite.

The major difficulty in the detection of planetary transit is to identify the false alarms due to photometric variations of stellar origin, as stellar activity. Bayesian methods (see e.g. Defaÿ et al. 2001), projects like STARE (Alonso et al. 2004) or the newest "supervised/unsupervised classification methods" (Debosscher et al. 2006) are studying the strategies to recognise these false alarms. Multi-colour information is obtained thanks to a bi-prism located in the focal block at few centimetres of the exoplanet CCDs, providing photometric information in three passbands. It has been shown that the coloured information decreases the false-alarm probability (Garrido 2000a).

8.2.3   The Additional Scientific Programmes of CoRoT

Although primarily driven by asteroseismology and exoplanet detection, CoRoT also accommodates Additional Programmes. This programmes include all scientific use of CoRoT data for purposes outside the Core Programme areas of exoplanet detection in the exoplanet field and asteroseismology in the astero-seismology field. Any other analysis of CoRoT light curves (rotation, activity, flaring, eclipsing binaries, etc) fall under the Additional Programmes.

The Additional Programmes section of CoRoT is available to the community after an Announcement of Opportunity (AO), and has the goal to maximise the scientific return of the mission. There are three possibilities to request CoRoT data within the Additional Programmes:

i. Half of the short runs scheduled for CoRoT are devoted to the Additional Programmes. During these short runs data from a specific target field is being obtained and they need not be devoted to asteroseismology or planet search.

ii. A few hundred windows of the exoplanet field during each long run are being available within the Additional Programmes.

iii. Archival data obtained within the Core Programme or the Additional Programmes can be requested.

In order to prepare the AOs mentioned above and help defining the CoRoT science, an Additional Program Working Group (APWG) was established[6]. There are several thematic teams included in the Additional Programmes, for example, groups on activity and rotation of stars, Be stars, binary stars, γ Doradus stars, pre-main sequence stars, etc. A detailed description on these working groups can be found in Weiss et al. (2004).

The AOs for observations are being issued each year. This programme is open to the entire astronomical community. Responses to the official AOs are been examined by the CoRoT Scientific Committee, which is in charge for the selection, taking into account the quality of the proposed science. Successful proposers will obtain status of a Guest Investigators and will have exclusive data rights for the science described in their proposals. The CoRoT Scientific Committee, however, will have the rights to use the same data for any other science. One year after the first release of the data to the Co- and/or Guest-Investigators (CoIs and/or GIs), the data will be available for the public.

---

[6]Website: http://www.univie.ac.at/asap/main.php?s=corot;corotAPWG.

8.3   The spacecraft design

The main technical characteristics of the mission, and in particular of the instrument, are described in detail in the CoRoT instrument handbook[7] and the reference ESA Publication on the pre-launch status of the CoRoT mission (Fridlund et al. 2006). Thus, the main characteristics are only briefly sketched out here. For a recent review of the technical descriptions and the behaviours in flight of the CoRoT satellite see Auvergne et al. (2009).

The CoRoT spacecraft is based on a PROTEUS platform (Plate-forme Reconfigurable pour l'Observation, pour les Télécommunications Et les Usages Scientifiques, see Landiech and Douillet 2004, for a detailed description), developed by CNES and Alcatel Space Industry (now renamed as Thales Alenia Space). This bus is designed for 500 Kg class satellites, operating in low earth orbit with a maximum altitude of 1 300 km. CoRoT is the third mission to use this platform and the associated generic ground control segment after Jason-1 and Calipso. An overview of the CoRoT satellite is shown in Fig. 8.3.
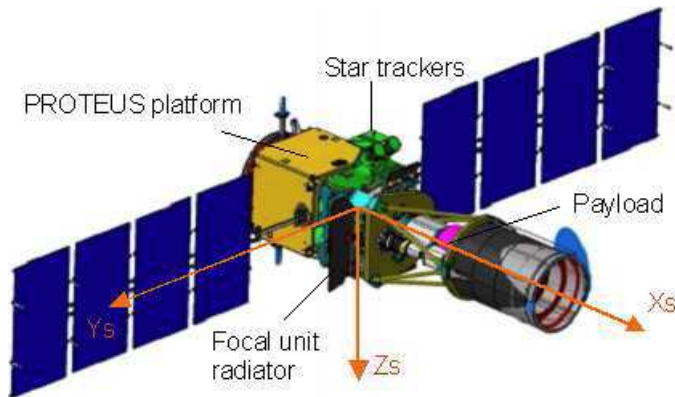
Figure 8.3: *Satellite overview with opened solar panels, dimensions:* 4.20 m × 9.60 m. Figure taken from CoRoT website at CNES.

---

[7]http://corotsol.obspm.fr/web-instrum/payload.param/.
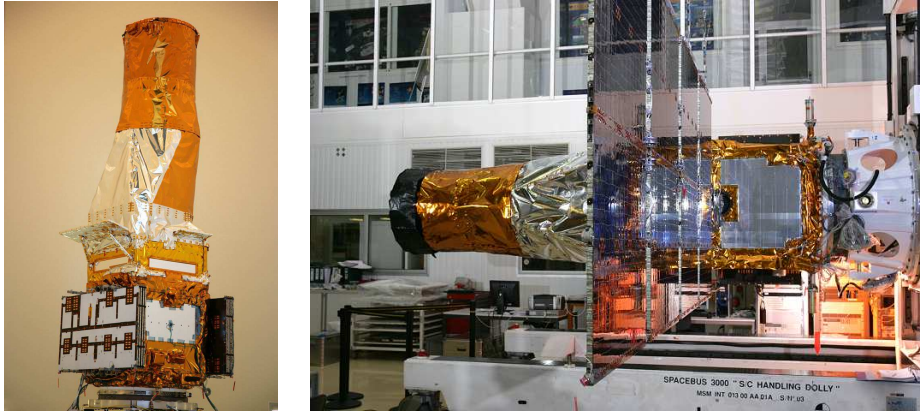
Figure 8.4: *Two views of the* CoRoT *satellite before launching on* 27th *of December 2006.* © Thales Alenia Space / JL Bazile.

The satellite is operated from the CoRoT Control Center, located in Toulouse (France), sharing the facilities of the PROTEUS satellite family. Communication with the satellite is provided by means of the CNES 2 GHz network, an antenna in Alcantara (Brazil) and another antenna in Vienna (Austria). The data is then distributed on the Internet to the mission's scientists. The volume of data to be transmitted daily to the ground is 1.5 Gb during observing runs.

The total weight of the satellite is 626 Kg, including 300 Kg for the payload. The power is provided by two solar arrays that feed directly into the battery giving a non regulated voltage in the interval $23 - 37$ V and a power of 1 kW. Two real images of the satellite before launching are depicted in Fig. 8.4. CoRoT is 4.10 m long and 1.984 m in diameter with closed solar wings.

The CoRoT payload is made up of the following subsystems (see Fig. 8.5 for an overview):

CoRoTel: An afocal telescope, with a diameter of 270 mm, composed of two parabolic mirrors, with a cylindrical baffle to stop the Earth straylight and a one-shot cover against blinding in early attitude acquisition phase.

CoRoTcam: A wide-field camera composed of a dioptric objective (six lenses)

and a focal unit equipped with four frame transfer 2048×4096 pixel CCDs working at $-40°C$. Two are dedicated to the seismology programme and the other two to the exoplanet programme. A dispersive device (bi-prism) is inserted in front of the two CCD matrices dedicated to exoplanets. A deep description of the CoRoTcam can be found in the mission design notes (Section 8.5).

CoRoTcase: The equipment bay supporting scientific data processing electronics (video electronics, extraction units and data processing units) and instrument housekeeping electronics (power distribution, fine thermal control, calibration management and synchronisation unit).
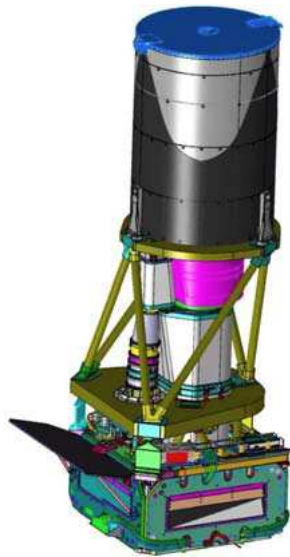
Figure 8.5: *Payload overview with the equipment bay in the lower part. The camera and the telescope are placed in the upper part. Figure taken from* CoRoT *website at* CNES.

Table 8.1: *Orbit parameters and associated properties of the* CoRoT *satellite.*

Semi-major axis (a)	7 274 km (altitude of 896 km)
Eccentricity (e)	0.00127° (circular)
Inclination (i)	90°
Right ascension of ascending node (Ω)	14.5° or 194.5° (before drift)
Period T	6 174 s (1 h 43 m)
Local time variation	−4 min / day

8.4   Mission scenario

As CoRoT flies on a PROTEUS bus, only low earth orbits are allowed. In order to observe the same direction of the sky for a long period of time (several months), not being blinded by the Sun or occulted by the Earth, the satellite must have a polar inertial orbit and a line of sight roughly perpendicular to the orbit plane. The orbit parameters are listed in Table 8.1.

Once given the orbital movement, the constraints to be taken into account for the orientation of the spacecraft are:

Sun glare: The observations are possible when the direction of the Sun is at more than 90° of the observed field.

Straylight scattered by the Earth: At the altitude of 896 km, the Earth is still seen as a big sphere and the limb is a source of scattered light. Considering that the line of sight must remain at more than $\theta = 20°$ from the limb (limit of baffle efficiency), the radius of the observation cone is $\gamma = \arccos(R/a) - \theta = 10°$ (see Fig. 8.6).

Roll domain: A roll angle of ±20° on the boresight axis, after alignment of the solar arrays for the optimum power budget. Such a rotation is helpful to optimise the projection of the target stars onto the CCD matrices (to put targets out from saturated columns, for instance).

Payload thermal constraints: Because of the focal unit radiator, the Ys+
satellite wall (see Fig. 8.7) must be in the shade as much as possible (north-
ward in winter, southward in summer). Ys+ will be exposed to the Sun
only when the Earth is close to the Line of Equinoxes (low solar declination,
high solar azimuth in the radiator reference frame).
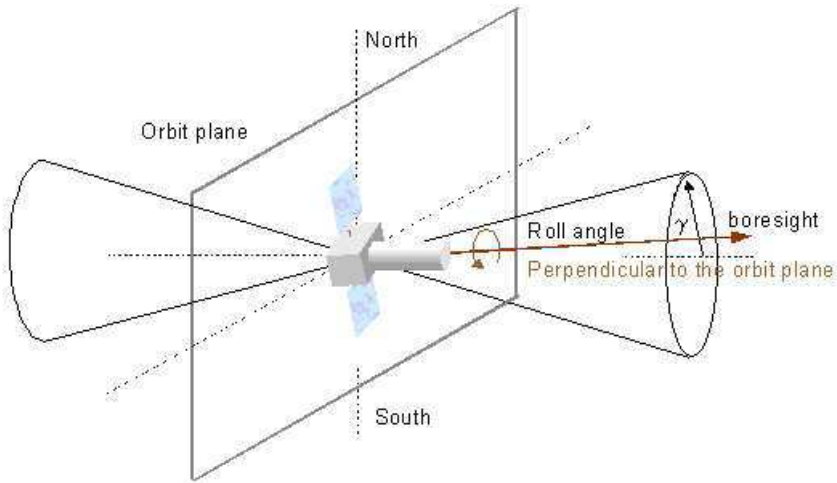
Figure 8.6: *Limits of the flight domain (inertial orbit) of* CoRoT *satellite. Figure
taken from* CoRoT *website at* CNES.

8.5 Mission design

Taking together the constraints which determine the mission scenario described
above, we obtain a set of rules that determines the design of the mission.

To keep scattered light to a minimum, when the Sun gets closer to the orbit
plane and is about to blind the telescope (twice a year), the spacecraft performs a
reversal attitude manoeuvre. This fact divide the year into two 6-month periods of
observation (by convention, summer and winter). The right ascension (RA) of the
orbit plane ($\Omega = 12.5°$) has been chosen after a ground preparatory observation
campaign: CoRoT will look in the sky at RA $= 6^{\mathrm{h}} 50'$ in winter (in *Serpens*
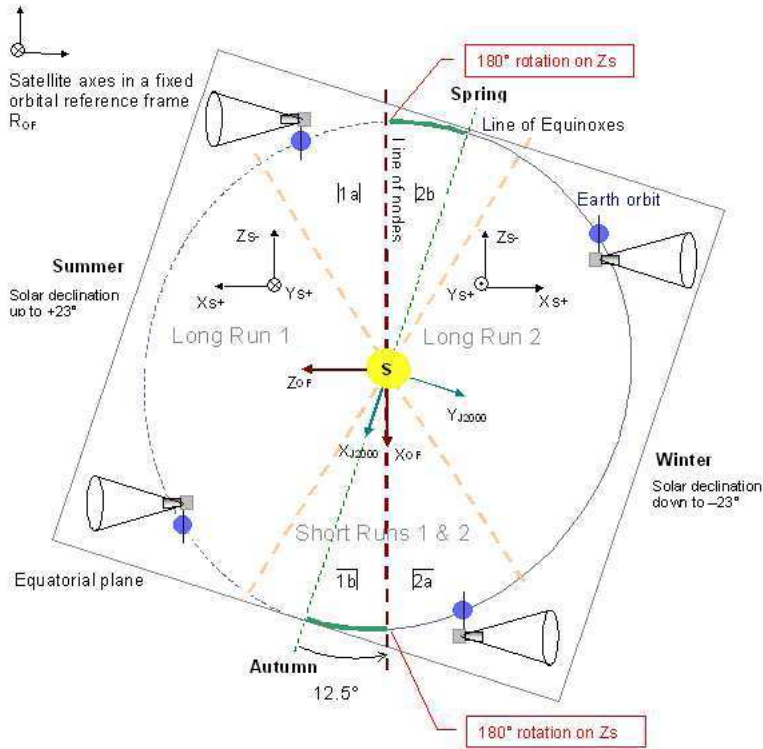
Figure 8.7: *The relative positions of* CoRoT *and the Sun during the year. The two long runs (Core Programme) and the four short runs (Exploratory Programme) are marked in the figure. Figure taken from* CoRoT *website at* CNES.

Cauda constellation towards the Galactic centre) and at RA = $18^{\mathrm{h}}\,50'$ in summer (in *Monoceros* constellation towards the Galactic anti-centre). Thanks to the baffle efficiency, it is possible to get closer to the Earth limb direction and thus orientate the satellite inside a cone with a 10° diameter. When projected onto the sky, this cone draws the two eyes of CoRoT (see Fig. 8.8), where will be selected the stellar fields to be observed.
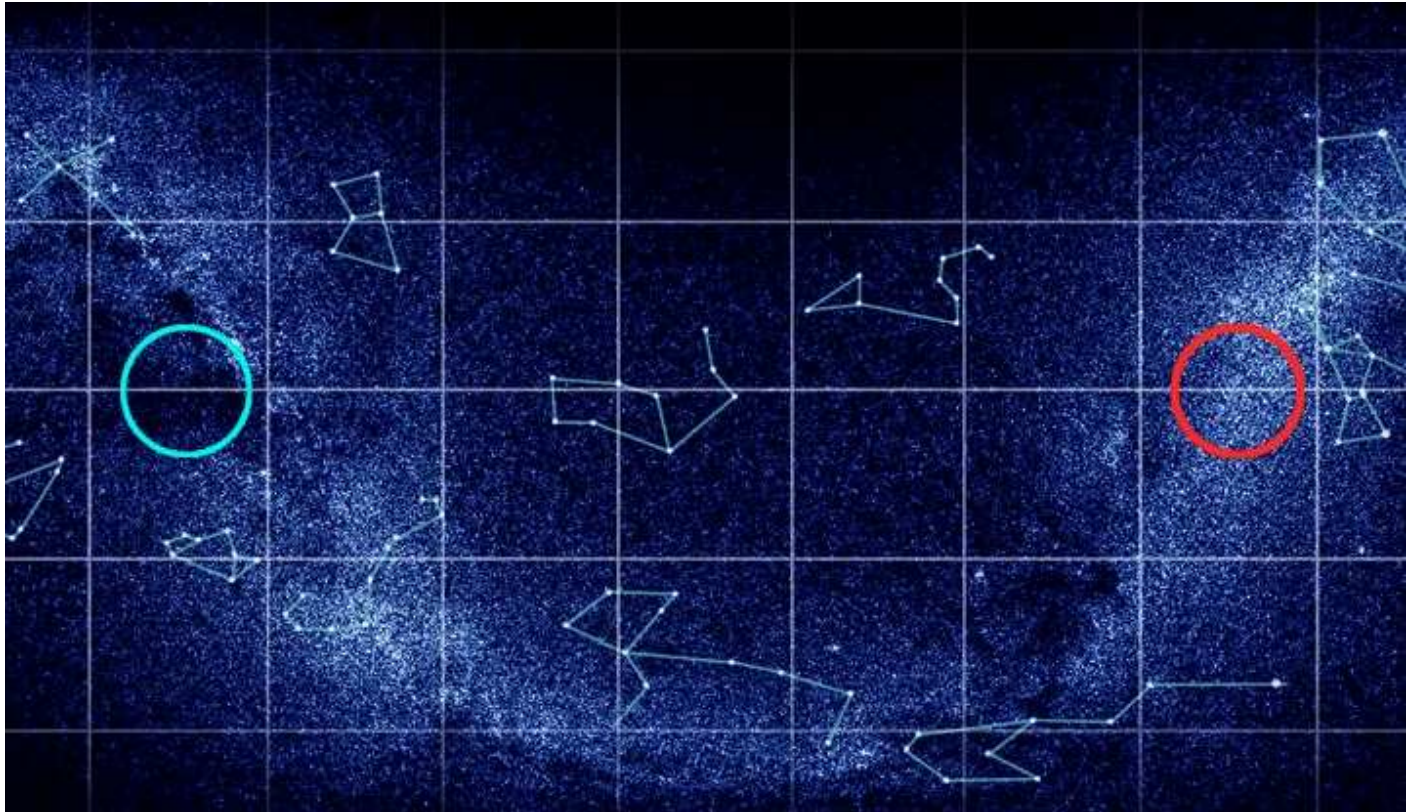
Figure 8.8: *The sky observed by* CoRoT *, towards the Galactic centre* (left) *and anti-centre* (right) *directions. Figure taken from* CoRoT *website at* CNES.

Two types of runs share the available time of observation:

Long runs: With a period of continuous observation of ~ 150 days. The long runs constitute the Core Programme devoted to seismology and Exoplanet Programme.

Short runs: With a period of continuous observation of 20 to 30 days. The short runs are equally shared by the Exploratory Programme of seismology and the Additional Programmes.

Each half year period contains a long run and one or two short runs. As a function of the right ascension of the depointing, the reversal manoeuvres are performed close to the line of nodes in a range of 20 days. During the observing runs (alternately 20 and 150 days), the spacecraft is 3-axis stabilised with asterocentric pointing. The jitter of stars on the detector is then less than 0.5 arcsec (0.2 pixels).

As mentioned in the satellite description section, the CoRoTcam includes four CCDs arranged in a square pattern, with a pixel scale of 13.5 μm, corresponding to 2.32 arcsec on the sky. Two of the CCDs are dedicated to asteroseismology, and two to planet finding, giving rectangular fields of $1.3° \times 2.6°$ for each programme (see Fig. 8.9). The asteroseismology CCDs are set slightly forwards of the focal plane to create a defocused image, and are read in frame transfer mode every second. Up to five stars with apparent magnitudes in the range $5.7 \leq V \leq 9.5$ mag are monitored on each CCD, and their light curves are transmitted to the ground with 32 s sampling (1 s on request). In addition, up to six 30×30 pixel windows can be transmitted to the ground every 32 s. The exoplanet CCDs are read every 32 s, and up to 6 000 stars per CCD in the range $11.5 \leq V \leq 16$ mag are monitored. Because of telemetry limitations, aperture photometry is performed on board and light curves with 512 s sampling are downloaded (32 s sampling is available for up to 500 stars per CCD). An objective prism inserted in the light path of the exoplanet CCDs gives rise to a very low-resolution spectrum at the location of each star, allowing the generation of 3-colour light curves for up to 5 000 stars with $V < 15$ mag using appropriately positioned apertures. Small windows spread over the CCD are used in both fields to monitor the background

level. The pointing of the satellite is adjusted based on astrometry from the asteroseismology channel. The relative position (left/right) of seismology and exoplanet channels has been defined at the same time as the orbit plane, as a compromise between the two programmes to set each half-field in the most favourable orientation inside the observed sky. In the first step of the CoRoT mission definitions, the candidates stars catalogue for the seismology mission holds 11 primary stars and 813 secondary stars. For the exoplanets mission it holds at least 200 000 candidates for observation.
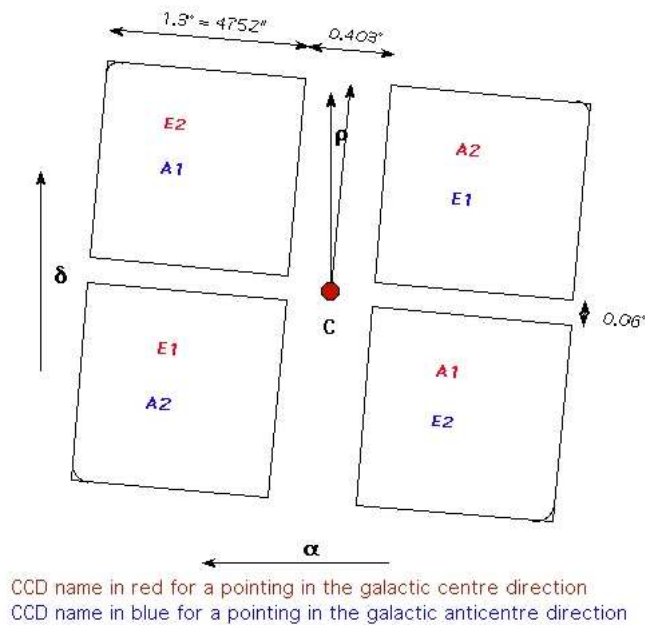
Figure 8.9: *Schematic layout of the focal plane. The CCD names* E1 *and* E2 *correspond to the exoplanet field and* A1 *and* A2 *to the asteroseismology field. The angles* α, δ *and* ρ *are respectively the right ascension and declination of the centre,* C, *of the focal plane, and the inclination of the longer side of the asteroseismology or exoplanet field to the meridian. Figure taken from* CoRoT *website at* CNES.

The 8th of March 2009 the satellite suffered a loss of communication with data processing unit number 1, processing data from one of the two photo-detector chains on the spacecraft. Science operations resumed early April 2009 with data processing unit number 1 offline while data processing unit number 2 operating

normally. The loss of photo-detector chain number one results in the loss of one CCD dedicated to asteroseismology and one CCD dedicated to planet detection. The field of view of the satellite is thus reduced by 50% and the loss of channel one seems to be permanent.

In telecommunications and electronics, the duty cycle is the fraction of time that a system is in an "active" state. Every interruption in the data makes the signal-to-noise decrease and affects the seismology spectrum by windowing. The mission scenario and the sensitivity of the equipment to radiations must guarantee continuous observations as much as possible. If it increases, a perturbation can be considered as a cause of unavailability. The duty cycle estimated values previous to the launch was around 97% over five moving days for seismology, actually it is around $90 - 98\%$. In the exoplanet field periodic crossings of the South Atlantic Anomaly turn to be the main contributor, and reduce it to 88% over a long run in the previous estimations. Actually it is around 86%.

8.6   Observing schedule and data products

The CoRoT satellite was successfully launched at 14:23:00 UTC on 27th of December 2006, atop a Soyuz 2.1b carrier rocket from Baïkonour Cosmodrome, in Kazakhstan (see Fig. 8.10). CoRoT subsequently reported first light on 18th of January 2007. Mission flight operations were originally scheduled to end 2.5 years from launch but actually flight operations have been extended to January 2010 and then to 2013 (see the Section 8.8 about CoRoT Two for more details).

As mentioned in the previous Section, the regular observing pattern for the CoRoT satellite is observing one target field for five months continuously (long run, abbreviated as LR), then switching to another field in the same direction for approximately 21 days (short run, abbreviated as SR) and then turning to face the opposite Galactic direction. This cycle will be repeated as long as the mission duration. Once the satellite was launched and after the commissioning period, where all the calibrations and engineering assessment were made, the CoRoT satellite performed the *initial run* (IRa1) on February 2007, monitoring the first

Figure 8.10: CoRoT *launch on December 2006 on board a* Soyuz 2.1в *rocket in Baïkonour (Kazakhstan). Figure taken from* CoRoT *website at* CNES.

targets. From this moment the spacecraft has been pointing alternatively towards the Galactic centre and anti-centre directions to perform the observations. These runs are named as LRc or SRc for the long and short runs in the Galactic centre direction and LRa or SRa for the long and short runs in the Galactic anti-centre direction, and they are followed by the number of the run. In Fig. 8.11 is showed the scheme of the CoRoT runs. The beginning and end date of the runs are not exactly the same for the seismology and exoplanet channel, depending on the runs, exoplanet runs begin three to five days after the seismology runs. Since LRc3, the CoRoT satellite is operating only with chain number 2 (data processing unit number 2 and CCDs A2 and E2) due to a failure system whose origin remains unknown yet.
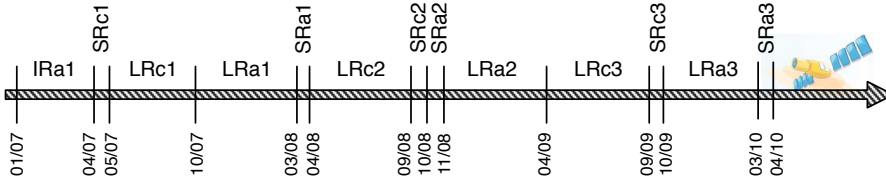
Figure 8.11: *Schedule of the runs planned for the* CoRoT *mission.*

Different products are obtained from data collected by the CoRoT satellite. From raw data (N0 products[8]), with important instrumental and environmental perturbations, to light curves ready to scientific analysis (N2 products). The aim of correcting the raw data is to optimise the duty cycle and reach the expected performances of the mission. A detailed description of the products can be retrieved from the CoRoT documentation web site[9] at the IAS (Institute d'Astrophysique Spatiale) Data Center. An overview of the whole process is showed in Fig. 8.12. The different data products obtained are:

N0 products: Raw data obtained at CoRoT Mission Center in CNES and retransmitted to the CoRoT Data Center (CDC) at LESIA. This data is not suitable for scientific use.

N1-Exo Alert products: Data received every week from CNES. After a local treatment (concatenation of daily files), data are forwarded to OAMP (Observatoire Astronomique Marseille-Provence) which manages the alert mode in order to oversample interesting stars.

N1 products: The following corrections are applied in order to obtain the N1 data products: offset subtraction, suppression of the outliers, correction of the electromagnetic interferences, gain correction, integration time correction, background subtraction and jitter correction. The pipeline N0–N1 is operated every one to seven days and therefore deals with short term corrections. Those data are restricted to a limited community. A complete review of the different correction pipelines can be found in Samadi et al. (2007).

---

[8]"N" refers to *niveau* in French, level in English.
[9]http://idoc-corot.ias.u-psud.fr/jsp/CorotHelp.jsp.

N2 products: Data received from LESIA to the IAS Data Center. The pipeline N1–N2 is operated once a run is finished. This data level corresponds to data "ready to use" by a scientist without a priory knowledge of the instrument. This means that data of this level should be easy to handle, and do not require the use of auxiliary data to use the main product: the light curves. Those data are available to about 70 CoIs and few GIs before becoming public.

N3 CVC products: The information present in the N3 product allow scientists to make candidate lists of their objects of study and to obtain some basic light curve information. This data includes a basic light curve modelling, sufficient for producing class memberships for each target. For every measured field, an ASCII file with CVC ("CoRoT Variability Classifier") results is delivered. For more details see Debosscher et al. (2009).
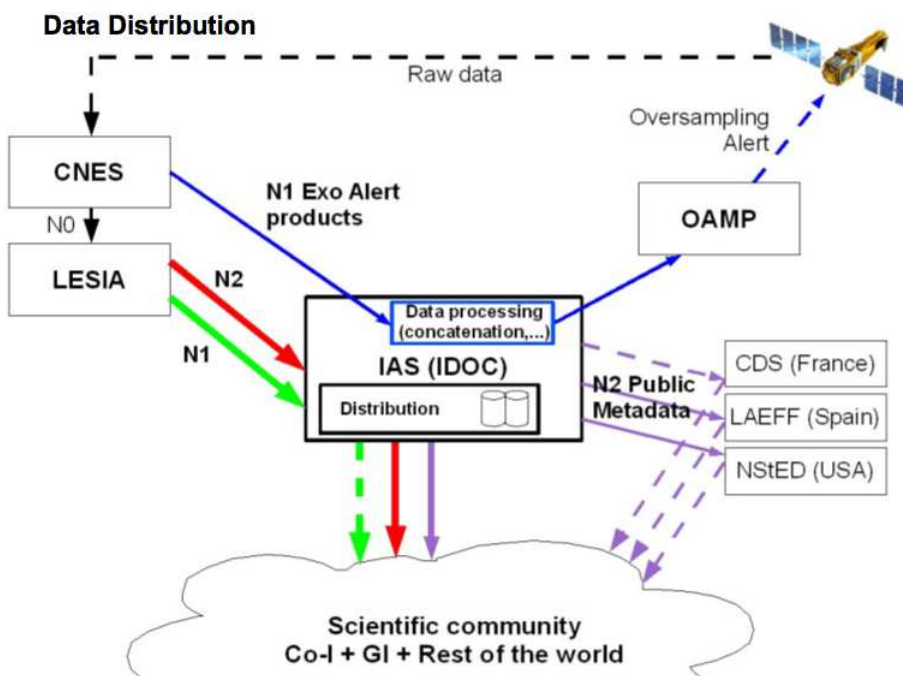
Figure 8.12: *Overview of the data acquisition process. Figure courtesy of H. Ballans.*

N2 Public Data are available since 19th of December 2008. N1 and N2 products are available through the interface or in a set of complete runs at the IAS Data Center website[10] of the CoRoT space mission. The N2 public metadata files are sent to the Scientific Data Center[11] at LAEFF (Laboratorio de Astrofísica Espacial y Física Fundamental) and NStED[12] (NASA/IPAC/NExSci Star and Exoplanet Database) at NASA for their own public interface. The data is also available through CDS[13] (Centre de Donées astronomiques de Strasbourg). N3 CVC products are available via the VizieR website[14].

As an example, for the IAS Data Center, since the end of December 2008 to January 2009 a total volume of 5.4 TB (compressed N2 products) has been downloaded from the CoRoT archive (484 GB through the search interface, and 4.9 TB as complete runs). In only one month (between December 2008 and January 2009), the N2 public archive was visited 210 times by 108 different users, this fact emphasises the importance of the CoRoT data to the scientific community.

8.7 Early results of the CoRoT space mission

On 22nd of October 2009 the scientific journal *Astronomy & Astrophysics* published a special issue devoted to the early results obtained with the CoRoT space mission. It includes 55 articles dealing with the primary goals of the CoRoT mission, that is, exoplanet hunting and asteroseismology, and also with other topics in stellar physics.

Up to now, 14 exoplanets have been discovered in the CoRoT data and confirmed by ground-based follow-up campaigns, the first one being CoRoT-1b (Snellen et al. 2009, discovered in May 2007). The difficulty with this exoplanet hunting is nicely illustrated by some papers (Queloz et al. 2009; Almenara et al. 2009) that describe the long process of deciphering the candidates and finally

---

[10] http://idoc-corot.ias.u-psud.fr/.
[11] http://sdc.cab.inta-csic.es/corotfa.
[12] http://nsted.ipac.caltech.edu/.
[13] http://cds.u-strasbg.fr/.
[14] http://vizier.u-strasbg.fr/viz-bin/VizieR?-source=J/A+A/506/519.

characterising a few stars hosting planets among tens of thousands. In this issue, two papers are devoted to the most exciting, and now famous, planet-hosting star: CoRoT-7. Léger et al. (2009) reported the discovery of CoRoT- 7b, the smallest exoplanet ever found, as was announced in February 2009 during the *First* CoRoT *International Symposium*. In a second article, Queloz et al. (2009) measured the mass of the planet ($5 \times$ Earth masses), using additional, ground-based measurements. They calculated its density (about $5.6 \, \mathrm{gr/cm^3}$), showing that CoRoT-7b is a rocky planet, just like the Earth. This is the first rocky exoplanet confirmed to date. Queloz et al. (2009) also discovered a third planet in the CoRoT-7 system. Now known as CoRoT-7c, it is another super-Earth exoplanet of about $8 \times$ Earth masses.

The accuracy of the CoRoT data is exemplified by the detection of the secondary transit of CoRoT-1b, when the planet passes behind its star. This is a real challenge because the amplitude of such an event is about one hundred parts per million. Comparing the depths of both transits provides information on the albedo of the planet, hence on the nature of its atmosphere (Alonso et al. 2009).

The primary goal of CoRoT is not only the exoplanet hunting, but also to studying the seismology of stars. This part of the mission is also a major step forward as illustrated by several papers that deal with the detection and measurements of solar-like oscillations in distant stars. CoRoT shows that the oscillations are generally more complicated than those of the Sun, which poses new problems of interpretation (e.g. García et al. 2009; Barban et al. 2009). Such oscillations have also been detected and quantified for the first time in many red giants, using data from the exoplanet search program (Hekker et al. 2009). The physical processes responsible for these oscillations are now understood (Dupret et al. 2009).

CoRoT also gave astonishing results about hot stars. The satellite observed a Be star during an outburst phase and measured the change in the oscillation spectrum during this rare event. These observations gave insight into the nature of the explosion (Huat et al. 2009a; Floquet et al. 2009). It will help in solving a question that has been pending for years: are oscillations the cause of the outburst? Moreover, for the first time, we have been able to observe simultaneously the rotational and the pulsational frequencies separate, constituting a proof of

the presence of pulsations in a Be star (Diago et al. 2009a, see Chapter 11).

During the first short run (SRc1) CoRoT has observed the δ Scuti star HD 174 936, revealing a total number of 422 frequencies (García Hernández et al. 2009). HD 174 936 has become the first δ Scuti star to be modelled using space-based photometry. The stellar modelling has confirmed a quasi-periodic pattern similar to the so-called large separation in solar-like stars.

Although primarily devoted to asteroseismology and exoplanet search, CoRoT also addresses many important topics in stellar physics. Several papers deal with stellar activity and report the detection of spots in the photospheres of the stars (Mosser et al. 2009), giving access to the rotation rate of the stars. In some cases, it is even possible to detect the latitude dependence of the rotation rate (Lanza et al. 2009). Significant progress in the modelling of fast-rotating stars will help in understanding these new data (Reese et al. 2009).

Actually, the CoRoT satellite has been orbiting the Earth for nearly three years and will be operated until 2013. This *Astronomy & Astrophysics* special issue nicely shows that it has already been a pioneering mission and has led to major insights in both exoplanetary and asteroseismic domains. The CoRoT successors are already on their way: the KEPLER mission by NASA, a super CoRoT devoted to finding Earth-size and smaller exoplanets, was launched in March 2009. Even more ambitious, the ESA project PLATO is still under assessment as a part of the ESA Cosmic Vision program for 2015–2025. PLATO will be able to combine the detailed study of the stellar interior and of the planetary environment of tens of thousands of bright stars.

8.8 CoRoT Two

The initial duration of the CoRoT mission was 2.5 years, but the scientific results up to now are of such importance that the mission extension has become obvious. CNES, together with its national partners (CNRS[15] and Observatoire de

---

[15]Centre National de la Recherche Scientifique: http://www.cnrs.fr/.

Paris–Meudon[16]) and international partners (Austria, Germany, Belgium, Brazil, ESA and Spain), has extended the operations of the CoRoT mission for three additional years, until 31st of March 2013. The decision was taken on 23rd of October 2009.

The success of this first phase of the mission and the impact of the early scientific results, described in the previous section, were the basis for the decision to extend the mission operations. The three year extension will be used to probe new types of stars and to revisit, and study in depth, those stars which have exhibited the most unexpected behaviour. The impact on the search for exoplanets will be an increase in the number of detections, and there will be particular emphasis on the search for "hot super-Earths", planets slightly more massive than the Earth but much closer to their parent star.

---

[16]Website: http://www.obspm.fr/.

I don't really want to stop the show,
But I thought you might like to know,
That the singer's going to sing a song,
And he wants you all to sing along.

Paul McCartney

9

The study of Be stars with CoRoT

In this Chapter we present the improvements that the CoRoT mission offers to the study of Be stars. Moreover, we also present the main objectives of the study of the Be phenomenon. Due to the interest of observing Be stars with CoRoT, a vigorous international collaboration has been established to propose such observations and to study and analyse the data of Be stars: The CoRoT Be Team, that will be described in the following. Finally, we present some instrumental effects present in the analysed N2 data for Be star light curves. These instrumental effects will be taken into account for the frequency analysis of the Be targets carried in the following Chapters.

9.1 What does CoRoT bring to the study of Be stars?

The final goal in Be star studies is to establish the pulsational behaviour of Be stars, which is still a matter of controversy. The CoRoT space mission is allowing the study of the internal structure of Be stars by means of asterosesimologic techniques. Unfortunately, to reach this objective we have to wait for theoretical models of the stellar stability for high rotational velocity stars.

In this sense, the CoRoT satellite provides us with unprecedented accuracy, long duration, highly sampled photometric data of Be stars. On average, one bright Be star is observed in each seismology field of CoRoT in the Core Programme, while a few tens of fainter Be stars are observed in each exoplanet field of CoRoT as part of the Additional Programme. As explained in Chapter 8, CoRoT observing runs last from a few weeks to five months. In the seismology field, the time sampling corresponds to one measurement every 32 s, while in the exoplanet field one measurement is obtained every 512 s. CoRoT data of Be stars will thus allow us to detect many frequencies with a precision in amplitude down to 10^{-6} mag, to disentangle very close frequencies ($\Delta\nu = 0.006 \, \mathrm{c\,d^{-1}}$) which could produce beatings and to detect low-amplitude modes.

In Fig. 9.1 we show a comparative illustration between the ground-based and CoRoT space-based photometric data obtained for the late Be star HD 50 209, studied in Chapter 11. In the left panels we have plot the data points obtained in both data sets, restricted to a time interval of 7 days. Top-left panel shows the observations of the star HD 50 209 carried by Gutiérrez-Soto et al. (2007a) at the OSN in 2006. Note that we only have measurements for several hours in each day, thus, the ground-based data show big gaps that will produce aliasing effects in the periodogram of this data. In the bottom-left panel the CoRoT data, obtained in the LRa1, for the same star is depicted. We clearly see the continuos observations of the CoRoT satellite. In the right panels of Fig. 9.1 we show the periodograms for both 7-day data sets. The OSN data yield to a peak at the frequency $0.48 \, \mathrm{c\,d^{-1}}$ and $1.48 \, \mathrm{c\,d^{-1}}$ due to the aliasing effect, while the CoRoT periodogram clearly shows the detection of three frequencies, being $1.48 \, \mathrm{c\,d^{-1}}$ the one with more am-
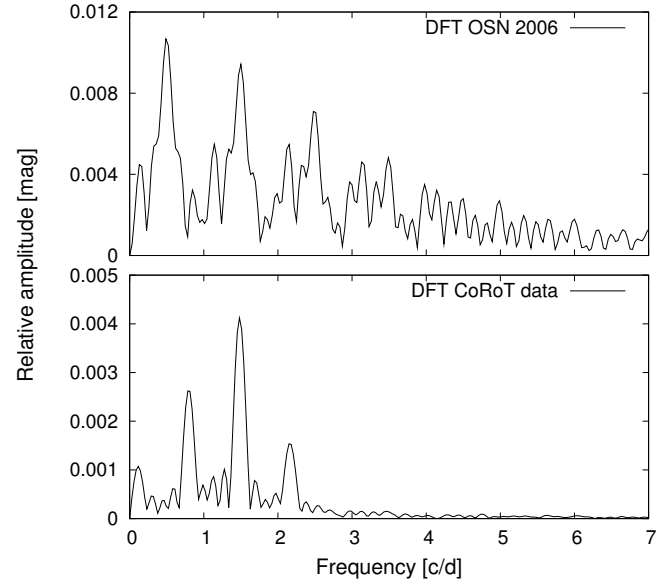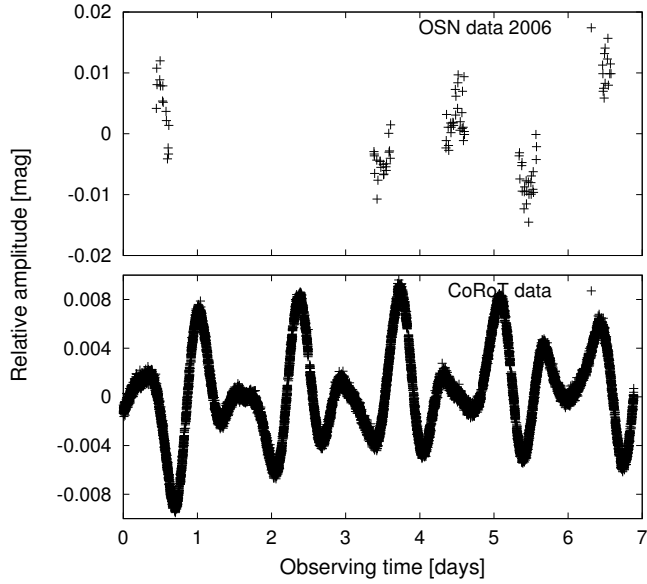
Figure 9.1: *Comparison between ground- and space-based photometry for the Be star* HD 50 209. *Left:* *Data sets for a 7-day time interval are depicted in left panels for the* OSN *and* CoRoT *observations obtained in* 2006 *and* 2007 (LRa1). *The amazing improvement of the* 32 s *sampling of the* CoRoT *data is clearly shown.* Right: *Periodograms for the data sets depicted in left panels. The periodoram obtained from the* OSN *data shows only one frequency with aliasing effects. On the other hand, the periodogram obtained from the* CoRoT *data shows three clearly frequencies.*

plitude. It is clear that the periodogram for the CoRoT data shows a higher signal to noise ratio, that allows a better detection of the frequencies. Moreover, the 1-day aliasing effects are not present in the CoRoT periodogram. As we have seen, the 7-day data set from the CoRoT observations allow us the detection of three significant frequencies. But a complete data set from a CoRoT run contains between 20 and 150 days which will allow the detection of many more frequencies. In Chapter 11 we will show that the continuous 134-day data obtained for the star HD 50 209 with CoRoT allow us the detection of 60 frequencies.

9.2 Objectives of the study of Be stars

In general, the main objectives of the study of Be stars with the CoRoT space mission are the following:

- Detect new pulsation periods, especially beating periods. The longtime coverage is needed for the detection of a beat phenomenon of non-radial pulsation modes in relation with recurrent outbursts.

- Perform a seismic modelling of their interior structure.

- Disentangle stable periods due to pulsations from transient periods due to rotational modulation of temporary, possibly magnetic, co-rotating structures.

- Better understand how the circumstellar disk is generated.

- Detect high degree p-modes of low amplitude in main sequence or slightly evolved early Be stars: Balona and Kambe (1999) have shown that predicted light amplitudes in V band for spherical harmonic degrees $\ell = 4, ..., 8$ are less than 1 mmag if the pulsational velocity amplitude is less than $20 \, \text{km} \, \text{s}^{-1}$.

- Detect low amplitude g-modes in late Be stars.

- Detect rotation and associated modulation.

- Study the influence of a magnetic field on pulsational characteristics.

9.3 The CoRoT Be Team

Due to the interest of observing Be stars with CoRoT, illustrated in the previous text, a vigorous international collaboration has been established to propose such observations and to study and analyse the data of Be stars which CoRoT is providing: the CoRoT Be Team[1], composed of members from several institutes of France, Spain, Brazil and Belgium under the coordination of Coralie Neiner (previously led by Anne-Marie Hubert) at the Observatoire de Paris–Meudon[2]. Ground-based observations are obtained in collaboration with other CoRoT groups and Chilean researchers. Seismic modelling is performed in collaboration with Japanese and Spanish researchers and the SIROCO[3] Project. The CoRoT Be Team has proposed to observe Be stars to the Scientific Committee in two ways:

- Observations of bright Be stars as secondary targets in the seismology fields as part of the Core Programme. The CoIs of CoRoT for the Be stars programme are Anne-Marie Hubert, Coralie Neiner and Eduardo Janot-Pacheco. Several Be stars have been included in the list of targets of the long runs, showed in Table 9.1. Several others are being considered to be included in successive long or short runs, but they are not programmed yet. The web site of the CoRoT Be Team provides the list of all bright seismology targets in the field of view of CoRoT with the observed and proposed ones.

- Observations of faint Be stars in the exoplanet fields as part of the Additional Programme, being Coralie Neiner and Anne-Marie Hubert the Guest Investigators (GIs) of this project. The CoRoT Be stars group is in charge of the selection of faint Be stars as additional targets in the programmes of CoRoT . For this purpose, the CoRoT Be Team searches for faint Be stars in the exoplanet fields of CoRoT using different methods:

    – A literature search, which gives usually any result, since there are not many known Be stars in the V range $12 - 16\,\mathrm{mag}$. We have used

---

[1]http://corotbe.obspm.fr/.
[2]http://www.obspm.fr/.
[3]http://siroco.obspm.fr.

the IPHAS. The INT/WFC Photometric Hα Survey (IPHAS[4]) is a survey of the Northern Galactic Plane being carried out, in Hα, R and I filters, with the Wide Field Camera (WFC) on the 2.5 m Isaac Newton Telescope (INT[5]).

– A large programme of ground-based photometry, using telescopes as e.g. the INT and through the Hα, R and I filters. We have performed observations for the IRa1, LRa1, LRC1 and LRA2 fields for tens of candidate Be stars.

– A study of the stars showing an excess in the infrared flux with the SPITZER[6] survey.

– A large program of ground-based spectroscopy, concerning two different resolutions: low-resolution spectra ($R \sim 1000$) obtained at the OSN[7], NOT[8], INT, and the 2.2m telescope in CAHA–Calar Alto[9] which confirms the emission in the Hα line of the candidate Be stars and give us an estimation of the spectral type. And medium-resolution spectra obtained at the VLT with the FLAMES[10] multi-fibre spectrograph. Actually, part of the IRa01 and LRa1 have been observed between November 2008 to March 2009 (ESO period 82). The observation of LRc1 was scheduled for July to August 2009 (ESO period 83). The observation of the remaining of IRa1 and LRa1, as well as the observation of LRa2 has been requested for January 2010 (ESO period 84). The analysis of the FLAMES spectra of the new Be stars is being performed by Thierry Semaan at the Observatoire de Paris–Meudon.

During the last years, the CoRoT Be Team has been working on the preparation of the CoRoT mission. The French-Belgian group have published several papers related to the Be stars and the CoRoT mission: Neiner et al. (2005b) identified new Be stars in the GAUDI database[11] (see Solano et al. 2005, for

---

[4]IPHAS website: http://www.iphas.org/.
[5]Isaac Newton Telescope: http://www.ing.iac.es/.
[6]SPITZER website at JPL/NASA: http://www.spitzer.caltech.edu/.
[7]Observatorio de Sierra Nevada: http://www.osn.iaa.es/.
[8]Nordic Optical Telescope: http://www.not.iac.es/.
[9]Centro Astronómico Hispano Alemán: http://www.caha.es/.
[10]Fibre Large Array Multi Element Spectrograph (see Pasquini et al. 2002, for details): http://www.eso.org/sci/facilities/paranal/instruments/flames/.
[11]http://sdc.laeff.inta.es/gaudi/.

Table 9.1: *Be stars selected as seismology secondary targets for the different runs.*

Run	Be star	Type	m_{V}
IRa1	HD 50 846	B5e binary	8.43
SRc1	HD 175 869	B9IIIe	5.56
LRc1	HD 181 231	B9Ve	8.58
LRa1	HD 49 330	B0e	8.92
	HD 50 209	B9Ve	8.33
SRa1	-	-	-
LRc2	-	-	-
SRc2	-	-	-
SRa2	-	-	-
LRa2	HD 51 193	B1Vnne	8.06
	HD 51 452	B0IIIne	8.08
LRc3	-	-	-
LRa3	HD 43 913	A0e	7.88

details). Frémat et al. (2006) determined the fundamental parameters of 64 Be stars, based on high-resolution spectroscopic data. Recently, Gutiérrez-Soto et al. (2007a) report a photometric study of Be stars located in the seismology fields of the CoRoT mission. The preparation and the status of the CoRoT Be targets previous to the launch of the satellite were presented in Gutiérrez-Soto (2006, Ph.D. thesis).

9.4 Instrumental effects in the CoRoT light curves

We have seen the great improvements in the study of Be stars derived from the CoRoT mission. However, the CoRoT data is also affected by instrumental effects that will be described in the following in order to help the understanding of the rest of Chapters. The data analysed in this Ph.D. thesis correspond to the calibrated N2 light curves that have been measured by the CoRoT satellite. In Chapter 10 we present the results of three Be stars observed during the IRa1 in the exoplanet field and in Chapter 11 we show the results for the late Be stat HD 50 209 observed during the LRa1 in the seismology field. Most of the

CoRoT light curves provided in the following are related to the CoRoT Julian Day (CoRoT JD). It is important to mention that the zero point for CoRoT JD is the 1st of January 2000, this means that

$$\text{CoRoT JD} = \text{JD} - 2\,451\,545 \qquad (9.1)$$

The CoRoT N2 data comes with unavoidable systematic effects: trends in the light curves due to changes in the amount of incident stray light during the run, periodic changes in flux caused by the satellite orbit and discontinuities in the light curves due to cosmic ray hits on the CCDs. Prior to the data analysis, we have removed all measurements having non-zero quality flags in the N2 product delivery, retaining only valid flux measurements. In this Section we present some common instrumental features detected in the light curve of the Be stars observed by the CoRoT mission until now. The signal acquired by the CoRoT CCDs represents the convolution of the signal coming from the star with both the spectral window and the modulation of the orbit.

9.4.1 Spurious signal

The Earth straylight introduces a periodic signal with period equal to orbital period ($1\,\text{h}\,43\,\text{min}$, $13.97\,\text{c}\,\text{d}^{-1}$, 161.689μHz) in the measured light curve of the stars. Even though the amplitudes of these peaks are low (typically below 900 parts per million, ppm hereafter), they clearly stand far above the low CoRoT noise level. Additional spurious frequencies at $2.007\,\text{c}\,\text{d}^{-1}$ ($23.15\,\mu$Hz) were detected, related to variations in the amount of received stray light due to the Earth's day/night cycle. These can cause sidelobes to appear around the orbital peaks as well (at $13.97\pm1\,\text{c}\,\text{d}^{-1}$, the same occurs for the higher harmonics). In Fig. 9.2, we show the spectral window for the star HD 175 869 studied by Gutiérrez-Soto et al. (2009b) and a zoom of the region about the orbital frequency.

In the majority of Be stars observed with CoRoT until now, the periodic signal originating in the star is within the frequency range of between 0 and $5\,\text{c}\,\text{d}^{-1}(0 - 60\,\mu$Hz). Therefore, the CoRoT spectral window produces a signal
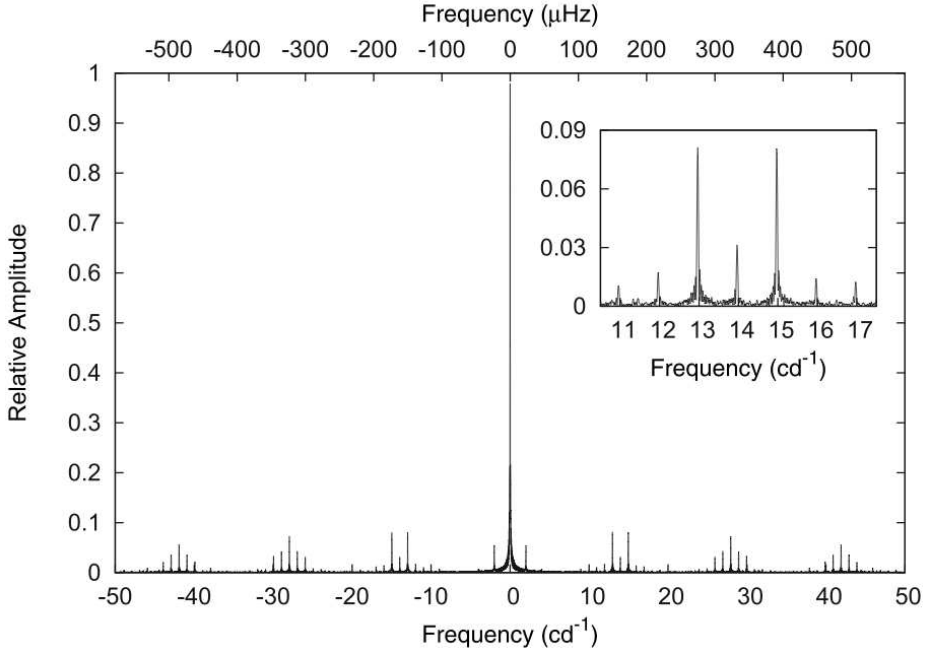
Figure 9.2: *Spectral window of the* CoRoT *light curve for the star* HD 175 869, *studied by [Gutiérrez-Soto et al. (2009b)](). The orbital period appears as a peak with a fundamental frequency of* $13.97\,\mathrm{c\,d^{-1}}$ *and a series of harmonic frequencies, with low amplitude, but that can trouble the detection and analysis of pulsation frequencies of the observed variable stars. Day/night peaks appear at* $\sim 2\,\mathrm{c\,d^{-1}}$, *and signal at* $13.97 \pm 1\,\mathrm{c\,d^{-1}}$ *is also present. Figure courtesy of J. Gutiérrez-Soto.*

in the same domain of the periodogram for all these stars. As shown in Fig. 9.3, aliases appear at frequencies $\nu_{\mathrm{star}} \pm n \times 13.97 \pm 1 \pm 2\,\mathrm{c\,d^{-1}}$, where n is a positive integer number, and ν_{star} is the stellar frequency. Therefore, for the majority of Be stars, aliases appear at frequencies higher than $10\,\mathrm{c\,d^{-1}}$, in groups of frequencies around the orbital frequency and its harmonics. Only aliases related to day/night variations are in the range from 0 to $10\,\mathrm{c\,d^{-1}}$, but those have quite negligible amplitudes. Spectral peaks related to the orbital frequency, day/night peaks and aliases were therefore ignored in the frequency analysis procedure.

Some early-type Be stars may exhibit higher stellar frequencies, as the star HD 49 330, also observed with CoRoT and analysed in Huat et al. (2009a). Vari-
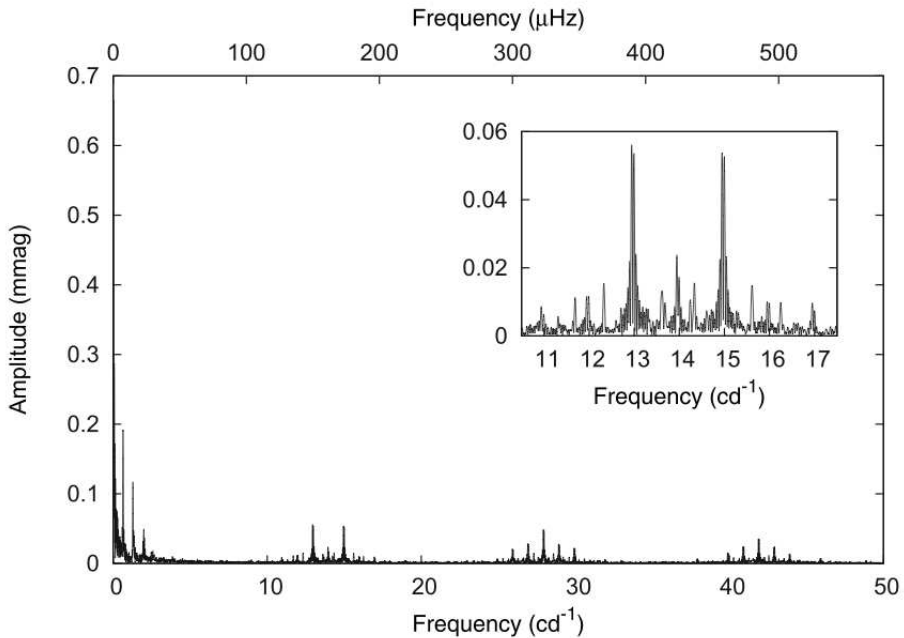
Figure 9.3: *Periodogram of the* CoRoT *light curve for the star* HD 175 869, *studied by* Gutiérrez-Soto et al. (2009b). *Figure courtesy of J. Gutiérrez-Soto.*

ations in frequencies of as high as $16 \, \mathrm{c\,d^{-1}}$ have been detected in this star. For these early-type Be stars, the spectral window produces a more random set of peaks and some caution is required when identifying frequencies coming from the star.

A linear interpolation filling the gaps is also provided by the CoRoT pipeline for the stars observed in the seismology fields. The spectral window of the interpolated data, hence, exhibits peaks neither in the orbital frequency nor day/night frequencies or combinations (see Fig. 9.4), since there are no gaps. The interpolation does not affect the scientific results for the majority of Be stars since the detected peaks appear at frequencies lower than the orbital frequency. An interpolation of the gaps with 2-order and 3-order polynomial functions give similar results within the errors. The interpolation of the gaps might affect the analysis

of other stars that have higher frequencies.
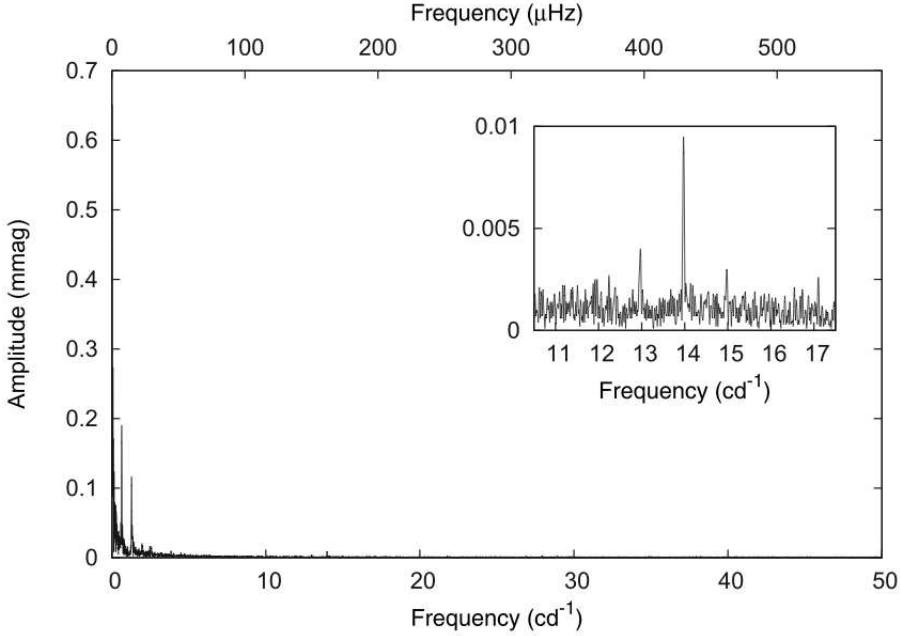
Figure 9.4: *Periodogram of the* CoRoT *light curve for the star* HD 175 869, *studied by Gutiérrez-Soto et al. (2009b), after filling the gaps with a linear interpolation. Figure courtesy of J. Gutiérrez-Soto.*

9.4.2   Modulation

Another instrumental feature is the modulation of the signal with the orbital frequency. The reason is that the CCD response depends on the temperature of the CCD, which depends on the position of the satellite with respect to the Sun, i.e., it varies with the orbital frequency. The signal coming from the star is then multiplied by the signal that varies with the orbit leading to a convolution of two signals in the Fourier domain. In Fig. 9.4, we see that the orbital frequency $(13.97 \, \text{c} \, \text{d}^{-1})$ and its harmonics are still present in the periodogram, even after filling the gaps with a linear interpolation.

9.4.3 Jittering

Usually CoRoT light curves present jumps in the data points. This change on measured flux is due to the jittering effect (see Fig. 9.5 for an example in the three channels data of the exoplanet CCDs). Jitter is the lack of stability of the attitude control system (ACS). This small motion of the satellite's line of sight pollutes the photometric signal because of flat-field and edge effects. The flat-field effect is due to variation in quantum efficiency between pixels. The edge effect is due to the photometric aperture (mask). If the mask is fixed at the CCD level and the observed star is in its centre, then satellite motion moves flux out of the mask, decreasing the measured integrated flux. Although jitter correction algorithms are applied to the CoRoT data pipeline, the analysed N2 products presented here are affected of this pollution in the photometry as we will see in the next Chapters.

9.4.4 Long-term trend

It is a common feature of the CoRoT light curves to show a linear or an almost linear decreasing pattern. In the case of Be stars, this trend could be related to the combination of two variations, one intrinsic to the star and another related to the instrument. As described in Chapter 2, Be stars are expected to have variability of the order of months to years because of changes in the disk. In addition, a slope has been detected in the light curve of all stars observed in the fields of CoRoT, probably due to the aging of the CCDs.

In the case of the exoplanet CCDs, the light curves come with three colour information (RGB). A separated examination of each colour light curve (only status zero points) shows long-term trends with different shapes, see Fig. 9.5. This fact evidences that, for exoplanet light curves, colour information cannot be used for frequency analysis. Therefore, for exoplanet data, we have analysed the "white" flux (R+G+B / 3), that also present long-term variations. In the other hand, the seismology CCDs provide monochromatic data.

We remove these long-term trends, in both exoplanet and seismology data, with a second-degree polynomial function. Nevertheless, some low frequencies close to $0\,c\,d^{-1}$ still appear in the analysis of the light curve. Some of them may be related to the correction of this slope and should be interpreted with caution. Some others can be identified with the beating frequency of the two real stellar frequencies with the highest amplitude or modes with $m = 0$ (see Chapter 11 or Diago et al. 2009a). Periods that have not been observed during at least 6 cycles ($P \geq T/6$) are considered with caution.
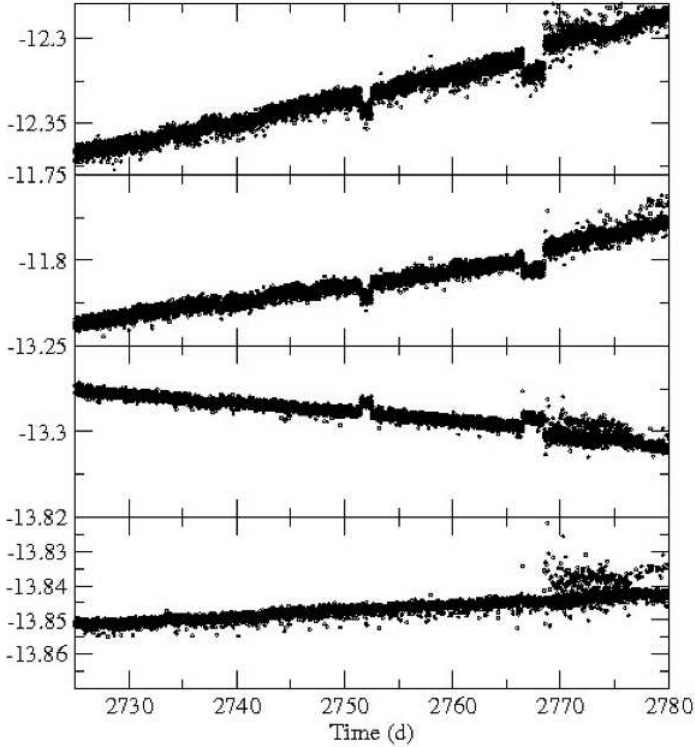
Figure 9.5: *Different long-term trends and jittering effects are present in the three channels of the exoplanet data of the* LRc1 *star* 100870830. *Vertical axis show magnitude in the blue channel* (first top panel), *green channel* (second panel), *red channel* (third panel) *and "white" flux* (bottom panel). *In this composition only points with "status=0" have been plotted. Figure courtesy of Juan Gutiérrez-Soto.*

We were talking
About the space between us all,
And the people
Who hide themselves behind a wall of illusion,
Never glimpse the truth,
Then it's far too late, when they pass away.

George Harrison

10

Be stars in the exoplanet fields of CoRoT

In addition to the bright Be stars observed in the CoRoT seismology fields as described in the previous chapters, CoRoT has also observed faint Be stars in the exoplanet fields. Although the photometric accuracy in the exoplanet fields is lower than in the seismology fields, in the former we have colour information that will be useful to identify modes in large amplitude pulsators, as shown in Garrido (2000b). As members of the CoRoT Be Team, we are in charge of the analysis of three of the Be stars observed in the initial run (IRa1) in the exoplanet CCDs of the CoRoT satellite. In this Chapter, we describe the analysis these three Be stars. We only performed the frequency analysis for these Be stars, a seismology study using colour information was, in that moment, beyond the scope of our work.

10.1 Observations and frequency analysis

To date, more than seven confirmed Be stars have been observed in the exoplanet fields of CoRoT during the IRa1. Some of these stars showed emission in the Hα line in the spectroscopic observations taken with CAFOS[1] at the 2.2 m telescope in Calar Alto (P.I.: Juan Fabregat). All of these confirmed Be stars have spectral types earlier than B5 and high-resolution spectra are need to have a better classification. The majority of these stars are highly variable when analysing their CoRoT light curves. In Table 10.1 we present a list of some of the candidate Be stars observed in the exoplanet CCDs of the IRa1. The time span of the IRa1 data is approximately of 54 days.

Table 10.1: *Be star candidates observed in the* IRa1 *run.*

CoRoT iD	Start	End	V Mag.	USNO-A2
102761769	03-02-2007	02-04-2007	13.08	0825-03100143
102792455	06-02-2007	02-04-2007	14.428	0825.03126936
102892638	06-02-2007	02-04-2007	13.264	0825.03227520
102964342	06-02-2007	02-04-2007	14.256	0825.03283067
102835370	06-02-2007	02-04-2007	14.541	0825.03176567
102847654	06-02-2007	02-04-2007	14.285	0825.03188171
102904910	03-02-2007	02-04-2007	13.773	0825-03237142
102719279	03-02-2007	02-04-2007	13.809	0825-03060502
102791482	03-02-2007	02-04-2007	12.596	0825-03126106
102798228	06-02-2007	02-04-2007	15.001	0825.03133704
102861867	06-02-2007	02-04-2007	15.17	0825.03201573
102973786	06-02-2007	02-04-2007	15.722	0825.03291744
102725623	03-02-2007	02-04-2007	14.82	0825-03066991
102766835	03-02-2007	02-04-2007	12.817	0825-03104592
102854684	06-02-2007	02-04-2007	12.539	-

For the three Be stars, the frequency analysis was performed in the "white" flux data (R+G+B / 3), using the methods described in Chapter 3. In the first stage, we search for frequencies in the light curves using the PASPER code (Diago et al. 2008a), based on standard Fourier transform. The second stage consists of improving with non-linear least squares fitting methods (local minimum) the estimation of initial frequencies detected with the code KURTZ _BOS. Finally, the amplitude,

---

[1]Calar Alto Faint Object Spectrograph:
http://www.caha.es/alises/cafos/cafos.html.

phase and signal to noise ratio are obtained for the improved frequencies.

As is often observed in Be stars, the detected frequencies range from 0.4 to $4\,\mathrm{c\,d^{-1}}$. The determined amplitudes range from 40 to a few $0.01\,\mathrm{mmag}$. For these three Be stars, the resolution in frequency for the spectral analysis is $1/2\,T \sim 1.43 \times 10^{-2}\,\mathrm{c\,d^{-1}}$ (Kallinger et al. 2008), T being the total interval covered by observations.

10.2   Results and discussion

Here we present a brief discussion on these three Be stars observed by the CoRoT satellite in the IRa1. The complete table with the detected frequencies, amplitudes, phases and S/N ratio can be retrieved in Table 10.2. A report on a few more stars of the IRa1 run studied by the CoRoT Be Team can be found in Gutierrez-Soto et al. (2008).

10.2.1   CoRoT star 102725623

As seen in Fig. 10.1, the CoRoT light curve of the star 102725623 shows a long-term trend larger than the total duration of the IRa1 run which would be produced by changes in the circumstellar disk. A jump in the data is also present due to a jittering effect in the CCDs. We have removed these trends by fitting a polynomial function of second degree without making assumptions on their origin. The initial data points affected by the jittering effect have been removed from the data before performing the spectral analysis. The resulting light curve is depicted in the bottom panel of Fig. 10.1. After removing these long-term variations, we found a significant peak at $f_1 = 0.897393\,\mathrm{c\,d^{-1}}$ with an amplitude of $0.4\,\mathrm{mmag}$ in the frequency domain of the short-term variability. The periodogram for this star is depicted in Fig 10.2 together with the phase diagram for the detected frequency. Another long-term frequency was found in the data. The frequency parameters are reported on Table 10.2.

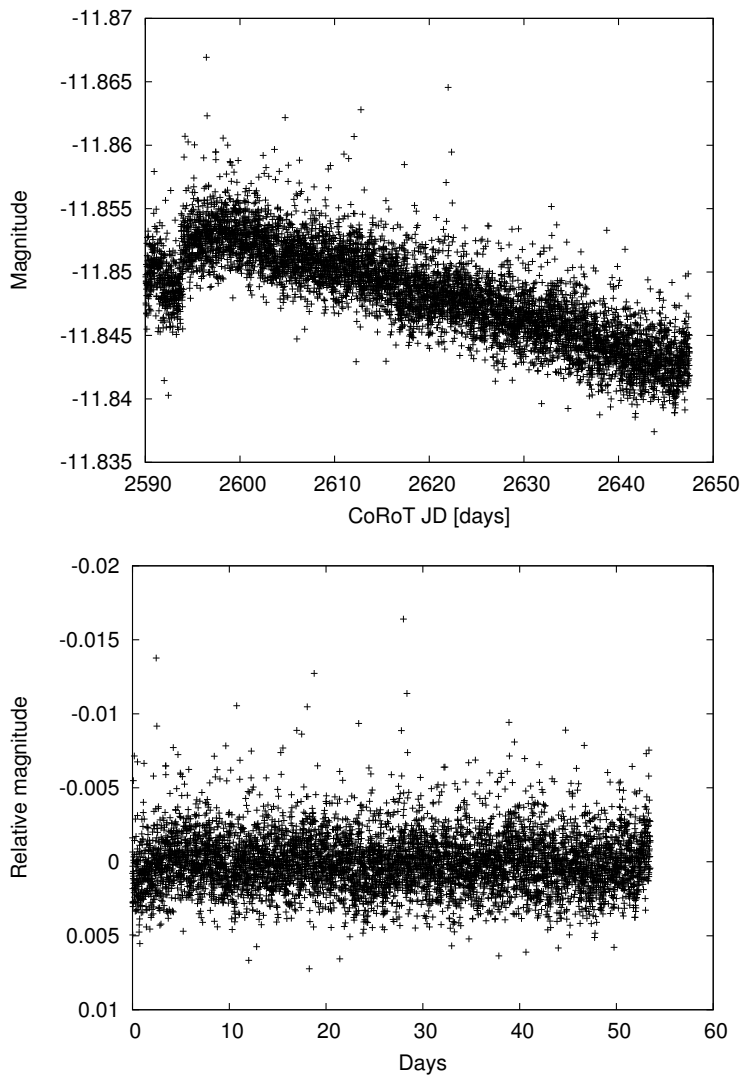**Figure 10.1:** Top: CoRoT *light curve of the star* 102725623. Bottom: *light curve of the star* 102725623 *after removing the long-term period and the jittering effect. The definition of the* CoRoT JD *is given in* Eq. 9.1.
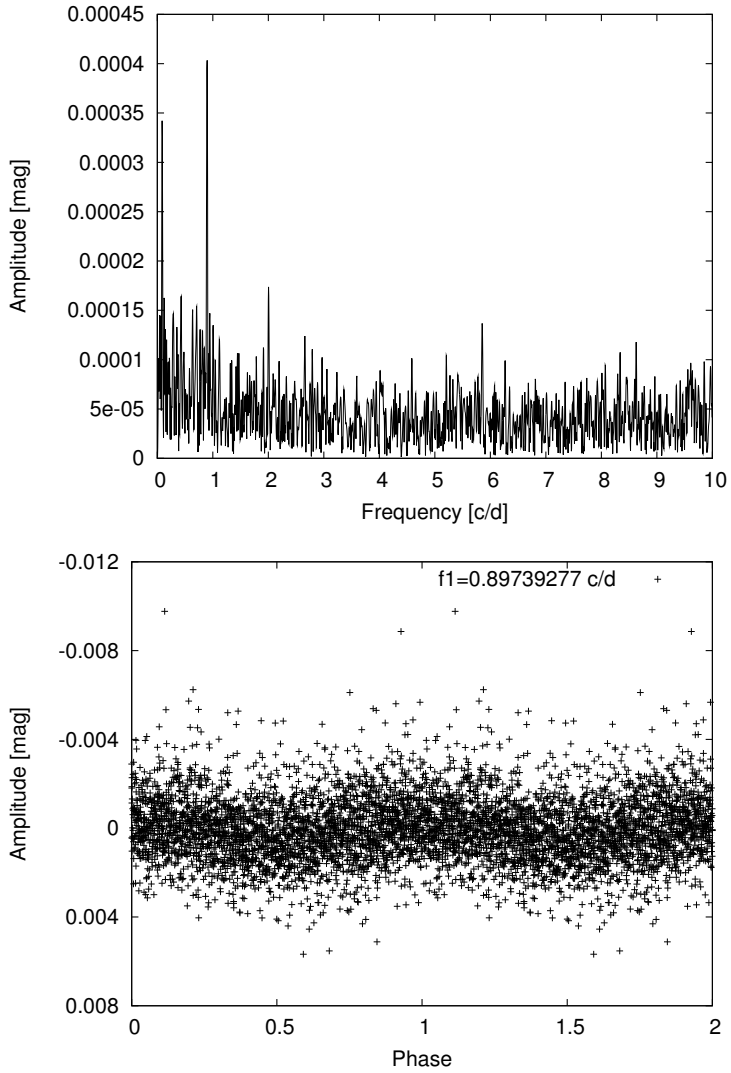
Figure 10.2: Top: *Periodogram for the* CoRoT *star 102725623.* Bottom: *Phase diagram for the frequency f_1 detected in the* CoRoT *star 102725623. Note that two cycles are shown for clarity.*

Concerning the spectroscopy data, for this star we have one *FLAMES* spectrum which have, unfortunately, very low resolution. Hence, no information about the $V \sin i$ could be extracted. Gutiérrez-Soto (2006, Ph.D. thesis) provided a B6 spectral type for this star. At the time this Ph.D. thesis is written the star 102725623 is still being studied in order to discover if it is a normal Be star or not. This star was also observed in the LRa1 by the CoRoT mission, therefore the analysis of this new data could give new insights on the nature of this star.

10.2.2   CoRoT star 102964342

In the top panel of Fig. 10.3 we present the light curve of the CoRoT star 102964342. A quasi-linear decreasing pattern of long period and an important jump in the data are present. The data points after the jump have been removed. In the bottom panel of Fig. 10.3 we depict the light curve after removing these effects.

From the spectral analysis we found five significant frequencies, reported in Table 10.2. The frequency $f_1 = 3.84457 \, \mathrm{c \, d^{-1}}$ is the one with greater amplitude, which is around $0.9 \, \mathrm{mmag}$. The frequency f_1 seems to be the first harmonic of f_2 because $2 \times f_2 \sim f_1$. In the upper panel of Fig. 10.4 we show the periodogram for the star 102964342. The phase diagram for frequency f_1 is plotted in the bottom panel of Fig. 10.4. Moreover, a couple of frequencies very close to f_2 appears in the significant frequency list. These two frequencies (f_4 and f_5) seem to be quasi-equidistant from f_2.

Concerning ground-based spectroscopy, this star was observed on 11th of March 2008 with the $2.2 \, \mathrm{m}$ telescope at Calar Alto with the spectrograph CAFOS. One low-resolution spectrum (B-200 grism, $4.71 \, \mathrm{\mathring{A}}$ / pix) was obtained for this star with a exposure time of $900 \, \mathrm{s}$ and signal to noise ratio of 80. The spectrum shows emission in the Hα line ($I_{\mathrm{e}}/I_{\mathrm{c}} = 2.75$) and the H$\beta$ line is partially filled with emission. It exhibits absorption in helium lines such as He I $4\,387 \, \mathrm{\mathring{A}}$, He I $4\,471 \, \mathrm{\mathring{A}}$, and no absorption in Mg II $4\,481 \, \mathrm{\mathring{A}}$. We estimate a spectral type between B1 and B2. Unfortunately, we cannot compute the $V \sin i$ from this low-resolution spectrum.

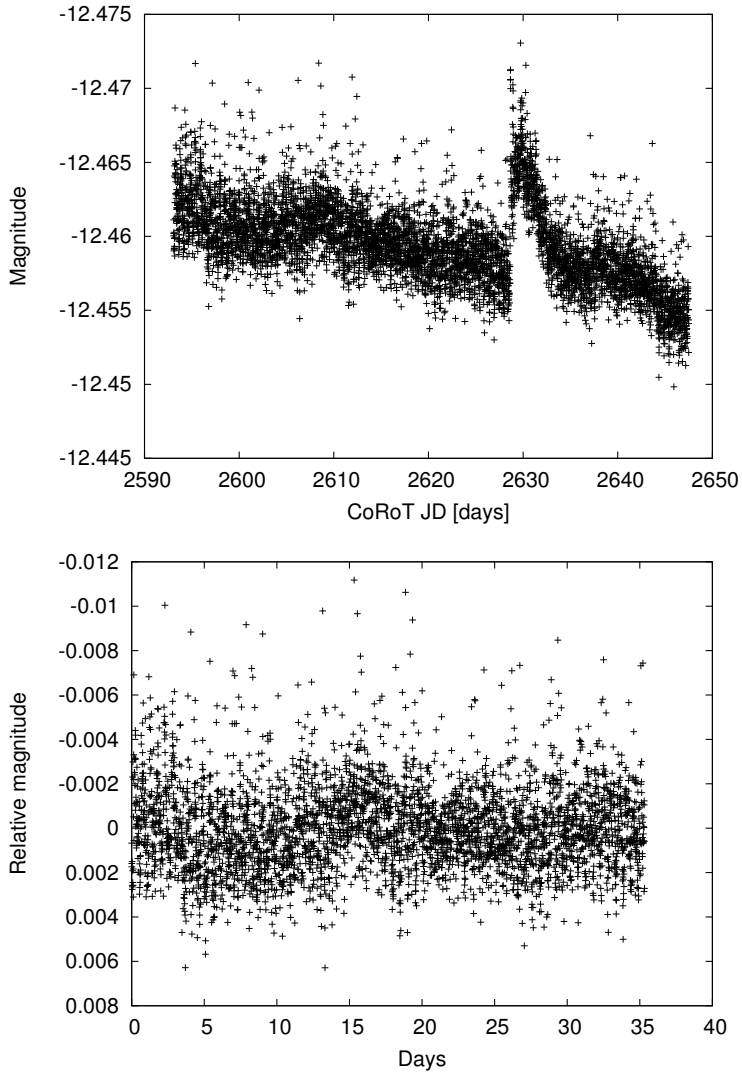**Figure 10.3:** Top: CoRoT *light curve of the star* 102964342. Bottom: *light curve of the star* 102964342 *detrended of the long-term period and the jittering effect. The definition of the* CoRoT JD *is given in* Eq. 9.1.
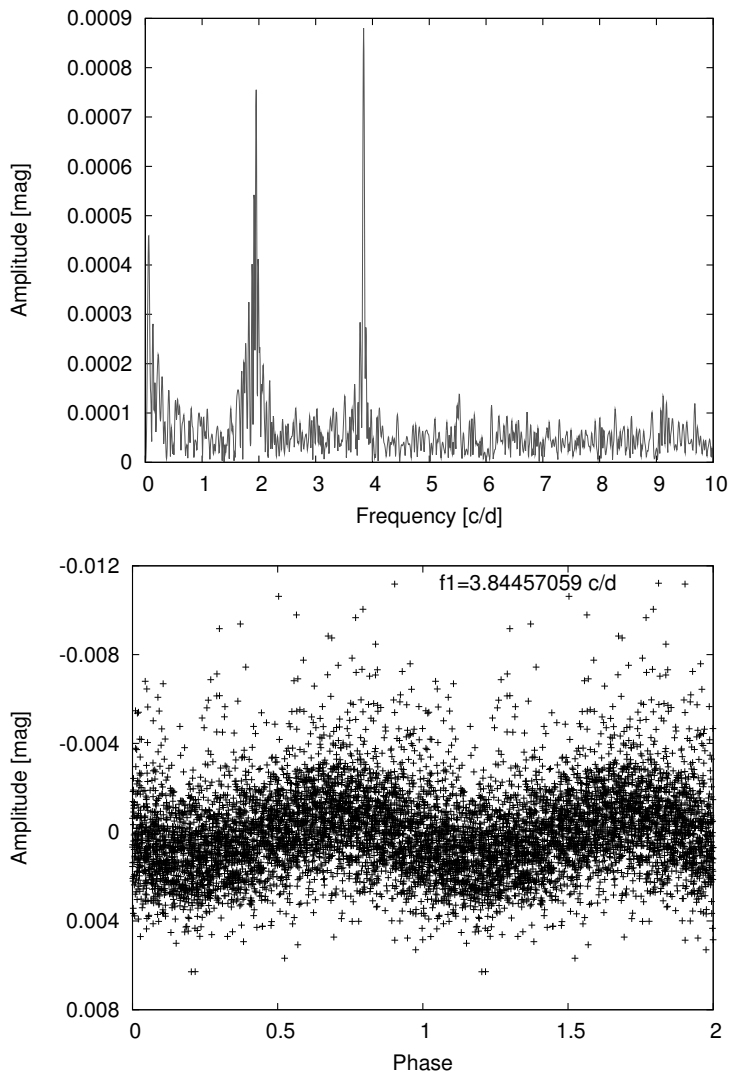
Figure 10.4: Top: *Periodogram for the* CoRoT *star* 102964342. Bottom: *Phase diagram for the frequency* f_1 *detected in the* CoRoT *star* 102964342. *Note that two cycles are shown for clarity.*

Table 10.2: *List of significant frequencies detected with* PASPER *for three Be stars observed in the exoplanet field during the* IRa1 *run with the* CoRoT *satellite.*

#	Freq. [$\mathrm{c\,d^{-1}}$]	Amp. [mmag]	Amp. Error [mmag]	Phase [0,1]	Ph. Error [0,1]	S/N ratio
			CoRoT iD 102725623			
1	0.89739277	0.40	0.0344	0.7419	0.0138	8.2
2	0.08600014	0.33	0.0342	0.2290	0.0167	6.8
			CoRoT iD 102964342			
1	3.84457	0.88	0.037	0.0442	0.0068	13.2
2	1.95343	0.81	0.039	0.1685	0.0077	12.1
3	0.05662	0.51	0.038	0.8086	0.0118	7.6
4	1.91945	0.41	0.038	0.3358	0.0146	6.2
5	1.97608	0.32	0.039	0.2700	0.0193	4.8
			CoRoT iD 102719279			
1	1.13317	11.35	0.46	0.7414	0.0065	10.1
2	1.16861	12.08	0.48	0.3130	0.0064	10.7
3	1.15624	9.60	0.49	0.3377	0.0082	8.6
4	2.32429	8.00	0.45	0.5693	0.0090	7.1
5	0.98222	5.81	0.45	0.5837	0.0124	5.2

10.2.3   CoRoT star 102719279

As seen in Fig. 10.5, the star 102719279 shows several fadings in its CoRoT light curve. A fading is an ejection of matter or outburst, but due to the inclination angle ($i \sim 90°$), the material in the envelope is shadowing the star (see Hubert and Floquet 1998, for some examples with HIPPARCOS data). From the light curve we see that a strong outburst occurs approximately at Julian day $2\,454\,151 - 2\,454\,152$ (CoRoT JD $2\,606 - 2\,607$ in the plot). Note that the outbursts produce a fading of $\sim 0.1\,\mathrm{mag}$ in the light curve. The amplitude of the oscillations increases until the strongest outburst occurs, and then suddenly the amplitude decreases while the average magnitude increases slowly to approximately reach the same level as before the outbursts. It is important to highlight that the outburst occurs when the amplitude of the variations is the largest.
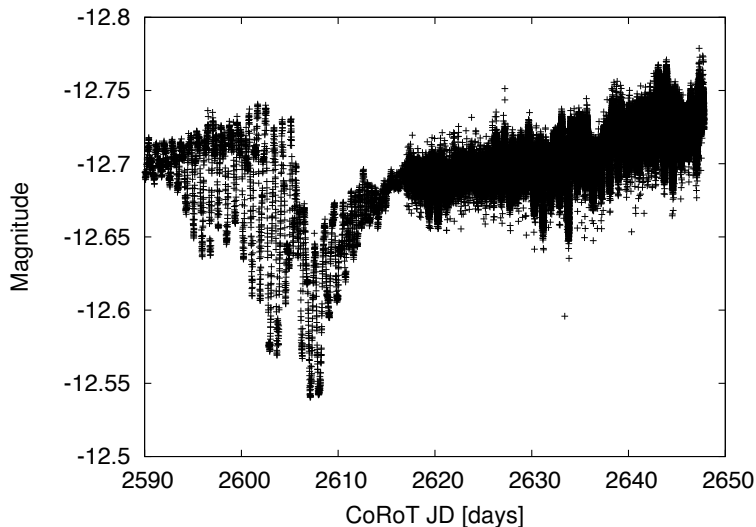
Figure 10.5: *Light curve of the* CoRoT *star* 102719279 *observed in the exoplanet field. The definition of the* CoRoT JD *is given in* Eq. 9.1.

From the Fourier analysis of the whole light curve, we detect several close frequencies around $1.16\,\mathrm{c\,d^{-1}}$ and the double $2.32\,\mathrm{c\,d^{-1}}$, and around $0.98\,\mathrm{c\,d^{-1}}$. As we noticed that the amplitudes change very much for the data points before and after the outbursts, we performed a Fourier analysis for both datasets (the frequencies reported on Table 10.2 corresponds to the analysis of the entire dataset). We clearly see in Fig. 10.6 that the amplitudes change dramatically for the frequencies close to one (the peaks disappear) and to $1.16\,\mathrm{c\,d^{-1}}$ (the amplitudes decreases from 20 to $5\,\mathrm{mmag}$). Therefore, this star shows us that there is a link between the outbursts and the change of amplitude. No spectra was available for this target.

10.3   Conclusions

In this preliminary study on Be stars from the CoRoT exoplanet field we have analysed the light curves of three faint Be stars, searching for short-term vari-
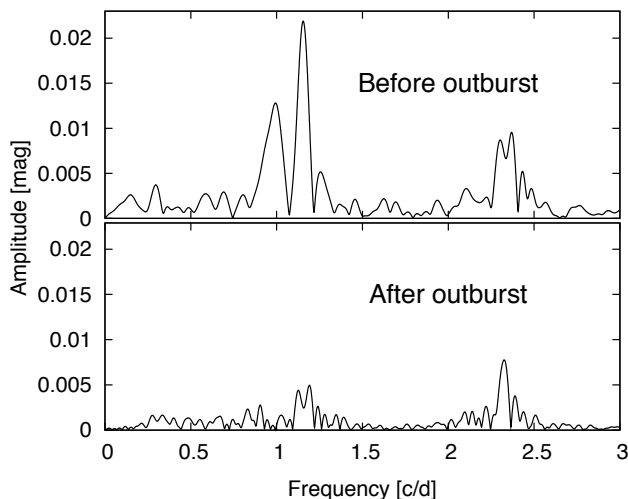
Figure 10.6: *Periodogram for the* CoRoT *Be star* 102719279 *before and after the outburst.*

ability, without making assumptions on the origin of these variations. The high precision, the high duty cycle and the long duration of the CoRoT observations have allowed us to detect many low-amplitude frequencies which would have never been detected from ground-based observations. These first light curves provided by the CoRoT satellite with the exoplanet CCDs have been a powerful example of the potential accuracy to be reached with the seismology CCDs. Moreover, these stars have been very useful targets to test our frequency analysis tools.

As a summary, we can conclude that Be stars are highly variable, as all the Be stars studied here present short-term variations. The Be stars 102964342 and 102719279 show multiple periods in their light curves, an evidence of non-radial pulsations. For the latter star, 102719279, a change of amplitude in the oscillations has been observed. Thus, a link between amplitude variations and outbursts has been found. In addition, we have shown that an outburst occurred when the amplitude of the oscillations was the largest for this Be star. This results suggests that the oscillations may be linked to the ejection of matter in this star,

as it was observed in the Be star μ Cen by Rivinius et al. (2001).

Therefore, we propose that the variations in the three studied Be stars are probably due to the presence of non-radial pulsations, since multiple frequencies have been clearly detected in the domain of β Cephei and SPB star pulsations.

I'd like to be under the sea,
In an octopus' garden in the shade.
He'd let us in, knows where we've been,
In his octopus' garden in the shade.

Ringo Starr

11

The Be star HD 50 209

In this Chapter we have studied the late Be star HD 50 209, observed by CoRoT in the seismology field. We present the frequency analysis, the study of the ground-based spectra and the asteroseismic interpretation of the observed frequencies.

The occurrence of pulsations in late B-type stars has been a matter of controversy in the recent literature. Hubert and Floquet (1998) showed that pulsations in B6-B9 type stars are much less common than in their early-type counterparts. Baade (1989) failed to detect line profile variations in the spectra of B8-B9.5 stars. However, Saio et al. (2007) presented the detection of low amplitude g-modes in the B8Ve star β CMi. To ascertain whether Be stars of all types do present pulsations is a key issue in order to establish the relation between non-radial pulsations and the mass ejection mechanisms.

11.1   Observations

HD 50 209 is a late Be star of spectral type B8IVe and $V = 8.36$ mag. It has been studied by Gutiérrez-Soto (2006, Ph.D. thesis) and Gutiérrez-Soto et al. (2007a) using data from Hipparcos[1], ASAS-3[2] and the OSN[3]. The Hipparcos data analysis yielded a frequency of variation at $1.689\,\mathrm{c\,d^{-1}}$ considered as uncertain and another frequency at $1.47\,\mathrm{c\,d^{-1}}$, although with a lower amplitude. From the OSN, the analysis revealed a frequency at $1.4889\,\mathrm{c\,d^{-1}}$. The analysis of the ASAS-3 dataset showed significant peaks at frequency $2.4803\,\mathrm{c\,d^{-1}}$ and $1.4747\,\mathrm{c\,d^{-1}}$.

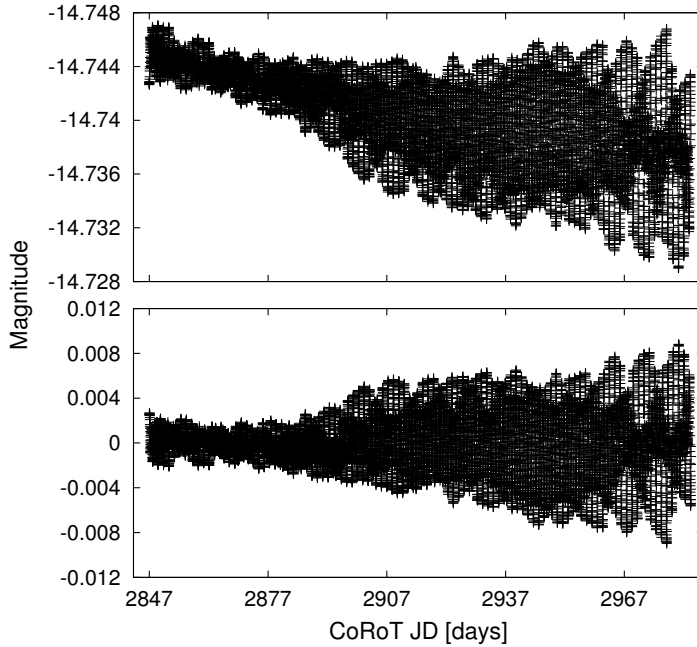
Figure 11.1: Top: CoRoT *light curve of the star* HD 50 209. Bottom: CoRoT *light curve detrended with a polynomial of second degree. The definition of the* CoRoT JD *is given in* Eq. 9.1.

---

[1] Hipparcos Project: http://www.rssd.esa.int/index.php?project=HIPPARCOS.
[2] All Sky Automated Survey: http://www.astrouw.edu.pl/asas/.
[3] Observatorio de Sierra Nevada: http://www.osn.iaa.es/.

The CoRoT satellite observed HD 50 209 in its seismology field. The observations span 136 days in the Galactic anti-centre direction (LRa1 run), between October 18th 2007 and March 3rd 2008, with a sampling of 32 s. The light curve contains 328 279 data points with a duty cycle of 89%.

As mentioned in Chapter 9, the orbital characteristics of the CoRoT satellite produce signal in the data at the orbital frequency (13.97 c d^{-1}, 161.689 μHz) and day/night peaks (2.007 c d^{-1}, 23.229 μHz) and their harmonics. For our purpose we have used the interpolated N2 data of this star, so the spectral window exhibits peaks neither in the orbital frequency nor day/night frequencies or combinations, since there are no gaps.

In Fig. 11.1 (top panel) we present the CoRoT light curve of HD 50 209. As it is common in the CoRoT data, an almost linear long-term decreasing pattern appears in the light curve (see Chapter 9 for details). We have removed these trends by fitting a polynomial function of second degree without making assumptions on their origin, obtaining the light curve depicted in the bottom panel of Fig. 11.1.

11.2 Frequency analysis

For the frequency analysis, we have employed the methods described in Chapter 3. Firstly, we have searched for frequencies in the data using the code PASPER. After fixing the number of statistical significant frequencies, we have computed a non-linear least-square fitting using the KURTZ_BOS routine. Finally, we have calculated the amplitudes and phases using least-square fitting again. For the Be star HD 50 209, the resolution in frequency of our analysis is $1/2\,T \sim 3.66 \times 10^{-3}$ c d^{-1} (Kallinger et al. 2008), T being the total interval covered by observations. The uncertainty on the detected frequencies is $\sqrt{3} \times 10^{-6}$ c d^{-1}. This value has been derived analytically using the formula given by Montgomery and O'Donogohue (1999), and taking into account the correlations in the residuals, as described by Schwarzenberg-Czerny (1991).

Table 11.1: *Principal frequencies of each set detected in* HD 50 209.

Set	Freq. [c d^{-1}]	Freq. [μHz]	Amp. [mmag]	Main freq.	Comment
F_1	1.48444	17.181	2.529	f_1	$f_5 + 2\,f_4$
	1.49028	17.248	1.616		
	1.47860	17.113	1.090		
	1.49613	17.316	0.653		
F_2	2.16238	25.027	0.904	f_2	$f_5 + 3\,f_4$
	2.16822	25.095	0.495		
F_3	0.79482	9.199	0.607	f_3	$f_5 + f_4$
	0.77874	9.013	0.407		
	0.80650	9.334	0.358		
F_4	0.67939	7.863	0.425	f_4	f_{rot}
	0.69108	7.998	0.368		
F_5	0.10811	1.251	0.202	f_5	
F_6	2.96889	34.362	0.121	f_6	$2\,f_1$
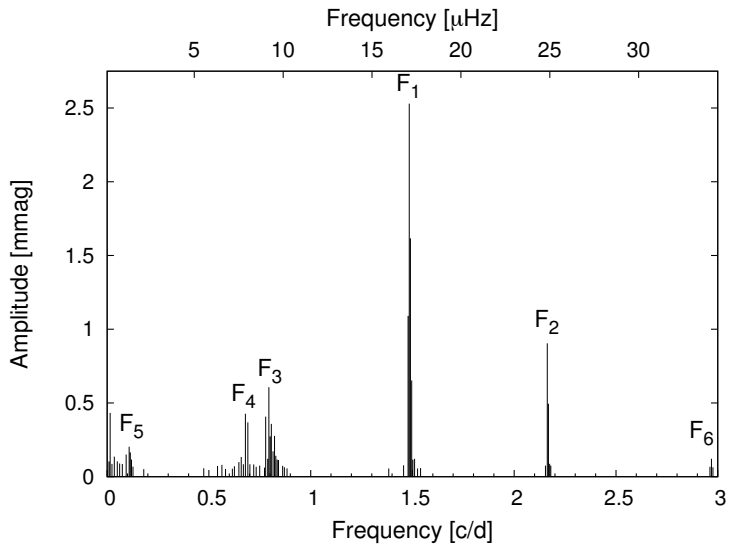
Figure 11.2: *The* 60 *significant frequencies detected for the star* HD 50 209 *revealing six different and separated frequency groups.*

From the frequency analysis, we obtain 60 significant frequencies. The frequencies with the highest amplitudes are listed in Table 11.1. The frequencies found are distributed in six main groups (named F_i with $i = 1, ..., 6$). All groups are clearly separated, except those centred on f_3 and f_4. In each group we note the existence of equidistant multiplets separated by intervals marginally larger than our frequency resolution. The entire set of 60 frequencies is listed in Table 11.2. Note that frequencies around $3/T \sim 0.022\,\mathrm{c\,d}^{-1}$ (0.255 μHz) or lower correspond to periods of the order of the entire dataset time-span, and hence should be considered with caution. They might be produced by the detrending process or artifacts of the frequency analysis. However, we have included them for completeness. The entire set of detected frequencies together with their amplitudes is plotted in Fig. 11.2. In Fig. 11.3 we provide the diagrams of the folded light curve with the two main frequencies f_1 and f_2. In Fig. 11.4 we display the complete Fourier spectrum for the HD 50 209 data.
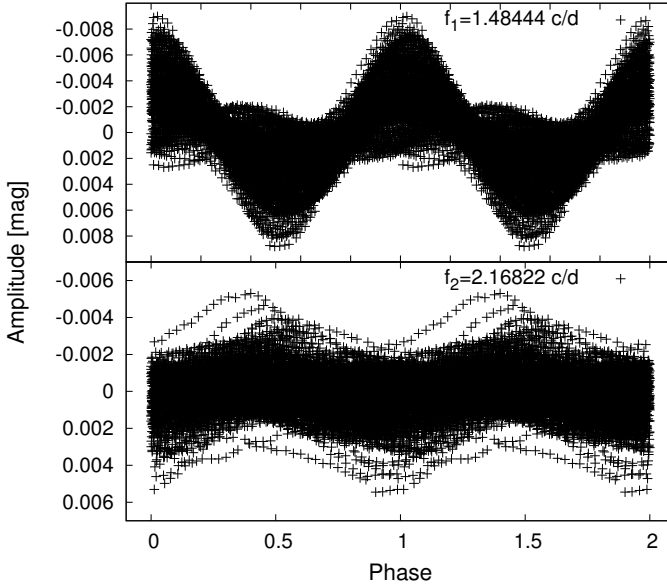
Figure 11.3: Top: *Phase diagram for the* HD 50 209 *data folded with the frequency* $f_1 = 1.48444\,\mathrm{c\,d}^{-1}$ *(17.181 μHz). Bottom:* Phase diagram for the HD 50 209 data, prewhitened *from the frequency* f_1 *and folded with the frequency* $f_2 = 2.16238\,\mathrm{c\,d}^{-1}$ *(25.02 7μHz). Note that two cycles are shown for clarity.*

Table 11.2: *Complete list of significant frequencies obtained with* PASPER *for the star* HD 50 209. *The time reference for the phase is* $HJD = 2\,454\,391.95$.

#	Freq. $[\mathrm{c\,d^{-1}}]$	Freq. $[\mu\mathrm{Hz}]$	Amp. [mmag]	Amp. error [mmag]	Phase [0,1]	Phase error [0,1]	S/N	Comment.
1	1.48444	17.181	2.5299	0.0011	0.7348	0.0001	265	f_1
2	1.49028	17.2486	1.6167	0.0012	0.1577	0.0001	169	
3	1.47860	17.1134	1.0901	0.0011	0.2747	0.0002	114	
4	2.16238	25.0275	0.9043	0.0010	0.9746	0.0002	94	f_2
5	0.79482	9.19931	0.6077	0.0011	0.9866	0.0003	63	f_3
6	1.49613	17.3163	0.6531	0.0011	0.2873	0.0003	68	
7	2.16822	25.0951	0.4953	0.0010	0.2636	0.0003	51	
8	0.01461	0.16909	0.4324	0.0010	0.2149	0.0004	45	$< 3/T$
9	0.77874	9.01319	0.4074	0.0010	0.0079	0.0004	42	
10	0.80650	9.33449	0.3583	0.0010	0.4104	0.0005	37	
11	0.67939	7.86331	0.4256	0.0010	0.3579	0.0004	44	f_4
12	0.69108	7.99861	0.3685	0.0009	0.5289	0.0004	38	
13	0.82258	9.5206	0.2768	0.0010	0.4198	0.0006	29	
14	0.80066	9.2669	0.2740	0.0011	0.1969	0.0006	28	
15	0.10811	1.25127	0.2030	0.0010	0.5750	0.0008	21	f_5
16	0.81527	9.436	0.1725	0.0009	0.2895	0.0009	18	
17	0.78897	9.1316	0.1214	0.0011	0.8024	0.0014	12	
18	0.09350	1.08218	0.1509	0.0009	0.4966	0.0010	15	

Continues on next page...

... continued from Table 11.2.

#	Freq. [c d^{-1}]	Freq. [μHz]	Amp. [mmag]	Amp. error [mmag]	Phase [0,1]	Phase error [0,1]	S/N	Comment.
19	0.03506	0.40578	0.1359	0.0009	0.3221	0.0011	14	
20	0.11396	1.31898	0.1647	0.0010	0.7770	0.0010	17	
21	1.51074	17.4854	0.1217	0.0009	0.2095	0.0012	12	
22	0.65894	7.62662	0.1333	0.0010	0.2271	0.0011	13	
23	2.96889	34.3622	0.1210	0.0009	0.7144	0.0012	12	f_6
24	0.07451	0.86238	0.0862	0.0009	0.2504	0.0017	9	
25	0.64725	7.49132	0.0980	0.0009	0.1021	0.0015	10	
26	0.82842	9.58819	0.1421	0.0010	0.7036	0.0011	14	
27	0.00876	0.10138	0.1040	0.0010	0.6659	0.0015	10	$< 3/T$
28	0.11980	1.38657	0.1164	0.0010	0.9496	0.0013	12	
29	0.83573	9.6728	0.1160	0.0010	0.5225	0.0013	12	
30	1.50197	17.3839	0.1158	0.0011	0.4101	0.0014	12	
31	0.84157	9.74039	0.1131	0.0010	0.7923	0.0014	11	
32	0.66916	7.74491	0.0847	0.0009	0.0830	0.0018	8	
33	0.74952	8.675	0.0751	0.0009	0.0087	0.0019	7	
34	0.04967	0.57488	0.1041	0.0009	0.5844	0.0014	10	
35	0.70131	8.11701	0.0854	0.0009	0.8694	0.0017	8	
36	0.02337	0.27048	0.0867	0.0009	0.2750	0.0017	9	$\sim 3/T$
37	0.06136	0.71018	0.0894	0.0009	0.8152	0.0017	9	

Continues on next page...

... continued from Table 11.2.

#	Freq. [c d^{-1}]	Freq. [μHz]	Amp. [mmag]	Amp. error [mmag]	Phase [0,1]	Phase error [0,1]	S/N	Comment.
38	0.56397	6.52743	0.0792	0.0009	0.1145	0.0018	8	
39	1.45668	16.8597	0.0774	0.0009	0.4253	0.0019	8	
40	0.62533	7.23762	0.0694	0.0009	0.1556	0.0021	7	
41	0.54205	6.27373	0.0726	0.0009	0.8328	0.0020	7	
42	0.86203	9.9772	0.0731	0.0009	0.7081	0.0020	7	
43	2.15361	24.926	0.0749	0.0009	0.2862	0.0019	7	
44	0.72030	8.33681	0.0829	0.0009	0.8066	0.0018	8	
45	2.96158	34.2775	0.0672	0.0009	0.4195	0.0021	7	
46	0.73199	8.47211	0.0681	0.0009	0.0589	0.0022	7	
47	0.12711	1.47118	0.0683	0.0009	0.1174	0.0021	7	
48	2.97619	34.4466	0.0640	0.0009	0.0250	0.0022	6	
49	2.17406	25.1627	0.0875	0.0010	0.5229	0.0019	9	
50	2.17991	25.2304	0.0755	0.0010	0.7423	0.0021	7	
51	1.53996	17.8236	0.0590	0.0009	0.4461	0.0024	6	
52	0.77290	8.9456	0.0615	0.0010	0.8969	0.0025	6	
53	1.38363	16.0142	0.0553	0.0009	0.7286	0.0026	5	
54	0.47484	5.49583	0.0574	0.0009	0.4781	0.0025	6	
55	0.61510	7.11921	0.0560	0.0009	0.2581	0.0026	5	
56	1.52535	17.6545	0.0559	0.0009	0.2121	0.0026	5	

Continues on next page...

... continued from Table 11.2.

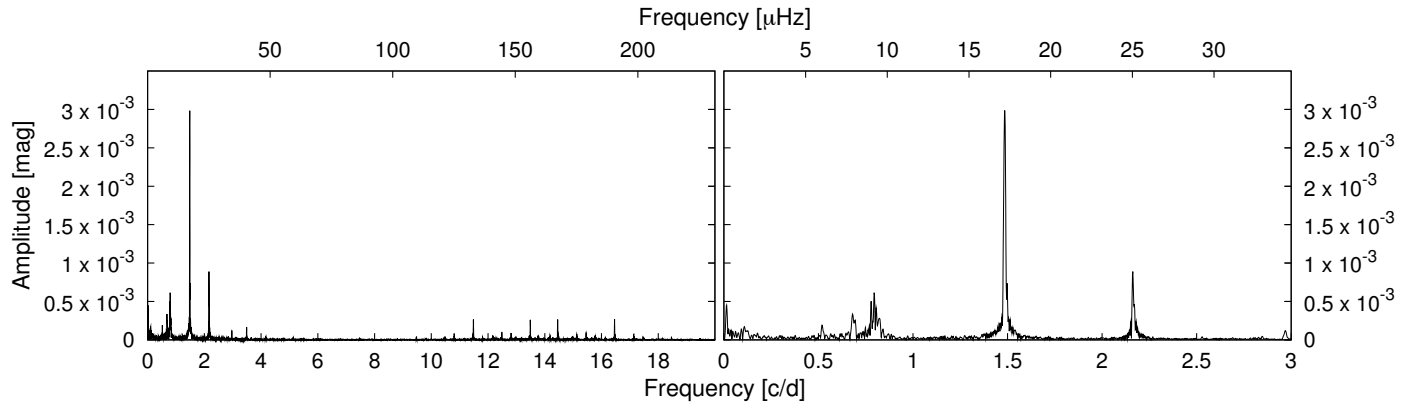| #	Freq. [c d^{-1}]	Freq. [μHz]	Amp. [mmag]	Amp. error [mmag]	Phase [0,1]	Phase error [0,1]	S/N	Comment.
57	0.87079	10.0786	0.0642	0.0009	0.8295	0.0023	6	
58	0.88394	10.2308	0.0567	0.0009	0.9051	0.0026	5	
59	0.58150	6.73032	0.0525	0.0009	0.6858	0.0028	5	
60	0.17971	2.07998	0.0515	0.0009	0.1046	0.0028	5	

Figure 11.4: Left: *Complete Fourier spectrum for* HD 50 209. *Spurious signal due to day/night cycle appears at signal at* $13.97 \pm 1 \, \mathrm{c \, d^{-1}}$. Right: *Fourier spectrum for* HD 50 209 *in the domain of the detected stellar frequencies.*

In addition, we performed a time-frequency analysis of the original light curve by applying the PASPER code to sliding windows with different sizes (for details on the method, see Huat et al. 2009a). The results presented in Fig. 11.5 show that all the main frequencies show large amplitude changes (see Section 11.4 for details).
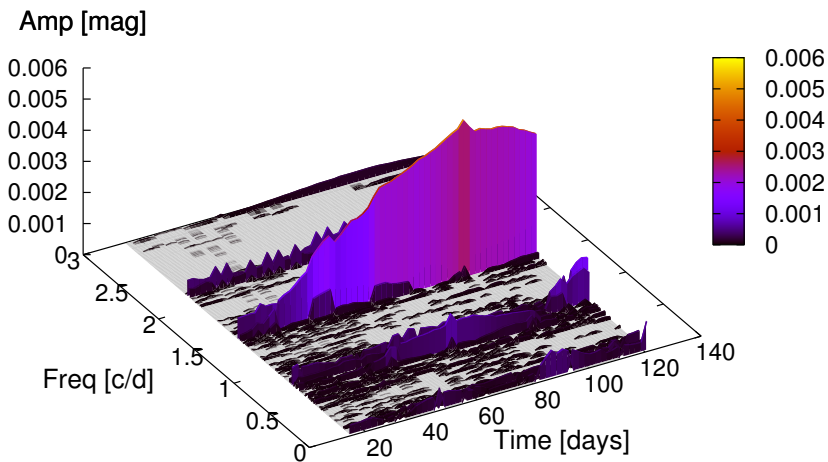

Figure 11.5: *3-D view of the frequencies determined using the time-frequency analysis with a sliding window of* 30 days. *The colour scale indicates the amplitude of the detected frequencies in* HD 50 209. *The time origin corresponds to* HJD = 2 454 391.95.
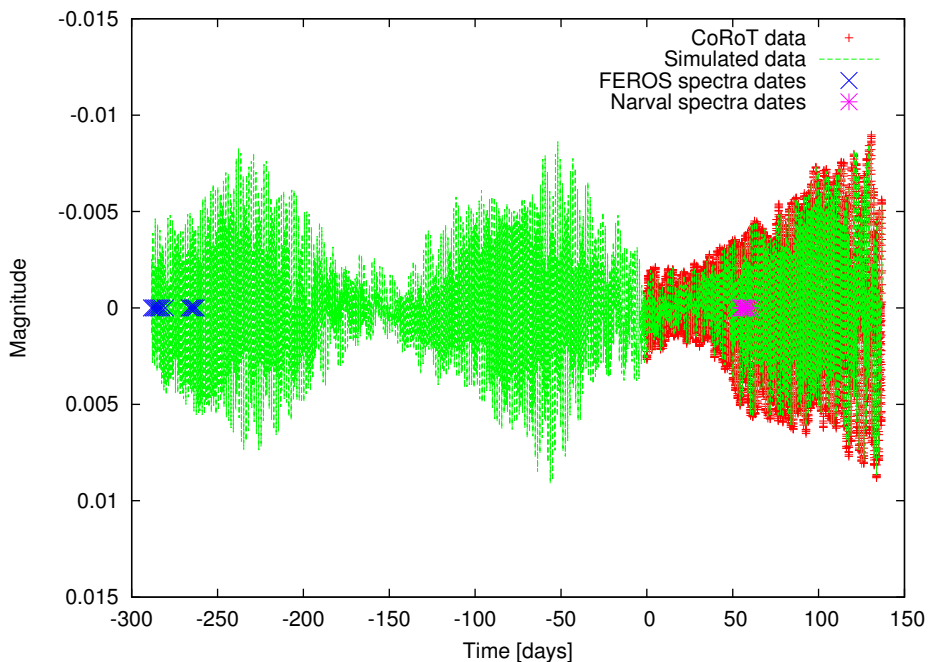
Figure 11.6: *Dates for the* FEROS *and the* Narval *spectra. We have also included the simulated light curve with the* 60 *frequencies found superimposed to the* CoRoT *observations. The time scale has been initialised at the begin of the* CoRoT LRa1 *run.*

11.3 Ground-based observations

High-resolution spectroscopy of HD 50 209 was obtained with the FEROS[4] spectrograph at the 2.2 m telescope in La Silla (Chile), in the framework of a large program complementary to the CoRoT mission. Observations were carried out one year prior to the LRa1 run of CoRoT to investigate spectroscopically the rapid variability previously detected in photometry by Gutiérrez-Soto et al. (2007a). Seventy spectra with high spectral resolution and high signal to noise ratio were obtained. Fourteen additional spectra were obtained with the Narval[5] spectropo-

---

[4]Fibre-fed Extended Range Optical Spectrograph (see Kaufer et al. 1999, for details): http://www.eso.org/sci/facilities/lasilla/instruments/feros/.
[5]Narval website: http://www.ast.obs-mip.fr/projets/narval/v1/.

larimeter at the TBL at Pic du Midi Observatory (France), contemporary to the CoRoT run. However, due to bad weather conditions, the signal to noise ratio is not high enough to search for low amplitude variability in the Narval data. The moment were the spectra were taken is depicted in Fig. 11.6. The plot depicts the synthetic light variations of the star HD 50 209 with the 60 detected frequencies. The non detection of line profile variations in the spectroscopic data may be due to the constructive beating at the moment when the spectra were taken. But this assumption is highly affected by systematic errors in the simulated data.

FEROS observations ($R = 48\,000$, $3\,600 - 9\,200\,\text{Å}$) were reduced with MI-DAS[6] (wavelength calibration, bias and flat field corrections and earth motion correction). For the Narval observations ($R = 65\,000$) the sum of the four sub-exposures obtained in Stokes V sequences were used. Exposures were reduced locally with LibrEsprit based on the Esprit software (Donati et al. 1997) and then summed. The continuum normalisation was carried out with IRAF[7].

The fundamental physical parameters of HD 50 209 have been accurately determined from the newly available spectroscopic data adopting a procedure described by Frémat et al. (2006) and correcting for gravitational darkening effects (Frémat et al. 2005). The obtained parameters are derived by fitting synthetic spectra to the observed one, adopting the different values of Ω/Ω_c presented in the first row of Table 11.3. The results are presented in Table 11.3 and are consistent with the previous parameter determination (Frémat et al. 2006).

Spectroscopic data also show that emission is present in the first Balmer lines and visible up to Hδ. Hα is a strong emission line ($EW = -19\,\text{Å}$, $I_{\max} = 4.68\,I_{\text{cont}}$) with inflection points on the wings and close double peaks at the centre. The line profile is typical of a Be star seen under a moderate inclination angle (Hanuschik et al. 1996). Hβ, Hγ and Hδ show a symmetrical and double-peaked

---

[6]The ESO-MIDAS system provides general tools for image processing and data reduction with emphasis on astronomical applications including imaging and special reduction packages for ESO instrumentation at La Silla and the VLT at Paranal. ESO-MIDAS is available under the GNU General Public License at http://www.eso.org/sci/data-processing/software/esomidas/.

[7]IRAF is distributed by the National Optical Astronomy Observatories, which is operated by the Association of Universities for Research in Astronomy (AURA), Inc., under cooperative agreement with the National Science Foundation. IRAF is available at http://iraf.noao.edu/iraf/web/iraf-homepage.html.

Table 11.3: *Fundamental parameters for* HD 50 209 *computed for different values of* Ω/Ω_c *and corrected for veiling. The errors in* T_{eff}, $\log g$ *and* $V \sin i$ *are taken from the apparent parameters.*

Ω/Ω_c	i [deg]	T_{eff} [K]	$\log g$ [cgs]	$V \sin i$ [$\mathrm{km\,s^{-1}}$]	M [$M_\odot$]	L [$L_\odot$]	R_{eq} [$R_\odot$]	f_{rot} [$\mathrm{c\,d^{-1}}$]
0.80	89 ± 20	13600 ± 1500	3.60 ± 0.11	192 ± 20	4.67 ± 0.95	2.97 ± 0.39	6.44 ± 1.53	0.60 ± 0.20
0.90	64 ± 14	13600 ± 1500	3.56 ± 0.11	205 ± 20	4.76 ± 1.02	3.02 ± 0.39	7.27 ± 1.74	0.62 ± 0.20
0.95	57 ± 15	13600 ± 1500	3.53 ± 0.11	211 ± 20	5.07 ± 1.15	3.08 ± 0.40	8.06 ± 2.03	0.62 ± 0.22
0.99	55 ± 12	13400 ± 1500	3.46 ± 0.11	221 ± 20	4.99 ± 1.22	3.14 ± 0.41	9.34 ± 2.35	0.58 ± 0.20

emission embedded in the broad wings of the photospheric profile (see Fig. 11.7). Moreover, numerous Fe II and Cr II lines as well as the IR Ca II triplet and O I 8 446 Å lines are in emission with a double component. Note that we have not found significant changes in the global emission state of HD 50 209 between the FEROS and NARVAL spectra taken about one year apart.

In addition, forbidden single-peaked [O I] 6 300 Å and [Fe II] emission lines are detected with a very weak intensity ($I \leq 1.01\%$ of the continuum, see Fig. 11.8). The star is isolated, outside any formation region. In addition, we found from the 2MASS[8] data that the infrared excess is much lower than the typical values for HAeBe stars, and it is close to the Be stars having strong emission. It could be an extreme Be star according to de Winter and Pérez (1998) or an unclB[e] star in the scheme proposed by the authors Lamers et al. (1998), though the B[e] character is very weak.
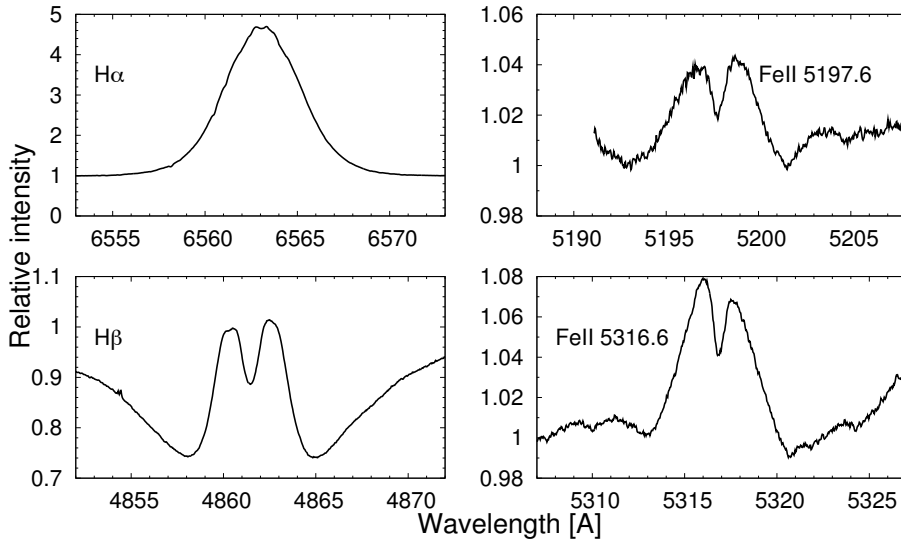

Figure 11.7: Left panels: Hα and Hβ emission. Right panels: Different emission lines in the Fe II region in the star HD 50 209. In all panels the horizontal axis is wavelength and the vertical one is relative intensity.
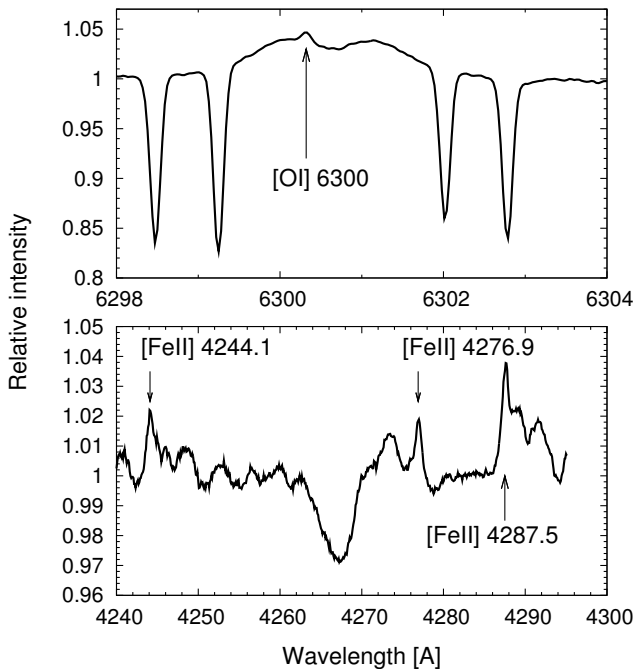
---

[8]2MASS at IPAC: http://www.ipac.caltech.edu/2mass/.

Figure 11.8: Top: *Forbidden emission line of* [O I] *at* 6 300 Å. Bottom: *Three forbidden emission lines of* [Fe II] *at* 4 244.1 Å *(21 F)*, 4 276.9 Å *(21 F) and* 4 287.5 Å *(7 F) from the spectra of* HD 50 209.

The mean Hα, Hβ and Fe II 5 197.6 Å and 5 316.6 Å profiles are shown in Fig. 11.7. The separation between the emission peaks and the lack of a shell profile exclude an inclination angle close to 90°, and hence the physical parameters in the first row of Table 11.3 are not suitable. This implies that the rotational frequency is at least 90% of the critical velocity. The shape of the Hα line profile and the forbidden lines discussed above indicate the presence of a very extended circumstellar disk.

In spite of the high quality of the FEROS spectra and the presence of rapid photometric variability apparent in the CoRoT data (see Fig. 11.1), we have not been able to detect periodic variability in purely photospheric lines of HD 50 209.

Some variability is present slightly above the detection limit but no consistent periodic behaviour could be established. Weak rapid variations were detected in the intensity of the V and R emission components of Balmer lines and their V/R ratio. Note also that the quantity $(V + R)/2$ seems to be slightly lower in the second part of the ESO run, suggesting a slight weakening of the emissivity of the disk. As shown in the mean variance in the $H\beta$ profile, the variability is concentrated in the emission part. Note that the variability is more conspicuous on certain days. Unfortunately, the gap between the two parts of the ESO run, the alternating of day/night and the weakness of variations prevent any reliable estimate on the time-scale of variations.

11.4   Discussion

As a result of our analysis, we have obtained 60 significant frequencies, grouped in six sets. In each set, different equidistant frequencies close to the main detected ones are present. The Fourier analysis of the light curve by means of sliding windows results in the detection of a significant variation of amplitude of the main frequencies (Fig. 11.5).

The first issue to be addressed is the presence of frequency multiplets and amplitude variations. Both phenomena are related, and can be due either to the presence of close frequencies or actual amplitude variations (Breger and Pamyatnykh 2006). The beating of two or more close frequencies will appear as a single frequency with variable amplitude when we split the data sample in shorter intervals, with the consequent loss of frequency resolution. On the other hand, true amplitude variability will produce peaks in the power spectrum broader than expected from the frequency resolution (as seen in Fig. 11.9), and the prewhitening of the main frequency will leave power in the wings of the main peak which will lead to false frequency doublets or multiplets.

In order to discriminate between the beating of several frequencies and an amplitude change of a single frequency we have applied the method described in Breger and Pamyatnykh (2006) to study the relationship between amplitude
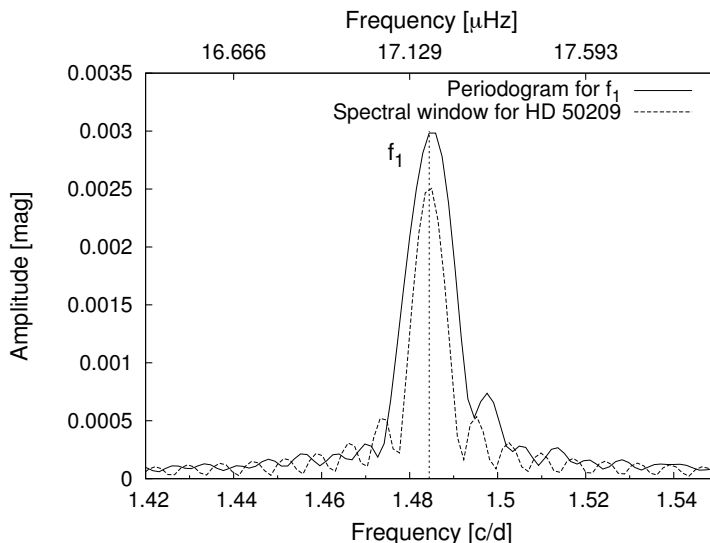
Figure 11.9: *Periodogram of the original light curve (solid line) and spectral window shifted at $f_1 = 1.48444 \, \mathrm{c\,d^{-1}}$ (dashed line). Note that the full width at half maximum of the peak in the periodogram at the frequency f_1 is broader than expected from the spectral window, suggesting the presence of more frequencies or amplitude changes. The vertical line indicates the position of the frequency f_1.*

variability and phase variations of an assumed single frequency. The idea behind this method is that the beating of frequencies will produce a phase variation with the same period as the beating period, while in the case of a single frequency with variable amplitude, the phase will remain constant.

We studied the six frequency groups with the above-mentioned method. However, the results obtained are inconclusive, for two main reasons:

1. The beat periods of the close frequencies are larger than the time coverage of CoRoT data (see Fig. 11.6), and hence, we cannot evaluate the consistency of the phase variations.

2. The phase variations predicted by the models with four or more frequencies are very small. At our detection level we were not able to discriminate between the predicted low amplitude variations and no variation at all.

Consequently, we cannot firmly reject either of the two interpretations.

In the following, we analyse the six main frequencies found, which, as discussed above, can be either single frequencies with variable amplitude or groups of close frequencies around a central value. The highest frequency, f_6, is the first harmonic of f_1, i.e. $f_6 = 2\,f_1$, and hence it will not be considered in the analysis. Frequencies f_5, f_3, f_1 and f_2 are equidistant within the frequency resolution at the 3-σ level, and the separation between them is the frequency f_4. Moreover, $f_4 = 0.67939\,\mathrm{c\,d^{-1}}$ is consistent with the rotational frequency of the star as given in Table 11.3. As a consequence, we have only two independent main frequencies, f_4 and f_5, and all the others are of the form $f_i = f_5 + n\,f_4$ with $n = 1, 2, 3$.

Let us recall, as described in Chapter 1 that the observed frequencies (ν_{obs}) in a rotating star are related to the pulsational frequency in the co-rotating frame by the expression:

$$\nu_{\mathrm{obs}} = |\,\nu_{\mathrm{corot}} - m\,\Omega\,| \tag{11.1}$$

where ν_{corot} is the frequency in the co-rotating frame and Ω is the rotational frequency of the star. From this expression, and considering f_4 as the rotational frequency as discussed above, the four frequencies f_5, f_3, f_1 and f_2 can be consistently interpreted as modes with the same pulsational frequency in the co-rotating frame and with $m = 0, -1, -2, -3$, respectively[9]. Therefore, we propose that there are four active pulsating modes, with the same frequency in the co-rotating frame, with spherical harmonic degree $\ell = 3$.

This interpretation has the difficulty that we only see $\ell = 3$ modes, and any $\ell = 1$ and $\ell = 2$ modes which must have higher amplitudes and hence, be more visible. Thus, another plausible interpretation is that we are observing only one group of pulsational frequencies, F_1, and the rotational frequency F_4. The rest of the peaks in the periodogram are combinations of these two groups of frequencies and therefore do not correspond to independent pulsational frequencies.

---

[9]Here we adopt the convention introduced by H. Saio. Negative m represents a pro-grade mode (in the co-rotating frame) with respect to the stellar rotation. Even (odd) modes are symmetric (anti-symmetric) with respect to the equatorial plane. The basis for this convention is that H. Saio assumes that $m > 0$ modes are not instables. See Saio et al. (2007) for details.

The fundamental parameters presented in Table 11.3 place HD 50 209 marginally outside the SPB instability strip calculated by Pamyatnykh (1999), although its position is compatible with the strip at the 1-σ error level. Hence, we consider that the pulsations detected are gravity modes typical of SPB stars. HD 50 209 is a SPBe star, the designation proposed by Walker et al. (2005a) for the Be stars pulsating in g-modes, considered as rapidly rotating counterparts of the SPB stars.

Due to the fact that in late-type B stars the frequencies of the g-modes in the co-rotating frame are much smaller than the rotational frequency, the frequencies of these modes in the observer's frame are close to $|m\,\Omega|$. This leads to the difficulty that the observed frequencies close to the expected rotational frequency can be either interpreted as g-mode pulsations (Walker et al. 2005a) or as rotational modulation (Balona 1995). In our case, we can for the first time discriminate between the rotational frequency and the frequency of the g-mode pulsation with azimuthal order $|m| = 1$, as we have detected both of them clearly separated by an interval much larger than the frequency resolution, thanks to the long duration of observations and precise measurements of CoRoT . We can be confident that the frequencies f_5, f_3, f_1 and f_2 are not related to the rotation and hence they are true gravity mode pulsations.

The frequency in the co-rotating frame of the detected modes, namely $f_5 = 0.10811\,\mathrm{c\,d^{-1}}$, is significantly lower than the frequencies commonly found for both SPB and SPBe stars. However, this low value is consistent with what is expected for an $m = 0$ mode in models of rapidly rotating late-type B stars (Walker et al. 2005a; Saio et al. 2007). The modelling of the detected pulsations will provide more insights into the nature of the pulsational modes.

11.5   Conclusions

The high precision photometry and long duration of continuous observations provided by the CoRoT mission has allowed the detection of g-mode pulsations in the late-type Be star HD 50 209. This supports the fact that all Be stars have

non-radial pulsations that could play a critical role in the mass ejection mechanism.

From our analysis, we propose that the star pulsates in four modes with the same frequency in the co-rotating frame with azimuthal order $m = 0, -1, -2, -3$. Other interpretations are also possible, though. We have also detected the rotational frequency, both as a significant peak in the power spectrum and as the separation of frequencies with different m. The accurate determination of the rotational period will play an important part in constraining the fundamental parameters of the star in order to perform the seismic modelling.

For the first time, we have been able to observe simultaneously the rotational frequency and the pulsational frequencies and separate them, implying that the frequencies we attribute to g-mode pulsations cannot be interpreted as the effect of the rotational modulation. This constitutes a proof of the presence of pulsations in HD 50 209.

And in the end,
The love you take
Is equal to the love you make.

Paul McCartney

12

Conclusions and future work

In this Ph.D. thesis we have developed the tools for carrying out the Fourier analysis of the high-precision light curves provided by the CoRoT satellite for several pre-selected Be stars. In order to test these tools we have selected B and Be stars from the Small and Large Magellanic Cloud (SMC and LMC) and we have searched for B-type pulsations in this low metallicity environments. The observational results in the Magellanic Clouds (MCs) have been very productive, confirming β Cephei and SPB-like pulsations in both clouds. Our results have been compared to those obtained for the Milky Way (MW).

Concerning the CoRoT data, the analysis method have been applied to several stars in the exoplanet and seismology fields of the CoRoT satellite, revealing interesting results and detecting different pulsational modes. The most amazing

result have been obtained for the Be star HD 50 209 finding for the first time the rotational splitting for such a rapidly rotating star and being able to confirm the presence of non-radial pulsations for this Be star. Taking together, the results derived from this project have allowed us a better understanding of the Be phenomenon.

Here we summarise the most important scientific results in the study of the Be stars derived from our work:

12.1   Conclusions in the Magellanic Clouds studies

- We have searched for short-term variability in a sample of 183 absorption-line B stars and 126 Be stars in the SMC and in a sample of 106 absorption-line B stars and 47 Be stars in the LMC, both samples with accurately determined physical parameters. We have studied their position in the theoretical H-R diagram and mapped the regions of pulsational instability in the SMC and in the LMC.

- In the SMC we have found nine pulsating absorption-line B stars. Among them, eight have periods longer than 0.5 days, characteristic of SPB-type stars. The region occupied by the SPB stars in the SMC is shifted towards higher temperatures with respect to the galactic SPB instability strip and to the predictions of recent models for $Z = 0.005$. The remaining star presents two short periods within the range of the β Cephei variables. This fact and its high effective temperature lead us to propose that it is indeed a β Cephei star. This is an interesting result as current stellar models do not predict β Cephei pulsations at the SMC metallicity. There are 32 pulsating stars among the Be star sample. Most of them are placed in the region occupied by the SPB stars in the H-R diagram of the SMC and present periods longer than 0.5 days. They are most probably g-mode SPB-like pulsators. Three pulsating Be stars are significantly hotter and present much shorter periods, within the range of the β Cephei stars. We propose that they are β Cephei-like pulsators.

- In the LMC we have found seven pulsating absorption-line B stars. Among

them, two stars are proposed to be SPB-like pulsators from their period distribution. As in the results obtained for the SMC, the position occupied by the LMC SPB stars in the H-R diagram seems to be shifted towards higher temperatures with respect to the Galactic SPB instability strip. The remaining five B stars present periods within the range of β Cephei variables. This fact and their high effective temperatures lead us to propose that they are indeed β Cephei stars. In the Be star sample, we have detected five pulsating stars, three of them showing multiperiodicity. According to the observed periods we interpret them as the g-mode SPB-like pulsators.

- For both the MCs the prevalence of pulsations among Be stars is significantly higher than among absorption-line B stars, much like as in the Galaxy. In the case of the SMC, we have found that 25.3% of Be stars present short-term variability, while only 4.9% of B star do pulsate. In the case of the LMC 23% of Be stars present short-term variability, while only the 7% of B stars do pulsate. The same result is obtained in the MW. These results indicate that the high-rotational velocity either contribute to trigger the development of non-radial pulsations or to enhance the amplitude of the existing modes. Alternatively, the prevalence of non-radial pulsations could be related to the yet unknown nature of the Be phenomenon.

- In the case of the SMC, both the fraction of SPB among B stars and pulsating Be stars among the whole sample of Be stars in the SMC are lower than in the Galaxy, indicating that the prevalence of pulsations is directly affected by the metallicity of the environment, as predicted by the current stellar models.

- We have undertaken a comparison of the prevalence of pulsating B-type stars in the SMC, LMC and MW. We note a decrease of the rates of pulsating B-type stars with decreasing metallicity as expected from the theory. However, it is clear from this work (and other above mentioned studies) that pulsations are still driven in B-type stars at low metallicity environments, not predicted by the recent calculations on stellar pulsation theory. This detection of pulsators at low-Z environments remains an enigma.

- In addition, we detect an increase of the rates of pulsating Be stars between the MW, LMC and SMC while the metallicity decreases. This may be

explained by the fact that SMC Be stars rotate faster than their counterparts in the LMC or in the MW. There is a similar trend in Ω/Ω_c for B stars, but their ratios are always lower than the minimal ratio from which the fast rotation effects on the stars are not negligible ($\Omega/\Omega_c \sim 70\%$). This fact could explain why there is an effect of the fast rotation between the LMC and SMC for Be stars and not for B stars.

12.2   Conclusions in the CoRoT data studies

- From our preliminary study of three faint Be stars observed in the CoRoT exoplanetary field we can conclude that Be stars are highly variable. A change of amplitude of the oscillations is observed along the light curve in one star (102719279), and it is linked to the outburst, as it was found for the Be star μ Cen with ground-based data (Rivinius et al. 2001) and for the star HD 49 330 with CoRoT data (Huat et al. 2009a; Floquet et al. 2009).

- The high precision photometry and long duration of continuous observations provided by the CoRoT mission has allowed the detection of g-mode pulsations in the late-type Be star HD 50 209. This supports the fact that all Be stars have non-radial pulsations that could play a critical role in the mass ejection mechanism.

- From our analysis of the Be star HD 50 209, we have found pulsation in four modes with the same frequency in the co-rotating frame with azimuthal order $m = 0, -1, -2, -3$. We have also detected the rotational frequency, both as a significant peak in the power spectrum and as the separation of frequencies with different m. The accurate determination of the rotational period will play an important part in constraining the fundamental parameters of the star in order to perform the seismic modelling.

- For the first time, we have been able to observe simultaneously the rotational frequency and the pulsational frequencies and separate them, implying that the frequencies we attribute to g-mode pulsations cannot be interpreted as the effect of the rotational modulation. This constitutes a proof of the presence of pulsations in HD 50 209.

12.3 Future work

The work presented here is the first part of a large project aimed at studying the physics of Be stars using data from the CoRoT satellite. The natural follow-up of our work is to continue the analysis of the data relative to Be stars produced by the CoRoT space mission. These new data will allow us to perform in-depth analysis of Be stars pulsational properties and to address most of the problems raised in this Ph.D. thesis in much deeper detail.

In addition, immediate follow-up studies of several particular topics presented in this work are the following:

- Obtain spectroscopic data of the pulsating B and Be stars detected in the SMC and LMC with enough signal to noise ratio in order to derive the chemical abundances for these stars. This would confirm if they are, in fact, true low-Z stars or enriched stars with a metallicity higher than the mean metallicity of the MCs. A collaboration with Christophe Martayan started during this Ph.D. thesis. Nowadays, we have allocated some time to get high-resolution spectra at the ESO/VLT with the spectrograph X-Shooter[1]. The results will be obtained during next year.

- We are planning to analyse the big sample of B-type stars observed by Martayan et al. (2008a) in the Hα survey of the SMC using the ESO/WFI[2]. This study will increase the statistics of B-type pulsators in low metallicity environments and gives new clues in the origin of the Be phenomenon. In this issue, we plan to collaborate with Luis Manuel Sarro, who works with automated classification of variable stars (Debosscher et al. 2007; Sarro et al. 2009).

- Perform spectroscopic observations of HD 50 209 in order to obtain a better signal to noise values. It would be interesting to obtain spectroscopic data

---

[1] X-Shooter is a single target spectrograph for the Cassegrain focus of one of the VLT Unit Telescopes. It is the first of the second generation instruments at VLT (see D'Odorico et al. 2006, for details): http://www.eso.org/sci/facilities/develop/instruments/xshooter/.

[2] The Wide Field Imager (WFI) is a focal reducer-type camera which is permanently mounted at the Cassegrain focus of the 2.2-m MPG/ESO telescope at La Silla (see Baade et al. 1999, for details): http://www.eso.org/sci/facilities/lasilla/instruments/wfi/.

matching with the maximum amplitude epochs.

- To continue analysing the upcoming CoRoT data of Be stars from the exoplanet and seismology fields scheduled for the next runs. The procedure will be the same as we have employed for the analysis of the HD 50 209 Be star. The analysis of the Be star HD 51 193 is on course and the results will be published during this year.

- In collaboration with specialised groups (e.g. Hideyuki Saio or the Dpto. de Física Estelar at IAA-CSIC[3]), perform the pulsational models of the analysed Be stars from the CoRoT mission, in particular, HD 50 209. This is a great challenge because the modelling of Be stars remains a difficult task due to their high-rotational velocity rates.

- Inside the CoRoT Be Team tasks, continue the photometric programme for the identification of new Be stars in the exoplanet fields for the successive CoRoT pointings.

- Our group is involved in a related project aimed at studying B and Be stars with the KEPLER satellite[4]. Much as the CoRoT exoplanet programme, the KEPLER mission is devoted to find Earth-size extrasolar planets with the transits technique and it also hosts an additional science programme to obtain photometric time series with different scientific purposes. Our objective with respect the KEPLER data is to operate in a similar way as we are doing with the CoRoT data. At the moment, we have observations for a confirmed Be star spanning 230 days with high-resolution spectra.

---

[3]http://www.iaa.es/.
[4]http://kepler.nasa.gov/.

Two of us wearing raincoats,
Standing solo in the Sun.
You and me chasing paper,
Getting nowhere on our way back home.

Paul McCartney

13

Addendum

The continuous work on this project has produced a lot of scientific results that has been distributed to the scientific community through publications in different specialised international journals, conferences, proceedings, etc. Here we attach the complete list of publications where the author of this Ph.D. thesis has been author or co-author.

13.1 Publications in International Refereed Journals

- *Pulsating B and Be stars in the Small Magellanic Cloud.*
  Journal: *Astronomy & Astrophysics.*
  Reference: Diago et al. (2008a).

- *The B0.5IVe* CoRoT *target* HD 49 330. *I. Photometric analysis from* CoRoT *data.*
  Journal: *Astronomy & Astrophysics.*
  Reference: Huat et al. (2009a).

- *The B0.5 IVe* CoRoT *target* HD 49 330. *II. Spectroscopic ground-based observations.*
  Journal: *Astronomy & Astrophysics.*
  Reference: Floquet et al. (2009).

- *Pulsations in the late-type Be star* HD 50 209 *detected by* CoRoT .
  Journal: *Astronomy & Astrophysics.*
  Reference: Diago et al. (2009a).

- *Low-amplitude variations detected by* CoRoT *in the B8IIIe star* HD 175 869.
  Journal: *Astronomy & Astrophysics.*
  Reference: Gutiérrez-Soto et al. (2009b).

- *The pulsations of the B5IVe star* HD 181 231 *observed with* CoRoT *and ground-based spectroscopy.*
  Journal: *Astronomy & Astrophysics.*
  Reference: Neiner et al. (2009a).

- *The effects of metallicity and rotation on B-type star pulsations. Study in the LMC and comparison between the MCs and the MW.*
  Journal: *Astronomy & Astrophysics.*
  Reference: Diago et al. (2010), submitted.

13.2 Publications in Proceedings of International Conferences

- *Variability of B and Be stars in the LMC/SMC: binaries and pulsations.*
  Journal: *Proceedings IAU Symposium No. 256.*
  Reference: Martayan et al. (2008b).

- *Pulsating B and Be stars in the Magellanic Clouds.*
  Journal: *Proceedings of the VIII Reunión Científica de la SEA, 2008.*
  Reference: Diago et al. (2010).

- *First results on Be stars with* CoRoT.
  Journal: *Proceedings of the Annual meeting of the French Society of Astronomy and Astrophysics, 2008.*
  Reference: Gutiérrez-Soto et al. (2008).

- *First results on the Be stars observed with the* CoRoT *satellite.*
  Journal: *Communications in Asteroseismology.*
  Reference: Gutierrez-Soto et al. (2008).

- *Pulsating B and Be stars in the Magellanic Cloud.*
  Journal: *Communications in Asteroseismology.*
  Reference: Diago et al. (2008b).

- *More on pulsating B-type stars in the Magellanic Clouds.*
  Journal: *Communications in Asteroseismology.*
  Reference: Diago et al. (2009b).

- *Low-amplitude variations detected by* CoRoT *in the late type Be star* HD 175 869.
  Journal: *Communications in Asteroseismology.*
  Reference: Gutiérrez-Soto et al. (2009a).

- *Application of the* TiSAFT *code (Time Series Analysis with Fisher's Test).*
  Journal: *Communications in Asteroseismology.*
  Reference: Huat et al. (2009b).

- *Preliminary results on the pulsations of Be stars with* CoRoT .
  Journal: *Communications in Asteroseismology.*
  Reference: Neiner et al. (2009b).

- *The study of Be stars with the* CoRoT *satellite.*
  Journal: *Proceedings of the XIX Reunión Científica de la SEA, 2010.*
  Reference: Diago et al. (2010), in preparation.

Part III

Appendixes

Blackbird singing in the dead of night,
Take these sunken eyes and learn to see.
All your life,
You are only waiting for this moment to be free.

Paul McCartney

A

Resumen en castellano

Esta parte constituye un resumen en castellano de los contenidos de esta tesis doctoral. Se trata de una breve descripción de los resultados y discusiones más interesantes de la tesis. No se incluyen figuras ni tablas, refiriéndonos siempre a las ya incluidas en el cuerpo principal del trabajo.

A.1 Introducción

A.1.1 Asterosismología

El objetivo de la asterosismología es describir el interior de las estrellas a partir de las oscilaciones. Evidentemente, el interior de las estrellas es, posiblemente, el lugar más difícil de estudiar de todo el Universo, ya que las condiciones especiales que allí se dan no pueden reproducirse en ningún laboratorio terrestre. Así, la importancia de esta ciencia en el estudio global de la física estelar es crucial. Los principios básicos de la asterosismología son, en esencia, similares a los que los geólogos usan en el estudio de seísmos terrestres. La asterosismología hace uso de descripciones matemáticas de las oscilaciones en cuerpos tridimensionales, creando para ello sofisticadas simulaciones numéricas. Es, por tanto, un claro ejemplo de una ciencia multidisciplinar. Para una descripción profunda de la asterosismología referimos al lector al capítulo 1 y al apéndice B, que constituyen un importante complemento para la comprensión del capítulo mencionado.

A lo largo del diagrama H-R se identifican una gran cantidad de estrellas pulsantes, tal y como podemos observar en la figura 1.7. La banda en la que aparecen la mayoría de estrellas pulsantes se denomina la *banda clásica de inestabilidad*, y en ella encontramos las estrellas pulsantes de tipo Cefeidas, RR Lyrae, δ Scutti, etc. En lo que refiere a esta tesis, nos centraremos en dos tipos concretos de estrellas pulsantes del diagrama H-R: las estrellas de tipo β Cephei y las SPB (de su acrónimo en inglés: Slowly Pulsating B star) . Ambos tipos de estrellas son pulsadores de tipo B situados cerca de la sección principal del diagrama H-R con el mecanismo κ actuando en los elementos pesados del grupo del Fe como motor impulsor de las pulsaciones.

- **Estrellas tipo β Cephei**

  El grupo de las estrellas de tipo β Cephei es conocido desde principios del siglo XIX y está formado por estrellas de tipos B tempranos con tipos espectrales entre B0.5 y B2 y clases de luminosidad entre II-III y V. Normalmente, las estrellas de tipo β Cephei suelen presentar variabilidad de corto periodo

tanto en su luminosidad como en su velocidad radial. Los periodos de pulsación de estas estrellas variables se sitúa entre 3 y 8 horas y están asociados a modos p de orden bajo y/o modos g.

- **Estrellas tipo SPB**

  Las estrellas SPB, del inglés *Slow Pulsating B stars*, fueron introducidas por primera vez por Waelkens (1991) como un grupo separado de estrellas variables con tipos espectrales entre B2 y B9 y masas de entre 3 y 7 $M_\odot$ que presentan multiperiodicidad. Los periodos típicos de entre 0.5 y 3 días y se atribuyen a pulsaciones no radiales en modos g de altos órdenes. Las estrellas SPB están situadas en temperaturas más bajas en la secuencia principal, justo debajo de las β Cephei, como puede observarse en la figura 1.9. Como se ha mencionado, la mayoría de estrellas pulsantes de tipo SPB presentan multiples periodos de variabilidad, lo que hace que se produzca el fenómeno conocido como *beating* de frecuencias con periodos de meses o años. Además, las estrellas SPB son consideradas como rotadores lentos, pues tienen, en media, un $V \sin i \leq 100\,\mathrm{km\,s^{-1}}$.

A.1.2   Estrellas de tipo Be

Las estrellas Be son objetos de secuencia principal, con alta velocidad de rotación, que presentan un exceso infrarrojo y emisión en las líneas de Balmer, debido a la presencia de una envoltura circumestelar concentrada en el ecuador y generada por eyecciones discretas de materia originado por mecanismos que todavía no son bien conocidos.

El caso de las estrellas Be es especialmente complejo. Un estudio publicado por Hubert and Floquet (1998) basado en fotometría del satélite HIPPARCOS mostró que la mayoría de las estrellas Be tempranas presentan variabilidad fotométrica de corto periodo (86%), mientras que el porcentaje disminuye en los tipos más tardíos (18% en el rango B6-B9). Estas variaciones de corto periodo son atribuidas a la presencia de pulsaciones no radiales en estas estrellas.

Teóricamente, como se ha visto anteriormente en el texto, a lo largo de todo el

rango del tipo espectral B podemos encontrar distintos tipos de estrellas pulsantes. Dado que el grupo de estrellas Be están formadas por estrellas masivas, los modos de oscilación que se esperan pueden estar causados tanto por modos p como por modos g.

Los mecanismos propuestos para explicar la eyección de materia y, por tanto, la formación del disco circumestelar que caracteriza a las estrellas Be, son hasta ahora, las pulsaciones no radiales y los campos magnéticos, combinados con la alta velocidad de rotación característica de este tipo de estrellas. En un trabajo reciente, Rivinius et al. (2001) ha demostrado que la interferencia constructiva de los diferentes modos de pulsación detectados determinan los episodios de pérdida de masa en la estrella Be μ Cen. La cuestión: "¿Es este tipo de mecanismo válido para el resto de estrellas Be?" continúa siendo un enigma.

A lo largo de este trabajo consideraremos que las variaciones de corto periodo observadas en las estrellas estudiadas son debidas a pulsaciones y no a otro tipo de mecanismos como podrían ser, por ejemplo, modulación rotacional o las manchas en la superficie estelar. Las razones que refuerzan esta suposición son dos:

- Las estrellas variables detectadas, tanto de tipo B como Be, están localizadas en las zonas de inestabilidad correspondientes a estrellas de tipo β Cephei o SPB. Por tanto, podemos suponer que las variaciones de corto periodo son debidas a modos p o g excitados por el mecanismo κ, tal y como ha sido observado por muchos autores (Balona and Kambe 1999; Jankov et al. 2000; Janot-Pacheco et al. 1999; Hubert et al. 1997; Floquet et al. 1996) y calculado en diversas modelizaciones teóricas (véase Balona and Dziembowski 1999, por ejemplo).

- El segundo argumento hace referencia a la dificultad de encontrar un modelo físico que explique las inhomogeneidades en la fotosfera o baja atmósfera de las estrellas Be. Las estrellas de tipo Be son completamente radiativas en sus capas más externas. Por tanto, no se pueden presumir mecanismos de tipo dinamo que produzcan campos magnéticos y den lugar a manchas en la superficie estelar. Actualmente no se ha encontrado ninguna evidencia de campo magnético en estrellas de tipo Be (Silvester et al. 2009; Wade

2010). Sin embargo, los modelos teóricos que atribuyen la variación de corto periodo a pulsaciones describen adecuadamente las frecuencias observadas en muchos de los trabajos recientes (véase, por ejemplo, los trabajos de Rivinius et al. 2003; Walker et al. 2005b,a; Saio et al. 2007, en los que se estudian las frecuencias detectadas en diversas estrellas observadas por la misión espacial MOST)

A.1.3   La misión espacial CoRoT

El satélite espacial CoRoT (de su descripción en inglés Co*nvection*, Ro*tation and planetary* T*ransits*) es una de de las misiones espaciales más importantes hoy en día. El objetivo principal de la misión es obtener fotometría de muy alta precisión para el estudio asterosismológico y la búsqueda de planetas extrasolares. La misión está liderada por la agencia francesa del espacio CNES con una importante participación internacional de la ESA (Agencia Espacial Europea), Alemania, Austria, Bélgica, Brasil y España. El satélite CoRoT está equipado con un pequeño telescopio de 27 cm y cuatro cámaras CCD con las que se están detectando variaciones en la intensidad de la luz proveniente de diferentes estrellas seleccionadas previamente para distintos objetivos científicos. El satélite CoRoT fue lanzado con éxito el pasado 27 de diciembre de 2006.

Los objetivos científicos del satélite CoRoT son dos, los cuales requieren de observaciones de larga duración obtenidas de forma ininterrumpida por el satélite desde el espacio. Cada uno de los objetivos ha sido asignado a un programa diferente, el cual, tiene una determinada configuración óptica y sensibilidad a la luz de los objetos seleccionados.

- **Programa de sismología estelar**

  Como se ha descrito antes, la asterosismología estudia la estructura interna de las estrellas a través de la interpretación de las oscilaciones detectadas. Así, el estudio de las oscilaciones estelares a partir de las variaciones en la luminosidad de la estrella o en las lineas espectrales nos permite conocer el interior de las estrellas. El programa de sismología estelar ha sido dividido en

dos subprogramas con diferentes objetivos: i) *el programa central*, dedicado al estudio de las capas internas y la física de los núcleos estelares; ii) *el programa exploratorio*, dedicado a la determinación de parámetros estelares.

Así, en el campo de sismología estelar o asterosismología se observan, en cada uno de los apuntados previstos, una o dos estrellas brillantes seleccionadas como objetivos principales del programa central y cerca de una decena de estrellas seleccionadas como objetivos secundarios del programa exploratorio.

- **Programa de búsqueda de exoplanetas**

  A partir del descubrimiento del primer planeta orbitando alrededor de una estrella distinta a nuestro Sol (exoplaneta) por parte de Mayor and Queloz (1995), el conocimiento e interés en la formación y búsqueda de planetas extrasolares ha aumentado considerablemente. El desafío de la misión CoRoT es la observación y detección, por primera vez, de planetas extrasolares de tipo terrestre utilizando el método de los tránsitos (ver figura 8.2). El método de los tránsitos se basa en la detección de una pequeña disminución de la luminosidad de la estrella cuando es ocultada por uno de los planetas que orbitan a su alrededor. Para ello, es necesario una precisión fotométrica sin precedentes y observaciones de muy larga duración.

  En el campo de exoplanetas se han fijado cerca de 12 000 estrellas por apuntado, de las cuales, unos cuantos centenares forman parte de un *programa adicional* con diferentes objetivos científicos que se seleccionan a partir de propuestas elaboradas por la comunidad científica en respuesta a distintos anuncios de oportunidad.

La misión espacial CoRoT ha sido diseñada con dos campos de visión, dos conos de $10°$ de radio centrados en el centro galáctico (coordenadas RA $= 18\,h50'$ y $\delta = 0°$) y anticentro galáctico (coordenadas RA $= 6\,h50'$ y $\delta = 0°$). Las observaciones se han planificado en apuntados continuados de larga duración (150 días – *long runs*) y de corta duración (20-30 días – *short runs*). Cada año se divide en distintos periodos de observación, que pueden consultarse en el capítulo 8, así como la cadena de producción y adquisición de datos de la misión espacial CoRoT.

El estudio de estrellas Be con CoRoT

Las listas de objetivos principales y secundarios para ser observados por el satélite CoRoT han sido confeccionadas con detenimiento durante los últimos años, dependiendo de su interés científico. Debido al interés de las estrellas Be, se ha establecido una colaboración internacional para el estudio de este tipo de estrellas con la misión espacial CoRoT, este grupo ha sido denominado *the* CoRoT *Be Team* y es el encargado de seleccionar estrellas Be como posibles candidatos a ser observados por el satélite CoRoT desde el espacio.

El CoRoT Be Team se encarga de proponer observaciones de estrellas Be por la misión CoRoT en dos sentidos:

- Observaciones de estrellas brillantes como objetos secundarios en los campos de sismología estelar. Varias estrellas han sido ya observadas por el satélite como objetos de los dos primeros apuntados largos. Otras han sido consideradas para los siguientes apuntados largos todavía por fijar.

- Observaciones de estrellas débiles en los campos de exoplanetas. Estas observaciones están comprendidas dentro del programa adicional. Distintas estrellas Be han sido ya observadas y muchas otras están siendo propuestas como respuesta a diferentes anuncios de oportunidad. El tratamiento y análisis de estos datos están totalmente bajo la responsabilidad de nuestro grupo.

El grupo del Observatorio Astronómico de la Universitat de València es el responsable del estudio fotométrico de las estrellas Be brillantes que han sido propuestas como objetos secundarios en los campos de asterosismología y de las estrellas Be débiles en los campos de exoplanetas. El trabajo realizado hasta ahora es el presentado en esta tesis.

A.2 Herramientas de análisis de datos

Para la detección de señales periódicas en las series fotométricas obtenidas en las observaciones de CoRoT en el grupo CoRoT Be Team utilizamos técnicas basadas en el análisis de Fourier. En el capítulo 3 se da una descripción detallada de la base matemática del análisis de Fourier.

En el grupo del Observatorio Astronómico de la Universitat de València hemos desarrollado el código de análisis PASPER (Diago et al. 2008a), en colaboración con Rafael Garrido y Juan Gutiérrez-Soto (Instituto de Astrofísica de Andalucía, IAA-CSIC). PASPER analiza el espectro de frecuencias en busca de la señal con mayor amplitud en el espacio de Fourier ajustando una función sinusoidal. Esto se realiza ajustando esta frecuencia detectada con mínimos cuadrados en el dominio temporal. PASPER está basado en la transformada discreta de Fourier (Deeming 1975), haciendo uso del periodograma de Lomb-Scargle (Lomb 1976; Scargle 1982). Cuando el programa encuentra una frecuencia se elimina su señal de los datos y se continúa la búsqueda de frecuencias en el residuo de esta sustracción. El programa continúa buscando frecuencias hasta que la señal/ruido de la frecuencia encontrada ya no es significativa. El criterio de parada usado por PASPER está basado en el trabajo descrito por Breger et al. (1993).

Una vez detectado el número de frecuencias significativas, el segundo paso es refinar este análisis para obtener una buena determinación de cada una de las frecuencias. Este paso se realiza utilizando un método de ajuste no lineal basado en mínimos cuadrados. Para ello, hacemos uso del código KURTZ_BOS, desarrollados por Juan Gutiérrez-Soto. Este código implementa el algoritmo de Kurtz, descrito en Kurtz (1985). Una vez detectada una frecuencia, el programa minimiza la varianza moviendo la frecuencia detectada en un pequeño intervalo centrado en esta frecuencia. La frecuencia refinada es eliminada de los datos y una nueva determinación empieza de nuevo hasta encontrar la segunda frecuencia. El código ajusta simultáneamente las dos frecuencias encontradas moviéndolas en pequeños intervalos para minimizar, de nuevo, su varianza y obtener el mejor ajuste. Este método es iterativo, finalizando al alcanzar el número máximo de frecuencias significativas detectadas con el código PASPER.

La determinación de las amplitudes y fases de las frecuencias mejoradas se realiza con mínimos cuadrados, haciendo uso de una función interna del código PASPER.

La resolución en la determinación de las frecuencias es, siguiendo el criterio de Rayleigh, $1/T$, siendo T el intervalo de tiempo de observación. A pesar de esto, Kallinger et al. (2008) propone un valor menos conservativo, basado en simulaciones Monte-Carlo. Este valor es de $1/(4T)$.

El error en la determinación de las frecuencias, amplitudes y fases se deriva del trabajo de Montgomery and O'Donogohue (1999). La correlación en los residuos del ajuste (Schwarzenberg-Czerny 1991) se tiene en cuenta multiplicando los errores en estas cantidades por $\sqrt{D}$, donde D es el número consecutivo de puntos correlacionados presentes en los datos.

Los manuales de uso de los programas PASPER y KURTZ_BOS se adjuntan en los apéndices C y D, respectivamente.

A.3   Estudio en las Nubes de Magallanes

El trabajo presentado en esta tesis comenzó en octubre de 2005, más de un año antes de que se lanzara el satélite CoRoT. Antes de que los primeros datos de la misión CoRoT comenzaran a llegar necesitábamos testear los códigos y comprobar que los resultados obtenidos eran satisfactorios. Para ello, se propuso una búsqueda de variabilidad de corto periodo en grandes muestras de estrellas de tipo B y Be de las Nubes de Magallanes (MCs). Algunos puntos clave para la realización de este estudio en las MCs fueron:

- Las muestras de estrellas B y Be de las MCs tenían una determinación minuciosa de los parámetros fundamentales, lo que nos permitía no solo realizar el estudio pulsacional, sino también mapear zonas de inestabilidad en las regiones de las MCs.

- La teoría de pulsación no predice pulsaciones de tipo SPB ni β Cephei en regiones de baja metalicidad. De este modo, la búsqueda de este tipo de estrellas masivas pulsante en la región de la Nube Pequeña de Magallanes (SMC) era un importante reto que podría confirmar o desmentir los cálculos teóricos.

- Una vez obtenidos los excelentes resultados en la SMC (que se describen a continuación), nos propusimos completar y extender el estudio a la Nube Grande de Magallanes (LMC) y comparar ambos resultados con los resultados conocidos para nuestra Galaxia (MW).

A.3.1   Interés del estudio en las MCs

El mecanismo κ en estrellas pulsantes de tipo β Cephei y SPB depende de la abundancia de los elementos más pesados de la estrella, especialmente de los del grupo del Fe. Es claro, por tanto, que las bandas de inestabilidad dependerán de la metalicidad (Z) del medio interestelar en el que esté inmerso la estrella. En el trabajo de Pamyatnykh (1999) se demuestra que las bandas de inestabilidad para

las estrellas de tipo β Cephei y SPB prácticamente desaparecen para $Z < 0.01$ y $Z < 0.006$, respectivamente. Miglio et al. (2007a,b) realizó nuevos cálculos basados en tablas de opacidad actualizadas y diferentes abundancias en metales, determinando que para una metalicidad de $Z = 0.005$, solo pulsaciones de tipo SPB pueden ser esperadas. No se predicen pulsaciones de tipo β Cephei para esa metalicidad. Más recientemente, nuevos cálculos realizados por Salmon et al. (2009) han demostrado que una metalicidad $Z \geq 0.007$ es necesaria para activar las pulsaciones de tipo β Cephei y $Z > 0.004$ para las de tipo SPB.

La metalicidad de las MCs se estima en $Z = 0.002$ para la SMC y $Z = 0.007$ para la LMC, de acuerdo con Maeder et al. (1999, y referencias internas). Podemos deducir, por tanto, que para la LMC se esperará encontrar muy pocas variables de tipo β Cephei y SPB y, en cambio, para la SMC no se espera encontrar ningún tipo de las dos variables anteriores.

A pesar de estas consideraciones teóricas, numerosos trabajos recientes han encontrado estrellas masivas pulsantes de tipo B en regiones de baja metalicidad (cf. Pigulski and Kołaczkowski 2002; Kołaczkowski et al. 2004, 2006; Diago et al. 2008a; Karoff et al. 2008; Sarro et al. 2009, por ejemplo). Estos resultados ponen de manifiesto que el mecanismo κ continúa activando las pulsaciones aún en regiones con poca abundancia en metales. Esta contradicción entre teoría y observaciones continúa sin poder ser explicada.

Para este estudio de estrellas de tipo B en las MCs hemos tomado series temporales fotométricas del proyecto MACHO. La larga duración de estas observaciones (de unos 2 690 días) nos da una amplia resolución en frecuencias, lo que nos permite distinguir entre frecuencias relativamente cercanas.

A.3.2   Conclusiones del estudio en la SMC

Para la SMC hemos analizado una muestra de 183 estrellas con lineas de absorción de tipo B y una muestra de 126 estrellas de tipo Be, para las cuales Martayan et al. (2007b) determinó los parámetros físicos. Esto nos ha permitido

estudiar la posición de las estrellas pulsantes de tipo B y Be de la SMC en el diagrama H-R. Se han determinado observacionalmente las bandas de inestabilidad para la SMC, como puede verse en las figuras 6.10 y 6.12 para las estrellas B y Be, respectivamente.

Se han encontrado nueve estrellas pulsantes de tipo B, ocho de las cuales parecen ser variables de tipo SPB. La región que ocupan estas posibles variables de tipo SPB en el diagrama H-R parece estar situada a una temperatura más alta con respecto a la región ocupada por las estrellas SPB observadas en la MW. La estrella restante podría ser considerada como una variable de tipo β Cephei con dos periodos de pulsación. Este hecho y el hecho de que es la estrella con mayor temperatura efectiva nos hace sospechar que se trata efectivamente de una variable de tipo β Cephei. Este es un resultado muy interesante, puesto que los modelos teórico actuales no predicen pulsaciones de tipo β Cephei para la metalicidad de la SMC.

Entre la muestra de estrellas Be se han encontrado 32 estrellas pulsantes. La mayoría de ellas están situadas en la región de las estrellas SPB del diagrama H-R, con periodos mayores a 0.5 días. Probablemente se trata de pulsadores en modos g de tipo SPB. Tres estrellas pulsantes de tipo Be se encuentran en zonas con temperaturas más altas, por lo que podrían ser consideradas como variables de tipo β Cephei.

Al igual que en los resultados obtenidos por Gutiérrez-Soto et al. (2007a), para la SMC se encuentran más pulsadores entre la muestra de estrellas Be que entre la muestra de estrellas B. Un 25.3% de las estrellas Be presentan variabilidad de corto periodo, mientras que solo un 4.9% de las estrellas de tipo B presenta este tipo de variabilidad. Este resultado nos indica que la alta velocidad de rotación presente en las estrellas de tipo Be podría favorecer la aparición de pulsaciones no radiales o intensificar las amplitudes de los modos ya presentes en estas estrellas. Alternativamente, esta presencia de pulsaciones no radiales podría estar relacionada con la naturaleza, todavía desconocida, del fenómeno Be.

Tanto los porcentajes de estrellas variables de tipo B sobre la muestra total de estrellas B como el porcentaje de estrellas variables de tipo Be sobre la muestra

total de estrellas Be en la SMC son menores que en la MW. Este resultado indica, claramente, que la presencia de pulsaciones está directamente afectada por la disminución de la metalicidad del medio interestelar de la SMC, tal y como predicen los modelos teóricos.

A.3.3   Conclusiones del estudio en la LMC

En la LMC hemos analizado una muestra de 106 estrellas con lineas de absorción de tipo B y una muestra de 47 estrellas de tipo Be, para las cuales Martayan et al. (2006a) determinó los parámetros físicos. Esto nos ha permitido, al igual que en la SMC, estudiar la posición de las estrellas pulsantes de tipo B y Be de la LMC en el diagrama H-R. Se han determinado observacionalmente las bandas de inestabilidad para la LMC, como puede verse en las figuras 7.4 y 7.7 para las estrellas B y Be, respectivamente.

Entre las estrellas con lineas de absorción de tipo B hemos encontrado siete variables de corto periodo. Dos de ellas han sido propuestas como variables de tipo SPB en función de los periodos encontrados. Al igual que para la SMC, la posición de las estrellas variables de tipo SPB en el diagrama H-R para la metalicidad de la LMC está situada a temperaturas efectivas más altas con respecto a las variables SPB detectadas en la MW. Las restantes cinco estrellas presentan periodos en el rango de las variables de tipo β Cephei. Este hecho, junto con las altas temperaturas efectivas de estas cinco estrellas hace que sean propuestas como candidatas a variables de tipo β Cephei.

En la muestra de estrellas Be hemos encontrado cinco estrellas pulsantes. Tres de ellas presentan multiperiodicidad. En relación a los periodos obtenidos, estas variables han sido propuestas como pulsadores en g modos de tipo SPB, pero las altas velocidades de rotación presentes en estas estrellas hacen que el resultado no sea concluyente.

El predominio de estrellas pulsantes en la muestra de estrellas Be es significativamente mayor que sobre la muestra de estrellas B. Hemos detectado que el

23% de las estrellas Be presentan variabilidad de corto periodo, mientras que tan solo el 7% de las estrellas B presentan este tipo de variabilidad. Este resultado concuerda con el obtenido en la SMC y la MW, reforzando el hecho de que la alta velocidad de rotación contribuye en la aparición de pulsaciones no radiales o amplifica los modos ya existentes en las estrellas pulsantes. Alternativamente, esta presencia de pulsaciones no radiales podría estar relacionada con la naturaleza, todavía desconocida, del fenómeno Be.

Finalmente, en este capítulo se ha llevado a cabo una minuciosa comparación entre el número de pulsadores de tipo B de la SMC, LMC y MW. Hemos encontrado una disminución en el porcentaje de estrellas pulsantes de tipo espectral B con el decrecimiento de la metalicidad del medio interestelar, tal y como se predice en la teoría de pulsación. No obstante, es evidente a la luz de los resultados de este trabajo que las pulsaciones siguen presentes en las estrellas de tipo espectral B aun en regiones pobres en metalicidad. Este hecho no ha podido ser explicado, aun, por la teoría de pulsación. Por tanto, el por qué de la detección de pulsadores de tipo SPB y β Cephei en regiones de baja metalicidad continúa siendo un enigma.

Además, hemos detectado un incremento en los porcentajes de estrellas Be pulsantes de la MW, LMC y SMC, mientras que la metalicidad decrece. Este fenómeno podría ser explicado por el hecho de que las estrellas Be de la SMC adquieren velocidades de rotación (Ω/Ω_c) mucho mayores que en la LMC o la MW. Se experimenta una disminución similar en cuanto a la velocidad de rotación de las estrellas B. No obstante, en este caso, los porcentajes están siempre por debajo del valor mínimo a partir del cual los efectos de alta rotación empiezan a aparecer $(\Omega/\Omega_c \sim 70\%)$. Este hecho podría explicar el por qué del aumento de pulsaciones en estrellas Be entre la LMC y la SMC y no en el caso de estrellas de tipo B.

A.4 Estudio de estrellas Be en el campo de exoplanetas de la misión CoRoT

Además de las estrellas Be brillantes observadas en el campo de sismología del satélite CoRoT, nuestro grupo también es el encargado de numerosas estrellas débiles seleccionadas en el campo de exoplanetas de la misión CoRoT. El objetivo es, no sólo el análisis fotométrico de las series temporales producidas por CoRoT, sino también la detección e identificación de estrellas de tipo Be para ser observadas durante futuros apuntados.

A.4.1 Resultados y discusión

En el campo de exoplanetas de la misión espacial CoRoT se han analizado los datos correspondientes a varias estrellas Be observadas en el IRa1. Para tres de estas estrellas Be se han encontrado resultados interesantes, que serán discutidos a continuación. La lista completa de estrellas observadas en este apuntado inicial se muestra en la tabla 10.1. Las observaciones de este apuntado inicial son de aproximadamente 54 días. Estas estrellas han sido analizadas utilizando los códigos descritos en las secciones anteriores.

CoRoT star 102725623

Para esta estrella el análisis de la serie fotométrica producida por el satélite CoRoT ha revelado una frecuencia significativa en $0.8974 \, \mathrm{c \, d^{-1}}$ con una amplitud de $0.4 \, \mathrm{mmag}$. También se ha encontrado otra frecuencia atribuida a variación de largo periodo. La curva de luz de esta estrella presenta también un decrecimiento de largo periodo, que ha sido corregido previamente al análisis de frecuencias. La espectroscopía de esta estrella tiene muy baja resolución y tan solo ha servido para clasificar esta estrella con el tipo espectral B6.

CoRoT star 102964342

La curva de luz de esta estrella muestra típicos saltos fotométricos producidos por efectos sistemáticos en las CCDs del satélite CoRoT. Estos efectos han sido corregidos previamente al análisis de frecuencias.

A partir del análisis fotométrico hemos detectado cinco frecuencias significativas. La frecuencia $f_1 = 3.8446\,\mathrm{c\,d^{-1}}$ es la predominante, pues es la que tiene una mayor amplitud (cerca de $0.9\,\mathrm{mmag}$). Tras un análisis detallado, observamos que la frecuencia f_1 podría ser el primer armónico de la frecuencia $f_2 = 1.9534\,\mathrm{c\,d^{-1}}$, puesto que $2f_2 \sim f_1$. En cualquier caso, la presencia de múltiples frecuencias apunta a la existencia de pulsaciones no radiales en esta estrella Be.

Para esta estrella se han obtenido también datos espectroscópicos de baja resolución con el telescopio de $2.2\,\mathrm{m}$ del CAHA (Centro Astronómico Hispano Alemán, en Calar Alto, Almería) utilizando el espectrógrafo CAFOS. A partir de estos datos, el tipo espectral de esta estrella correspondería entre B1 y B2. Lamentablemente, no se pudo deducir el $V \sin i$ a partir de estos espectros de baja resolución.

CoRoT star 102719279

La estrella Be 102719279 observada por el satélite CoRoT muestra varios desvanecimientos en su curva de luz. Estos desvanecimientos o *fadings* son debidos a eyecciones de materia o *outburst* por parte de la estrella. Debido al ángulo de inclinación con que el satélite CoRoT observa la estrella ($i \sim 90°$), el material eyectado oculta la estrella (cf. Hubert and Floquet 1998, para ver algunos ejemplos con datos de la misión espacial HIPPARCOS). Observando la curva de luz, parece que ocurre un outburst cerca del día juliano $2\,454\,141$, un segundo outburts parece ocurrir cerca del día juliano $2\,454\,148$ y un tercero, más intenso, alrededor de los días julianos $2\,454\,151 - 2\,454\,152$. Podemos ver en la figura 10.5 que los outbursts producen fadings de unas $100\,\mathrm{mmag}$ en la curva de luz. La amplitud de la oscilación se incrementa hasta alcanzar el momento en que se produce el

outburst más intenso. A continuación, la amplitud decae mientras la magnitud de la estrella se recupera lentamente hasta alcanzar los niveles previos al outburst. En este caso, el outburst parece coincidir con el momento en que la amplitud de la oscilación alcanza su máximo. Como ha sido observado para la estrella μ Cen por Rivinius et al. (2001).

Del análisis de Fourier de esta estrella se detectan varias frecuencias cercanas al valor $1.16\,\mathrm{c\,d}^{-1}$, su doble $2.32\,\mathrm{c\,d}^{-1}$ y cercanas a $0.98\,\mathrm{c\,d}^{-1}$. Como hemos comprobado, las amplitudes de las frecuencias cambian radicalmente de los días anteriores a los posteriores al outburst, por lo que ha sido necesario un análisis a cada uno de los conjuntos de datos por separado. Podemos ver los cambios de amplitud en la figura 10.6. Al igual que para la estrella descrita anteriormente, la presencia de múltiples frecuencias pone de manifiesto la existencia de pulsaciones no radiales en esta estrella Be.

A.5   La estrella Be HD 50 209 observada por la misión espacial CoRoT

La estrella HD 50 209 está clasificada como una estrella de tipo espectral B8IVe, con una magnitud $V = 8.36$. Ha sido estudiada previamente por Gutiérrez-Soto (2006) y Gutiérrez-Soto et al. (2007a), usando datos del satélite HIPPARCOS, ASAS-3 y del Observatorio de Sierra Nevada (OSN) en Granada. A partir de los datos de HIPPARCOS se detectaron dos frecuencias en $1.689\,\mathrm{c\,d^{-1}}$ y $1.47\,\mathrm{c\,d^{-1}}$, aunque con bajas amplitudes. Los datos del OSN revelaron una frecuencia en $1.4889\,\mathrm{c\,d^{-1}}$. Finalmente, el análisis de los datos de ASAS-3 mostraron picos significativos en las frecuencias $2.4803\,\mathrm{c\,d^{-1}}$ y $1.4747\,\mathrm{c\,d^{-1}}$.

La presencia de pulsaciones en estrellas de tipo B tardíos ha sido un tema de controversia en la literatura reciente. Hubert and Floquet (1998) mostraron que las pulsaciones en tipos espectrales tardíos B6-B9 son mucho menos comunes que en sus respectivos tipos tempranos. Baade (1989) no fue capaz de detectar variaciones en el perfil de linea en el espectro de varias estrellas de tipos B8 a B9.5. Saio et al. (2007) detectó modos g con poca amplitud en la estrella de tipo B8Ve β CMi. Por tanto, la tarea de averiguar cuándo las estrellas de Be de cualquier tipo presentan o no pulsaciones es una cuestión clave para establecer una relación entre pulsaciones no radiales y mecanismos de pérdida de masa.

El satélite CoRoT observó la estrella HD 50 209 en el campo de sismología. Las observaciones duraron 136 días en la dirección de anticentro galáctico en el apuntado LRa1, entre los días 18 de octubre de 2007 y 3 de marzo de 2008. La curva de luz que produjo el satélite contiene la información fotométrica en sus 328 279 puntos.

A.5.1   Análisis de frecuencias de HD 50 209

El análisis de frecuencias se realizó utilizando los códigos descritos previamente: PASPER y KURTZ_BOS. En este caso, las características orbitales de la misión

CoRoT aparecen reflejadas en el análisis de frecuencias, detectando una señal en $13.97\,\mathrm{c\,d^{-1}}$, correspondiente al periodo orbital del satélite y en $2.007\,\mathrm{c\,d^{-1}}$, correspondiente a la frecuencia día/noche del mismo satélite. Estas frecuencias y sus armónicos han sido eliminadas de la lista de frecuencias significativas. La lista completa de las frecuencias derivadas del análisis espectral se encuentran en la tabla 11.2, con un total de 60 frecuencias significativas.

Las frecuencias detectadas se agrupan en seis conjuntos. Cada conjunto está claramente separado del resto, excepto un par de ellos, como puede verse en la figura 11.2. En cada conjunto podemos observar la existencia de multipletes casi equidistantes y separados por intervalos ligeramente mayores a la resolución espectral.

A.5.2   Espectroscopía de HD 50 209

Para la estrella HD 50 209 se obtuvo espectroscopía de alta resolución utilizando el instrumento FEROS en el telescopio de 2.2 m del Observatorio de La Silla (Chile). Diecisiete espectros de alta resolución con alta señal ruido fueron obtenidos. Catorce espectros adicionales complementaron los datos espectroscópicos. Estos últimos catorce espectros fueron obtenidos con el instrumento Narval en el telescopio TBL del Observatorio de Pic du Midi (Francia).

A partir de estos espectros se determinaron los parámetros fundamentales de HD 50 209 utilizando el mismo método que el descrito en Frémat et al. (2006). Los resultados para los distintos valores de Ω/Ω_c se presentan en la tabla 11.3 y son consistentes con las determinaciones previos por parte de (Frémat et al. 2006).

A pesar de la alta calidad de los espectros proporcionados por el instrumento FEROS y de las variaciones detectadas en los datos fotométricos de CoRoT , no hemos podido detectar ninguna variabilidad periodica en el espectro de HD 50 209.

A.5.3 Discusión de los resultados

El primer hecho al que se debe hacer referencia es la presencia de multipletes en el análisis de frecuencias. Sabemos que la aparición de estos multipletes puede deberse a la presencia real de frecuencias cercanas o a la variación de la amplitud de una única frecuencia (Breger and Pamyatnykh 2006). Para poder discernir si se trata de verdaderas frecuencias cercanas o de la variación de la amplitud de una sola frecuencia hemos aplicado el método descrito en (Breger and Pamyatnykh 2006), pero los resultados obtenidos no han sido concluyentes y por tanto, no podemos afirmar o rechazar ninguna de las dos hipótesis sobre el origen de estos multipletes.

Del análisis exhaustivo de los multipletes y su distribución en diversos grupos se observa que realmente solo tenemos dos grupos independientes de frecuencias (f_4 y f_5), puesto que el resto son de la forma $f_i = f_5 + n\,f_4$ con $n = 1, 2, 3$. La frecuencia f_6 sería el primer armónico de f_1 y por tanto quedaría fuera del análisis. Recordemos que la frecuencia observada en una estrella (ν_{obs}) en rotación están relacionadas con la frecuencia de pulsación en el sistema de co-rotación (ν_{corot}) por la expresión:

$$\nu_{\mathrm{obs}} = |\,\nu_{\mathrm{corot}} - m\,\Omega\,| \tag{A.1}$$

donde Ω es la frecuencia de rotación de la estrella. A partir de la expresión A.1 y considerando f_4 como la frecuencia de rotación, el resto de frecuencias f_5, f_3, f_1 y f_2 podrían ser interpretadas como modos de una misma frecuencia de rotación en el sistema de co-rotación con $m = 0, -1, -2, -3$, respectivamente[1]. De este modo, la estrella presentaría cuatro modos de pulsación activos, con la misma frecuencia en el sistema de co-rotación, presentando un valor $\ell = 3$.

No obstante, esta interpretación presenta un inconveniente importante: los modos correspondientes a $\ell = 1, 2$ no están siendo detectados, cuando son los que tienen mayor amplitud y por tanto, deberían de ser más fáciles de detectar. Por tanto, otra interpretación posible sería la existencia de un solo grupo de frecuencias de pulsación (F_1) junto con la frecuencia de rotación (F_4). Siendo el

---

[1]En este caso concreto estamos utilizando la notación propuesta por H. Saio, en la que los valores negativos de m representan modos en el sentido de giro de la estrella. Véase Saio et al. (2007) para más detalles.

resto de frecuencias combinaciones de estos dos grupos. No obstante, solo con nuestras observaciones no podemos discernir cuál de estas interpretaciones es la correcta.

Los parámetros fundamentales de la estrella HD 50 209 la sitúan ligeramente fuera de la banda de inestabilidad de las estrellas variables de tipo SPB calculada por Pamyatnykh (1999), aunque su posición es compatible si consideramos un error de 1-σ. Por tanto, consideraremos que las pulsaciones detectadas en HD 50 209 se deben a modos g típicos de variables SPB. De este modo, HD 50 209 sería un nuevo ejemplo de variable SPBe, cuya designación fue acuñada por Walker et al. (2005a).

Debido al hecho de que en las estrellas de tipo B tardío las frecuencias asociadas a modos g en el sistema de co-rotación de la estrella son mucho más pequeñas que la frecuencia de rotación, las frecuencias de estos modos en el sistema propio del observador están muy próximas a $|\,m\,\Omega\,|$. Esto nos conduce a la posibilidad de confundir las frecuencias cercanas a la frecuencia de rotación como un modo g más de pulsación (Walker et al. 2005a) o como una modulación de la rotacional (Balona 1995). En nuestro caso, por primera vez, hemos podido diferenciar entre la frecuencia de rotación y la frecuencia de pulsación en modos g con orden acimutal $|\,m\,| = 1$.

A.5.4 Conclusiones

La alta precisión y calidad de la fotometría obtenida por el satélite CoRoT así como la larga duración de las observaciones ha permitido la detección de pulsaciones en modos g en la estrella de tipo Be tardía HD 50 209. Esta detección refuerza el hecho de que todas las estrellas Be tienen pulsaciones no radiales y que éstas juegan un importante papel en los mecanismos de eyección de masa asociados al fenómeno Be.

Se han encontrado pulsaciones en cuatro modos con una misma frecuencia en el sistema de co-rotación con diferentes órdenes acimutales, aunque otras interpreta-

ciones son también plausibles. Además, se ha detectado la frecuencia de rotación de la estrella. La determinación precisa del periodo de rotación de la estrella será de vital importancia en la determinación de los parámetros fundamentales para futuros estudios de modelización asterosismológica.

Por primera vez se ha observado simultáneamente la frecuencia de rotación y las frecuencias de pulsación de forma separada, lo cual implica que las frecuencias que en este trabajo se atribuyen a modos g no pueden ser debidas a efectos de modulación rotacional. Este último hecho constituye una prueba de la presencia de pulsaciones en HD 50 209.

A.6 Conclusiones generales y trabajo futuro

El objetivo principal de este proyecto ha sido el estudio de las características pulsacionales de las estrellas de tipo Be utilizando datos de la misión espacial CoRoT. Para ello, en una primera fase del proyecto, se han desarrollado las herramientas necesarias y se han testeado en estrellas de tipo B y Be de las Nubes de Magallanes. Este estudio inicial ha proporcionado nuevas evidencias en la existencia de estrellas variables de tipo β Cephei y SPB en regiones interestelares de baja metalicidad. En una segunda fase del proyecto hemos empezado a trabajar con los datos que actualmente está proporcionando la misión CoRoT. Se han analizado varias estrellas Be del campo de exoplanetas y una estrella Be del campo de sismología estelar, la cual ha proporcionado nuevos resultados de gran impacto científico. Por lo tanto, podemos dar por alcanzado el objetivo principal de este proyecto.

A.6.1 Trabajo futuro

La misión espacial CoRoT continúa produciendo nuevos datos sobre estrellas Be seleccionadas por nuestro grupo, tanto en el campo de exoplanetas como en el de sismología estelar, además el tiempo de vida de la misión ha sido recientemente aumentado, por lo que la continuación inmediata de esta tesis es clara: continuar analizando datos sobre estrellas de tipo Be. Estos nuevos datos permitirán profundizar en el estudio del fenómeno Be y resolver los enigmas que aun permanecen sin resolver en este campo.

Además, se abren nuevas posibilidades y lineas de trabajo inmediatas derivadas de el trabajo desarrollado en este proyecto:

- Obtener datos espectroscópicos de las estrellas pulsantes B y Be de las Nubes de Magallanes para mejorar la determinación de las abundacias en metales de estas estrellas. De este modo podríamos confirmar si realmente son estrellas pulsantes con bajo contenido en metales o si son estrellas enriquecidas.

Durante el desarrollo de esta tesis se ha establecido una colaboración con el Christophe Martayan para obtener espectros de alta resolución con el espectrógrafo X-Shooter[2] en el ESO/VLT. Se espera presentar los primeros resultados durante el año que viene.

- Realizar un análisis similar al realizado para las MCs en una gran muestra de estrellas observadas por Martayan et al. (2008a) en el estudio Hα de la SMC usando el instrumento ESO/WFI[3]. En este sentido, pretendemos establecer una colaboración con Luis Manuel Sarro, quien tiene una gran experiencia en el campo de clasificación automatizada de estrellas variables (Debosscher et al. 2007; Sarro et al. 2009). Este estudio ayudaría a aumentar las estadísticas de estrellas pulsantes en medios con baja metalicidad y arrojaría más luz al origen del fenómeno Be.

- Obtener espectros de la estrella HD 50 209 con una mayor señal ruido. Sería interesante obtener espectros que coincidan con las épocas de mayor amplitud en las frecuencias observadas en este estudio.

- Continuar analizando series fotométricas de estrellas Be proporcionadas por la misión espacial CoRoT. Actualmente estamos analizando la estrella Be HD 51 193, cuyos resultados serán publicados a lo largo de este año.

- En colaboración con otros grupos (como por ejemplo, Hideyuki Saio o el Dpto. de Física Estelar del IAA-CSIC), desarrollar modelos teóricos de pulsación para las estrellas Be analizadas y proporcionadas por la misión CoRoT. El obtener modelos teóricos es un gran reto porque actualmente los modelos existentes no contemplan la alta rotación en sus cálculos.

- Continuar identificando nuevas estrellas Be para ser observadas posteriormente por la misión CoRoT.

- Nuestro grupo está implicado en el estudio de estrellas B y Be con el satélite Kepler. Por lo tanto, esta nueva misión proporcionará nuevas series fotométricas de estrellas B y Be para ser analizadas. Actualmente ya se ha observado una estrella Be confirmada, para la cual se han obtenido datos fotométricos de 230 días de duración. Espectros de alta resolución ya han sido obtenidos para esta estrella.

---

[2]http://www.eso.org/sci/facilities/develop/instruments/xshooter/.
[3]http://www.eso.org/sci/facilities/lasilla/instruments/wfi/.

The long and winding road,
That leads to your door
Will never disappear.
I've seen that road before.
It always leads me here,
Lead me to your door.

Paul McCartney

B

Basic equations of non-radial pulsations

Here we give the basic equations of hydrodynamics, equilibrium configuration in stars, and non-radial oscillations in stars. In this brief resume we will not derive the equations neither discuss them, because they are described in several books of fluid dynamics and astrophysics. For a deep description we refer to Cox (1980), Unno et al. (1989) or Aerts et al. (2010). Moreover, there are several lecture notes on this matter that can give a comprehensive analysis of the equations, for example Scuflaire and Thoul (2002) or Christensen-Dalsgaard (2003).

B.1 Mathematical preliminaries

Here we present some relations in spherical polar coordinates that will be needed in the following. The spherical polar coordinates and the Cartesian coordinates are related through:

$$
\begin{aligned}
x &= r \sin\theta \cos\varphi \\
y &= r \sin\theta \sin\varphi \\
z &= r \cos\theta
\end{aligned}
$$
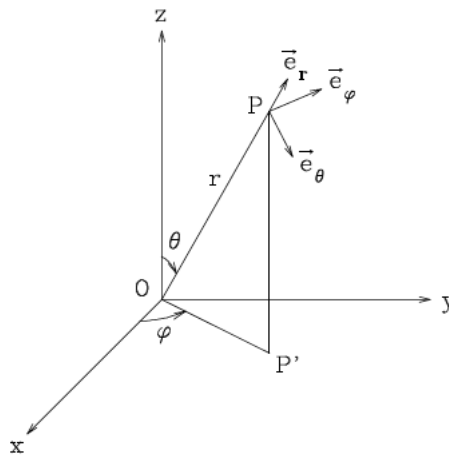
Figure B.1: *The spherical coordinates*

Let $\{\vec{e_r}, \vec{e_\theta}, \vec{e_\varphi}\}$ be the unit vectors in the r, θ and φ directions and let V be a general scalar field. Then, each vector $\vec{a}$ of the field V can be written as

$$
\vec{a} = a_r \vec{e_r} + a_\theta \vec{e_\theta} + a_\varphi \vec{e_\varphi}
$$

The *horizontal component* (or, properly speaking the *tangential component*) of

the vector $\vec{a}$ is defined as:

$$\vec{a_\perp} = a_\theta \vec{e_\theta} + a_\varphi \vec{e_\varphi} \tag{B.1}$$

We define the following vectors and scalar quantities:

1. **Gradient of the scalar field V:**

$$\nabla V := \frac{\partial V}{\partial r} \vec{e_r} + \frac{1}{r} \frac{\partial V}{\partial \theta} \vec{e_\theta} + \frac{1}{r \sin \theta} \frac{\partial V}{\partial \varphi} \vec{e_\varphi} \tag{B.2}$$

that is a vector field which points in the direction of the greatest rate of increase of the scalar field V, and whose magnitude is the greatest rate of change.

2. **Divergence of $\vec{a}$:**

$$\nabla \cdot \vec{a} := \frac{1}{r^2} \frac{\partial}{\partial r}(r^2 a_r) + \frac{1}{r \sin \theta} \frac{\partial}{\partial \theta}(\sin \theta \, a_\theta) + \frac{1}{r \sin \theta} \frac{\partial}{\partial \varphi}(a_\varphi) \tag{B.3}$$

3. **Laplacian of V:**

$$\triangle V := \nabla \cdot (\nabla V) =$$
$$= \frac{1}{r^2} \frac{\partial}{\partial r} \left(r^2 \frac{\partial V}{\partial r} \right) + \frac{1}{r \sin \theta} \frac{\partial}{\partial \theta} \left(\sin \theta \frac{1}{r} \frac{\partial V}{\partial \theta} \right) + \frac{1}{r \sin \theta} \frac{\partial}{\partial \varphi} \left(\frac{1}{r \sin \theta} \frac{\partial V}{\partial \varphi} \right) \tag{B.4}$$

B.2 General equations of hydrodynamics

Two formalisms are commonly used to describe the motion of a fluid: the *Eulerian* and the *Lagrangian* descriptions. In the Lagrange formalism, each fluid particle is assigned a label and followed in its motion as in classical mechanics. The particle label could be for example its initial position $\vec{r_0}$. We will more generally use some vector $\vec{a}$ as label. The fluid is then described by the functions $\vec{r}(\vec{a}, t)$, $\rho(\vec{a}, t)$, $P(\vec{a}, t)$, ...

In the Euler formalism, particles are not followed one by one. Rather, at each

position $\vec{r}$, the fluid is described by the functions $\vec{v}(\vec{r}, t)$, $\rho(\vec{r}, t)$, $P(\vec{r}, t)$, ...

In particular, time derivatives in these two formalisms do not have the same meaning: in the Lagrange formalism $\partial/\partial t$ its the time derivative following the motion of the fluid, while in the Euler formalism this symbol represents the time derivative at given point. Therefore, we have

$$\frac{\partial \vec{r}}{\partial t} = \vec{v} \quad \text{in the Lagrange formalism,}$$

$$\frac{\partial \vec{r}}{\partial t} = 0 \quad \text{in the Euler formalism.}$$

In the Euler formalism we introduce the differential operator called Strokes derivative, or derivative with respect to t following the fluid. For a quantity X, it is defined as

$$\frac{dX}{dt} := \frac{\partial X}{\partial t} + \vec{v} \cdot \nabla X \tag{B.5}$$

It is clear that

$$\left(\frac{\partial X}{\partial t} \right)_{Lagrange} = \frac{dX}{dt} \tag{B.6}$$

The two formalisms are often used simultaneously. To prevent any confusion, we use the notation $\partial/\partial t$ for $(\partial/\partial t)_{Euler}$ and d/dt for the operator $(\partial/\partial t)_{Lagrange}$. This convention is in agreement with the relationship B.6 between the Strokes derivative and the Lagrangian time derivative.

The basic equations that describe a non-magnetic self-gravitating spherically symmetric gaseous sphere without taking convective and viscous effects into account, are the following equations of hydrodynamics:

B.2.1   Continuity equation

The continuity equation represents the mass conservation. It can be written as

$$\frac{\partial \rho}{\partial t} + \nabla \cdot (\rho \, \vec{v}) = 0 \quad \text{or} \quad \frac{d\rho}{dt} + \rho \, \nabla \cdot \vec{v} = 0 \tag{B.7}$$

where $\vec{v}$ and ρ are respectively the local velocity and density.

B.2.2   Momentum conservation equation

The momentum equation is given by

$$\frac{\partial \vec{v}}{\partial t} + \vec{v} \cdot \nabla \vec{v} = -\nabla \Phi - \frac{\nabla P}{\rho} \quad \text{or} \quad \frac{d\vec{v}}{dt} = -\nabla \Phi - \frac{\nabla P}{\rho} \tag{B.8}$$

where P is the total pressure (gas, radiation and turbulent pressure) and Φ is the gravitational potential. The latter fullfills the equation of Poisson:

$$\triangle \Phi = 4 \, \pi \, G \, \rho \tag{B.9}$$

where G is the Gravitational Constant.

B.2.3   Energy conservation

The energy conservation is written as

$$T \left(\frac{\partial S}{\partial t} + \vec{v} \cdot \nabla S \right) = \varepsilon - \frac{\nabla \cdot \vec{F}}{\rho} \quad \text{or} \quad T \frac{dS}{dt} = \varepsilon - \frac{\nabla \cdot \vec{F}}{\rho} \tag{B.10}$$

where T is the local temperature, S the entropy per mass unit, ε the rate of energy generation per mass unit and $\vec{F}$ the energy flux density.

B.2.4   Transport equation

The energy transport in a star is either achieved through radiation or through convection so we note the total flux as $\vec{F} = \vec{F_R} + \vec{F_C}$ with $\vec{F_R}$ being the radiative flux and $\vec{F_C}$ the convective flux of the star. In the bulk of the star the diffusion approximation is valid because the mean free path of the photons (typically some cm in the solar interior) is much smaller than the distance to overcome to reach the surface. The radiative flux is therefore, to a good approximation, given by the diffusion equation:

$$\vec{F_R} = -K\nabla T \tag{B.11}$$

where K is the radiative conductivity coefficient, that can be written in terms of the Rosseland mean opacity κ as

$$K = -\frac{4\,a\,c_*\,T^3}{3\,\kappa\,\rho} \tag{B.12}$$

being $a = 7.56 \cdot 10^{-15}$ cgs the radiation density constant and c_* the velocity of light.

B.2.5   Material equations

In addition to the partial differential equations and the associated boundary conditions, we also need the equations describing the behaviour of the matter as a function of its chemical composition and the thermodynamic variables. This equations are sometimes called constitutive equations or material equations. They include the equation of state , the opacity κ and the nuclear energy generation rate ε. We assume that ρ and T are independent thermodynamic variables. The properties of the matter can be described by relations of the form

$$P = P(\rho, T, \chi_i), \ S = S(\rho, T, \chi_i), \ \kappa = \kappa(\rho, T, \chi_i), \ \varepsilon = \varepsilon(\rho, T, \chi_i), \ ...$$

where χ_i denotes the chemical composition in terms of i different elements. Note that the nuclear energy generation rate ε is usually the result of many nuclear reactions whose rates depends on elements with very small abundances, very

short lifetimes and not described by χ_i. It is only when these elements reach their equilibrium abundance values that ε can be considered as a function of ρ, T and χ_i.

B.3   Stellar equilibrium configuration

Since the equilibrium state is spherically symmetric, the structure depends only on the distance r to the centre. In the spherical polar coordinates $\{r, \theta, \varphi\}$ (described in detail in B.1) the basic equations of hydrodynamics are rewritten as

$$\frac{1}{\rho}\frac{dP}{dr} + \frac{d\Phi}{dr} = 0 \tag{B.13}$$

$$\frac{1}{r^2}\frac{d}{dr}\left(r^2\frac{d\Phi}{dr}\right) = 4\pi\,G\rho \tag{B.14}$$

$$\varepsilon - \frac{1}{\rho r^2}\frac{d}{dr}\left(r^2 F\right) = 0 \tag{B.15}$$

$$F = -\frac{4\,a\,c\,T^3}{3\,\kappa\,\rho}\frac{dT}{dr} \quad \text{(radiative zone)} \tag{B.16}$$

In the Eq. B.16 the energy transport is considered only by radiation. When convection is present, the convective flux must be included.

Let M_r be the mass of the sphere of radius r and L_r its luminosity, i.e.:

$$M_r = \int_0^r 4\,\pi\,r^2\,\rho dr \tag{B.17}$$

$$L_r = 4\,\pi\,r^2\,F \tag{B.18}$$

Then, the equations presented above take their standard form of equations of stellar structure:

$$\frac{dP}{dr} = -\rho g, \quad \text{where} \quad g = \frac{GM_r}{r^2} \tag{B.19}$$

$$\frac{dM_r}{dr} = 4\pi r^2 \rho \tag{B.20}$$

$$\frac{dL_r}{dr} = 4\pi r^2 \rho\, \varepsilon \tag{B.21}$$

$$\frac{dT}{dr} = -\frac{3\kappa\rho}{4\,a\,c_*}\frac{1}{T^3}\frac{L_r}{4\,\pi r^2} \quad \text{(radiative zone)} \tag{B.22}$$

In some evolution phases, the models are not in thermal equilibrium and there is a term involving the derivative of the entropy in the energy conservation equation. In what follows, we will not consider out-of-thermal-equilibrium models.

We must add the boundary conditions to these equations, but we will not go into details in these matters. A more detailed description on equilibrium configurations, can be found on the book by Kippenhahn and Weigert (1990).

The convective zones of the star are delimited through the Schwarzschild criterion used by Ledoux and Walraven (1958) to denote the degree of convective instability ($A > 0$) or stability ($A < 0$), and it is related to the Brunt-Väisälä frequency N by:

$$A := \frac{N^2}{g} = \frac{d\ln\rho}{dr} - \frac{1}{\Gamma_1}\frac{d\ln P}{dr} \tag{B.23}$$

where $g = (GM_r)/r^2$ and Γ_1 is one of the adiabatic coefficients, defined as:

$$\Gamma_1 := \left(\frac{\partial\ln P}{\partial\ln\rho}\right)_{\text{ad}} \quad \text{and} \quad \Gamma_3 - 1 := \left(\frac{\partial\ln \mathrm{T}}{\partial\ln\rho}\right)_{\text{ad}} \tag{B.24}$$

Moreover, the stellar parameters ρ, T, P, ... are obtained form the *mixing-length theory* (MLT) of convection. This is a local time-independent theory in which one assumes that the mean free path of a convective element, l, can be well described as

$$l = \alpha_{\text{MLT}}H_P = -\alpha_{\text{MLT}}\left(\frac{d\ln P}{dr}\right)^{-1} \tag{B.25}$$

where H_P is the pressure scale height and α_{MLT} is the mixing-length parameter, which is of order unity ($\alpha_{\text{MLT}} \sim 1.8$ for the Sun). The precise location of the transformation from a radiative to a convective region is very difficult to determine. The reason is that it depends on a poorly known phenomenon called

convective overshooting, which is a term to express that the convective cells do not stop abruptly once entering a radiative zone. Convective overshooting is usually parametrised by the so-called *overshooting parameter* α_{ov} defined as the fractional length, expressed in units of H_P, over which the convective cells still move while entering the radiative zone. Typical values for α_{ov} considered in stellar modelling range from 0.0 to 0.3. A very important subject of research in stellar structure is to find accurate observational constraints on this poorly known parameter.

B.4   Perturbation analysis

At each given time a pulsating star is not in equilibrium but the position, density, pressure and temperature of a mass element vary periodically around their equilibrium value. So, it is possible to write any variable X as the sum of its equilibrium or unperturbed value X_0 and a small perturbation δX, obtaining

$$X = X_0 + \delta X$$

Substituting these expressions into the hydrodynamical equations and keeping only terms up to first order in the perturbed quantities, one gets linear equations. These equations are much easier to study than the original equations, and their solutions are very useful approximations. This method makes it possible to study the stability of the stellar models against sufficiently small perturbations. It will not, however, give us any information on the stability against finite amplitude perturbations, or metastable states, on limited cycles close to unperturbed solutions. It will also not give us the pulsation amplitude of a variable star. If the unperturbed configuration is stationary, the coefficients of the linearised equations are time-independent. We can then write the general solution as a linear combination of simple solutions which depend exponentially on the time as e^{st} (s can be complex) and which are normal modes. In the case of a mechanical system with a finite number of degrees of freedom, there is also a finite number of normal modes. Here, we have an infinite number of degrees of freedom and there exists an infinite number of normal modes of oscillation (as in the case of a vibrating string). A given mode is stable if $\Re s < 0$, unstable if $\Re s > 0$. A stellar

configuration is stable if *all* its normal modes are stable, but it is unstable as soon as *one* mode is unstable. In the exceptional case where the stability of one or several modes is marginal ($\Re s = 0$), the other modes being stable, the linear analysis does not give the information on whether the considered model is stable or not.

B.4.1   Lagrangian and Eulerian perturbations

To the two formalisms of hydrodynamics correspond two types of perturbations. For a physical quantity X whit an equilibrium value is X_0, the Lagrangian perturbation δX is described by

$$X(\vec{a}, t) = X_0(\vec{a}, t) + \delta X(\vec{a}, t)$$

and the Eulerian perturbation X' described by

$$X(\vec{r}, t) = X_0(\vec{r}, t) + X'(\vec{r}, t)$$

The relation between the Lagrangian and the Eulerian perturbations of the quantity X is given by

$$\delta X = X' + \delta r \cdot \nabla X_0$$

Since the perturbed variable X does not enter into the perturbation equations, but only the quantities X_0, δX and X', it is convenient to omit the subscript "'0'" in the perturbed value of the variable. In that case, the above relation will then be rewritten as

$$\delta X = X' + \delta r \cdot \nabla X \tag{B.26}$$

B.4.2   Perturbation of the differential equations

Before perturbing the hydrodynamic equations, we define the velocity vector,$\vec{v}$, as the derivative of the vector $\vec{r}$:

$$\vec{v} := \frac{d\vec{r}}{dt} \tag{B.27}$$

Thus, the perturbation of $\vec{v}$ results:

$$\partial\vec{v} = \frac{\partial\delta\vec{r}}{\partial t} \quad \text{and} \quad \vec{v}' = \frac{d\delta\vec{r}}{dt} \tag{B.28}$$

In the case of a star without rotation and convection this velocity will be the only velocity field, and we define it as $\delta\vec{v} = \vec{v}' = \vec{v}$, if it do not drive us to confusion. Then, taking into account only terms of first order in the basic equations of hydrodynamics given in the previous Section, we obtain:

Continuity equation:

$$\delta\rho + \rho \cdot \nabla\delta\vec{r} = 0 \quad \text{or} \quad \rho' + \nabla \cdot (\rho\,\delta\vec{r}) = 0 \tag{B.29}$$

Momentum equation:

$$\rho\frac{\partial\vec{v}}{\partial t} + \nabla P' + \rho\nabla\Phi' + \rho'\nabla\Phi = 0 \tag{B.30}$$

Poisson equation:

$$\triangle\Phi' = 4\,\pi\,G\,\rho' \tag{B.31}$$

Energy conservation equation:

$$\rho\,T\,\frac{\partial\delta S}{\partial t} = \left(\rho\,\varepsilon - \nabla \cdot \vec{F}\right)' \tag{B.32}$$

Radiative transfer equation:

$$\vec{F}' = -K'\,\nabla T - K\,\nabla T' \tag{B.33}$$

The system of equations has to be closed by adding the perturbed versions of the chosen boundary conditions, which we do not outline here for brevity. These five equations are partial derivative equations that depend on time t and $\vec{r}$ in the perturbation variables and $\vec{v}$. The coefficients of the perturbation variables of the equilibrium depend only on the radial coordinate r.

For thus, we can separate the time dependence part of the equations from the rest and write this part in the form $e^{i\,\nu_k\,t}$, where ν_k depends on each particular solution. Then, the general solution for each variable $\vec{X}$ of the lineal system will result in the form:

$$\vec{X}(\vec{r}, t) = \Re\left\{ \sum_{k=0}^{\infty} A_k \vec{X}_k(\vec{r})\, e^{i\,\nu_k\,t} \right\} \tag{B.34}$$

Taking this into account and considering $\vec{v} = i\,\nu\,\delta\vec{r}$, the Eqs. B.30 and B.32 can be written as

$$-\nu^2 \delta\vec{r} + \frac{1}{\rho}\nabla P' + \nabla\Phi' + \frac{\rho'}{\rho}\nabla\Phi = 0 \tag{B.35}$$

$$i\,\nu\,\rho\,T\,\delta S = (\rho\varepsilon)' - \nabla\cdot\vec{F}' \tag{B.36}$$

B.5   Equations for non-radial oscillations

Now its time to use the polar spherical coordinates described in Section B.1, because in the equilibrium state the star is assumed to be in spherical symmetry. We consider the displacement vector as

$$\delta\vec{r} = \xi_r \vec{e_r} + \xi_\theta \vec{e_\theta} + \xi_\varphi \vec{e_\varphi} \tag{B.37}$$

The horizontal component of the vector comes from Eq. B.1 and it is defined as $\xi_\perp := (0, \xi_\theta, \xi_\varphi)$.

Then, the perturbed hydrodynamic equations are rewritten as follows

Components of the momentum equation:

$$-\nu^2\xi_r + \frac{1}{\rho}\frac{\partial P'}{\partial r} - \nu^2\xi_\perp + \nabla_\perp\left(\frac{P'}{\rho} + \Phi'\right) + \frac{\partial \Phi'}{\partial r} + \frac{\rho'}{\rho}\frac{d\Phi}{dr} = 0 \qquad \text{(B.38)}$$

Separating the radial and the angular components, we have:

$$-\nu^2\xi_r + \frac{1}{\rho}\frac{\partial P'}{\partial r} + \frac{\partial \Phi'}{\partial r} + \frac{\rho'}{\rho}\frac{d\Phi}{dr} = 0 \qquad \text{(B.39)}$$

$$-\nu^2\xi_\perp + \nabla_\perp\left(\frac{P'}{\rho} + \Phi'\right) = 0 \qquad \text{(B.40)}$$

Continuity equation:

$$\frac{\delta\rho}{\rho} + \frac{1}{r^2}\frac{\partial r^2\xi_r}{\partial r} + \nabla_\perp \cdot \xi_\perp = 0 \qquad \text{(B.41)}$$

Using the Eq. B.40 we obtain

$$\frac{\delta\rho}{\rho} + \frac{1}{r^2}\frac{\partial r^2\xi_r}{\partial r} + \frac{1}{\nu^2}\nabla_\perp^2\left(\frac{P'}{\rho} + \Phi'\right) = 0 \qquad \text{(B.42)}$$

where

$$\nabla_\perp^2 = \frac{1}{r^2}\frac{1}{\sin^2\theta}\left[\sin\theta\frac{\partial}{\partial\theta}\left(\sin\theta\frac{\partial}{\partial\theta}\right) + \frac{\partial^2}{\partial\varphi^2}\right] \qquad \text{(B.43)}$$

Poisson equation:

$$\frac{1}{r^2}\frac{\partial}{\partial r}\left(r^2\frac{\partial\Phi'}{\partial r}\right) + \nabla_\perp^2\Phi' = 4\pi G\rho' \qquad \text{(B.44)}$$

Energy conservation:

$$i\nu\rho T\,\delta S = (\rho\varepsilon)' - \frac{1}{r^2}\frac{\partial r^2 F'_r}{\partial r} + \nabla_\perp^2(KT') \qquad \text{(B.45)}$$

Components of the transport equation:

$$F'_r = -K'\frac{\partial T}{\partial r} - K\frac{\partial T'}{\partial r} \qquad \text{(B.46)}$$

$$F'_\perp = -K\nabla_\perp T' \qquad \text{(B.47)}$$

Using some thermodynamic relations the number of variables of the system can be reduced, in our case we are not going to describe this process. After some manipulations, the non-adiabatic system of lineal equations can be written as follows:

$$
\begin{cases}
\frac{1}{\rho'}\frac{dP'}{dr} + \frac{g}{\rho c^2}P' + (N^2 - \nu^2)\xi_r + \frac{d\Phi'}{dr} = g\nabla_{\mathrm{ad}}\frac{T\rho}{P}\delta S \\[2ex]
\frac{1}{r^2}\frac{dr^2\xi_r}{dr} + \frac{1}{\Gamma_1}\frac{d\ln P}{dr}\xi_r + \left(1 - \frac{L_\ell^2}{\nu^2}\right)\frac{P'}{\rho c^2} - \frac{\ell(\ell+1)}{\nu^2 r^2}\Phi' = \nabla_{\mathrm{ad}}\frac{\rho T}{P}\delta S \\[2ex]
\frac{1}{r^2}\frac{d}{dr}\left(r^2\frac{d\Phi'}{dr}\right) - \frac{\ell(\ell+1)}{r^2}\Phi' - 4\pi G\rho\left(\frac{P'}{\rho c^2} + \frac{N^2}{g}\xi_r\right) = -4\pi G\nabla_{\mathrm{ad}}\frac{\rho^2 T}{P}\delta S \\[2ex]
K\frac{dT'}{dr} = -F_r' - K\frac{dT}{dr} \\[2ex]
(\rho\varepsilon)' - \frac{1}{r}\frac{dr^2 F_r'}{dr} - \frac{\ell(\ell+1)}{r^2}KT' = i\nu\rho T\delta S
\end{cases}
\tag{B.48}
$$

where the parameter L_ℓ is the Lamb frequency defined as

$$
L_\ell^2 := \frac{\ell(\ell+1)c^2}{r^2}
\tag{B.49}
$$

being c the speed of sound. Moreover, the adiabatic gradient of temperature ∇_{ad} and the coefficient Γ_1 are defined as

$$
\nabla_{\mathrm{ad}} = \left(\frac{\partial\ln T}{\partial\ln P}\right)_S \quad \text{and} \quad \Gamma_1 = \left(\frac{\partial\ln P}{\partial\ln\rho}\right)_S
\tag{B.50}
$$

As we can see, we have reduced the lineal problem to a set of differential equations in one coordinate r. As we can observe, this set of equations does not depend on the value m, it means that each solution has a $(2\ell+1)$-degeneration in m. This fact is due to the absence of magnetic fields or rotation in the model as we are assuming spherical symmetry. It is possible to show the existence of this degeneracy through theory of groups (Perdang 1968).

B.6 The adiabatic and Cowling approximations

B.6.1 The adiabatic case

In the adiabatic case we take into account the fact that the characteristic timescale for energy transfer in a star is much larger than the characteristic dynamical timescale (except in the external layers of the star). It is therefore natural, as a first approximation, to neglect transport phenomena and energy production for perturbations which evolve on a dynamical timescale. The energy conservation equation then becomes

$$\delta S = 0 \tag{B.51}$$

This equation describes an adiabatic perturbation.

Using this approximation, in the system of Eqs. B.48 the mechanic equations are decoupled from the thermic ones. Then, we obtain a three-equation system to resolve the pulsations in a star:

$$
\begin{cases}
\frac{1}{r^2}\frac{d}{dr}\left(r^2 g\right) - \frac{g}{c^2}\xi_r + \left(1 - \frac{L_\ell^2}{\nu^2}\right)\frac{P'}{\rho c^2} &= \frac{\ell(\ell+1)}{\nu^2 r^2}\Phi' \\[2ex]
\frac{1}{\rho}\frac{dP'}{dr} + \frac{g}{\rho c^2}P' + (N^2 - \nu^2)\xi_r &= -\frac{d\Phi'}{dr} \\[2ex]
\frac{1}{r^2}\frac{d}{dr}\left(r^2 \frac{d\Phi'}{dr}\right) - \frac{\ell(\ell+1)}{r^2}\Phi' &= 4\pi G \rho \left(\frac{P'}{\rho c^2} + \frac{N^2}{g}\xi_r\right)
\end{cases}
\tag{B.52}
$$

In this approximation the thermodynamic equations can be simplified as

$$\delta\rho = \frac{\delta P}{c^2} \quad \text{or} \quad \frac{\delta T}{T} = (\Gamma_3 - 1)\frac{\delta\rho}{\rho} \tag{B.53}$$

where c the sound speed. Thus, the variables to solve the system are reduced to four: ξ_r, P', Φ' and $\frac{d\Phi'}{dr}$.

We still have to specify the boundary conditions which must be satisfied by the solutions of this system. At $r = 0$ some coefficients of the differential system are singular. We impose to the solutions to remain regular at that point. So two

of the conditions to have regular solutions in $r = 0$ are that $\xi_r \sim r^{\ell-1}$, whereas $P' \sim r^\ell$ and $\Phi' \sim r^\ell$. In the special case of radial oscillation we impose $\xi_r \sim r$. Moreover, on the stellar surface we demand continuity for Φ' an its derivative at the surface radius $r = R$ and we impose $\delta P = 0$. For more details see the Section 18.1 in Unno et al. (1989) and Section 17.6 in Cox (1980).

B.6.2   The Cowling approximation

The approximation introduced by Cowling (1941) is very useful because, together with the adiabatic case, introduces a significant simplification in the system of pulsation Eqs. B.48. This approximation consists of neglecting the Eulerian perturbation of the gravitational potential, i.e. $\Phi' = 0$. This approximation is specially true for the high order modes (n or ℓ high).

Considering the Cowling approximation ($\Phi' = 0$), the system of Eqs. B.52 presented in the adiabatic case is simplified to the following system formed by two differential equations with two unknowns:

$$\begin{cases} \frac{1}{r^2}\frac{dr^2\xi_r}{dr} - \frac{g}{c^2}\xi_r + \left(1 - \frac{L_\ell^2}{c^2}\right)\frac{P'}{\rho c^2} &= 0 \\[3mm] \frac{1}{\rho}\frac{dP'}{dr} + \frac{g}{\rho c^2}P' + (N^2 - \nu^2)\xi_r &= 0 \end{cases} \tag{B.54}$$

We can make the following change of variables

$$\begin{aligned} a(r) &= r^2\xi_r e^{-\int_0^r \frac{g}{c^2}dr} \\[3mm] b(r) &= \frac{P'}{\rho}e^{-\int_0^r \frac{N^2}{g}dr} = \nu^2\, r\, |\xi_r|\, e^{-\int_0^r \frac{N^2}{g}dr} \end{aligned} \tag{B.55}$$

Applying this change of variables at the system B.54 we obtain

$$\begin{cases} \frac{da}{dr} &= h(r)\frac{r^2}{c^2}\left(\frac{L_\ell^2}{\nu^2} - 1\right)b \\[3mm] \frac{db}{dr} &= \frac{1}{r^2 h(r)}(\nu^2 - N^2)a \end{cases} \tag{B.56}$$

where

$$h(r) = e^{\int_0^r \left(\frac{N^2}{g} - \frac{g}{c^2} \right) dr} \tag{B.57}$$

B.7 Pressure and gravity modes

The differential system describing the non-radial oscillations of a star can only be solved analytically in the very unrealistic case of a homogeneous model. This case will nevertheless reveal the different types of non-radial modes, as seen in Fig. B.2.
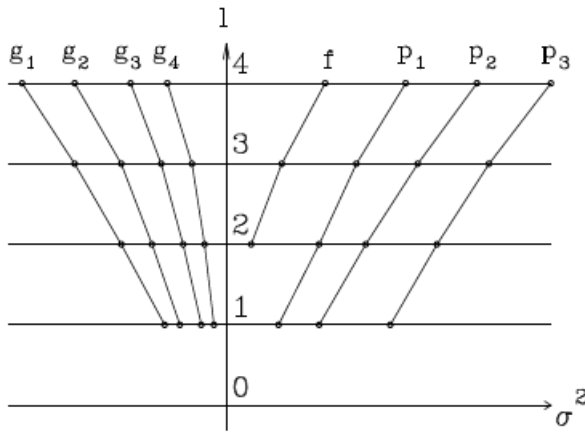
Figure B.2: *Frequencies of non-radial modes of the homogeneous model. The value σ^2 means the same as ν^2. Figure taken from Scuflaire and Thoul (2002).*

For each couple of indices (ℓ, m), the differential system describing the non-radial oscillations of a star (assuming adiabatic and Cowling approximations) transforms into a Sturm-Liouville problem taking appropriate boundary conditions. In this case, for modes with high frequencies ν, the term L_ℓ^2/ν^2 can be neglected. With this simplification we obtain a Sturm-Liouville problem with infinitely countable number of increasing eigenvalues $\nu^2 \to \infty$. These modes are named *pressure modes*. On the other hand, for very low frequencies, $N^2 - \nu^2 \approx N^2$.

This time the Sturm-Liouville problem has decreasing eigenvalues $\nu^2 \to 0$. These modes are called *gravity modes*. Finally, when $\ell > 1$, there is a stable mode, whose frequency is lower than those of the p-modes. It is called the *fundamental mode* or f-mode.

For more realistic models, the differential system is too complicated and cannot be solved analytically. Numerous numerical integrations show that the non-radial modes of physically realistic models can be classified as those of the homogeneous model. The result is exactly the same if the model is entirely convective. If the model is entirely radiative, the g-modes are stable. Their frequencies are lower than the f-mode and p-modes frequencies and have an accumulation point at 0. If the model has both radiative and convective zones, there are two spectra of g-modes, one stable (those with real values for ν, i.e. $\nu^2 > 0$) and the other unstable (those with imaginary values for ν, i.e. $\nu^2 < 0$), as shown in Fig. B.3. The stable modes are labelled g^+ and the unstable are labelled g^-.
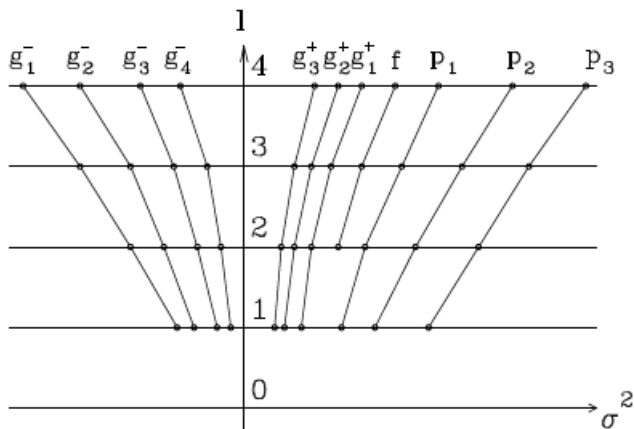
Figure B.3: *Frequencies of non-radial modes of a physical model. The value σ^2 means the same as ν^2. Figure taken from Scuflaire and Thoul (2002).*

The non-radial modes can be physically described as follows: The p-modes are acoustic modes. The g^--modes describe the convective instability. The g^+-modes are internal gravity waves. In very concentrated models, the low n order p-modes and g^+-modes can present a mixed character and behave as gravity waves in the

central regions of the star and as acoustic waves in the external layers. Usually, we restrict to the gravity modes that are dynamically stable, and the superscript "+" is dropped and one simply uses the term g-modes.

Thus, the frequency spectra in a real star is a combination of p-modes with high frequencies (low periods) and g-modes with low frequencies (high periods). When it is also present the f-mode with no nodes in the star. Each mode p_i or g_i is associated with an eigenfrequency ν_i. It means that for the mode p_i or g_i, the associated eigenfunction has i nodes in the interior of the star.

B.8   Physic nature of the oscillation modes

This study is carried out under the adiabatic and cowling approximation assumptions. The acoustic and gravity waves which are responsible for non-radial oscillations are propagative in the radial direction only in restricted regions depending on the properties of the waves. The global non-radial oscillations are standing waves which are formed by reflection of the waves at both sides of a propagative region. In other words, the oscillation are trapped in a propagative region. The trapping of oscillations is of fundamental importance in the theory on non-radial oscillations.

In the local treatment, we assume the coefficients of Eqs. B.54 to be constant. Then, the solutions will be functions like

$$a(r), b(r) \propto e^{i\, k_r\, r} \tag{B.58}$$

where

$$k_r^2 = \frac{(\nu^2 - L_\ell^2)(\nu^2 - N^2)}{\nu^2 c^2} \tag{B.59}$$

The Eq. B.59 is the dispersion relation, which relates the wave number k_r to the frequency. The appearance of the Brunt-Väisälä (N) and Lamb frequencies (L_ℓ) as critical frequencies should be noted.

1. If $\nu^2 > N^2, L_\ell^2$ or $\nu^2 < N^2, L_\ell^2 \implies k_r \in \mathbb{R}$ and we obtain a oscillatory solution, so the waves can propagate in radial directions.

2. If $N^2 > \nu^2 > L_\ell^2$ or $N^2 < \nu^2 < L_\ell^2 \implies i\, k_r \in \mathbb{R}$ and we obtain a exponential solution, that means that the amplitude of the solution changes exponentially in r. Thus, the acceptable solution, in a physic meaning, represents a dumped oscillation travelling through the interior of a surface of radius r (*evanescence zone E*) and another reflected to the exterior.

3. If $N^2 < \nu^2 < 0$. This situation is only possible in unstable dynamical zones of convection. This case is possible because $N^2 < 0$ in convective zones. The study of this case is out of the aims of this work.

So, it is clear that the Brunt-Väisälä (N) and Lamb frequencies (L_ℓ) delimit the different propagation zones of the waves in a star. The points with $k_r^2 = 0$ are called return points. Then, it is said that the modes are trapped in this propagating oscillatory zones (propagating zones). We now introduce the horizontal number k_h by

$$k_h^2 = \frac{L_\ell^2}{c^2} \tag{B.60}$$

The dispersion Eq. B.59 is then rewritten as

$$\nu^4 - (N^2 + k^2 c^2)\nu^2 + N^2 k_h^2 c^2 = 0 \tag{B.61}$$

with $k^2 = k_r^2 + k_h^2$.

Then, we have two possibilities:

1. $\nu^2 > N^2, L_\ell^2$. For simplicity we study the limit case $\nu^2 >> N^2, L_\ell^2$. In this case

$$k^2 = \frac{\nu^2}{c^2} \tag{B.62}$$

this relation is that one characterising an acoustic wave, being the sound speed which characterises this dynamical propagation. For thus, in this region, the pressure is the main restoring force and we denote this zone as *Pressure zone* (P). The stable modes trapped in the P zone will be called *p*-modes, pressure modes.

2. $\nu^2 < N^2, L_\ell^2$. Assuming simplifications similar to the previous case we derive that

$$k^2 = \frac{N^2 k_h^2}{\nu^2} \qquad (\text{B.63})$$

in which the Brunt-Väisälä frequency is the responsible of dynamic propagation. The restoring force associated to the Brunt-Väisälä frequency is due to the density differences in the neighbourhood of displacement of a fluid element under the action of gravity. This force is also known as buoyancy. Therefore, the propagation zone where the buoyancy is the restoring force is called *Gravity zone* (G), and thus, the stable trapped modes in the G zone are called *g*-modes, gravity modes.

B.8.1 Propagation diagram of the modes

As described above, the *p*-modes and *g*-modes have an oscillatory behaviour only in the so-called *trapping regions* or *mode cavities*. Outside of these regions they decrease exponentially. The localisation of the cavities depends on the frequency of the mode and so is different for different modes. For *p*-modes, an oscillatory motion occurs for $\nu^2 > N^2, L_\ell^2$. This denotes the *p*-mode cavity. The *g*-modes (in fact g^+-modes), on the other hand, are trapped whenever $0 < \nu^2 < N^2, L_\ell^2$. These *g*-mode cavities are situated much deeper in the star than the *p*-mode cavities. We show the *p*-mode and *g*-mode cavities for a real stellar model computed by A. Claret in Fig. 1.5.

In order to visualise the condition of wave trapping in realistic stellar models, a diagram in which L_ℓ^2 and N^2 are plotted as function of the radial coordinate r should be instructive. This diagram is called a *propagation diagram*. Let be ω^2 denote the square of the dimensionless frequency, i.e.

$$\omega^2 = \frac{\nu^2 R^3}{GM} \qquad (\text{B.64})$$

with G the gravitational constant, M the stellar mass, R the stellar radius and ν the pulsational frequency. In Fig. 1.5 we display the propagation diagram of a stellar model of $1.8 M_\odot$. In this figure, the horizontal lines indicate that the

oscillation frequencies of several modes, and the dotes on the lines indicate the nodes of the eigenfunctions $\xi_r(r)$ of each mode. The nodes for the p-modes and g-modes appear, respectively, in the P and G propagative zones. This figure clearly shows that p-modes and g-modes are trapped in the P zone and the G zone, respectively. We finally mention that, during the course of the evolution of a star, its modes may become of *mixed nature*, i.e. an oscillatory behaviour in an inner g-mode cavity but in an outer p-mode cavity. In such a case the p-mode and g-mode cavities are situated much closer to each other than in Fig. 1.5.

B.9   Non-adiabatic asteroseismology

In this brief notes, we only describe the dynamically stable adiabatic oscillations in non-rotating and non-magnetic spherical star, that are strictly periodic. In mathematical terms, the eigenfunctions and eigenvalues are purely real. Oscillations in nature are, however, inevitably non-adiabatic. It means that the energy exchange among mass elements occurs during oscillations and governs the vibrational stability (amplitude growth or decay) of the star. This corresponds to the fact that the eigenfunctions and eigenfrequencies are complex (non-real) in the mathematical description of linear non-adiabatic oscillations. In Dupret (2001) and Dupret et al. (2002) can be found a detailed treatment of the outer boundary conditions in the non-radial adiabatic case and a detailed treatment of the pulsation in the very external layers of the star. The non-adiabatic case is no described in this brief Appendix.

B.10   Computing oscillations in stars

There are different tools to compute and model the non-radial pulsations observed in stars. These tools include codes to calculate the non-adiabatic observables needed for instability analysis. The observables are then used for mode identification within the framework of multicolour photometry. In this Section we want to describe briefly the oscillation codes used during the stay in the Instituto de

Astrofísica de Andalucía (IAA-CSIC) at Granada.

1. The evolutionary code CESAM (Code d'Evolution Stellaire Adaptatif et Modulaire, Morel 1997; Morel and Lebreton 2008) computes the stellar models[1].

2. The GRAnada oscillation Code (GRACO) described in Moya et al. (2004) and Moya and Garrido (2008) provides diagnostics on the instability and non-adiabatic observables required for fitting the multicolour photometric observations. In this code the non-adiabatic pulsation equations are solved mainly following Unno et al. (1989), including the non-adiabatic pulsation treatment of the atmosphere proposed by Dupret et al. (2002). Although including this atmosphere-pulsation interaction does not have any significant influence on the modal stability, it does allow theoretical predictions to be compared with photometric colour observations (see Moya et al. 2004, for more details). The atmospheres were reconstructed at specific Rosseland optical depths ($\tau = 1$) until the last photospheric edge of the star was reached.

3. For rotating adiabatic oscillations computations, the oscillation code FILOU (Tran Minh and Léon 1995; Suárez 2002) provides adiabatic oscillation modes corrected for the effects of rotation up to second order (centrifugal and Coriolis forces), including second order effects of near degeneracy that are expected to be significant for moderately high rotational velocities Soufi et al. (1998). See also Suárez et al. (2006) for recent details about FILOU. Indeed, two or more modes, close in frequency, are rendered *degenerate* by rotation under certain conditions, corresponding to selection rules. In particular, these rules select modes with the same azimuthal order m and degrees ℓ differing by 0 or 2 (Soufi et al. 1998). If we consider two generic modes $\alpha_1 \equiv (n, \ell, m)$ and $\alpha_2 \equiv (n', \ell', m')$ under these conditions, near degeneracy occurs for $|\nu_{\alpha_1} - \nu_{\alpha_2}| \leq \nu_\Omega$, where ν_{α_1} and ν_{α_2} represent the eigenfrequency associated to modes α_1 and α_2, respectively, and ν_Ω represents the stellar rotational frequency (see Goupil et al. 2000, for more details).

---

[1] Available at http://www.oca.eu/cesam/.

Child-like, no-one understands,
Jack-knife in your sweaty hands.
Some kind of innocence is measured out in years,
You don't know what it's like to listen to your fears.

John Lennon

C
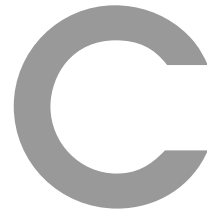
User Guide: PASPER - version 2.25

Code author: Pascual David Diago Nebot[1], February 2010.

C.1   Use Policy

You have permission to use this software freely, but:

1. The author of this code has to be informed of any use or modification of the original package provided.

---

[1]e-mail: Pascual.Diago@uv.es

2. The author of this software has to be a co-author of every publication in which this code has been used.

3. This code cannot be transferred to a third party without the permission of the author.

4. Cite the PASPER code as: "... the frequency analysis was performed with PASPER (Diago et al. 2008a) ...", with the reference:
   Diago, P. D., Gutiérrez-Soto, J., Fabregat, J., and Martayan, C.: 2008, A&A 480, 179

   Cite the PASPER code in LaTeX as: "... the frequency analysis was performed with \textsc{pasper} \citep[][]{2008A&A...480..179D} ...", with this Bibtex entry:

```
@ARTICLE{2008A&A...480..179D,
   author = {{Diago}, P.~D. and {Guti{\'e}rrez-Soto}, J. and
   {Fabregat}, J. and {Martayan}, C.},
    title = "{Pulsating B and Be stars in the Small Magellanic
    Cloud}",
  journal = {\aap},
archivePrefix = "arXiv",
   eprint = {0709.4573},
 keywords = {stars: emission-line, Be, stars: oscillations,
 stars: early-type, stars: statistics, galaxies: Magellanic
 Clouds},
     year = 2008,
    month = mar,
   volume = 480,
    pages = {179-186},
      doi = {10.1051/0004-6361:20078754},
   adsurl = {http://adsabs.harvard.edu/abs/
   2008A%26A...480..179D},
   adsnote = {Provided by the SAO/NASA Astrophysics
   Data System}
}
```

C.2 Introduction

The PASPER code (Diago et al. 2008a) is a package of functions programmed in Python and developed for the astronomical time series analysis. The code uses standard Fourier analysis techniques and least-square fitting in a similar way to the software PERIOD04 (Lenz and Breger 2005). An important advantage of this code is the batch analysis mode, very useful for long sets of observations. This code has been developed by Diago in collaboration with Garrido and Gutiérrez-Soto.

PASPER acts as an interface between different routines written by other persons in different programming languages:

- `freq`, written by Garrido in FORTRAN77. This routine finds frequencies one by one computing the Fourier Transform (Lomb-Scargle periodogram) and then adjusting parameters of a sinusoidal function using least-square fitting.

- `prog_pol_mul_sigma`, written by Gutiérrez-Soto. This routine fits polynomial functions to the data.

- `binning_media_corot5`, written by Gutiérrez-Soto. This routine make new data using a binning function.

The main program in the package PASPER is `freqPy`. Although, you can perform many different actions with PASPER. For example, fit polynomial functions to your data, calculate the parameters (amplitude, phase and signal to noise) of a list of frequencies, plot periodograms, phases, light-curves, etc.

C.2.1 The `freqPy` routine

`freqPy` is a modification of the original program `freq` written by Garrido. It allows us to perform a Fourier analysis of a time series. Here goes a brief description of how `freqPy` carries with the data analysis:

Fourier analysis is applied to time series. The program finds frequencies one by one by computing the Fourier transform (Lomb-Scargle periodogram) and then adjusts parameters of a sinusoidal function using a least-square fitting (this two subroutines are based on the `FORTRAN77` routine `freq` written by Garrido). Then this frequency is removed (prewhitened) of the original data and a new step is started finding a new frequency. The subsequent least-square fitting is made allowing the two frequencies to move in order to get the minimum variance. The method is iterative ending when removing of a new frequency is not statistically significant (Breger et al. 1993).

Finally the program adjusts the amplitude, phase and S/N parameters to the list of frequencies obtained. This is made with least-square fitting again. In this stage we obtain the *frequency list* with the parameters, the *periodograms* for each frequency and we can do the different *phase plots* of each frequency in our analysis.

Note that `freqPy` calculates the periodograms with amplitude instead of power.

C.2.2 Some mathematics

Here go a brief descriptions of some terms we use in `freqPy` and `freqPyLSQ` functions:

Let be $X = [T_i, M_i]$ the light-curve that we are analysing, where T_i is the time column vector and M_i is the magnitude column vector for $i = 1, ..., N$. Being N the total observation samples and $[\nu_{ini}, \nu_{fin}]$ the frequency interval where we are searching for significant frequencies.

We define the *frequency accuracy* of a time sequence as:

$$\text{freq. accur.} :\sim \frac{1}{T_N - T_1}$$

We define the *number of steps of the periodogram* as:

$$N_{steps} := (\nu_N - \nu_1) \cdot resolution \cdot (T_N - T_1)$$

where the *resolution* means the number of points that we obtain for each peak of the periodogram in our DFT calculation. In PASPER the maximum number of steps in the DFT calculation is $N_{stepMAX} = 300\,000$.

Finally, we define the *step in the DFT* as:

$$dftstep := \frac{1}{resolution \cdot (T_N - T_1)}$$

C.2.3   Stop criterion

The method used by PASPER in order to determine whether the frequencies are statistically significant or not is the *signal-to-noise amplitude ratio requirement* described in Breger et al. (1993). This method basically consists in the calculation of the SNR of each peak in the periodogram. To calculate the SNR of each peak, the signal (S) is the amplitude of the peak for each frequency obtained. And the noise (N) is assumed to be the average amplitude in the residual periodogram after the *prewhitening* of all the frequencies detected. The interval of frequencies where it is calculated depend on the frequencies one is studying (in our case we are searching for frequencies between $\nu = 0$ and $\nu = 10$, and we use a 5 c/d frequency interval). Breger et al. (1993) shown that for a multi-site campaign a $S/N \geq 4$ might be a good criterion to distinguish between peaks due to real frequencies and noise. Note that the criterion is conservative, by using amplitudes rather than power (amplitude squared).

C.2.4   Error in the frequencies

We calculated the frequency resolution following the Rayleigh criterion, i.e., $1/T$, where T is the time duration of the light curve. However, Kallinger et al. (2008)

propose a less conservative criterion, based on Monte-Carlo simulations, by using $1/(4T)$.

For the error in the frequency, amplitude, and phase values, we use the analytic formula from Montgomery and O'Donogohue (1999). These errors are also calculated in the determination of amplitudes and phases by AMPHI. The correlations in the residuals of the fitting (Schwarzenberg-Czerny 1991) are taken into account by multiplying the errors by $\sqrt{D}$, where D is the number of consecutive datapoints that are correlated.

C.3   The pasper package

The folder `pasperVX.XX/` contains:

- `freq/` folder with the `FORTRAN77` routines written by Garrido.

- `plot/` folder with the `bash` routines to plot the data with `Gnuplot`.

- `doc/` folder with the User Guide of the version.

- The files with the `C` routines written Gutiérrez-Soto:

    - `pasper_fitpol`

    - `func_pol_mul.c`

    - `prog_pol_mul_sigma.c`

    - `prog_pol_mul_sigma` (the compiled program).

- `binning_media_corot5.f` file, the program to make a binning in the data.

- `pasper.py` file with the `Python` library.

- `pasperstartup.py` file, a script to start PASPER.

- `freqPy.input` file, a configuration file to run PASPER in batch-mode.

- `README.txt` file with the notes of the version.

C.4   Installing pasper

- **Previous software request (Linux systems):**

  1. `Python`

  2. `iPython`

  3. `Python` libraries: `Matplotlib`, `SciPy` and `NumPy`.

  4. A `FORTRAN77` and `C` compilers: `gFortran` and `gcc`.

  5. Common Linux programs: `awk` and `Gnuplot`

  6. The GSL libraries. Visit http://www.gnu.org/software/gsl/ and follow the installation steps.

  After installing all these software, please update the database of your system, with the command line:

  `> updatedb`

  Note for MAC OS users: these programs can be installed under `Fink` or `MacPorts` projects. Detailed instructions (in Spanish) for MAC OS users can be found in the `doc/` folder of the PASPER package.

- **Compiling the programs**

  1. `freq`: in the `freq/` folder, type:

     `> gfortran -o freqpasper freqNewPASPERV2.0-MUT.for`
     `mynv16nd.for`

  2. `binning`: in the `pasperVX.XX` folder, type:
     `> gfortran -o binning binning_media_corot5.f`

  3. `pasper_fitpol`: in the `pasperVX.XX` folder, type:
     `> gcc -o prog_pol_mul_sigma prog_pol_mul_sigma.c`
     `func_pol_mul.c -lgsl -lgslcblas -lm`

     Note for MAC OS users: `Fink` and `MacPorts` install the GNU utilities in the directories `/sw/` and `/opt/local/`, respectively. Therefore, we have to specify the correct path for the libraries. For a `MacPorts` installation we type:

```
> gcc -o prog_pol_mul_sigma prog_pol_mul_sigma.c
func_pol_mul.c -I/opt/local/include -L /opt/local/lib/
-lgsl -lgslcblas -lm
```

- **Changing the paths in** PASPER

  Using a text editor, open the files,

  1. `pasper.py`, and add your corresponding path for your PASPER version in `PATH`, in line 7, e.g.:

     `PATH = '/home/pasdiane/programas/pasperVX.XX/'`

  2. `pasperstartup.py`, and add your corresponding path for your PASPER version in `PATHPASPER`, in line 1, e.g.:

     `PATHPASPER = '/home/pasdiane/programas/pasperVX.XX'`

- **Changing the bashrc file:**

  We recommend to add the PASPER `PATH` to the `bashrc` file. This allows you to run the `pasper_fitpol` routine in any directory and the plot commands from the Linux shell. You can modify the `/etc/bashrc` (you need to be superuser), and automatically all users have the `PATH_PASPER` in they `PATHS`. If you are not the superuser of the system, you can modify your `/home/user/.bashrc` file. In both cases, add to the `bashrc` file the lines:

  `PATH_PASPER=/path_to_pasperVX.XX`

  `PATH_PASPER_PLOT=/path_to_pasperVX.XX/plot`

  `$PATH=$PATH:your_custom_paths:$PATH_PASPER:$PATH_PASPER_PLOT`

  `export PATH`

  Finally, add the alias in the `bashrc` file:

  `alias pasper='ipython -pylab -i $PATH_PASPER/pasperstartup.py'`

  `alias pasper_batch='python $PATH_PASPER/pasper.py'`

  Remember to compile the `bashrc` file with:

  `> source /etc/bashrc` (as su and as normal user)

- **Plotting data**

  In the `pasperVX.XX/plot/` folder, open the `compos.awk` file and do the following:

– For Linux users, remove the first line: `#!/opt/local/bin/awk -f`.

– For MAC OS users, keep the first line: `#!/opt/local/bin/awk -f`.

Moreover, if you are a MAC OS user, you need to open the terminal preferences and uncheck the option `export LANG variable` in the advanced settings tab. The Unicode UTF-8 language has to be enabled.

C.5 Running pasper

You can run PASPER typing in the line command shell:

> `pasper`

Then, you will be launched to an `iPython` console, and you can launch any function from this command line.

WARNING!: PASPER uses temporal files with the "freq" extension. Be careful because any previous file with this extension on your working directory will be deleted.

To exit from the `iPython` console type `Ctr + D`.

PASPER can also run in a *batch-mode* directly from the line command shell, for do that, you have to edit the `freqPy.input` file and type the command:

> `pasper_batch`

See Section C.6 for more information.

C.6   Using pasper

From the `iPython` console you can launch any function of the PASPER package. In general, the usage is as follows:

>>> `pasper.function(params)`, or

>>> `function(params)`

For several functions you have to load the data previously in the `iPython` console:

>>> `your_variable = function_for_load_data('your_data_file')`

>>> `function(your_variable, other_parameters)`

In the other hand, other functions can be called indicating the name of the data file present in the current directory with the command:

>>> `function('your_data_file')`

To learn how to use each function see the Section C.7 or type in the shell the command:

>>> `help (function)`

C.6.1   Preparing your data to use it with pasper

Firstly, your data has to be in a two or three columns format, i.e.:

[TIME, MAG] or [TIME, MAG, ERR_MAG]

Be sure that no one of your files in the working directory is named with the

"freq" extension.

C.6.2   Handling your data in pasper

For some functions explained in this Section you have to load previously the light-curve data in a variable with the command:

```
>>> variable = cargar('your_data')
```

Some other functions work without loading the data files. See Section C.7 for a complete explanation of each function.

The PASPER package allows you to perform different actions:

- Make a binning in the data with the `pasper_bin` function in the command line shell.

- De-trend a polynomial function of the data with the function `fitpol` from the `iPython` console, or directly from the command line shell with the command `pasper_fitpol`.

- See the statistics of a file with the `stats` function.

- Perform a σ-clipping to the data use the `sigmaclip` function.

- Delete data points in two different ways:

  - Delete the points with magnitude greater/lower than an specific value (with `quitarmaggt` and `quitarmaglt`).

  - Delete the points with time values greater/lower than an specific one (with `quitartimegt` and `quitartimelt`.)

- We use in the DFT calculations the term *resolution* in spite of the *DFT step in frequencies*. But we have added to PASPER some functions to convert the DFT step into resolution and viceversa (`dftstep2res` and `res2dftstep`). Moreover, you can obtain the maximum value for the DFT resolution of a

light-curve with `resolucion` or the equivalently, the minimum step in the DFT calculation with `dftstep`.

Remember that in PASPER the maximum number of steps in the DFT calculation is $N_{stepMAX} = 300\,000$.

If you have modified your original data, you have to save this data before performing the frequency analysis with `freqPy`. For this, you can use `guardar` routine.

C.6.3 Plotting your data in pasper

In PASPER you have different plotting commands to use with your data:

- Functions to plot non-loaded files. From the `iPython` shell, you can tip:
  - `ver` and `vererror` can show you the light-curve shape without or with errorbars.
  - `fase` is used when you have a residuals file (from `freqPy`) and you want to see a phase diagram.
  - `window` is used when you have a window file (from `freqPy`) and you want to see it.
  - `periodograma` is used when you have a DFT file (from `freqPy`) and you want to see the periodogram for different frequencies. It allows you to save an eps figure or a zoom in the values needed.
  - `peaks` is used to plot the frequency values versus their amplitudes in an impulse diagram.

  Type the name of the function in the shell to see the help manual.

- Functions to plot loaded files: The `plot` function is used when you have a variable in `iPython` an you want to plot one column versus another column.

- Functions to plot loaded or non-loaded files: The function `histo` plot an histogram of the second column of the data (usually the magnitude).

Moreover, you can use the plotting functions located in the folder `plot/` in any directory on the command-line shell, because during the installation we have add the `PATH_PASPER_PLOT` variable to the `PATH`. This functions allow you to save all figures in *eps* format. See the usage of this functions typing the name of the function in the command-line shell.

C.6.4   Performing a frequency analysis with freqPy

To perform the frequency analysis, you have to run `freqPy` in the PASPER console. It only needs the file name of the data you want to analyse. For example if you want to analyse the file `my\_data.txt`, you do not have to load it, you only have to type:

```
>>> freqPy('my_data.txt')
```

Then, the program will begins and will ask you for other parameters:

- Frequency range: you have to put integer numbers, with 0 as initial frequency.

- Resolution: it means the number of points that you will got for each lobe in the DFT.

- Minimum value for the signal to noise. The criterion used by `freqPy` has been explained above in the text.

When the `freqPy` function ends, it will create different files:

- A `.log` file with the results of the analysis (frequency, amplitude, phase and signal to noise).

- A `.dft` file with the first column being the different frequency steps and the i column being the amplitude of the periodogram for the $i - 1$ frequency ($i \geq 2$). (Remember that this program uses amplitude and not power).

- A `.res` file with the first column being the original time column, and the i column the residuals after the least-squares fitting fitting for the $i-1$ frequencies ($i \geq 2$).

- A `.raf` file. It is a one column file that contains the residual after every fit. The first row is the residuals of the originals, and the i row is the residuals after the least-squares fitting of the $i-1$ frequencies ($i \geq 2$).

- `.win` file with the spectral window of the data that you are analysing.

- `.num` file to take it as input for the program NUMEROLOGY (only available for the CoRoT Be Team).

After the frequency analysis, you can plot the different results obtained (periodograms, phases, spectral window, etc.) or you can run NUMEROLOGY.

In `freqPy`, the following parameters are fixed:

- File type, set in two columns file $[TIME, MAG]$.

- Number of harmonics, fixed in 1.

- Artificial mean, set in the value 0.

If you want to perform a frequency analysis changing this values, you can run `freqPyPRO`, typing:

```
>>> freqPyPRO('my_data.txt')
```

And the function will ask you for:

- File type: 2 or 5 columns.

- Number of harmonics you want to use in the calculation (1 to 4).

- Artificial mean: it is the value for the DFT that you want in the frequency $\nu = 0$. By default you have to assign 0.

- Frequency range: you have to put integer numbers, with 0 as initial frequency.

- Resolution: it means the number of points that you will got for each lobe in the DFT.

- Minimum value for the signal to noise. The criterion used by `freqPy` has been explained above in the text.

C.6.5 `freqPy` with a configuration file

If you want to use the same parameters for all light-curves in your analysis, you can create a `freqPy.input` file in your working directory, with each row being:

1. File extension, for example: `.dat` or `.txt`

2. Initial frequency: necessary 0

3. Final frequency: (integer number)

4. Resolution.

5. Minimum value for S/N.

You have an example file in the `pasperVX.XX/` folder. Then, you have to run the command:

```
>>> freqPyMUT('my_data')
```

The `freqPyMUT` routine creates the same outputs as the `freqPy` routine.

C.6.6 `freqPy` in batch-mode

If you have many light-curves to analyse and the `freqPy` parameters are the same for all data files, you can run `freqPy` in batch-mode directly from the command-

line console. For this, create the configuration file `freqPy.input` as explained in Section C.6.5, and run in your working directory:

```
> pasper_batch
```

The batch-mode can also run in the `iPython` console with the command:

```
>>> freqPyBATCH()
```

When you run PASPER in batch-mode, you obtain for all light-curves the `.log`, `.win`, `.res`, `.raf`, `.dft` and `.num` files plus a `freqPy.batch` file with the information of the batch-mode analysis.

C.6.7 Adjusting amplitude, phase and S/N to the detected frequencies with `freqPyLSQ`

If you have a list of frequencies and you want to calculate the amplitude, phase and signal to noise, you can use the `freqPyLSQ` routine typing:

```
>>> freqPyLSQ('freqs_file', 'your_data_file')
```

The program will ask you for the frequency range and the resolution used in the frequency determination. At the end, it will create a `.log` file with the parameters of the fitting and a `.num` file for use it in NUMEROLOGY.

You can run `freqPyLSQ` in batch mode modifying the file `pasper.py`. For this, you have to open with a text editor the `pasper.py` file and uncomment the `freqPyLSQBATCH()` and comment the `freqPyBATCH()` row in the last rows of the file:

```
if __name__ == "__main__":
print '\t\tRunning in BATCH-MODE...\n'
print '----------------------------------\n'
```

```
# Uncomment the following row to use pasperbatch in freqPy MODE
freqPyBATCH()
# Uncomment the following row to use pasperbatch in freqPyLSQ MODE
#freqPyLSQBATCH()
```

C.7   Function documentation

Here we describe the different functions that can be executed with the PASPER
package. Note in the functions that when appears 'file' it means that the data
file has not to be loaded. And when appears data it means that the data file has
to be loaded previously.

cargar (*nom*)

```
Implementation of the load function for pasper. Loads ASCII files.
Usually: TIME, MAG, ERRMAG.
Usage:
>>> data = cargar('file')
```

dfstep2res (*data*, *dftstep*, *fini*, *ffin*)

```
Function to convert the DFT frequency step into resolution of the DFT.
Usage:
>>> res = dftstep2res(data, dftstep, freq_initial, freq_final)
>>> res = dftstep2res('file', dftstep, freq_initial, freq_final)
```

dftstep (*data*, *fini*, *ffin*)

```
Function to calculate the minimum step in the DFT calculation.
Usage:
```

```
>>> df = dftstep(data, freq_initial, freq_final)
>>> df = dftstep('file', freq_initial, freq_final)
```

dondeestafreq (*freq, fini, ffin, bin*)

```
Subfunction of SN.
Function to calculate the interval where a frequency is.
Usage:
>>> position = dondeestafreq(freq, freq_initial, freq_final, binning)
position is an integer
```

fase (*freq, numfreq, nom*)

```
Function to plot the magnitude with a frequency folding (phase) with Gnuplot.
Usage:
>>> fase(frequency, number_of_frequency, 'file')
Where number_of_frequency means if the frequency is the first (1), second (2),
etc... 'file' can be .dat or .res
The data is taken from the .res file given by freqPy.
```

fitpol (*nom, grado*)

```
Function to fit polynomial function to the data. It creates a .log file with the
information of the fitting and a _respol#.dat file with the residuals of the
fitting.
Usage:
>>> fitpol('file', degree)

Or directly from the command line shell:
> pasper_fitpol [file (ONLY 2 cols)] [Degree]
```

freqinterface (*caso*, *harms*, *nom*, *modo*, *mediaart*, *resol*, *fini*, *ffin*)

```
Interface (API) for call freq from Python in a semi-interactive mode.
```

freqparams (*caso*, *harms*, *nom*, *modo*, *mediaart*, *resol*, *fini*, *ffin*)

```
Function to generate the parameters file for use freqPy.
```

freqPy (*nom*)

```
Function to use the program FREQ.FOR (by Rafa Garrido) in a Python console.
We use here freqNewPASPER-MUT.for, a Freq.for version.
It uses 1 harmonic and artificial mean value = 0 in the calculation.
The data file has to be in 2 columns format: [TIME, MAG]
Inputs:
          - Filename of the data
          - Resolution
          - Initial Frequency
          - Final Frequency
          - Signal to noise criterion
Output:
          - List of significant frequencies
          - Log file with the frequencies, amplitudes, phases and Signals to noise
            obtained.
          - .win, .dft, .raf, .res, .num files (see description in the user guide).
Usage:
>>> freqPy('data_file')
```

freqPyBATCH ()

```
Function to launch freqPy in a BATCH-MODE. It calls the freqPyMUT routine for
different files in the current directory using a configuration file.
It uses 1 harmonic and artificial mean value = 0 in the calculation.
The data file has to be in 2 columns format: [TIME, MAG]
```

```
Configuration file: 'freqPy.input' with the parameters:
                - File extension of the file to analyze: (.txt or .dat or ...)
                - Initial frequency: (Obligatory 0)
                - Final frequency: (integer)
                - Resolution: (run previously freqPy or resolucion to check the
                  maximum)
                - Minimum value for the S/N: (default 4)
Outputs:
        - For each file:
                - Log file with the frequencies, amplitudes, phases and Signals
                  to noise obtained.
                - .win, .dft, .raf, .res, .num files.
        - 'freqPy.batch' file with information of the batch analysis.
Usage:
>>> freqPyBATCH
Edit previously the 'freqPy.input' file.

NOTE: pasper can run in BATCH-MODE without logging in an iPython shell.
For do that, type in the Linux shell (after editing the 'freqPy.input'
configuration file):
> pasper_batch
```

freqPyLSQ (*frecvect*, *nom*)

```
Function to calculate the parameters (amplitude, phase and Signal to noise) of
a frequency list given. It uses the freqPy routine.
You need to have the frequency list in a file in the same directory of the data.
It uses 1 harmonic and artificial mean value = 0 in the calculation.
The data file has to be in 2 columns format: [TIME, MAG]
Inputs:
        - Resolution
        - Initial Frequency
        - Final Frequency
Output:
        - Log file with the frequencies, amplitudes, phases and Signals to noise
          obtained with the LSQ routine.
        - .num file for Numerology program.
Usage:
>>> freqPyLSQ('frequencies_file', 'data_file')
```

freqPyMUT (*nom*)

```
Function to use freqPy in automatic mode using the configuration file
'freqPy.input' with the parameters of the analysis.
It uses 1 harmonic and artificial mean value = 0 in the calculation.
The data file has to be in 2 columns format: [TIME, MAG]
Inputs:
        - name of the file.
        - Configuration file: 'freqPy.input' with the parameters:
                - File extension of the file to analyze: (.txt or .dat or ...)
                - Initial frequency: (Obligatory 0)
                - Final frequency: (integer)
                - Resolution: (run previously freqPy or resolucion to check the
                  maximum value allowed).
                - Minimum value for the S/N: (default 4)
Output:
        - List of significant frequencies
        - Log file with the frequencies, amplitudes, phases and Signals to noise
          obtained.
        - .win, .dft, .raf, .res, .num files (see description in the user guide).
Usage:
>>> freqPyMUT('data_file')
Edit previously the 'freqPy.input' file.
```

freqPyPRO (*nom*)

```
Function to use the program FREQ.FOR (by Rafa Garrido) in a Python console.
We use here freqNewPASPER-MUT.for, a Freq.for version.
freqPyPRO allows you to configure all the parameters.
Inputs:
        - Filename of the data
        - Number of harmonics in the calculation.
        - Type of data.
        - Artificial Mean
        - Resolution
        - Initial Frequency
        - Final Frequency
        - Signal to noise criterion
Output:
        - List of significant frequencies
```

```
        - Log file with the frequencies, amplitudes, phases and Signals to noise
          obtained.
        - .win, .dft, .raf, .res, .num files (see description in the user guide).
Usage:
>>> freqPyPRO('data_file')
```

guardar (*nom*, *variable*)

```
Implementation of the save function for pasper. Saves variables to ASCII files.
Usage:
>>> guardar('file', data)
```

histo (*data*, *bins*)

```
Function to plot an histogram of the data. This function uses matplotlib.
Can be used with loaded data or with data files from the current directory.
Usage:
>>> histo(data, number_of_bins)
>>> histo('file', number_of_bins)
```

noext (*nom*, *num*)

```
Function to delete the extension from a given file.
Usage:
>>> new_name = noext('file', number_of_letters_of_the_ext)
Note: number_of_letters_of_the_ext has to include the point.
```

periodograma (*numfreq*, *nom*)

```
Function to plot the DFT of a time series with Gnuplot.
Usage:
```

```
>>> periodograma(number_of_frequency, 'file')
Where number_of_frequency means if the frequency is the first (1), second (2),
etc...
The data is taken from the .dft file given by freqPy
'file' can be .dat or .dft
```

plot (*data*, *X*, *Y*)

```
Plots one column versus another column from the variable data, uses matplotlib.
Usage:
>>> plot(data, column1, column2)
Note: data has to be a declared variable in Python.
For plot files you have to use the function ver/vererror.
```

quitarmaggt (*data*, *gt*)

```
Function to remove data in a variable. It removes the data with magnitude greater
than an specified quantity.
Usage:
>>> new_data = quitarmaggt(data, values_greater_than_this_will_be_removed)
>>> new_data = quitarmaggt('file', values_greater_than_this_will_be_removed)
```

quitarmaglt (*data*, *lt*)

```
Function to remove data in a variable. It removes the data with magnitude lower
than an specified quantity.
Usage:
>>> new_data = quitarmaglt(data, values_lower_than_this_will_be_removed)
>>> new_data = quitarmaglt('file', values_lower_than_this_will_be_removed)
```

quitartimegt (*data*, *gt*)

```
Function to remove data in a variable. It removes the data with time greater
```

than an specified quantity.
Usage:
```
>>> new_data = quitartimegt(data, values_greater_than_this_will_be_removed)
>>> new_data = quitartimegt('file', values_greater_than_this_will_be_removed)
```

quitartimelt (*data*, *lt*)

Function to remove data in a variable. It removes the data with time lower
than an specified quantity.
Usage:
```
>>> new_data = quitartimelt(data, values_lower_than_this_will_be_removed)
>>> new_data = quitartimelt('file', values_lower_than_this_will_be_removed)
```

res2dftstep (*data*, *res*, *fini*, *ffin*)

Function to convert the resolution in each peak of the DFT into frequency
step in the DFT calculation.
Usage:
```
>>> df = res2dftstep(data, res, freq_initial, freq_final)
>>> df = res2dftstep('file', res, freq_initial, freq_final)
```

resolucion (*data*, *fini*, *ffin*)

Function to calculate the maximum resolution to uses in freqPy for the data.
The term resolution means the number of points that we obtain for each peak of
the periodogram in our DFT calculation.
Usage:
```
>>> res = resolucion(data, freq_initial, freq_final)
>>> res = resolucion('file', freq_initial, freq_final)
```

ruido (*periodograma*, *fini*, *ffin*, *bin*)

Subfunction of SN.

Function to calculate the noise of a periodogram, with a corresponding binning.
Usually uses a bin of 5 c/d
WARNING!: The frequency calculations have to begin in 0.
Usage:
```
>>> noise_value = ruido(dft, freq_initial, freq_final, binning)
%REVISAR PARA CUALQUIER RANGO DE FREQS
```

sigmaclip (*data*, *nsigmas*)

Function to make a n-sigma clipping in the data.
Can be used with loaded data or with data files in the current directory.
Usage:
```
>>> new_data = sigmaclip(data, number_of_sigmas)
>>> new_data = sigmaclip('file', number_of_sigmas)
```

SN (*periodograma*, *freq*, *amp*, *fini*, *ffin*, *bin*)

Function to calculate the Signal to Noise amplitude ratio of a frequency.
It uses a binning (See Breger et al. 1993).
Usage:
```
>>> signal_to_noise = SN(dft, freq, amplitude, freq_initial, freq_final, binning)
```

stats (*data*)

Function to obtain the statistics of the data. It returns a vector with different
information:
Initial_Time, Num_Days, Num_Points, Mag_Max, Mag_Min, Mag_Mean, Mag_Med, Mag_Sigma,
Mag_Var

Can be used with loaded data or with data files in the current directory.
Usage:
```
>>> [T0, NDays, NPoints, MagMax, MagMin, MagMean, MagMed, MagSigma, MagVar] =
= stats(data)
>>> [T0, NDays, NPoints, MagMax, MagMin, MagMean, MagMed, MagSigma, MagVar] =
= stats('file')
```

ver (*nom*)

```
Function to plot time versus magnitude with Gnuplot.
Usage:
>>> ver('file')
```

vererror (*nom*)

```
Function to plot time versus magnitude with Gnuplot, with the errors in magnitude.
Usage:
>>> vererror('file')
```

window (*nom*)

```
Function to plot the spectral window of a time series with Gnuplot.
Usage:
>>> window('file')
The data is taken from the .win file given by freqPy
'file' can be .dat or .win
```

C.8   Authors

This software has been written by Pascual D. Diago Nebot (Observatori Astronòmic de la Universitat de València and Valencian International University, VIU) with financial support of the Spanish "Plan Nacional de Investigación Científica, Desarrollo e Innovación Tecnológica" and FEDER, through contract AYA2007-62487. The initial work of P. D. Diago was also supported by a FPU grant from the Spanish "Ministerio de Educación y Ciencia". This software uses programs written by Rafael Garrido Haba and Juan Gutiérrez-Soto (Instituto de Astrofísica de Andalucia-CSIC).

C.9   Acknowledgements

Thanks to Rafael Garrido Haba for having provided us with his original code `freq` and for his useful comments and support in every moment. Thanks to Juan Gutiérrez-Soto for his help and support to develop this software. And finally, thanks to my Ph.D. tutor Juan Fabregat for the support in every moment.

Carve your number on my wall,
And maybe you will get a call from me,
If I needed someone.

George Harrison

D

User Guide: KURTZ_BOS - version 1.0

Code author: Juan Gutiérrez-Soto[1], February 2008.

D.1   The algorithm

The objective of the KURTZ_BOS program is to find frequencies in a light curve. It is based on Fourier analysis and least-square fitting.

The procedure is the following:

---

[1]e-mail: jgs@iaa.es

1. Search for the first frequency with the highest amplitude by using the Kurtz algorithm (Kurtz 1985). This algorithm is based on the Discrete Fourier Transform (DFT), but four to six times faster.

2. Once we have found a frequency, we move around this frequency (local fitting) to find the frequency which gives the least residual, by a least-square fitting to a sinusoidal function. The function to be fitted is

$$f(x) = Const + Amp * \sin\left(2\pi(t * freq + phase)\right) \tag{D.1}$$

   The program uses the GSL library (Galassi et al. 2006) for the least-square fitting. KURTZ_BOS does not use the Levenberg-Marquardt algorithm for non-linear least-square fitting, it just finds the residual of the fit for a sample of trial frequencies and then it takes the one with least residual.

3. Having found a frequency, the program calculates the corresponding constant, amplitude and phase, following Eq. D.1. Then, it removes this signal to the light curve, obtaining the residual light curve.

4. The Kurtz algorithm is used again to find the the frequency with the highest amplitude in the residual light curve.

5. Now that we have found two frequencies (from item 2 and 4), we move around this pair of frequencies (local fitting) to find the frequencies which give the best fit to the original data. The function which is fitted is the Eq. D.1, but for two frequencies.

6. As in item 3, having found two frequencies, we calculate the corresponding parameters and we remove the signal from the light curve.

Then, the program iterates until it reaches the number of frequencies given by the user.

NOTE: The local fitting (fine tuning around a frequency) is only applied to frequencies which are higher than $6/T$, where T is the time span of the data. Frequencies lower than $6/T$ are too close to 0 and then the program would take too much time for finding these frequencies. Moreover, these frequencies may be due

to long term trends that are better to remove with other methods. Therefore, the frequencies obtained with this program lower than $6/T$ are those found directly by the Fourier analysis.

D.2   Usage

D.2.1   Online-help

If you type

```
> kurtz_bos
```

Then you will get the following output

```
Usage: kurtz_bos --input-file|-i FILE1 --output-file|-o FILE2 \
            --input-file-freq|-f FILE3\
            --number-lines|-l INTEGER1 \
            [--number-frequencies|-n INTEGER3] \
            [--ending-frequency|-e REAL1] \
            [--step-frequency|-s REAL2]

     kurtz_bos --command-file|-F FILE

     kurtz_bos --create-template|-T FILE

     kurtz_bos --version|-v
     kurtz_bos --help|-h            (prints a detailed help)
```

Options which are not within brackets are mandatory. For the user convenience most long name options (those beginning with a double dash; e.g. -number-points) may be abbreviated either by typing enough characters so that

there is no ambiguity with another option or by typing the corresponding short option (a single letter preceded by a single dash; e.g. -N). For options that take an argument, the kind of argument is indicated; arguments come in two flavours: numbers (here, INTEGER stands for integers and REAL for floating point numbers) and strings (here FILE). Arguments may be separated from the option's short or long name by a space or by the equal sign.

A detailed help can be obtained with the following command:

```
> kurtz_bos --help
```

Then you will get the following output

```
Usage: kurtz_bos --input-file|-i FILE1 --output-file|-o FILE2 \
           --number-lines|-l INTEGER1 \
           [--input-file-freq|-f FILE3]\
           [--number-frequencies|-n INTEGER2] \
           [--ending-frequency|-e REAL1] \
           [--step-frequency|-s REAL2]

     where FILE1 and FILE2 are the names of the input and
     output files; FILE3 is the name of the file of input
     frequencies
     INTEGER1 is the number of lines of the input file;
     INTEGER2 is the number of frequencies
     (default: 5); REAL1 (> 0) is the maximum frequency
     (default: 10.0); REAL2 (> 0) is the frequency step
     (default: 0.001)

     kurtz_bos --command-file|-F FILE [--number-frequencies|-n \
     INTEGER] [--ending-frequency|-e REAL1] [--step-frequency|-s \
     REAL2]

       The values of the parameters are written in a command file
```

```
   of name given by FILE. For the user's convenience, the
   program can generate a template of such a file (see below).


   If non-mandatory options are not given values in the
   command file, they may be given values by adding them to
   this command line (e.g., -F cmdfile.txt -s 0.15 -n 20).

 kurtz_bos --create-template|-T FILE

   Creates a template command file of name given by FILE,
   appropriate to the chosen operation mode.


   In all the above, the options within brackets are not
   mandatory.
   The non-mandatory options that take an argument are given
   a default value; these are:
   - number of frequencies: 5
   - maximal frequency: 10.0
   - frequency step: 0.001.

 kurtz_bos --version|-v

   Prints the version number of the program.

 kurtz_bos --help|-h

   Prints this message.
```

D.2.2   Parameters

The **mandatory** parameters of the program are the following:

- -input-file | -i FILE1, i.e. the input file containing the light curve. Note

that it should contain only two columns, time and magnitude (or flux).

- -output-file | -o FILE2, i.e. the output file where the detected frequencies are going to be saved.

- -number-lines | -l INTEGER1, i.e. the number of lines in the input file (the Linux command "wc -l file" gives you the number of lines of a file).

The **optional** parameters of the program are the following:

- -input-file-freq | -f FILE3, i.e. the input file containing a set of initial frequencies. Note that it should contain only 1 column with the frequencies.

- -number-frequencies | -n INTEGER2, i.e. the number of frequencies that we are searching for. The default is 5. Note that the number of requested frequencies should be larger than the number of frequencies given in the optional input-file-freq.

- -ending-frequency| -e REAL1, i.e. we are searching for frequencies in the range between 0 and this frequency. The default is 10, i.e. the default range is [0,10].

- -step-frequency| -s REAL2. This number is the step in frequencies for the Fourier analysis calculations. The default is 0.001.

D.2.3   Typical use

Generally speaking, we recommend using a command file rather than a command line, the latter putting the user more at risk of making mistakes.

1. Create a command file template, `file.par`, say:

   > kurtz_bos -T file.par

   The `file.par` will contain:

```
# Command file for kurtz_bos.

# If a line with a keyword is commented, this means
# that the corresponding keyword will be ascribed
# a default value; comment out the line and give a
# value if the default value does not suits your needs.

input-file =
output-file =
number-lines =

#input-file-freq =
#number-frequencies =      # (default: 5)
#ending-frequency =        # (default: 10.0
#step-frequency =          # (default: 0.001)
```

Note that the first three parameters are **mandatory** and they should be filled while the other four are optional. If you want to change the optional parameters, you should remove the # and fill the parameter. See Section D.3 for some examples.

2. Run the program with the following command:

```
> kurtz_bos -F file.par
```

D.3   Examples

D.3.1   Find five frequencies in a light curve

We are going to find five frequencies in the input file toto.dat in the frequency range [0,10] with a step in frequency of $0.001 \, \mathrm{c} \, \mathrm{d}^{-1}$. The time in the light curve is in days. First of all, we need to know the number of lines in toto.dat, in the terminal:

```
> wc -l toto.dat
> 3682 toto.dat
```

Now we create a command file template

```
> kurtz_bos -T toto.par
```

And then we fill the input file, output file and number of lines of the command file `toto.par`.

```
input-file = toto.dat
output-file = toto.kb
number-lines = 3682

#input-file-freq =
#number-frequencies =        # (default: 5)
#ending-frequency =          # (default: 10.0
#step-frequency =            # (default: 0.001)
```

Note that if we want to change the number of frequencies from the default, we need to remove the # and fill the parameter. Idem for the ending-frequency and step-frequency.

D.3.2 Improve two frequencies that I have found with another program

If we have used another program to search for frequencies and we want to improve these frequencies, we have to create a file, which we will call `toto.freq`, with the two frequencies, as in the example:

```
1.173244589
0.9826453009
```

Then we fill the command file `toto.par`

```
input-file = toto.dat
output-file = toto.kb
number-lines = 3682

input-file-freq = toto.freq
number-frequencies = 2        # (default: 5)
#ending-frequency =           # (default: 10.0)
#step-frequency =             # (default: 0.001)
```

D.3.3 We found three frequencies with kurtz_bos but now we want to find seven more

We have to create a file, which we will call `toto.freq`, with the three frequencies, as in the example:

```
1.173244589
0.9826453009
0.035
```

And then we fill the command file `toto.par`

```
input-file = toto.dat
output-file = toto.kb
number-lines = 3682

input-file-freq = toto.freq
```

```
number-frequencies = 10       # (default: 5)
#ending-frequency =           # (default: 10.0
#step-frequency =             # (default: 0.001)
```

D.4   Authors

This program has been developed by Juan Gutiérrez-Soto with the collaboration of Rafael Garrido Haba in the elaboration of the algorithm. The interface (command file and line commands) has been fully developed by Bernard Leroy.

I listen for your footsteps coming up the drive,
Listen for your footsteps, but they don't arrive.
Waiting for your knock, dear, on my old front door,
I don't hear it,
Does it mean you don't love me anymore?

Ringo Starr

E

Small Magellanic Cloud appendix

This appendix contains additional plots from Chapter 6.
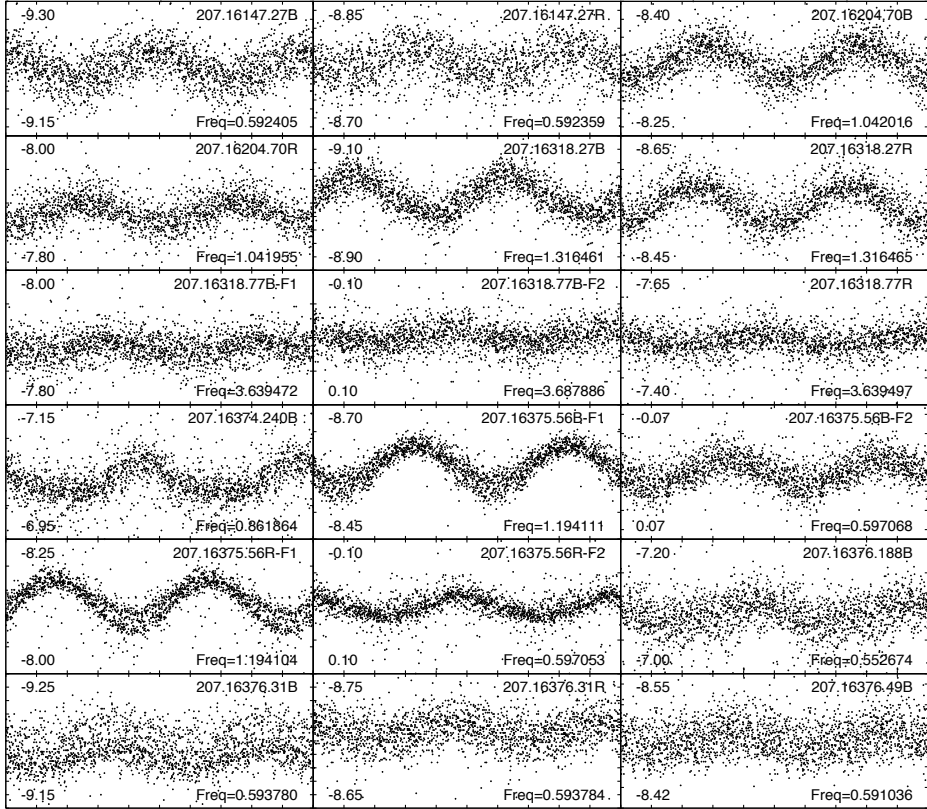
Figure E.1: *Phase plots of absorption-line B SMC stars showing short-term variability folded with the frequency given in each panel. Phases span from 0 to 2. Magnitude range in the B or R filter is denoted inside each panel in the left side. In the right lower corner we show the frequency in $c\,d^{-1}$. When the star is multiperiodic, the frequency used in the plot is given by the label F1, F2, F3 or F4 inside each panel.*
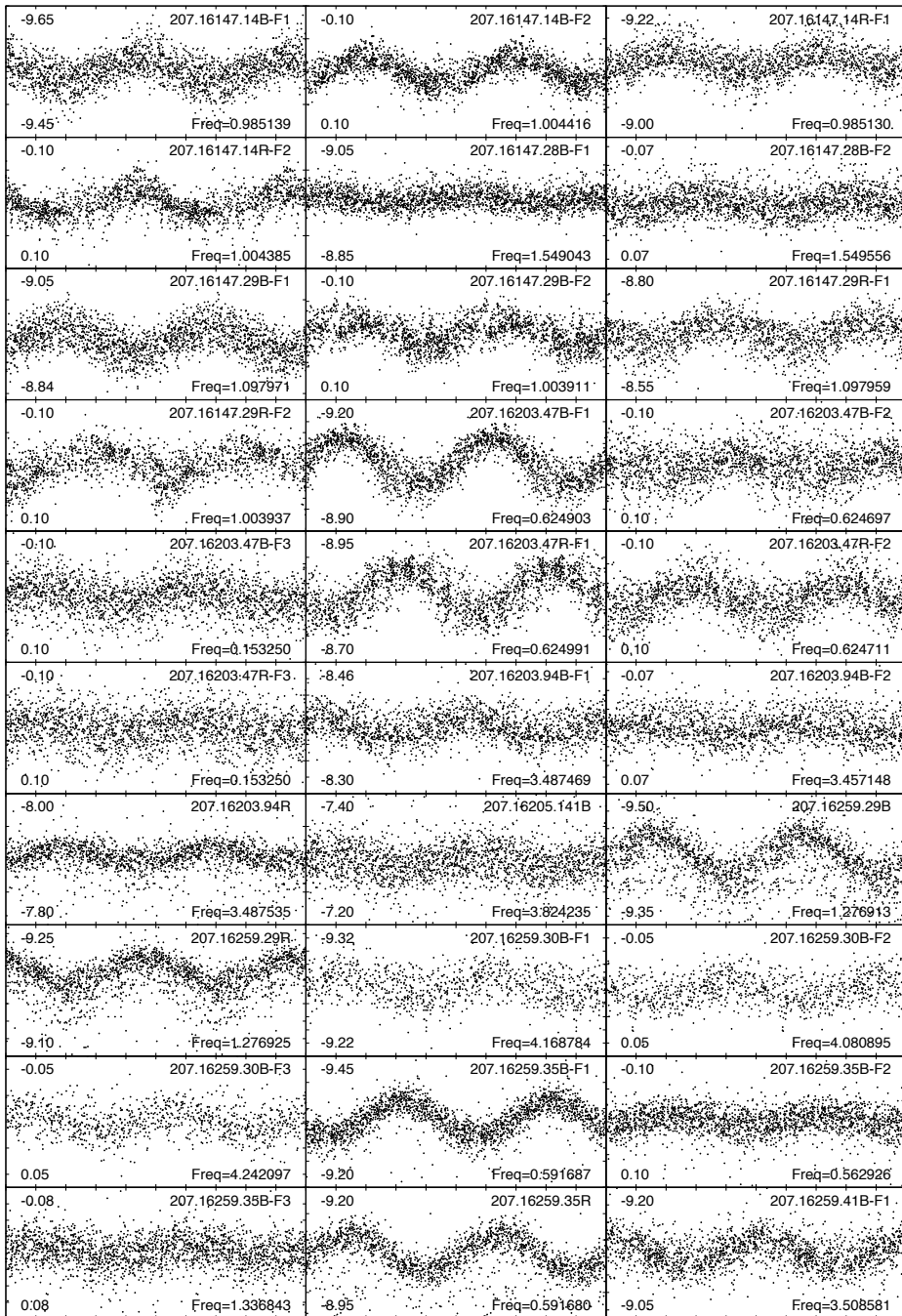
Figure E.2: *Phase plots of Be stars showing short-term variability. Axes as in* Fig. E.1.
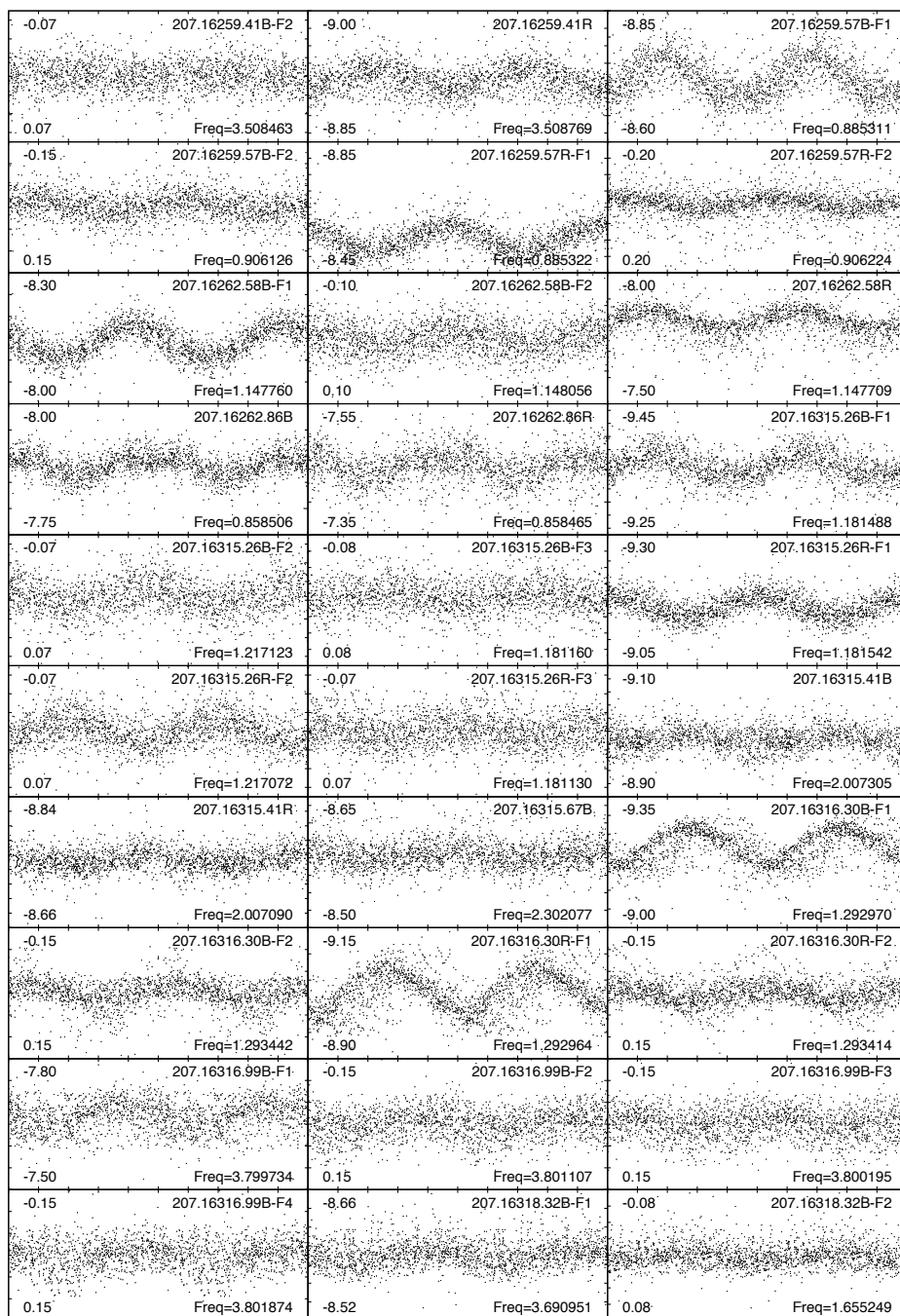
Figure E.3: *Continued from* Fig. E.2.
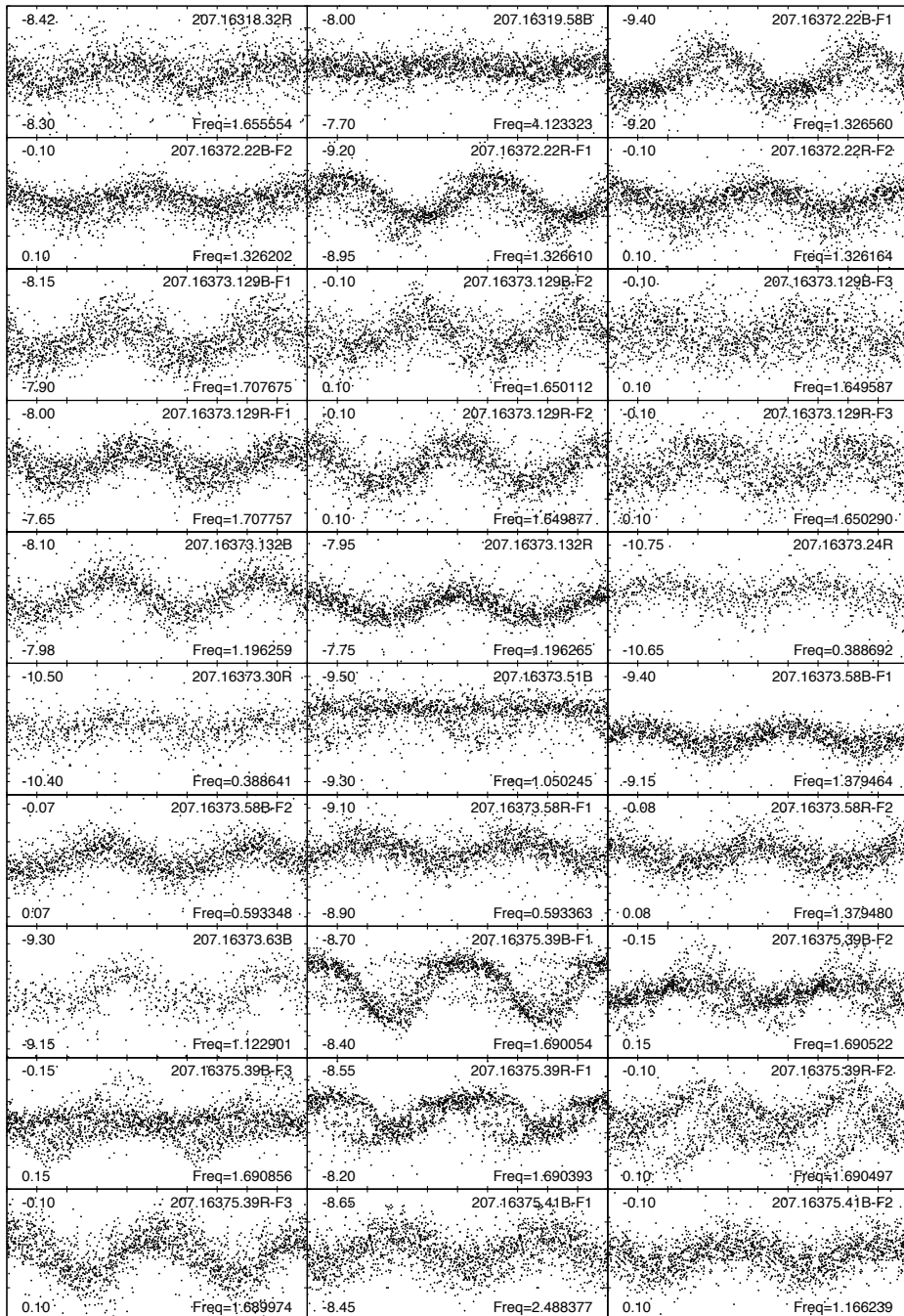
Figure E.4: *Continued from* Fig. E.3.
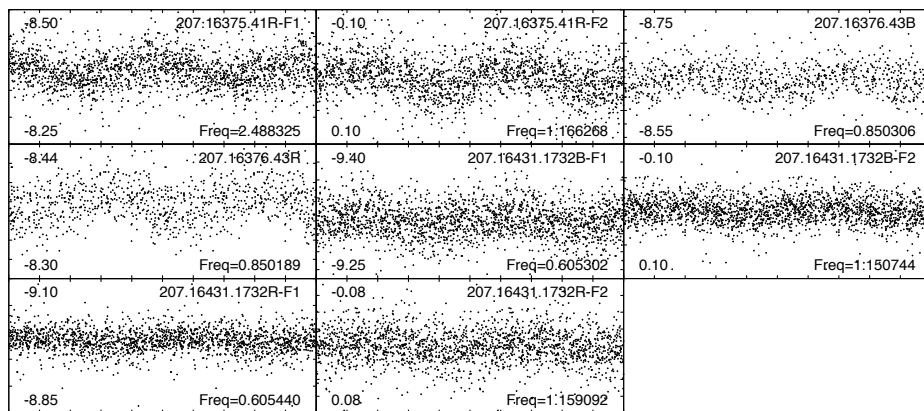
Figure E.5: *Continued from* Fig. E.4.

Bibliography

Aerts, C.: 2005, *Asteroseismology (Lecture notes)*, Universities of Leuven and Nijmegen

Aerts, C., Christensen-Dalsgaard, J., and Kurtz, D. W.: 2010, *Asteroseismology*

Aerts, C., De Cat, P., Cuypers, J., Becker, S. R., Mathias, P., De Mey, K., Gillet, D., and Waelkens, C.: 1998, *Astronomy & Astrophysics* **329**, 137

Alcock, C., Allsman, R. A., Alves, D. R., Axelrod, T. S., Becker, A. C., Bennett, D. P., Cook, K. H., Drake, A. J., Freeman, K. C., Geha, M., Griest, K., Lehner, M. J., Marshall, S. L., Minniti, D., Peterson, B. A., Popowski, P., Pratt, M. R., Nelson, C. A., Quinn, P. J., Stubbs, C. W., Sutherland, W., Tomaney, A. B., Vandehei, T., Welch, D. L., and The MACHO Collaboration: 1999, *Publications of the Astronomical Society of the Pacific* **111**, 1539

Almenara, J. M., Deeg, H. J., Aigrain, S., Alonso, R., Auvergne, M., Baglin, A., Barbieri, M., Barge, P., Bordé, P., Bouchy, F., Bruntt, H., Cabrera, J., Carone, L., Carpano, S., Catala, C., Csizmadia, S., de La Reza, R., Deleuil, M., Dvorak, R., Erikson, A., Fridlund, M., Gandolfi, D., Gillon, M., Gondoin, P., Guenther, E., Guillot, T., Hatzes, A., Hébrard, G., Jorda, L., Lammer, H., Léger, A., Llebaria, A., Loeillet, B., Magain, P., Mayor, M., Mazeh, T., Moutou, C., Ollivier, M., Pätzold, M., Pont, F., Queloz, D., Rauer, H., Régulo, C., Renner, S., Rouan, D., Samuel, B., Schneider, J., Shporer, A., Wuchterl, G., and Zucker, S.: 2009, *Astronomy & Astrophysics* **506**, 337

Alonso, R., Alapini, A., Aigrain, S., Auvergne, M., Baglin, A., Barbieri, M., Barge, P., Bonomo, A. S., Bordé, P., Bouchy, F., Chaintreuil, S., de La Reza, R., Deeg, H. J., Deleuil, M., Dvorak, R., Erikson, A., Fridlund, M., de Oliveira Fialho, F., Gondoin, P., Guillot, T., Hatzes, A., Jorda, L., Lammer, H., Léger, A., Llebaria, A., Magain, P., Mazeh, T., Moutou, C., Ollivier, M., Pätzold, M., Pont, F., Queloz, D., Rauer, H., Rouan, D., Schneider, J., and Wuchterl, G.: 2009, *Astronomy & Astrophysics* **506**, 353

Alonso, R., Deeg, H. J., Brown, T. M., and Belmonte, J. A.: 2004, in F. Favata, S. Aigrain, & A. Wilson (ed.), *Stellar Structure and Habitable Planet Finding*, Vol. 538 of *ESA Special Publication*, pp 255–259

Ando, H. and Osaki, Y.: 1975, *Publications of the Astronomical Society of Japan* **27**, 581

Auvergne, M., Bodin, P., Boisnard, L., Buey, J., Chaintreuil, S., Epstein, G., Jouret, M., Lam-Trong, T., Levacher, P., Magnan, A., Perez, R., Plasson, P., Plesseria, J., Peter, G., Steller, M., Tiphène, D., Baglin, A., Agogué, P., Appourchaux, T., Barbet, D., Beaufort, T., Bellenger, R., Berlin, R., Bernardi, P., Blouin, D., Boumier, P., Bonneau, F., Briet, R., Butler, B., Cautain, R., Chiavassa, F., Costes, V., Cuvilho, J., Cunha-Parro, V., de Oliveira Fialho, F., Decaudin, M., Defise, J., Djalal, S., Docclo, A., Drummond, R., Dupuis, O., Exil, G., Fauré, C., Gaboriaud, A., Gamet, P., Gavalda, P., Grolleau, E., Gueguen, L., Guivarc'h, V., Guterman, P., Hasiba, J., Huntzinger, G., Hustaix, H., Imbert, C., Jeanville, G., Johlander, B., Jorda, L.,

Journoud, P., Karioty, F., Kerjean, L., Lafond, L., Lapeyrere, V., Landiech, P., Larqué, T., Laudet, P., Le Merrer, J., Leporati, L., Leruyet, B., Levieuge, B., Llebaria, A., Martin, L., Mazy, E., Mesnager, J., Michel, J., Moalic, J., Monjoin, W., Naudet, D., Neukirchner, S., Nguyen-Kim, K., Ollivier, M., Orcesi, J., Ottacher, H., Oulali, A., Parisot, J., Perruchot, S., Piacentino, A., Pinheiro da Silva, L., Platzer, J., Pontet, B., Pradines, A., Quentin, C., Rohbeck, U., Rolland, G., Rollenhagen, F., Romagnan, R., Russ, N., Samadi, R., Schmidt, R., Schwartz, N., Sebbag, I., Smit, H., Sunter, W., Tello, M., Toulouse, P., Ulmer, B., Vandermarcq, O., Vergnault, E., Wallner, R., Waultier, G., and Zanatta, P.: 2009, *Astronomy & Astrophysics* **506**, 411

Baade, D.: 1982a, *Astronomy & Astrophysics* **105**, 65

Baade, D.: 1982b, *Astronomy & Astrophysics* **110**, L15

Baade, D.: 1989, *Astronomy & Astrophysics* **222**, 200

Baade, D. and Balona, L. A.: 1994, in L. A. Balona, H. F. Henrichs, & J. M. Le Contel (ed.), *Pulsation; Rotation; and Mass Loss in Early-Type Stars*, Vol. 162 of *IAU Symposium*, p. 311

Baade, D., Meisenheimer, K., Iwert, O., Alonso, J., Augusteijn, T., Beletic, J., Bellemann, H., Benesch, W., Böhm, A., Böhnhardt, H., Brewer, J., Deiries, S., Delabre, B., Donaldson, R., Dupuy, C., Franke, P., Gerdes, R., Gilliotte, A., Grimm, B., Haddad, N., Hess, G., Ihle, G., Klein, R., Lenzen, R., Lizon, J., Mancini, D., Münch, N., Pizarro, A., Prado, P., Rahmer, G., Reyes, J., Richardson, F., Robledo, E., Sanchez, F., Silber, A., Sinclaire, P., Wackermann, R., and Zaggia, S.: 1999, *The Messenger* **95**, 15

Baglin, A., Weiss, W. W., and Bisnovatyi-Kogan, G.: 1993, in W. W. Weiss & A. Baglin (ed.), *IAU Colloq. 137: Inside the Stars*, Vol. 40 of *Astronomical Society of the Pacific Conference Series*, p. 758

Baker, N. and Kippenhahn, R.: 1962, *Zeitschrift fur Astrophysik* **54**, 114

Balona, L. A.: 1990, *Monthly Notices of the Royal Astronomical Society* **245**, 92

Balona, L. A.: 1992, *Monthly Notices of the Royal Astronomical Society* **256**, 425

Balona, L. A.: 1993, *Monthly Notices of the Royal Astronomical Society* **260**, 795

Balona, L. A.: 1995, *Monthly Notices of the Royal Astronomical Society* **277**, 1547

Balona, L. A. and Dziembowski, W. A.: 1999, *Monthly Notices of the Royal Astronomical Society* **309**, 221

Balona, L. A. and Jerzykiewicz, M.: 1993, *Monthly Notices of the Royal Astronomical Society* **260**, 782

Balona, L. A. and Kambe, E.: 1999, *Monthly Notices of the Royal Astronomical Society* **308**, 1117

Barban, C., Deheuvels, S., Baudin, F., Appourchaux, T., Auvergne, M., Ballot, J., Boumier, P., Chaplin, W. J., García, R. A., Gaulme, P., Michel, E., Mosser, B., Régulo, C., Roxburgh, I. W., Verner, G., Baglin, A., Catala, C., Samadi, R., Bruntt, H., Elsworth, Y., and Mathur, S.: 2009, *Astronomy & Astrophysics* **506**, 51

Bessell, M. S.: 1990, *Publications of the Astronomical Society of the Pacific* **102**, 1181

Bordé, P., Rouan, D., and Léger, A.: 2001, *Comptes Rendus Physique* **7**, 1049

Breger, M. and Pamyatnykh, A. A.: 2006, *Monthly Notices of the Royal Astronomical Society* **368**, 571

Breger, M., Stich, J., Garrido, R., Martin, B., Jiang, S. Y., Li, Z. P., Hube, D. P., Ostermann, W., Paparo, M., and Scheck, M.: 1993, *Astronomy & Astrophysics* **271**, 482

Bretthorst, G. L.: 2003, *Frequency estimation and generalized Lomb-Scargle periodograms*, pp 309–329, Statistical Challenges in Astronomy

Brewer, E. C.: 1894, *Dictionary of Phrase and Fable*

Brown, T. M. and Gilliland, R. L.: 1994, *Annual Review of Astronomy & Astrophysics* **32**, 37

Castelli, F., Gratton, R. G., and Kurucz, R. L.: 1997, *Astronomy & Astrophysics* **318**, 841

Catala, C., Mangeney, A., Gautier, D., Auvergne, M., Baglin, A., Goupil, M. J., Michel, E., Zahn, J. P., Magnan, A., Vuillemin, A., Boumier, P., Gabriel, A., Lemaire, P., Turck-Chieze, S., Dzitko, H., Mosser, B., and Bonneau, F.: 1995, in R. K. Ulrich, E. J. Rhodes Jr., & W. Dappen (ed.), *GONG 1994. Helio- and Astro-Seismology from the Earth and Space*, Vol. 76 of *Astronomical Society of the Pacific Conference Series*, p. 426

Catala, C. and the PLATO consortium: 2008, *Journal of Physics Conference Series* **118(1)**, 012040

Chauville, J., Zorec, J., Ballereau, D., Morrell, N., Cidale, L., and Garcia, A.: 2001, *Astronomy & Astrophysics* **378**, 861

Christensen-Dalsgaard, J.: 2002, *Reviews of Modern Physics* **74**, 1073

Christensen-Dalsgaard, J.: 2003, *Stellar Oscillation (Lecture notes)*, Institut for Fysik og Astronomi, Aarhus Universitet Teoretisk Astrofysik Center, Danmarks Grundforskningsfond

Christensen-Dalsgaard, J. and Berthomieu, G.: 1991, *Theory of solar oscillations*, pp 401–478

Christy, R. F.: 1966, *Annual Review of Astronomy & Astrophysics* **4**, 353

Collins, II, G. W.: 1987, in A. Slettebak and T. P. Snow (eds.), *IAU Colloq. 92: Physics of Be Stars*, pp 3–19

Collins, II, G. W. and Truax, R. J.: 1995, *Astrophysical Journal* **439**, 860

Cowling, T. G.: 1941, *Monthly Notices of the Royal Astronomical Society* **101**, 367

Cox, A. N., Morgan, S. M., Rogers, F. J., and Iglesias, C. A.: 1992, *Astrophysical Journal* **393**, 272

Cox, J. P.: 1980, *Theory of stellar pulsation*

Cox, J. P. and Whitney, C.: 1958, *Astrophysical Journal* **127**, 561

Cunha, M. S., Aerts, C., Christensen-Dalsgaard, J., Baglin, A., Bigot, L., Brown, T. M., Catala, C., Creevey, O. L., Domiciano de Souza, A., Eggenberger, P., Garcia, P. J. V., Grundahl, F., Kervella, P., Kurtz, D. W., Mathias, P., Miglio, A., Monteiro, M. J. P. F. G., Perrin, G., Pijpers, F. P., Pourbaix, D., Quirrenbach, A., Rousselet-Perraut, K., Teixeira, T. C., Thévenin, F., and Thompson, M. J.: 2007, *Astronomy and Astrophysics Review* **14**, 217

de Cat, P.: 2002, in C. Aerts, T. R. Bedding, and J. Christensen-Dalsgaard (eds.), *IAU Colloq. 185: Radial and Nonradial Pulsations as Probes of Stellar Physics*, Vol. 259 of *Astronomical Society of the Pacific Conference Series*, p. 196

de Winter, D. and Pérez, M. R.: 1998, in A. M. Hubert and C. Jaschek (eds.), *B[e] stars*, Vol. 233 of *Astrophysics and Space Science Library*, p. 269

Debosscher, J., Aerts, C., and Vandenbussche, B.: 2006, in C. Aerts & C. Sterken (ed.), *Astrophysics of Variable Stars*, Vol. 349 of *Astronomical Society of the Pacific Conference Series*, p. 219

Debosscher, J., Sarro, L. M., Aerts, C., Cuypers, J., Vandenbussche, B., Garrido, R., and Solano, E.: 2007, *Astronomy & Astrophysics* **475**, 1159

Debosscher, J., Sarro, L. M., López, M., Deleuil, M., Aerts, C., Auvergne, M., Baglin, A., Baudin, F., Chadid, M., Charpinet, S., Cuypers, J., De Ridder, J., Garrido, R., Hubert, A. M., Janot-Pacheco, E., Jorda, L., Kaiser, A., Kallinger, T., Kollath, Z., Maceroni, C., Mathias, P., Michel, E., Moutou, C., Neiner, C., Ollivier, M., Samadi, R., Solano, E., Surace, C., Vandenbussche, B., and Weiss, W. W.: 2009, *Astronomy & Astrophysics* **506**, 519

Deeming, T. J.: 1975, *Astrophysics and Space Science* **36**, 137

Defaÿ, C., Deleuil, M., and Barge, P.: 2001, *Astronomy & Astrophysics* **365**, 330

Deubner, F.: 1975, *Astronomy & Astrophysics* **44**, 371

Diago, P. D., Gutiérrez-Soto, J., Auvergne, M., Fabregat, J., Hubert, A., Floquet, M., Frémat, Y., Garrido, R., Andrade, L., de Batz, B., Emilio, M., Espinosa Lara, F., Huat, A., Janot-Pacheco, E., Leroy, B., Martayan, C., Neiner, C., Semaan, T., Suso, J., Catala, C., Poretti, E., Rainer, M., Uytterhoeven, K., Michel, E., and Samadi, R.: 2009a, *Astronomy & Astrophysics* **506**, 125

Diago, P. D., Gutiérrez-Soto, J., Fabregat, J., and Martayan, C.: 2008a, *Astronomy & Astrophysics* **480**, 179

Diago, P. D., Gutiérrez-Soto, J., Fabregat, J., and Martayan, C.: 2009b, *Communications in Asteroseismology* **158**, 184

Diago, P. D., Gutierrez-Soto, J., Fabregat, J., Martayan, C., and Suso, J.: 2008b, *Communications in Asteroseismology* **157**, 299

Diago, P. D., Gutiérrez-Soto, J., Fabregat, J., Martayan, C., and Suso, J.: 2010, in J. M. Diego, L. J. Goicoechea, J. I. González-Serrano, & J. Gorgas (ed.), *Highlights of Spanish Astrophysics V*, p. 401

D'Odorico, S., Dekker, H., Mazzoleni, R., Vernet, J., Guinouard, I., Groot, P., Hammer, F., Rasmussen, P. K., Kaper, L., Navarro, R., Pallavicini, R., Peroux, C., and Zerbi, F. M.: 2006, in *Society of Photo-Optical Instrumentation Engineers (SPIE) Conference Series*, Vol. 6269 of *Presented at the Society of Photo-Optical Instrumentation Engineers (SPIE) Conference*

Domiciano de Souza, A., Kervella, P., Jankov, S., Abe, L., Vakili, F., di Folco, E., and Paresce, F.: 2003, *Astronomy & Astrophysics* **407**, L47

Donati, J.-F., Semel, M., Carter, B. D., Rees, D. E., and Collier Cameron, A.: 1997, *Monthly Notices of the Royal Astronomical Society* **291**, 658

Dupret, M., Belkacem, K., Samadi, R., Montalban, J., Moreira, O., Miglio, A., Godart, M., Ventura, P., Ludwig, H., Grigahcène, A., Goupil, M., Noels, A., and Caffau, E.: 2009, *Astronomy & Astrophysics* **506**, 57

Dupret, M., De Ridder, J., Neuforge, C., Aerts, C., and Scuflaire, R.: 2002, *Astronomy & Astrophysics* **385**, 563

Dupret, M. A.: 2001, *Astronomy & Astrophysics* **366**, 166

Dziembowski, W. A., Moskalik, P., and Pamyatnykh, A. A.: 1993, *Monthly Notices of the Royal Astronomical Society* **265**, 588

Dziembowski, W. A. and Pamyatnykh, A. A.: 1993, *Monthly Notices of the Royal Astronomical Society* **262**, 204

Eddington, A. S.: 1926, *The Internal Constitution of the Stars*

Eyer, L. and Mowlavi, N.: 2008, *Journal of Physics Conference Series* **118(1)**, 012010

Fabregat, J.: 2003, in C. Sterken (ed.), *Interplay of Periodic, Cyclic and Stochastic Variability in Selected Areas of the H-R Diagram*, Vol. 292 of *Astronomical Society of the Pacific Conference Series*, p. 65

Fabregat, J. and Torrejón, J. M.: 2000, *Astronomy & Astrophysics* **357**, 451

Feast, M. W.: 1972, *Monthly Notices of the Royal Astronomical Society* **159**, 113

Floquet, M., Hubert, A., Huat, A., Frémat, Y., Janot-Pacheco, E., Gutiérrez-Soto, J., Neiner, C., de Batz, B., Leroy, B., Poretti, E., Amado, P., Catala, C., Rainer, M., Diaz, D., Uytterhoeven, K., Andrade, L., Diago, P. D., Emilio, M., Espinosa Lara, F., Fabregat, J., Martayan, C., Semaan, T., and Suso, J.: 2009, *Astronomy & Astrophysics* **506**, 103

Floquet, M., Hubert, A. M., Hubert, H., Janot-Pacheco, E., Caillet, S., and Leister, N. V.: 1996, *Astronomy & Astrophysics* **310**, 849

Foster, G.: 1995, *Astronomical Journal* **109**, 1889

Frémat, Y., Neiner, C., Hubert, A., Floquet, M., Zorec, J., Janot-Pacheco, E., and Renan de Medeiros, J.: 2006, *Astronomy & Astrophysics* **451**, 1053

Frémat, Y., Zorec, J., Hubert, A.-M., and Floquet, M.: 2005, *Astronomy & Astrophysics* **440**, 305

Fridlund, M., Baglin, A., Lochard, J., and Conroy, L. (eds.): 2006, *The CoRoT Mission Pre-Launch Status - Stellar Seismology and Planet Finding*, Vol. 1306 of *ESA Special Publication*

Frost, E. B.: 1902, *Astrophysical Journal* **15**, 340

Galassi, M., Davies, J., Theiler, J., B., G., G., J., M., B., and F., R.: 2006, *GNU Scientific Library Reference Manual, revised and updated second edition, GNU Free Software Foundation*, The corresponding software can be found at http://www.gnu.org/software/gsl/

García, R. A., Régulo, C., Samadi, R., Ballot, J., Barban, C., Benomar, O., Chaplin, W. J., Gaulme, P., Appourchaux, T., Mathur, S., Mosser, B., Toutain, T., Verner, G. A., Auvergne, M., Baglin, A., Baudin, F., Boumier, P., Bruntt, H., Catala, C., Deheuvels, S., Elsworth, Y., Jiménez-Reyes, S. J., Michel, E., Pérez Hernández, F., Roxburgh, I. W., and Salabert, D.: 2009, *Astronomy & Astrophysics* **506**, 41

García Hernández, A., Moya, A., Michel, E., Garrido, R., Suárez, J. C., Rodríguez, E., Amado, P. J., Martín-Ruiz, S., Rolland, A., Poretti, E., Samadi, R., Baglin, A., Auvergne, M., Catala, C., Lefevre, L., and Baudin, F.: 2009, *Astronomy & Astrophysics* **506**, 79

Garrido, R.: 2000a, in T. Teixeira & T. Bedding (ed.), *The Third MONS Workshop: Science Preparation and Target Selection*, p. 103

Garrido, R.: 2000b, in M. Breger & M. Montgomery (ed.), *Delta Scuti and Related Stars*, Vol. 210 of *Astronomical Society of the Pacific Conference Series*, p. 67

Gautschy, A. and Saio, H.: 1993, *Monthly Notices of the Royal Astronomical Society* **262**, 213

Gautschy, A. and Saio, H.: 1995, *Annual Review of Astronomy & Astrophysics* **33**, 75

Gautschy, A. and Saio, H.: 1996, *Annual Review of Astronomy & Astrophysics* **34**, 551

Gough, D. and Toomre, J.: 1991, *Annual Review of Astronomy & Astrophysics* **29**, 627

Gough, D. O.: 1990, in Y. Osaki & H. Shibahashi (ed.), *Progress of Seismology of the Sun and Stars*, Vol. 367 of *Lecture Notes in Physics, Berlin Springer Verlag*, p. 283

Gough, D. O.: 1993, in J.-P. Zahn & J. Zinn-Justin (ed.), *Astrophysical Fluid Dynamics - Les Houches 1987*, pp 399–560

Goupil, M., Dziembowski, W. A., Goode, P. R., and Michel, E.: 1996, *Astronomy & Astrophysics* **305**, 487

Goupil, M., Dziembowski, W. A., Pamyatnykh, A. A., and Talon, S.: 2000, in M. Breger & M. Montgomery (ed.), *Delta Scuti and Related Stars*, Vol. 210 of *Astronomical Society of the Pacific Conference Series*, p. 267

Grebel, E. K. and Richtler, T.: 1992, *Astronomy & Astrophysics* **253**, 359

Grebel, E. K., Roberts, W. J., and Brandner, W.: 1996, *Astronomy & Astrophysics* **311**, 470

Grebel, E. K., Roberts, W. J., Will, J., and de Boer, K. S.: 1993, *Space Science Reviews* **66**, 65

Grundahl, F., Christensen-Dalsgaard, J., Kjeldsen, H., Jørgensen, U. G., Arentoft, T., Frandsen, S., and Kjærgaard, P.: 2009, *ArXiv e-prints*

Gutiérrez-Soto, J.: 2006, *Ph.D. thesis*, Observatori Astrònomic de la Universitat de València. Universitat de València

Gutiérrez-Soto, J., Fabregat, J., Suso, J., Lanzara, M., Garrido, R., Hubert, A., and Floquet, M.: 2007a, *Astronomy & Astrophysics* **476**, 927

Gutiérrez-Soto, J., Fabregat, J., Suso, J., Suárez, J. C., Moya, A., Garrido, R., Hubert, A., Floquet, M., Neiner, C., and Frémat, Y.: 2007b, *Astronomy & Astrophysics* **472**, 565

Gutiérrez-Soto, J., Floquet, M., Neiner, C., Hubert, A., Frémat, Y., Andrade, L., de Batz, B., Diago, P. D., Emilio, M., Fabregat, J., Facanha, W., Huat, A., Janot-Pacheco, E., Leroy, B., Martayan, C., Suso, J., and Garrido, R.: 2009a, *Communications in Asteroseismology* **158**, 208

Gutiérrez-Soto, J., Floquet, M., Samadi, R., Neiner, C., Garrido, R., Fabregat, J., Frémat, Y., Diago, P. D., Huat, A., Leroy, B., Emilio, M., Hubert, A., Andrade, O. T. L., de Batz, B., Janot-Pacheco, E., Espinosa Lara, F., Martayan, C., Semaan, T., Suso, J., Auvergne, M., Chaintreuil, S., Michel, E., and Catala, C.: 2009b, *Astronomy & Astrophysics* **506**, 133

Gutierrez-Soto, J., Neiner, C., Hubert, A., Floquet, M., Huat, A., Diago, P. D., Fabregat, J., Leroy, B., De Batz, B., Andrade, L., Emilio, M., Facanha, W., Fremat, Y., Janot-Pacheco, E., Martayan, C., and Suso, J.: 2008, *Communications in Asteroseismology* **157**, 70

Gutiérrez-Soto, J., Neiner, C., Hubert, A., Floquet, M., Huat, A., Diago, P. D., Fabregat, J., Leroy, B., de Batz, B., Andrade, L., Emilio, M., Facanha, W., Frémat, Y., Janot-Pacheco, E., Martayan, M., Suso, J., and Garrido, R.: 2008, in C. Charbonnel, F. Combes, & R. Samadi (ed.), *SF2A-2008*, p. 475

Hanuschik, R. W., Hummel, W., Sutorius, E., Dietle, O., and Thimm, G.: 1996, *Astronomy & Astrophysics Supplement Series* **116**, 309

Hart, J., van Hermelen, J., Hovey, G., Freeman, K. C., Peterson, B. A., Axelrod, T. S., Quinn, P. J., Rodgers, A. W., Allsman, R. A., Alcock, C., Bennett, D. P., Cook, K. H., Griest, K., Marshall, S. L., Pratt, M. R., Stubbs, C. W., and Sutherland, W.: 1996, *Publications of the Astronomical Society of the Pacific* **108**, 220

Harvey, J. W.: 1988, in J. Christensen-Dalsgaard & S. Frandsen (ed.), *Advances in Helio- and Asteroseismology*, Vol. 123 of *IAU Symposium*, p. 497

Hekker, S., Kallinger, T., Baudin, F., De Ridder, J., Barban, C., Carrier, F., Hatzes, A. P., Weiss, W. W., and Baglin, A.: 2009, *Astronomy & Astrophysics* **506**, 465

Huat, A., Hubert, A., Baudin, F., Floquet, M., Neiner, C., Frémat, Y., Gutiérrez-Soto, J., Andrade, L., de Batz, B., Diago, P. D., Emilio, M., Espinosa Lara, F., Fabregat, J., Janot-Pacheco, E., Leroy, B., Martayan, C., Semaan, T., Suso, J., Auvergne, M., Catala, C., Michel, E., and Samadi, R.: 2009a, *Astronomy & Astrophysics* **506**, 95

Huat, A., Leroy, B., and Diago, P. D.: 2009b, *Communications in Asteroseismology* **158**, 211

Hubeny, I. and Lanz, T.: 1995, *Astrophysical Journal* **439**, 875

Hubert, A. M. and Floquet, M.: 1998, *Astronomy & Astrophysics* **335**, 565

Hubert, A. M., Floquet, M., Hao, J. X., Caillet, S., Catala, C., Foing, B. H., Neff, J. E., Huang, L., Hubert, H., Barban, C., Baudrand, J., Cao, H., Char, S., Chatzichristou, H., Cuby, J. G., Czarny, J., Dreux, M., Felenbok, P., Guerin, J., Hron, J., Huovelin, J., Jankov, S., Jiang, S., Le Contel, J. M., Maitzen, H. M., Petrov, P., Savanov, I., Shcherbakov, A., Simon, T., Stee, P., Tuominen, I., and Zhai, D.: 1997, *Astronomy & Astrophysics* **324**, 929

Hubert, A. M., Floquet, M., and Zorec, J.: 2000, in M. A. Smith, H. F. Henrichs, & J. Fabregat (ed.), *IAU Colloq. 175: The Be Phenomenon in Early-Type Stars*, Vol. 214 of *Astronomical Society of the Pacific Conference Series*, p. 348

Iglesias, C. A. and Rogers, F. J.: 1996, *Astrophysical Journal* **464**, 943

Jankov, S., Janot-Pacheco, E., and Leister, N. V.: 2000, *Astrophysical Journal* **540**, 535

Janot-Pacheco, E., Jankov, S., Leister, N. V., Hubert, A. M., and Floquet, M.: 1999, *Astronomy & Astrophysics Supplement Series* **137**, 407

Jaschek, M., Slettebak, A., and Jaschek, C.: 1981, *Be star terminology.*

Jasniewicz, G. and Thevenin, F.: 1994, *Astronomy & Astrophysics* **282**, 717

Kallinger, T., Reegen, P., and Weiss, W. W.: 2008, *Astronomy & Astrophysics* **481**, 571

Karoff, C., Arentoft, T., Glowienka, L., Coutures, C., Nielsen, T. B., Dogan, G., Grundahl, F., and Kjeldsen, H.: 2008, *Monthly Notices of the Royal Astronomical Society* **386**, 1085

Kaufer, A., Stahl, O., Tubbesing, S., Nørregaard, P., Avila, G., Francois, P., Pasquini, L., and Pizzella, A.: 1999, *The Messenger* **95**, 8

Keller, S. C., Bessell, M. S., and Da Costa, G. S.: 2000, in M. A. Smith, H. F. Henrichs, & J. Fabregat (ed.), *IAU Colloq. 175: The Be Phenomenon in Early-Type Stars*, Vol. 214 of *Astronomical Society of the Pacific Conference Series*, pp 75–+

Keller, S. C., Grebel, E. K., Miller, G. J., and Yoss, K. M.: 2001, *Astronomical Journal* **122**, 248

Keller, S. C., Wood, P. R., and Bessell, M. S.: 1999, *Astronomy & Astrophysics Supplement Series* **134**, 489

Kelvin, L.: 1863, → *Thomson (1863)*

Kippenhahn, R. and Weigert, A.: 1990, *Stellar Structure and Evolution*

Kjeldsen, H. and Baade, D.: 1994, in L. A. Balona, H. F. Henrichs, and J. M. Le Contel (eds.), *Pulsation; Rotation; and Mass Loss in Early-Type Stars*, Vol. 162 of *IAU Symposium*, p. 29

Koestler, A.: 1959, *The Sleepwalkers, the Macmillan company, New York*

Kołaczkowski, Z., Pigulski, A., Soszyński, I., Udalski, A., Kubiak, M., Szymański, M., Żebruń, K., Pietrzyński, G., Woźniak, P. R., Szewczyk, O., and Wyrzykowski, Ł.: 2006, *Memorie della Societa Astronomica Italiana* **77**, 336

Kołaczkowski, Z., Pigulski, A., Soszyński, I., Udalski, A., Szymañski, M., Kubiak, M., Zebruń, K., Pietrzyński, G., Woźniak, P. R., Szewczyk, O., and Wyrzykowski, L.: 2005, *Beta Cephei stars in the LMC*

Kołaczkowski, Z., Pigulski, A., Soszyński, I., Udalski, A., Szymański, M., Kubiak, M., Żebruń, K., Pietrzyński, G., Woźniak, P. R., Szewczyk, O., Wyrzykowski, L., and The Ogle Team: 2004, in D. W. Kurtz and K. R. Pollard (eds.), *ASP Conf. Ser. 310: IAU Colloq. 193: Variable Stars in the Local Group*, p. 225

Korn, A. J., Keller, S. C., Kaufer, A., Langer, N., Przybilla, N., Stahl, O., and Wolf, B.: 2002, *Astronomy & Astrophysics* **385**, 143

Koubský, P., Harmanec, P., Hubert, A. M., Floquet, M., Kubát, J., Ballereau, D., Chauville, J., Božić, H., Holmgren, D., Yang, S., Cao, H., Eenens, P., Huang, L., and Percy, J. R.: 2000, *Astronomy & Astrophysics* **356**, 913

Kubiak, M.: 1990, *Acta Astronomica* **40**, 355

Kurtz, D. W.: 1982, *Monthly Notices of the Royal Astronomical Society* **200**, 807

Kurtz, D. W.: 1985, *Monthly Notices of the Royal Astronomical Society* **213**, 773

Kurtz, D. W.: 2006, in C. Sterken and C. Aerts (eds.), *Astrophysics of Variable Stars*, Vol. 349 of *Astronomical Society of the Pacific Conference Series*, p. 101

Kurucz, R.: 1993, *ATLAS9 Stellar Atmosphere Programs and 2 km/s grid. Kurucz CD-ROM No. 13. Cambridge, Mass.: Smithsonian Astrophysical Observatory, 1993.* 13

Lamers, H. J. G. L. M., Zickgraf, F.-J., de Winter, D., Houziaux, L., and Zorec, J.: 1998, *Astronomy & Astrophysics* **340**, 117

Landiech, P. and Douillet, F.: 2004, in B. Warmbein (ed.), *Small Satellites, Systems and Services*, Vol. 571 of *ESA Special Publication*

Lanza, A. F., Aigrain, S., Messina, S., Leto, G., Pagano, I., Auvergne, M., Baglin, A., Barge, P., Bonomo, A. S., Collier Cameron, A., Cutispoto, G., Deleuil, M., de Medeiros, J. R., Foing, B., and Moutou, C.: 2009, *Astronomy & Astrophysics* **506**, 255

Ledoux, P.: 1951, *Astrophysical Journal* **114**, 373

Ledoux, P. and Walraven, T.: 1958, *Handbuch der Physik* **51**, 353

Lee, U.: 2006, *Monthly Notices of the Royal Astronomical Society* **365**, 677

Léger, A., Rouan, D., Schneider, J., Barge, P., Fridlund, M., Samuel, B., Ollivier, M., Guenther, E., Deleuil, M., Deeg, H. J., Auvergne, M., Alonso, R., Aigrain, S., Alapini, A., Almenara, J. M., Baglin, A., Barbieri, M., Bruntt, H., Bordé, P., Bouchy, F., Cabrera, J., Catala, C., Carone, L., Carpano, S., Csizmadia, S., Dvorak, R., Erikson, A., Ferraz-Mello, S., Foing, B., Fressin, F., Gandolfi, D., Gillon, M., Gondoin, P., Grasset, O., Guillot, T., Hatzes, A., Hébrard, G., Jorda, L., Lammer, H., Llebaria, A., Loeillet, B., Mayor, M., Mazeh, T., Moutou, C., Pätzold, M., Pont, F., Queloz, D., Rauer, H., Renner, S., Samadi, R., Shporer, A., Sotin, C., Tingley, B., Wuchterl, G., Adda, M., Agogu, P., Appourchaux, T., Ballans, H., Baron, P., Beaufort, T., Bellenger, R., Berlin, R., Bernardi, P., Blouin, D., Baudin, F., Bodin, P., Boisnard, L., Boit, L., Bonneau, F., Borzeix, S., Briet, R., Buey, J., Butler, B., Cailleau, D., Cautain, R., Chabaud, P., Chaintreuil, S., Chiavassa, F., Costes, V., Cuna Parrho, V., de Oliveira Fialho, F., Decaudin, M., Defise, J., Djalal, S., Epstein, G., Exil, G., Fauré, C., Fenouillet, T., Gaboriaud, A., Gallic, A., Gamet, P., Gavalda, P., Grolleau, E., Gruneisen, R., Gueguen, L., Guis, V., Guivarc'h, V., Guterman, P., Hallouard, D., Hasiba, J., Heuripeau, F., Huntzinger, G., Hustaix, H., Imad, C., Imbert, C., Johlander, B., Jouret, M., Journoud, P., Karioty, F., Kerjean, L., Lafaille, V., Lafond, L., Lam-Trong, T., Landiech, P., Lapeyrere, V., Larqué, T., Laudet, P., Lautier, N., Lecann, H., Lefevre, L., Leruyet, B., Levacher, P., Magnan, A., Mazy, E., Mertens, F., Mesnager, J., Meunier, J., Michel, J., Monjoin, W., Naudet, D., Nguyen-Kim, K., Orcesi, J., Ottacher, H., Perez, R., Peter, G., Plasson, P., Plesseria, J., Pontet, B., Pradines, A., Quentin, C., Reynaud, J., Rolland, G., Rollenhagen, F., Romagnan, R., Russ, N., Schmidt, R., Schwartz, N., Sebbag, I., Sedes, G., Smit, H., Steller, M. B., Sunter, W., Surace, C., Tello, M., Tiphène, D., Toulouse, P., Ulmer, B., Vandermarcq, O., Vergnault, E., Vuillemin, A., and Zanatta, P.: 2009, *Astronomy & Astrophysics* **506**, 287

Leighton, R. B., Noyes, R. W., and Simon, G. W.: 1962, *Astrophysical Journal* **135**, 474

Lenz, P. and Breger, M.: 2005, *Communications in Asteroseismology* **146**, 53

Lomb, N. R.: 1976, *Astrophysics and Space Science* **39**, 447

Maeder, A., Grebel, E. K., and Mermilliod, J.-C.: 1999, *Astronomy & Astrophysics* **346**, 459

Maeder, A. and Meynet, G.: 2001, *Astronomy & Astrophysics* **373**, 555

Maintz, M., Rivinius, T., Štefl, S., Baade, D., Wolf, B., and Townsend, R. H. D.: 2003, *Astronomy & Astrophysics* **411**, 181

Marshall, S.: 1994, in H. T. MacGillivray (ed.), *Astronomy from Wide-Field Imaging*, Vol. 161 of *IAU Symposium*, pp 67–+

Martayan, C., Baade, D., and Fabregat, J.: 2008a, in C. Charbonnel, F. Combes, & R. Samadi (ed.), *SF2A-2008*, pp 497–+

Martayan, C., Diago, P., Gutiérrez-Soto, J., Fabregat, J., Hubert, A., Floquet, M., Neiner, C., and Mekkas, M.: 2008b, *ArXiv e-prints*

Martayan, C., Floquet, M., Hubert, A. M., Gutiérrez-Soto, J., Fabregat, J., Neiner, C., and Mekkas, M.: 2007a, *Astronomy & Astrophysics* **472**, 577

Martayan, C., Frémat, Y., Hubert, A., Floquet, M., Zorec, J., and Neiner, C.: 2006a, *Astronomy & Astrophysics* **452**, 273

Martayan, C., Frémat, Y., Hubert, A.-M., Floquet, M., Zorec, J., and Neiner, C.: 2007b, *Astronomy & Astrophysics* **462**, 683

Martayan, C., Hubert, A. M., Floquet, M., Fabregat, J., Frémat, Y., Neiner, C., Stee, P., and Zorec, J.: 2006b, *Astronomy & Astrophysics* **445**, 931

Martín, S., Bossi, M., and Zerbi, F. M.: 2003, *Astronomy & Astrophysics* **401**, 1077

Mayor, M. and Queloz, D.: 1995, *Nature* **378**, 355

Mazzali, P. A., Lennon, D. J., Pasian, F., Marconi, G., Baade, D., and Castellani, V.: 1996, *Astronomy & Astrophysics* **316**, 173

Meilland, A., Stee, P., Zorec, J., and Kanaan, S.: 2006, *Astronomy & Astrophysics* **455**, 953

Mennickent, R. E., Pietrzyński, G., Gieren, W., and Szewczyk, O.: 2002, *Astronomy & Astrophysics* **393**, 887

Meynet, G. and Maeder, A.: 2000, *Astronomy & Astrophysics* **361**, 101

Miglio, A.: 2006, in C. Aerts & C. Sterken (ed.), *Astrophysics of Variable Stars*, Vol. 349 of *Astronomical Society of the Pacific Conference Series*, p. 297

Miglio, A., Montalbán, J., and Dupret, M.-A.: 2007a, *Monthly Notices of the Royal Astronomical Society* **375**, L21

Miglio, A., Montalbán, J., and Dupret, M.-A.: 2007b, *Communications in Asteroseismology* **151**, 48

Montgomery, M. and O'Donogohue, D.: 1999, *Delta Scuti Newsletter* **13**, p28

Morel, P.: 1997, *Astronomy & Astrophysics Supplement Series* **124**, 597

Morel, P. and Lebreton, Y.: 2008, *Astrophysics and Space Science* **316**, 61

Mosser, B., Appourchaux, T., Catala, C., Buey, J., and the SIAMOIS team: 2008, *Journal of Physics Conference Series* **118(1)**, 012042

Mosser, B., Baudin, F., Lanza, A. F., Hulot, J. C., Catala, C., Baglin, A., and Auvergne, M.: 2009, *Astronomy & Astrophysics* **506**, 245

Moya, A. and Garrido, R.: 2008, *Astrophysics and Space Science* **316**, 129

Moya, A., Garrido, R., and Dupret, M. A.: 2004, *Astronomy & Astrophysics* **414**, 1081

Narwid, A., Kołaczkowski, Z., Pigulski, A., and Ramza, T.: 2006, *Memorie della Societa Astronomica Italiana* **77**, 342

Neiner, C., Floquet, M., Hubert, A. M., Frémat, Y., Hirata, R., Masuda, S., Gies, D., Buil, C., and Martayan, C.: 2005a, *Astronomy & Astrophysics* **437**, 257

Neiner, C., Gutiérrez-Soto, J., Baudin, F., de Batz, B., Frémat, Y., Huat, A. L., Floquet, M., Hubert, A., Leroy, B., Diago, P. D., Poretti, E., Carrier, F., Rainer, M., Catala, C., Thizy, O., Buil, C., Ribeiro, J., Andrade, L., Emilio, M., Espinosa Lara, F., Fabregat, J., Janot-Pacheco, E., Martayan, C., Semaan, T., Suso, J., Baglin, A., Michel, E., and Samadi, R.: 2009a, *Astronomy & Astrophysics* **506**, 143

Neiner, C., Gutiérrez-Soto, J., Floquet, M., Huat, A., Hubert, A., de Batz, B., Leroy, B., Frémat, Y., Andrade, L., Diago, P. D., Emilio, M., Fabregat, J., Janot-Pacheco, E., Martayan, C., Semaan, T., and Suso, J.: 2009b, *Communications in Asteroseismology* **158**, 319

Neiner, C. and Hubert, A.: 2009, *Communications in Asteroseismology* **158**, 194

Neiner, C., Hubert, A., and Catala, C.: 2005b, *Astrophysical Journal Supplement Series* **156**, 237

Neiner, C., Hubert, A., Frémat, Y., Floquet, M., Jankov, S., Preuss, O., Henrichs, H. F., and Zorec, J.: 2003, *Astronomy & Astrophysics* **409**, 275

Osaki, J.: 1975, *Publications of the Astronomical Society of Japan* **27**, 237

Osaki, Y.: 1971, *Publications of the Astronomical Society of Japan* **23**, 485

Osaki, Y.: 1974, *Astrophysical Journal* **189**, 469

Pamyatnykh, A. A.: 1999, *Acta Astronomica* **49**, 119

Pasquini, L., Avila, G., Blecha, A., Cacciari, C., Cayatte, V., Colless, M., Damiani, F., de Propris, R., Dekker, H., di Marcantonio, P., Farrell, T., Gillingham, P., Guinouard, I., Hammer, F., Kaufer, A., Hill, V., Marteaud, M., Modigliani, A., Mulas, G., North, P., Popovic, D., Rossetti, E., Royer, F., Santin, P., Schmutzer, R., Simond, G., Vola, P., Waller, L., and Zoccali, M.: 2002, *The Messenger* **110**, 1

Pekeris, C. L.: 1938, *Astrophysical Journal* **88**, 189

Perdang, J.: 1968, *Astrophysics and Space Science* **1**, 355

Pigulski, A.: 2005, *Acta Astronomica* **55**, 219

Pigulski, A. and Kołaczkowski, Z.: 2002, *Astronomy & Astrophysics* **388**, 88

Porter, J. M. and Rivinius, T.: 2003, *Publications of the Astronomical Society of the Pacific* **115**, 1153

Provost, J.: 2000, in E. Michel and A. Hui-Bon-Hoa (ed.), *CoRoT Milestone 2000*, available at http://www.lesia.obspm.fr/projets/corotswg/MilestoneProc/SWGproc2000.html

Queloz, D., Bouchy, F., Moutou, C., Hatzes, A., Hébrard, G., Alonso, R., Auvergne, M., Baglin, A., Barbieri, M., Barge, P., Benz, W., Bordé, P., Deeg, H. J., Deleuil, M., Dvorak, R., Erikson, A., Ferraz Mello, S., Fridlund, M., Gandolfi, D., Gillon, M., Guenther, E., Guillot, T., Jorda, L., Hartmann, M., Lammer, H., Léger, A., Llebaria, A., Lovis, C., Magain, P., Mayor, M., Mazeh, T., Ollivier, M., Pätzold, M., Pepe, F., Rauer, H., Rouan, D., Schneider, J., Segransan, D., Udry, S., and Wuchterl, G.: 2009, *Astronomy & Astrophysics* **506**, 303

Quirrenbach, A., Bjorkman, K. S., Bjorkman, J. E., Hummel, C. A., Buscher, D. F., Armstrong, J. T., Mozurkewich, D., Elias, II, N. M., and Babler, B. L.: 1997, *Astrophysical Journal* **479**, 477

Reese, D., Lignières, F., and Rieutord, M.: 2006, *Astronomy & Astrophysics* **455**, 621

Reese, D. R., MacGregor, K. B., Jackson, S., Skumanich, A., and Metcalfe, T. S.: 2009, *Astronomy & Astrophysics* **506**, 189

Renzini, A. and da Costa, L.: 1999, *The Messenger* **98**, 33

Renzini, A. and da Costa, L. N.: 1997, *The Messenger* **87**, 23

Ritter, A.: 1879, *Wiedemanns Annual*, Vol. 8

Rivinius, T., Baade, D., Stefl, S., and et al.: 1998a, in L. Kaper & A. W. Fullerton (ed.), *Cyclical Variability in Stellar Winds*, p. 207

Rivinius, T., Baade, D., Stefl, S., Stahl, O., Wolf, B., and Kaufer, A.: 1998b, *Astronomy & Astrophysics* **336**, 177

Rivinius, T., Baade, D., and Štefl, S.: 2003, *Astronomy & Astrophysics* **411**, 229

Rivinius, T., Baade, D., Štefl, S., Townsend, R. H. D., Stahl, O., Wolf, B., and Kaufer, A.: 2001, *Astronomy & Astrophysics* **369**, 1058

Robinson, T. R. and Grubb, T.: 1869, *Royal Society of London Philosophical Transactions Series I* **159**, 127

Rogers, F. J. and Iglesias, C. A.: 1992, *Astrophysical Journal Supplement Series* **79**, 507

Rolleston, W. R. J., Brown, P. J. F., Dufton, P. L., and Howarth, I. D.: 1996, *Astronomy & Astrophysics* **315**, 95

Rosseland, S.: 1949, *The pulsation theory of variable stars.*

Royer, F., Melo, C., Mermilliod, J., North, P., Do Nascimento, Jr., J. D., de Medeiros, J. R., Grebel, E. K., and Maeder, A.: 2004, in A. Maeder & P. Eenens (ed.), *Stellar Rotation*, Vol. 215 of *IAU Symposium*, p. 71

Sabogal, B. E., Mennickent, R. E., Pietrzyński, G., and Gieren, W.: 2005, *Monthly Notices of the Royal Astronomical Society* **361**, 1055

Saio, H., Cameron, C., Kuschnig, R., Walker, G. A. H., Matthews, J. M., Rowe, J. F., Lee, U., Huber, D., Weiss, W. W., Guenther, D. B., Moffat, A. F. J., Rucinski, S. M., and Sasselov, D.: 2007, *Astrophysical Journal* **654**, 544

Salmon, S., Montalbán, J., Miglio, A., Morel, T., Dupret, M., and Noels, A.: 2009, in J. A. Guzik & P. A. Bradley (ed.), *American Institute of Physics Conference Series*, Vol. 1170 of *American Institute of Physics Conference Series*, pp 385–387

Samadi, R., Fialho, F., Costa, J. E. S., Drummond, R., Pinheiro Da Silva, L., Baudin, F., Boumier, P., and Jorda, L.: 2007, *ArXiv Astrophysics e-prints*

Sarro, L. M., Debosscher, J., López, M., and Aerts, C.: 2009, *Astronomy & Astrophysics* **494**, 739

Savonije, G. J.: 2005, *Astronomy & Astrophysics* **443**, 557

Scargle, J. D.: 1982, *Astrophysical Journal* **263**, 835

Schaerer, D., Charbonnel, C., Meynet, G., Maeder, A., and Schaller, G.: 1993, *Astronomy & Astrophysics Supplement Series* **102**, 339

Schaller, G., Schaerer, D., Meynet, G., and Maeder, A.: 1992, *Astronomy & Astrophysics Supplement Series* **96**, 269

Schmidtke, P. C., Chobanian, J. B., and Cowley, A. P.: 2008, *Astronomical Journal* **135**, 1350

Schwarzenberg-Czerny, A.: 1991, *Monthly Notices of the Royal Astronomical Society* **253**, 198

Scuflaire, R.: 1974, *Astronomy & Astrophysics* **36**, 107

Scuflaire, R. and Thoul, A.: 2002, *Stellar Stability and Asteroseismology (Lecture notes)*, Institute of Astrophysics and Geophysics of the University of Liège

Seaton, M. J.: 1996, *Monthly Notices of the Royal Astronomical Society* **279**, 95

Secchi, A.: 1866, *Astronomische Nachrichten* **68**, 63

Shibahashi, H. and Osaki, Y.: 1976, *Publications of the Astronomical Society of Japan* **28**, 199

Silvester, J., Neiner, C., Henrichs, H. F., Wade, G. A., Petit, V., Alecian, E., Huat, A., Martayan, C., Power, J., and Thizy, O.: 2009, *Monthly Notices of the Royal Astronomical Society* **398**, 1505

Slettebak, A.: 1982, *Astrophysical Journal Supplement Series* **50**, 55

Slettebak, A.: 1988, *Publications of the Astronomical Society of the Pacific* **100**, 770

Smith, M. A.: 1980, *Astrophysical Journal* **240**, 149

Smith, M. A., Henrichs, H. F., and Fabregat, J. (eds.): 2000, *The Be Phenomenon in Early-Type Stars*, Vol. 214 of *Astronomical Society of the Pacific Conference Series*

Snellen, I. A. G., de Mooij, E. J. W., and Albrecht, S.: 2009, *Nature* **459**, 543

Solano, E., Catala, C., Garrido, R., Poretti, E., Janot-Pacheco, E., Gutiérrez, R., González, R., Mantegazza, L., Neiner, C., Fremat, Y., Charpinet, S., Weiss, W., Amado, P. J., Rainer, M., Tsymbal, V., Lyashko, D., Ballereau, D., Bouret, J. C., Hua, T., Katz, D., Lignières, F., Lüftinger, T., Mittermayer, P., Nesvacil, N., Soubiran, C., van't Veer-Menneret, C., Goupil, M. J., Costa, V., Rolland, A., Antonello, E., Bossi, M., Buzzoni, A., Rodrigo, C., Aerts, C., Butler, C. J., Guenther, E., and Hatzes, A.: 2005, *Astronomical Journal* **129**, 547

Soszynski, I., Zebrun, K., Udalski, A., Wozniak, P. R., Szymanski, M., Kubiak, M., Pietrzynski, G., Szewczyk, O., and Wyrzykowski, L.: 2002, *Acta Astronomica* **52**, 143

Soufi, F., Goupil, M. J., and Dziembowski, W. A.: 1998, *Astronomy & Astrophysics* **334**, 911

Stankov, A. and Handler, G.: 2005, *Astrophysical Journal Supplement Series* **158**, 193

Stee, P.: 2000, in M. A. Smith, H. F. Henrichs, & J. Fabregat (ed.), *IAU Colloq. 175: The Be Phenomenon in Early-Type Stars*, Vol. 214 of *Astronomical Society of the Pacific Conference Series*, p. 129

Stein, R. F. and Leibacher, J.: 1974, *Annual Review of Astronomy & Astrophysics* **12**, 407

Stellingwerf, R. F.: 1978, *Astrophysical Journal* **224**, 953

Sterken, C. and Jerzykiewicz, M.: 1988, *Monthly Notices of the Royal Astronomical Society* **235**, 565

Stoeckley, T. R.: 1968, *Monthly Notices of the Royal Astronomical Society* **140**, 141

Stubbs, C. W., Marshall, S., Cook, K. H., Hills, R. F., Noonan, J., Akerlof, C. W., Alcock, C. R., Axelrod, T. S., Bennett, D., Dagley, K., Freeman, K. C., Griest, K., Park, H., Perlmutter, S., Peterson, B. A., Quinn, P. J., Rodgers, A. W., Sosin, C., and Sutherland, W. J.: 1993, in M. M. Blouke (ed.), *Society of Photo-Optical Instrumentation Engineers (SPIE) Conference Series*, Vol. 1900 of *Presented at the Society of Photo-Optical Instrumentation Engineers (SPIE) Conference*, pp 192–204

Suárez, J. C.: 2002, *Ph.D. thesis*, Observatoire de Paris

Suárez, J. C., Goupil, M. J., and Morel, P.: 2006, *Astronomy & Astrophysics* **449**, 673

Tassoul, M.: 1980, *Astrophysical Journal Supplement Series* **43**, 469

Thomson, W.: 1863, *Phil. Trans. Royal Society London*, Vol. 153

Townsend, R. H. D.: 2005, *Monthly Notices of the Royal Astronomical Society* **364**, 573

Tran Minh, F. and Léon, L.: 1995, in I. W. Roxburgh & J.-L. Masnou (ed.), *Physical Processes in Astrophysics*, pp 219–221

Unno, W.: 1975, *Publications of the Astronomical Society of Japan* **27**, 81

Unno, W., Osaki, Y., Ando, H., Saio, H., and Shibahashi, H.: 1989, *Nonradial oscillations of stars*

Vakili, F., Mourard, D., Stee, P., Bonneau, D., Berio, P., Chesneau, O., Thureau, N., Morand, F., Labeyrie, A., and Tallon-Bosc, I.: 1998, *Astronomy & Astrophysics* **335**, 261

Van Bever, J. and Vanbeveren, D.: 1997, *Astronomy & Astrophysics* **322**, 116

Vaníček, P.: 1971, *Astrophysics and Space Science* **12**, 10

Wade, G. A.: 2010, in C. Neiner, G. A. Wade, G. Meynet & G. Peters (ed.), *Active OB stars: structure, evolution, mass loss and critical limits*, IAU Symposium 272, in preparation

Waelkens, C.: 1991, *Astronomy & Astrophysics* **246**, 453

Waelkens, C., Aerts, C., Kestens, E., Grenon, M., and Eyer, L.: 1998, *Astronomy & Astrophysics* **330**, 215

Walker, G., Matthews, J., Kuschnig, R., Johnson, R., Rucinski, S., Pazder, J., Burley, G., Walker, A., Skaret, K., Zee, R., Grocott, S., Carroll, K., Sinclair, P., Sturgeon, D., and Harron, J.: 2003, *Publications of the Astronomical Society of the Pacific* **115**, 1023

Walker, G. A. H.: 2008, *Journal of Physics Conference Series* **118(1)**, 012013

Walker, G. A. H., Kuschnig, R., Matthews, J. M., Cameron, C., Saio, H., Lee, U., Kambe, E., Masuda, S., Guenther, D. B., Moffat, A. F. J., Rucinski, S. M., Sasselov, D., and Weiss, W. W.: 2005a, *Astrophysical Journal Letters* **635**, L77

Walker, G. A. H., Kuschnig, R., Matthews, J. M., Reegen, P., Kallinger, T., Kambe, E., Saio, H., Harmanec, P., Guenther, D. B., Moffat, A. F. J., Rucinski, S. M., Sasselov, D., Weiss, W. W., Bohlender, D. A., Božić, H., Hashimoto, O., Koubský, P., Mann, R., Ruždjak, D., Škoda, P., Šlechta, M., Sudar, D., Wolf, M., and Yang, S.: 2005b, *Astrophysical Journal Letters* **623**, L145

Weiss, W. W., Aerts, C., Aigrain, S., Alecian, G., Antonello, E., Baglin, A., Bazot, M., Collier-Cameron, A., Charpinet, S., Gamarova, A., Handler, G., Hatzes, A., Hubert, A., Lammer, H., Lebzelter, T., Maceroni, C., Marconi, M., de Martino, D., Janot-Pacheco, E., Pagano, I., Paunzen, E., Pinheiro, F. J. G., Poretti, E., Ribas, I., Ripepi, V., Roques, F., Silvotti, R., Surdej, J., Vauclair, G., Vauclair, S., and Zwintz, K.: 2004, in F. Favata, S. Aigrain, & A. Wilson (ed.), *Stellar Structure and Habitable Planet Finding*, Vol. 538 of *ESA Special Publication*, pp 435–444

White, T. R., Brewer, B. J., Bedding, T. R., Stello, D., and Kjeldsen, H.: 2010, *Communications in Asteroseismology* **161**, 39

Zerbi, F. M., Garrido, R., Rodriguez, E., Krisciunas, K., Crowe, R. A., Roberts, M., Guinan, E. F., McCook, G. P., Sperauskas, J., Griffin, R. F., and Luedeke, K. D.: 1997, *Monthly Notices of the Royal Astronomical Society* **290**, 401

Zhevakin, S. A.: 1952, *Astron. Zhurnal* **29**, 37

Zhevakin, S. A.: 1953, *Astron. Zhurnal* **30**, 161

Zhevakin, S. A.: 1963, *Annual Review of Astronomy & Astrophysics* **1**, 367

Zorec, J., Frémat, Y., and Cidale, L.: 2005, *Astronomy & Astrophysics* **441**, 235

List of Tables

List of Figures

Agradecimientos

There are places I remember
All my life, through some have changed,
Some forever, not for better,
Some have gone and some remain.

John Lennon & Paul McCartney

Esta tesis doctoral ha sido fruto del trabajo y esfuerzo de un gran número de personas, a las cuales quiero agradecer su colaboración y participación en este gran proyecto. Sin ellos y sin sus valiosas aportaciones este trabajo no hubiera sido posible.

Primeramente, quiero dar las gracias a mis directores de tesis, Juan Fabregat y Juan Gutiérrez-Soto, por su dedicación y paciencia conmigo. A Juan Fabregat por ofrecerme la oportunidad de trabajar a su lado, por tener siempre un momento para charlar, por las fructíferas discusiones y por sus buenas explicaciones y razonamientos. A Juan Gutiérrez-Soto, por adentrarme en el mundo de la investigación, un trabajo "*a veces tan duro y a veces tan gratificante*", por tener tantísima paciencia conmigo y por responder a las mil y una preguntas que siempre tengo para él. Gracias a los dos por vuestro apoyo en todo momento y por acceder a ser mis directores de tesis.

El trabajo inicial de esta tesis sobre pulsaciones en estrellas masivas de las nubes de Magallanes se ha beneficiado enormemente de la colaboración de Christo-phe Martayan, gracias a él, a sus aportaciones y a sus estudios hemos podido realizar esta primera parte de la tesis, obteniendo resultados muy interesantes. En lo que corresponde al código PASPER creado para el análisis automático de frecuencias, quiero agradecer a Rafa Garrido que nos facilitara su código FORTRAN, *freq.for*. Sin esta aportación todo hubiera sido bastante más complicado y tedioso.

En estos años de preparación (y ahora de análisis de datos) de la misión CoRoT la comunicación y discusión con los miembros del CoRoT Be Team han sido muy enriquecedoras. Por esto, quiero dar las gracias a todos los integrantes del CoRoT Be Team, muy especialmente a los miembros pertenecientes al GEPI del Observatoire de Paris–Meudon. En particular quiero dar las gracias a Coralie Neiner por su amable acogida, a Anne-Marie Hubert y a Michèle Floquet por estar siempre dispuestas a revisar nuestros trabajos, a Bernard Leroy por trabajar con Juan Gutiérrez-Soto y conmigo en el desarrollo y mejora de los códigos y a Yves Frémat por la determinación de parámetros para el estudio de la estrella Be HD 50 209.

Quiero dar las gracias a la gente que conocí en el Instituto Astrofísica de Andalucía (IAA–CSIC) durante mi estancia en Granada. Gracias a Andy Moya y Juan Carlos por enseñarme tanto sobre evolución estelar, por enseñarme a usar sus códigos de oscilación y por ser tan buena gente. Gracias también a Pedro Amado, Susana Martín y Cristina Rodríguez por compartir buenos almuerzos, risas y ciencia. Y sobretodo, gracias a Rafa Garrido por darme la oportunidad de formar parte de un grupo tan dinámico y motivador, y por enseñarme que "*la transformada de Fourier lo ve todo*".

Gracias también a Slavek Rucinski, por darme la oportunidad de observar en el DDO de Toronto (Canadá) antes de que fuera cerrado. Fue una gran experiencia para un joven astrónomo como yo. Gracias también a Julia Suso, por compartir noches de observación en el INT del Observatorio de Roque de Los Muchachos en La Palma y por apoyarme siempre en todo momento.

Quiero agradecer especialmente el esfuerzo realizado por los evaluadores de esta tesis doctoral: Andy Moya, Enrique Solano y Julia Suso. Gracias por acceder a corregir esta tesis y por vuestros comentarios y sugerencias tan acertados. Sin duda, han sido claves en la elaboración final del texto de esta tesis doctoral.

Un agradecimiento muy especial va para la gente del Observatori Astronòmic de la Universitat de València. Todos y cada uno de ellos son excelentes investigadores y mejores personas. Todos forman un grupo muy unido en el que me siento totalmente integrado. Gracias a todos los que habéis pasado por el Observatori: Vicent Martínez, Julia Suso, Juan Fabregat, Fernando Ballesteros, Amelia Ortíz y Alberto Fernández, Miquel Gómez, Vicent Peris, Mauro Stefanon y Elisa Nespoli, Pablo Arnalte, Lara Santolaya, Mariana Lanzara, Jorge Alonso, Pablo de la Cruz, Laura Moll, Juan Gutiérrez-Soto, Teresa Gallego, Toni Peña, María Herrero, Sofía Fuentes y Lupe Almodóvar (seguro que me dejo a alguien). Gracias por los buenos ratos que hemos pasado y por los que están por venir.

También quiero agradecer a mis compañeros de la VIU (Valencian International University) el apoyo constante para que pudiera llevar a cabo esta tesis doctoral. A todos ellos: ¡mil gracias! y mucho ánimo a los que estáis todavía con vuestras tesis.

Gracias muy especiales a mis compañeros de carrera, en la Facultat de Matemàtiques de la Universitat de València, con los que he compartido los muchos de los mejores momentos de mi vida: fiestas, exámenes, ratos de cafetería, cenas de Navidad, días Sivera, semanas culturales, finales con el OBM, clases de estadística Bayesiana, de Geometría Afín y Proyectiva, discursos de JoseRa, ... Gracias por ser apoyo y motivación constantes: Ana, Anabel, Bea, Diego, Dioni, Elena, Isa, Jannet, JoseRa, Jota, Lledó, Mario, Marta, Pol, Paula, Pili, Raúl, Rafa, Rebeca, Rob, Rosaura, Rubia, Suárez, ...